Titre: Title:	Nuclear reactor kinetics based on hierarchical nodal analysis
Auteur: Author:	Siamak Kaveh-Khorie
Date:	2000
Type:	Mémoire ou thèse / Dissertation or Thesis
Référence: Citation:	Kaveh-Khorie, S. (2000). Nuclear reactor kinetics based on hierarchical nodal analysis [Thèse de doctorat, École Polytechnique de Montréal]. PolyPublie. https://publications.polymtl.ca/7530/

URL de PolyPublie: PolyPublie URL:	https://publications.polymtl.ca/7530/
Directeurs de recherche: Advisors:	Jean Koclas, & Robert Roy
Programme: Program:	Non spécifié

UNIVERSITÉ DE MONTRÉAL

NUCLEAR REACTOR KINETICS BASED ON HIERARCHICAL NODAL ANALYSIS

SIAMAK KAVEH-KHORIE
DÉPARTEMENT DE GÉNIE MÉCANIQUE
ÉCOLE POLYTECHNIQUE DE MONTRÉAL

THÈSE PRÉSENTÉE EN VUE DE L'OBTENTION
DU DIPLÔME DE PHILOSOPHIAE DOCTOR
(GÉNIE NUCLÉAIRE)
AOÛT 2000

UNIVERSITÉ DE MONTRÉAL

ÉCOLE POLYTECHNIQUE DE MONTRÉAL

Cette thèse intitulée :

NUCLEAR REACTOR KINETICS BASED ON HIERARCHICAL NODAL ANALYSIS

présentée par: KAVEH-KHORIE Siamak

en vue de l'obtention du diplôme de: Philosophiae Doctor

a été dûment acceptée par le jury d'examen constitué de:

M. ROZON Daniel, Ph.D., président

M. KOCLAS Jean, Ph.D., membre et directeur de recherche

M. ROY Robert, Ph.D., membre et codirecteur de recherche

M. TEYSSEDOU Alberto, Ph.D., membre

M. ROUBEN Benjamin, Ph.D., membre

DEDICATION

To

my father

my mother

ACKNOWLEDGEMENTS

I would like to thank my thesis supervisors, Drs. J. Koclas and R. Roy, for their invaluable guidance, insightful advice, and encouragement during the course of this research project. Without their vast knowledge and experience, this investigation could not have been accomplished.

I would also like to thank all the members of my jury for taking the time to read my thesis and particularly for doing so on such short notice.

It is a pleasure to thank Drs. A. Teyssedou and D. Rozon for their support during my time as a student at École Polytechnique de Montréal.

I am also indebted to Dr. P. Tye, who kindly accepted to read and correct the entire text in a short period of time.

The list of friends who have been generous with their support is very long indeed. Rather than risk omission of a single name, I hope that a grateful general acknowledgment will express my sincere gratitude for their precious encouragement.

Last but not least, I wish to record my very special appreciation to my life companion and wife, Lina, for her support, patience and understanding throughout my long preoccupation with the present research.

RÉSUMÉ

L'analyse des phénomènes transitoires simulant le comportement des réacteurs nucléaires de puissance nécessite une somme considérable de ressources informatiques. L'objectif de cette thèse est de développer un algorithme numérique efficace et précis pour résoudre l'équation spatio-temporelle de diffusion de neutrons. La nouvelle méthodologie ici développée a pour nom la «cinétique hiérarchique nodale»: la hiérarchie consistant à définir un ou plusieurs maillages plus grossiers sur lesquels le calcul complet du réacteur peut être effectué à un moindre coût. Afin de préserver l'exactitude de ces calculs grossiers, le maillage fin du problème original est projeté vers un maillage plus grossier en utilisant la théorie d'équivalence généralisée introduisant des facteurs appelés de discontinuité. Deux formalismes cinétiques hiérarchiques nodaux seront établis: l'approche hiérarchique en temps et en espace. Dans le formalisme hiérarchique en temps, la solution du problème à mailles grossières agit comme solution pour le prochain pas de temps (ou tout au moins une partie de cette solution). Dans le formalisme hiérarchique en espace, ces solutions intermédiaires à mailles grossières sont plutôt employées afin d'accélérer le taux de convergence du problème fin.

Les nombreuses simulations numériques (conçues tant en mode statique que dynamique) permettent de mieux juger des différentes applications de la théorie d'équivalence généralisée et ainsi d'évaluer correctement la performance de la cinétique hiérarchique nodale. Toutes les simulations utilisent un modèle relativement réaliste du réacteur CANDU-6. Les résultats obtenus prouvent que l'emploi de la formulation hiérarchique en temps conduit à une réduction d'au moins 85% en temps de calcul par rapport à la solution directe tout en préservant l'exactitude de la solution. De plus, il est démontré qu'en utilisant l'approche hiérarchique en espace, qui est en fait une méthode multigrille, le nombre d'itérations pour un critère donné de convergence peut être réduit d'au moins 50%, ce qui contribue également à réduire grandement le temps de calcul.

ABSTRACT

The analysis of nuclear reactor power transients requires a considerable amount of computational resources. The main objective of the present thesis is to establish a new solution algorithm called hierarchical nodal kinetics whose main objective is to reduce the computing costs of the time-dependent calculations without introducing unacceptable inaccuracies in the solution. The basis of the method is the definition of one or more intermediate coarser grids over which the reactor problem is solved at a much lower computational cost. To preserve the accuracy of the coarse calculations, the projection of the reactor problem from the finer grids to the coarser meshes is carried out using generalized equivalence theory and so-called discontinuity factors. Two formalisms of hierarchical nodal kinetics are established, time hierarchy and space hierarchy approaches. In the time hierarchy formalism, the solution of the reactor over the coarse grids is treated as the reactor solution (or a part of the reactor solution) for the next time step. In the space hierarchy formalism, the intermediate coarse solutions are used to accelerate the convergence rate of the fine grid problem.

Numerous simulations for both static and dynamic calculations are designed and performed to better understand different aspects of using generalized equivalence theory and thus to correctly evaluate the performance of the hierarchical nodal kinetics method. All test cases are performed for a relatively realistic model of a CANDU-6 reactor. The results obtained from the use of the time-hierarchy formalism resulted in a performance increase of at least 85% compared to the reference solution while maintaining accuracy of the solution. Furthermore, it is demonstrated that by using the space-hierarchy approach, which is a multigrid method, the number of iterations necessary for a given convergence criterion can be reduced by least 50% resulting in a considerable saving in total CPU time.

CONDENSÉ EN FRANÇAIS

Objectifs de l'étude

Un calcul précis de la puissance produite par le cœur d'un réacteur nucléaire au cours du suivi d'un phénomène transitoire est essentiel tout autant pour les applications de design que pour opération sécuritaire du réacteur. Ces transitoires couvrent une large gamme d'événements: allant de l'épuisement du combustible du cœur aux accidents nucléaires catastrophiques. Il est prouvé que les équations de diffusion, dans plusieurs cas, décrivent suffisamment bien le comportement neutronique du cœur de réacteur.

Malgré l'augmentation substantielle de la vitesse et de la mémoire des équipements informatiques disponibles ces dernières années, la solution numérique de ces équations de diffusion est encore loin d'être pratique pour des calculs effectués régulièrement. Le coût considérable de ces calculs est normalement induit par la prise en compte de la géométrie tridimensionnelle compliquée du cœur d'un réacteur de puissance dans le calcul du flux neutronique. Par exemple, pour un réacteur CANDU, un calcul transitoire typique nécessite près de 10000 mailles, ce qui demande une très grande consommation de temps de calcul. Supporté par ces constatations, l'objectif principal du présent travail est d'établir un nouvel algorithme de solution appelé «cinétique hiérarchique nodale» et visant la réduction du coût de calcul, sans introduire d'inexactitude inacceptable sur la solution. Le deuxième objectif de ce travail est d'évaluer la performance, sur le plan numérique, et ce en utilisant un modèle relativement réaliste du réacteur CANDU-6.

La théorie d'équivalence nodale

Le volume global du réacteur peut être partagé en nœuds homogénéisés et relativement grands ne se chevauchant pas. Ces nœuds sont soit véritablement homogènes d'un point de vue physique, soit ils seront forcés à être homogènes (en utilisant des valeurs nodales

de sections efficaces et de coefficients de diffusion à la fois pondérées par les éléments de volume et par le flux).

L'hétérogénéité inhérente du cœur d'un réacteur implique que la première alternative n'est pas réaliste hormis dans le réflecteur tandis que la seconde pourrait conduire à des erreurs substantielles dans les calculs de flux. La réponse à la question suivante est donc d'une importance primordiale:

"Comment les paramètres équivalents de diffusion peuvent-ils être définis ou évalués approximativement pour toutes les régions du réacteur de sorte que les applications qui en résultent présentent un minimum d'erreur dans les calculs transitoires de flux?"
La réponse à cette question est fondamentalement similaire à la solution du problème d'homogénéisation rencontré lorsque l'équation du transport doit être approchée par celle de la diffusion (connu aussi comme le problème d'homogénéisation de cellules ou d'assemblages); dans ce problème, on définit typiquement des paramètres de diffusion équivalents permettant de reproduire les calculs de transport au niveau de l'assemblage (Henry, 1975; Smith, 1986).

Cette similarité permettrait d'adopter les techniques avancées d'homogénéisation d'assemblage aux calculs transitoires d'un réacteur. Parmi ces techniques, la théorie d'équivalence nodale (NET) est la procédure la plus appropriée pour les calculs spatio-temporels du réacteur. En trois dimensions, la théorie d'équivalence nodale introduite six paramètres ajustables par groupe d'énergie et par nœud, ce qui nous force à conserver six courants d'interface moyennés par nœud et par groupe. Deux variétés de théorie d'équivalence nodale ont été développées: la théorie d'équivalence (ET) (Koebke, 1978) et la théorie d'équivalence généralisée (GET) (Smith, 1980). Dans les deux approches, le flux homogène transverse est considéré discontinu aux interfaces nodales. La somme des discontinuités est mesurée par la définition de facteurs hétérogènes (ET) ou facteurs de discontinuité (GET). Les valeurs de ces facteurs de

discontinuité ou d'hétérogénéité sont déterminées de façon à apparier les valeurs homogénéisées des courants d'interface aux valeurs hétérogènes correspondantes. La différence entre ces deux approches réside principalement dans le fait que, dans l'approche ET, les coefficients de diffusion et les facteurs de continuité sont ajustés simultanément tandis que, dans l'approche GET, les coefficients de diffusion sont arbitraires et les facteurs de discontinuité sont de fait les seuls paramètres ajustables. Dans le domaine de la cinétique des réacteurs, l'approche GET semble être l'approche la plus largement appliquée.

La cinétique hiérarchique nodale

L'essentiel de cette méthode consiste à définir un ou plusieurs maillages grossiers intermédiaires sur lesquels le problème du réacteur est résolu avec une baisse significative du coût de calcul. Afin de préserver l'exactitude des calculs grossiers, la projection du problème du réacteur du maillage fin au maillage plus grossier est faite en utilisant la théorie d'équivalence généralisée (Smith, 1980). Deux formalismes de la cinétique hiérarchique nodale sont établis: l'approche hiérarchique en temps et celle hiérarchique en espace.

La hiérarchie en temps

Dans le formalisme hiérarchique en temps, la solution du réacteur sur les maillages grossiers est traitée comme la solution du réacteur (ou une partie de la solution du réacteur) pour le prochain pas de temps. Ce concept peut être adapté aisément aux différentes approches conventionnelles. Par exemple, la fonction de forme issue d'un calcul quasi-statique peut être calculée en utilisant deux tailles de nœud (fine et grossière) où chaque taille correspond à un élément hiérarchique en temps. Il est supposé que la fonction de forme plus grossière variera plus vite que celle des nœuds plus fins. Donc, la fonction de forme dans les nœuds plus grossiers devrait être calculée plus souvent. La théorie d'équivalence nodale nous assure de préserver tous les taux de

réaction par groupe, toutes les concentrations de précurseurs de neutron ainsi que tous les courants d'interface, et ce pour chaque maille grossière. Sur les niveaux hiérarchiques en temps les plus fins, les équations de cinétique sont résolues. À tout pas de temps, les paramètres cinétiques sont définis par des intégrales moyennées par le flux et les sections efficaces des régions grossières. De là, ces paramètres doivent être mis à jour au bout de chaque pas de temps pour refléter toutes les variations possibles de sections efficaces dans le cœur. Plus le nombre de régions grossières est petit, moins ces calculs ne consomment de temps en comparaison de la méthode quasi - statique améliorée. Sur les pas de temps de mesure intermédiaire, la fonction de forme est intégrée sur des nœuds grossiers. Enfin, après beaucoup de calculs à maillage grossier, la fonction de forme du maillage de référence fin est recalculée en utilisant les équations sous leur forme multigroupe complète.

Un autre exemple de l'approche hiérarchique en temps peut être illustré par la définition d'uniquement deux niveaux en temps afin d'évaluer le flux de neutrons: un niveau fin et un niveau grossier. Pour la plus petite mesure en temps, les équations de diffusion multigroupe (mais pas les équations de forme) sont résolues sur des nœuds représentant les zones spatiales homogénéisées des nœuds fins. Après beaucoup ou peu de calculs grossiers (dépendant de la sévérité de la transitoire), les équations de diffusion multigroupe sont résolues sur le maillage fin. La solution de ce niveau fin est alors employée pour ré - homogénéiser les nœuds. Selon la nature de la transitoire, il peut même être possible d'introduire davantage de niveaux hiérarchiques en temps afin de calculer le flux neutronique.

La hiérarchie en espace

Dans le formalisme hiérarchique en espace, les solutions intermédiaires sont plutôt employées pour accélérer le taux de convergence du problème à maillage fin. Fondée

sur cette philosophie, une nouvelle procédure géométrique de type multigrille complète est proposée. Cette procédure repose sur une suite d'étapes:

1. La sélection géométrique des maillages grossiers: toute structure grossière peut être définie tant qu'elle peut être spatialement homogénéisée en utilisant la théorie d'équivalence nodale.
2. La procédure de restriction avant lissage: la théorie d'équivalence nodale résout exactement le problème d'homogénéisation lorsque suffisamment de solutions fines locales hétérogènes sont connues ou rapprochées dans chaque nœud. Les paramètres d'équivalence nodale obtenus par ces solutions fines locales rendent compte de toute hétérogénéité inhérente aux maillages grossiers. De là, le flux de diffusion aux nœuds grossiers peut être employé pour fournir les solutions locales approximatives aux nœuds fins. Conséquemment, la théorie d'équivalence nodale peut être employée comme un opérateur de restriction dans une méthode d'accélération multigrille pour toute méthode classique de relaxation.
3. La procédure de lissage: A cette étape, les équations de la cinétique spatio-temporelle pour les maillages grossiers sont définis et résolus. Plus le nombre de régions grossières est petit, plus le temps de calcul requis pour cette étape est négligeable. La solution du problème grossier représente presque exactement l'intégrale à chaque nœud grossier des taux moyens de réaction dans chaque groupe énergétique, ainsi que les intégrales des termes de courants à chaque groupe et sur toutes les surfaces de chaque nœud grossier pour la prochaine étape de temps. Les erreurs minimes dans les calculs à maillage grossier sont dues à l'emploi du flux de diffusion à l'étape actuelle de temps (plutôt que la valeur moyenne en temps) pour calculer les paramètres grossiers de région (sections efficaces, coefficients de diffusion et facteurs de discontinuité).
4. La procédure d'interpolation (après lissage): à cette étape, la solution doit être interpolée sur les nœuds fins. Le choix de l'opérateur d'interpolation

dépend fortement de la façon par laquelle la discrétisation en espace est réalisée. Par exemple dans certaines méthodes nodales, la méthode de reconstruction de la puissance de crayon (Koebke et Wagner, 1977; Koebke et Hetzelt, 1985) est un bon candidat. Le concept de fonction de forme employé dans cette méthode représente une correction fine sur le maillage et, de là, une composante de haute fréquence qui peut être amortie rapidement en utilisant une méthode itérative conventionnelle (Al-Chalabi et Turinsky, 1994).

Itération sur le maillage fin: Une fois que la procédure d'interpolation est complétée, le problème original de niveau fin peut être résolu en utilisant le flux interpolé comme approximation initiale. Les économies sur les itérations fines compensent habituellement le coût nécessaire pour obtenir la solution initiale pour le maillage fin . Un avantage de cette procédure multigrille réside dans le fait que même les techniques d'accélération de convergence supplémentaire peuvent être réalisées pour les itérations à maillage fin.

L'approximation des paramètres d'équivalence

Il est clair que le succès de cet algorithme dépend principalement de l'exactitude des calculs grossiers intermédiaires, laquelle exactitude dépend à son tour de la façon dont les paramètres d'équivalence sont estimés afin de refléter correctement les changements dans l'état du réacteur. Dans le but de diminuer le nombre nécessaire de calculs fins dans les calculs statiques et dynamiques, un traitement, employé couramment dans des procédures similaires, permet d'établir une base de données de paramètres d'équivalence pour chacun des mécanismes de réactivité. Quand plus d'un de ces mécanismes sont présents dans le coeur du réacteur, ces données cataloguées sont interpolées sur les diverses variables indépendantes et les paramètres approximatifs d'équivalence nodale. La cinétique hiérarchique nodale recommande plutôt l'emploi de

la distribution dynamique du flux de diffusion pour évaluer les facteurs dynamiques de discontinuité constants par morceaux.

Le développement du logiciel

Fondée sur cette nouvelle procédure de résolution, un nouveau logiciel informatique nommé NDF a été développé (Kaveh et al. 1998, 1999a, 1999b). Le logiciel NDF combine trois aspects majeurs: calculateur à maillage fin, à maillage grossier et modules de cinétique. Utilisant la procédure de contrôle de langage CLE-2000 (Roy, 2000), le logiciel NDF est capable de réaliser des calculs dynamiques et statiques de cœur basés sur les différentes variétés de cinétique hiérarchique nodale. Tous les coefficients de diffusion et de sections efficaces macroscopiques pour les cellules unitaires (de niveau fin) sont pré-calculés en utilisant le code de transport DRAGON (Marleau *et al.* 1996). De plus, en tirant parti d'une pleine représentation de tous les déplacements de mécanismes prévus dans le logiciel DONJON (Varin *et al.* 1996), l'ensemble des modules NDF est capable d'exécuter des calculs compliqués statiques et dynamiques lié au contrôle et aux dispositifs de sécurité dans un réacteur CANDU. Le logiciel NDF intègre essentiellement les modules suivants :

a) La module de niveau fin

Il a été prouvé que, parmi plusieurs méthodes disponibles, la méthode de différences finies centrées, laquelle représente l'ordre le plus bas de toute approximation nodale, est suffisamment précise pour l'étude des réacteurs CANDU avec une maillage de l'ordre d'une cellule unitaire (soit une grappe de combustible, son gainage et le modérateur l'entourant) (Koclas, 1998). Les approximations d'ordre supérieur de la méthode nodale produiraient seulement une amélioration marginale dans la distribution de flux. L'élimination des flux de surface en appliquant la continuité flux/courant à travers chaque interface conduit aux équations impliquant seulement les moyennes de flux aux nœuds. S'appuyant sur ces faits, une méthode de différences finies centrées est

appliquée pour produire le niveau fin ou la solution hétérogène d'un modèle d'un réacteur. Reproduire cette solution exacte à un coût informatique bas est la motivation ultime derrière la cinétique hiérarchique nodale.

b) La module de niveau grossier

La procédure d'homogénéisation du maillage grossier est exécutée dans le contexte des différences finies centrées à cause de sa nature simple qui est d'avoir seulement une inconnue par nœud et par groupe énergétique. De plus, les termes d'union ne sont pas dépendants des flux ou des courants et donc ne nécessite pas davantage d'itérations. Le module de niveau grossier consiste donc en deux sous-modules. Dans le premier sous-module, la solution de niveau fin obtenue est utilisée pour homogénéiser tous les nœuds basés sur la théorie d'équivalence nodale dans le contexte de la méthode des différences finies centrées. Le second sous-module résout les équations de cinétique spatio-temporelle des nœuds homogénéisés en appliquant l'algorithme modifié des différences finies.

c) La module de cinétique

La difficulté majeure, à cette étape, vient de la raideur («stiffness») des équations cinétiques du réacteur. Pour aborder ce problème, la méthode généralisée de Runge-Kutta (GRK4A) de la famille Kaps-Rentrop (Sánchez, 1989) a été choisie et appliquée. A cette étape, les sections efficaces et les flux dépendant du temps représentent les effets de perturbations du cœur du réacteur pendant la transitoire. Puisque la fonction de forme est supposée constante entre deux calculs de forme, les paramètres cinétiques ne sont pas exacts et il en résulte une certaine marge d'erreur introduite dans la solution.

d) La méthode d'intégration en temps

Afin de gérer la stabilité et la convergence de la solution dépendante du temps, le schéma de différences q-finies (Nakamura, 1977) est une des procédures les mieux établies. Donc, la mise en oeuvre complète de la méthode thêta sur les niveaux fins et sur les nœuds a été réalisée. Dans la version actuelle de NDF, les valeurs de thêta peuvent être différentes pour le flux et les précurseurs de neutrons retardés, et elles sont spatialement indépendantes.

Les résultats numériques

De nombreuses simulations (tant pour les calculs statiques que dynamiques) ont été conçues et exécutées afin de mieux comprendre les différents aspects de l'utilisation de la théorie généralisée d'équivalence, et ainsi d'évaluer correctement la performance de la cinétique hiérarchique nodale. Tous les cas d'essai ont été exécutés pour un modèle relativement réaliste d'un réacteur CANDU-6. Certaines conclusions importantes qui en découlent seront esquissées ici.

Les calculs statiques

1 Peu importe le nombre de maillages grossiers, en utilisant des valeurs exactes de paramètres d'équivalence, une reproduction très fidèle de la valeur propre fondamentale du réacteur ainsi que des flux moyens aux nœuds est réalisable. Cependant, les erreurs des flux nodaux synthétisés pour des cas à maillage grossier plus large sont plus grandes que celles obtenues sur des maillages légèrement moins grossiers. Ce comportement peut être attribué principalement aux erreurs inhérentes du calcul à point flottant.

2 Aucun modèle réutilisable pour la dépendance de paramètres d'équivalence (surtout des facteurs de discontinuité) envers les positions de mécanismes n'a pu être établi.

3 L'utilisation des paramètres d'équivalence de référence pour les barres de compensation et les autres dispositifs mécaniques de contrôle conduiraient à des erreurs significatives dans les calculs du flux grossier. Ces erreurs sont beaucoup plus petites pour les contrôleurs liquides car leurs sections efficaces d'absorption sont beaucoup plus petites que celles des barres.

4 Imposer la préservation des taux de réaction globaux (en utilisant seulement les sections efficaces pour des nœuds grossiers) peut considérablement réduire l'erreur moyenne dans les calculs de flux grossier. Tandis qu'exiger seulement l'exactitude des facteurs de discontinuité conduirait à une hausse considérable des erreurs dans les calculs de flux grossier. Ce n'est pas surprenant car utiliser des valeurs exactes de facteurs de discontinuité permet uniquement de conserver les courants grossiers de surface sans conserver réellement les taux globaux de réaction.

5 Il est clair que la contrainte due au nombre substantiel de mécanismes de réactivité, considérant toutes les positions possibles de ces mécanismes pour générer une base de données, ne serait pas pratique. De plus, puisque les valeurs de paramètres d'équivalence dépendent de la configuration grossière de la géométrie, il ne serait pas imaginable de créer une base de données pour toutes les configurations possibles de géométrie grossière. Une relation non-linéaire existe entre les paramètres d'équivalence et les distributions de flux, empêchant toute superposition ou interpolation simple des valeurs de la base de données de produire des estimations acceptables pour les valeurs des paramètres d'équivalence. De plus, les calculs de flux grossier sont très sensibles aux valeurs de paramètres d'équivalence, et des valeurs inexactes de paramètres d'équivalence (obtenues à partir de la base de données) pourraient engendrer des erreurs substantielles dans les calculs de flux.

6 La dépendance de paramètres d'équivalence sur la distribution de flux crée aussi des changements non négligeables dans les paramètres d'équivalence nécessaires au suivi de charge xénon. De là, l'emploi de paramètres constants d'équivalence

pendant une très longue transitoire telle que ceux qui impliquent des variations de la concentration en xénon pourrait détériorer la précision des résultats.

Les calculs dynamiques

Afin d'évaluer la performance de la cinétique hiérarchique nodale dans les simulations dynamiques, trois scénarios transitoires sont sélectionnés. Dans les deux premiers, la réponse du système de régulation du réacteur due à des perturbations substantielles est simulée. Le troisième scénario est une simulation simplifiée d'une perte de caloporteur.

1. Le premier scénario est la simulation d'une éjection hypothétique de barre. Les résultats obtenus en employant la cinétique hiérarchique nodale (dans l'approche quasi – statique étendue) procure une performance accrue de 85% à 150% sur la solution de référence tout en préservant l'exactitude de la solution. À première vue, le gain général est moindre que celui escompté. Cependant, il peut être démontré que ces différences sont principalement dues au temps de calcul nécessaire pour exécuter et transférer des données entre les différents modules.
2. Dans le deuxième scénario, la réponse du système de régulation du réacteur à une perturbation très substantielle est simulée. Cet essai peut être considéré comme relativement plus intense en comparaison du scénario #1. Le gain général en performance de temps obtenu en employant la cinétique hiérarchique nodale (dans l'approche quasi–statique étendue) est d'environ 98% à 125% par rapport à la solution de référence.
3. Dans le troisième scénario, un modèle simplifié d'une perte de caloporteur est développé. La première conclusion est que les approches quasi - statiques (classique ou étendue) ne sont pas efficaces pour ces types de transitoire. Leur déficience peut être attribuée à l'hypothèse d'une fonction de forme constante sur un certain temps. De là, les erreurs pour ces cas sont générées

pendant les calculs de cinétique ponctuelle et même la mise à jour fréquente des fonctions de forme fines ou grossières ne conduit pas à une amélioration notable de la solution finale. Ainsi, on prévoit que l'emploi de deux niveaux de calcul de flux serait beaucoup plus efficace pour cette analyse de perte de caloporteur. Dans l'analyse détaillée des résultats, l'exactitude de cette approche à deux niveaux dépend fortement du volume des mailles grossières et il est conclu qu'un nombre minimum de mailles grossières est nécessaire pour garantir son emploi. La contribution considérable des erreurs liées à l'emploi de grilles plus grossières est générée pendant la procédure de reconstruction. Traiter cet effet en définissant une plus petite représentation grossière du réacteur est la solution la plus simple à ce problème. Une conclusion très importante soutenue par de nombreux essais est que l'emploi d'une tabulation des facteurs de discontinuité statique résulterait en erreur considérable pour les calculs de flux. Il a été prouvé que l'approche de la cinétique hiérarchique nodale, qui est d'utiliser des facteurs dynamiques de discontinuité constants par morceaux, est supérieure à l'emploi de facteurs de discontinuité statique interpolés (au moins pour les réacteurs de type CANDU). Autrement dit, utiliser des arrêts sur image du flux dynamique représentant l'état réel du réacteur s'avère un choix intrinsèque pour calculer des facteurs de discontinuité sans décalage par rapport aux distributions de flux statiques.

Dans la dernière partie, la performance du formalisme hiérarchique en espace, qui est une approche multigrille, est évaluée. Il est trouvé que, pour les cas avec un petit nombre de maillages fins, la méthode n'amènerait pas d'économie significative du temps de calcul. Cependant, quand le nombre de nœuds nécessaires augmente, la méthode devient rapidement plus efficace. Dans une analyse de perte de caloporteur, il est montré que le nombre nécessaire d'itérations pour un critère donné de convergence peut

être réduit par un facteur d'au moins 50%, conduisant à une économie substantielle du temps de calcul.

TABLE OF CONTENTS

LIST OF FIGURES

LIST OF TABLES

LIST OF APPENDICES

LIST OF SYMBOLS

$B_{gu\pm}^{i,j,k}$	Coefficient, coarse-mesh finite difference, u-direction ($u = x, y, z$) ..... [--]
$E_{gu\pm}^{i,j,k}$	Coefficient, coarse-mesh finite difference modified by discontinuity factors, u-direction ($u = x, y, z$) ..... [--]
C_n	Delayed neutron precursor concentration (nth group) ..... [cm^{-3}]
dSIGT1	Change in fast-group absorption cross section ..... [%]
dSIGT2	Change in thermal-group absorption cross section ..... [%]
dFU1±	Change in fast-group discontinuity factor (U-direction, U=X,Y,Z) ..... [%]
dFU2±	Change in thermal-group discontinuity factor (U-direction, U=X,Y,Z) ..... [%]
dSIGF1	Change in fast-group fission cross section ..... [%]
dSIGF2	Change in thermal-group fission cross section ..... [%]
dSCg →g'	Change in scattering cross section ..... [%]
D	Number of delayed neutron precursor groups ..... [--]
$e_g^{i,j,k}$	Relative nodal group flux error ..... [--]
$e_{\max}^{i,j,k}$	Maximum nodal group flux error ..... [--]
$\bar{e}$	Average total nodal group flux error ..... [--]
$e^{\omega h}$	Error in smoothing ..... [--]
$f_{gu}^{\pm}$	Discontinuity factors, group g, u-direction (x, y, and z) ..... [--]
G	Number of energy groups ..... [--]
$I_h^{\omega h}$	Restriction operator ..... [--]
$I_{\omega h}^{h}$	Interpolation operator ..... [--]
r^h	Defect ..... [--]
PHI1	Fast-group neutron flux ..... [$cm^{-2}.s^{-1}$]
PHI2	Thermal-group neutron flux ..... [$cm^{-2}.s^{-1}$]
R	Partially empty supernode ..... [--]

R_f	Fine mesh inside the reactor core	[--]
R_e	Empty fine nodes inside a partially empty supernode	[--]
t	time	[s]
$T(t)$	Amplitude function	[--]
$V^{i,j,k}$	Fine mesh volume	[cm^3]
$V^{I,J,K}$	Coarse mesh volume	[cm^3]

β	Total delayed neutron fraction	[--]
β_n	Fraction of all fission neutrons appearing from nth precursor group	[--]
$\beta_n(t)$	Delayed neutron fraction from nth precursor group (point kinetics)	[--]
$\overline{\beta}(t)$	Effective delayed neutron fraction (point kinetics)	[--]
ε	Weighting parameter for correction terms	[--]
λ_n	Decay constant of nth precursor group	[--]
$\Lambda(t)$	Mean neutron generation time	[s]
$\rho(t)$	Dynamic reactivity	[mk]
θ	Weighting coefficient (θ-method)	[--]
ω	Dynamic frequency	[s^{-1}]
ω	Mesh order (greater than unity)	[--]
χ_g^p	Group prompt energy spectrum	[--]

$$[D]=\begin{pmatrix} D_1 & 0 & . & . \\ 0 & D_2 & . & . \\ . & . & . & . \\ 0 & . & . & D_G \end{pmatrix}$$ Diagonal matrix of diffusion coefficients ..... $[cm]$

$$[H]=\begin{bmatrix} H_{11} & H_{12} \\ H_{21} & H_{22} \end{bmatrix}$$ Coefficient matrix ..... [--]

$$\left[\bar{J}\right]=\begin{pmatrix} \bar{J}_1 \\ \bar{J}_2 \\ . \\ \bar{J}_G \end{pmatrix}$$ Column vector of currents ..... $[cm^{-2}.s^{-1}]$

$$[S]=\begin{pmatrix} S_1 \\ S_2 \\ . \\ S_G \end{pmatrix}$$ Column vector of shape function ..... $[cm^{-2}.s^{-1}]$

$$[\mathrm{v}]=\begin{pmatrix} \mathrm{v}_1 & 0 & . & . \\ 0 & \mathrm{v}_2 & . & . \\ . & . & . & . \\ 0 & . & . & \mathrm{v}_G \end{pmatrix}$$

Diagonal matrix of velocities ..... $[cm.s^{-1}]$

$$[W]=\begin{pmatrix} W_1 \\ W_2 \\ . \\ W_G \end{pmatrix}$$ Column vector of weight function ..... [--]

$$[\Phi]=\begin{pmatrix} \Phi_1 \\ \Phi_2 \\ . \\ \Phi_G \end{pmatrix}$$ Column vector of fluxes ..... $[cm^{-2}.s^{-1}]$

$$[\Sigma] = \begin{pmatrix} \Sigma_{t1} - \Sigma_{s1\leftarrow 1} & -\Sigma_{s1\leftarrow 2} & \cdot & -\Sigma_{s1\leftarrow G} \\ -\Sigma_{s2\leftarrow 1} & \Sigma_{t2} - \Sigma_{s2\leftarrow 2} & \cdot & -\Sigma_{s2\leftarrow G} \\ \cdot & \cdot & \cdot & \cdot \\ -\Sigma_{sG\leftarrow 1} & -\Sigma_{sG\leftarrow 2} & \cdot & \Sigma_{tG} - \Sigma_{sG\leftarrow G} \end{pmatrix}$$

Square matrix of cross sections ..... $[cm^{-1}]$

$$[\nu\Sigma_f] = \begin{pmatrix} \nu\Sigma_{f1} \\ \nu\Sigma_{f2} \\ \cdot \\ \nu\Sigma_{fG} \end{pmatrix}$$

Column vector of ν times the fission cross section... $[cm^{-1}]$

$$[\chi^p] = \begin{pmatrix} \chi_1^p \\ \chi_2^p \\ \cdot \\ \chi_G^p \end{pmatrix}$$

Column vector of prompt energy spectrum ..... [--]

$$[\chi_n^d] = \begin{pmatrix} \chi_{n1}^d \\ \chi_{n2}^d \\ \cdot \\ \chi_{nG}^d \end{pmatrix}$$

Column vector of delayed neutron spectra ..... [--]

LIST OF ABBREVIATIONS

AB ..... Adjuster Bank

DF ..... Discontinuity Factors

ET ..... Equivalence Theory

GET ..... Generalized Equivalence Theory

HNK ..... Hierarchical Nodal Kinetics

IQS ..... Improved Quasi-Static

LOCA ..... Loss Of Coolant Accident

LZC ..... Liquid Zone Controller

MCAB ..... Mechanical Control Absorber Banc

NET ..... Nodal Equivalence Theory

RRS ..... Reactor Regulating System

INTRODUCTION

The accurate calculation of the power produced throughout a nuclear reactor core during transient operation is essential to both the design and the safe operation of the reactor. These transients cover a wide range of events from core fuel depletion to catastrophic accident excursions. Adequate physical and mathematical models have been developed to describe the time-dependent neutronic and thermal-hydraulic behavior of a reactor. In thermal-hydraulics models, the physical model is expressed by a set of sophisticated coupled partial differential equations. In neutronics, due to the presence of distribution functions, the physical parameters are rather governed by the integro-differential equations. Numerous sophisticated numerical methods have been developed to solve this set of integro-differential equations, the so-called transport equations. However, these methods are normally very expensive from the point of view of the computational resources required. Hence, the extension of these methods to the time-dependent problems, which often need thousands of calculations, is practically unmanageable. Therefore, further approximations are necessary to reduce the complexity of the transport equations. The most common way to reduce the complexity of the transport equations is the diffusion approximation. The direct mathematical result of this approximation is to alter the transport equations from the integro-differential equations to a set of elliptic-parabolic-type partial differential equations known as diffusion equations. It is proved that the diffusion equations, in many instances, adequately describe the neutronic behavior of the reactor core. Nonetheless, despite the substantial increase in both speed and memory of the computer hardware in recent years, the numerical solution of these resulting diffusion equations is still far from being practical for regular calculations. The considerable cost of the calculations is normally due to the three-dimensional nature of the flux distribution through a large and often geometrically complicated core. For example, for a CANDU reactor, a typical transient calculation requires about 10000 mesh points, making the corresponding transient calculations very time consuming.

Based on these facts, the main objective of the present work is to develop a new solution algorithm called hierarchical nodal kinetics, whose goal is to reduce the computing costs of the time-dependent calculations without introducing unacceptable inaccuracies in the solution. The second objective of the present work is to assess the performance of the resulting numerical scheme using a relatively realistic model of a CANDU-6 reactor.

The proposed solution method is presently restricted to the diffusion equations since it is unlikely that the dynamic behavior of the reactor, in the foreseeable future, will receive a more rigorous treatment than that represented by time-dependent diffusion equations. It is thus assumed that all diffusion parameters are rigorously pre-calculated using a transport-to-diffusion homogenization procedure.

The organization of this thesis is outlined here:

- Chapter one briefly reviews the various methods developed for treating both the spatial and temporal variables of the time-dependent diffusion equations.
- Chapter two consists of three parts. In the first part, a brief description of nodal equivalence theory will be presented. In the second one, the methodology of hierarchical nodal kinetics will be thoroughly discussed. Finally, in the last section, the implementation of hierarchical nodal kinetics in the computer code NDF will be described.
- Chapter three essentially deals with different aspects of applying nodal equivalence theory for the steady-state calculations of a typical CANDU-6 reactor. Emphasis will be on the practical aspects such as the effect of the number of coarse nodes in the precision of the coarse-level calculations, the sensitivity of the equivalence parameters to the reactivity-device positions and the error in the flux calculations due to the use of a set of reference equivalence parameters.

- Chapter four presents the numerical results obtained from the use of hierarchical nodal kinetics for the transient simulations of a CANDU-6 reactor. The results are then compared to those obtained from the direct and improved quasi-static methods emphasizing both the precision of the results and the speed of calculations. Three transient scenarios are selected. In the first two the response of the reactor regulating system to the substantial perturbations are simulated. The third scenario is a simulation of a LOCA (Loss of Coolant Accident).
- Chapter five gives the conclusions and recommendations for future work.

CHAPTER 1

REVIEW OF REACTOR KINETICS

This chapter provides a summary of the various methods available for treating both spatial and temporal variables of the space-time kinetics equations in the multigroup diffusion approximation. Furthermore, an outline of some of the numerical procedures used to solve the resulting algebraic equations will be presented.

1.1 Governing Equations

It is well established that few-group neutron diffusion theory is a sufficiently accurate model for dynamic behavior of a nuclear reactor core. Limitations of this theory are well documented in the literature (Henry, 1975). The space-time kinetics equations (also known as time-dependent diffusion equations) are represented by (Koclas, 1996):

$$[v]^{-1}\frac{\partial}{\partial t}[\Phi] = -\bar{\nabla}\cdot[\bar{J}] - [\Sigma]\cdot[\Phi] + (1-\beta)[\chi^p][\nu\Sigma_f]^T[\Phi] + \sum_{n=1}^{D}[\chi_n^d]\lambda_n C_n \qquad (1.1)$$

$$[\bar{J}] = -D\bar{\nabla}[\Phi] \qquad (1.2)$$

$$\frac{\partial C_n}{\partial t} = \beta_n[\nu\Sigma_f]^T - \lambda_n C_n \qquad (1.3)$$

where the notation is standard. The parabolic equation (1.1) in conjunction with appropriate initial and boundary conditions form a well-defined mathematical problem to be solved. Since it is impossible to find an analytic solution for these three-dimensional equations, numerical procedures are necessary for treating both the spatial and temporal variables.

1.2 Numerical Methods

The numerical solution methods can be divided into three major categories: direct methods, space-time factorization procedures and synthesis methods. The direct

methods are characterized by a straightforward discretization of the spatial or temporal variables to form a set of coupled algebraic equations. The space-time factorization methods involve a factorization of group fluxes into two parts: first the amplitude function that is only time-dependent and second the shape function, which is time-, and weakly space-dependent. Finally, synthesis methods use a linear combination of predetermined time-dependent spatial distributions to approximate the group fluxes.

1.2.1 Direct Spatial Methods

The starting point for all practical spatial methods is the superposition of a grid or mesh structure on the region of the solution. Based on the particular discretization method employed, the unknown flux values may be defined either as constant values at the corners of the mesh boxes or as averages over the entire mesh boxes. Using the average flux values may also introduce further unknowns such as partial currents, or the components of the net current at the interfaces between the grids. The direct spatial methods can be classified into three groups: finite difference methods, coarse-mesh methods, and nodal methods

1.2.1.1 Finite-Difference Methods

These methods are extensions of the well-known procedures for solving the static diffusion equations to time-dependent cases. The first step is partitioning of the reactor core into a number of contiguous rectangular parallelepipeds. The difference equations (balance equations) for group flux and precursor concentrations are then obtained by integrating equations (1.1) through (1.3) over volume elements surrounding each point. Applying low-order-difference approximations (Taylor series expansions) of the flux and precursors within each small volume and the imposition of the average flux and current continuity at the boundaries results in a set of coupled algebraic equations. For all grids lying on the external boundary of the region of solution, the external boundary conditions are used instead of continuity conditions. Depending on where the unknowns

are defined, two varieties of finite difference can be defined. In the mesh-corner approach, all the unknowns are defined at the corners of the mesh boxes; while in the mesh-centered finite difference (also known as coarse-mesh finite difference) the unknowns are rather defined as the average of unknowns at the centers of the grids. Using the 7-point approximation, both approaches will result in a set of spatially discretized equations in the following form (Nakamura, 1977; Adams, 1977; Koclas, 1998):

$$\begin{aligned}\frac{V^{i,j,k}}{v_g}\frac{\partial}{\partial t}\Phi_g^{i,j,k}(t) = {} & B_{gx+}^{i,j,k}(t)\Phi_g^{i+1,j,k}(t)+B_{gx-}^{i,j,k}(t)\Phi_g^{i-1,j,k}(t)+B_{gy+}^{i,j,k}(t)\Phi_g^{i,j+1,k}(t)+\\ & B_{gy-}^{i,j,k}(t)\Phi_g^{i,j-1,k}(t)+B_{gz+}^{i,j,k}(t)\Phi_g^{i,j,k+1}(t)+B_{gz-}^{i,j,k}(t)\Phi_g^{i,j,k-1}(t)-\\ & [B_{gx+}^{i,j,k}(t)+B_{gx-}^{i,j,k}(t)+B_{gy+}^{i,j,k}(t)+B_{gy-}^{i,j,k}(t)+B_{gz+}^{i,j,k}(t)+\\ & B_{gz-}^{i,j,k}(t)+V^{i,j,k}\Sigma_{tg}^{i,j,k}]\Phi_g^{i,j,k}(t)+V^{i,j,k}\sum_{g'=1}^{G}\Sigma_{sgg'}^{i,j,k}\Phi_g^{i,j,k}(t)\\ & +V^{i,j,k}\chi_g^p(1-\beta)\sum_{g'=1}^{G}\nu\Sigma_{fg'}^{i,j,k}\Phi_{g'}^{i,j,k}(t)+V^{i,j,k}\sum_{n=1}^{D}\chi_{ng}^d\lambda_n C_n^{i,j,k}(t)\end{aligned} \tag{1.4}$$

where $B_{gu\mp}^{i,j,k}(t)$ are time-dependent coupling coefficients in the u-direction ($u = x$, y, or z). The associated precursor concentrations are expressed by:

$$\frac{d}{dt}C_n^{i,j,k}(t) = -\lambda_n C_n^{i,j,k}(t)+\beta_n\sum_{g'=1}^{G}\nu\Sigma_{fg'}^{i,j,k}\Phi_{g'}^{i,j,k}(t) \tag{1.5}$$

The nuclear properties (macroscopic cross sections and diffusion coefficients) are assumed to be spatially constant over each mesh box. Finite-difference methods possess several advantages over other schemes. These methods are conceptually simple and the resulting algebraic equations are such that only adjacent nodes are coupled by spatial leakage. This coupling pattern makes finite-difference methods very efficient for numerical treatment and consequently results in shorter computation time per unknown. Moreover, efficient solution of the resulting stiff coupled first-order temporal equations is possible using numerous available numerical methods. Another important property of the finite-difference technique is that it can be shown to converge to the exact solution

of space-time kinetics equations as both spatial and temporal mesh spacings become increasingly small. This means that the spatial errors will vanish in the fine-mesh limit and, as a result, exact detailed flux and reaction-rate distributions will be obtained from such a solution.

Abu-Shumays and Hageman (1975) have derived a number of higher-order finite-difference equations for regular mesh arrays, but at a cost of a more complicated coupling. They also have derived finite-difference equations for an arbitrary quadrilateral mesh where the mesh lines are parallel. Considering the number of the published research works as a criterion, it seems that these higher-order finite-difference methods have not been widely employed for the purpose of reactor kinetics.

1.2.1.2 Coarse-Mesh Methods

One of the disadvantages of finite-difference schemes is that mesh spacing must be on the order of the smallest group-wise diffusion length to maintain the accuracy of the resulting solution (Adams, 1977, Sutton and Aviles, 1996). This condition results in a very large number of unknowns (particularly for LWR reactors), which means huge execution times to achieve an acceptable degree of accuracy in the flux solution. To deal with this problem, different coarse-mesh methods have been developed by several groups. These methods achieve an acceptable degree of accuracy using higher-order approximations of the spatial variation of the unknowns within grids much larger than those necessary for finite-difference techniques. The flux-expansion method (Langenbuch, *et al.*, 1977a and 1977b) is one of the most well-known coarse-mesh methods. The flux expansion method solves the space-time kinetics equations using an asymmetric weighted residual method with polynomial basic functions defined for each *coarse* mesh box. In this method, the flux shape is approximated in terms of basic functions and the flux values at seven supporting points (center point of the box and center points of each of six sides of the mesh box). The resulting matrix equation has a

structure similar to those obtained from the finite-difference technique, thus any numerical scheme developed for the finite-difference method can be used for its solution.

Another well-known coarse-mesh method is the finite element method (Kang and Hansen, 1973; Nakamura, 1977). In this method, the group flux is approximated as a sum of multi-dimensional polynomials. These polynomials are zero everywhere outside of the finite volumes of the corresponding mesh boxes. Finite-element methods require more unknowns per mesh point than finite-difference methods, hence, the coupling coefficients are much more complicated than those of finite-difference methods. However, finite-element methods in general are more accurate than finite-difference methods. Finite-element methods also converge to the exact solution of the space-time kinetics equations as the mesh spacing becomes increasingly small. Another advantage of the finite-element method is that it is not limited to regular mesh. Hence the number of mesh points can be increased in the regions where more precision is required.

1.2.1.3 Nodal Methods

All nodal methods consist of three major steps:

- First, dividing the reactor volume into relatively large, non–overlapping nodes,
- second, integrating the time-dependent diffusion equations over each node resulting in nodal equations with nodal average fluxes and surface average currents as the unknowns,
- third, defining additional relationships between surface average currents and the node-averaged fluxes to close the set of nodal equations.

In the early nodal methods, (Wachspress *et al.*, 1962) different sorts of coupling parameters were used to define these additional relationships. These coupling parameters were normally calculated for a set of reference situations using a fine

solution method such as the finite-difference method. These constant parameters were then used to eliminate the partial currents during reactor power transients. Evidently, these coupling parameters are not accurate for situations different from the reference configurations.

In the modern nodal methods (called transverse integrated nodal methods), the relationships between the surface average currents and the node average fluxes are obtained using the transverse integration procedure. This procedure consists of integrating the space–time kinetics equations over two-dimensional cross sections of the node in the plane perpendicular to each of the Cartesian directions. This procedure will result in three sets of one-dimensional equations for transverse leakage terms. It is the solution of these one-dimensional equations that provides the relationships between the node-averaged fluxes and the interface-averaged net or partial currents. However, in practice, solving these one-dimensional equations requires that the dependence of the net transverse leakage on the spatial variables as well as temporal variable be known, which is practically impossible. To deal with this problem, numerous approximation methods have been developed. One of the most popular approximations for time derivative terms is the exponential transform (Shober *et al.*, 1977). For the spatial variation of the transverse leakage, two categories of the approximation procedure have been developed: polynomial procedures and analytic methods. In the polynomial methods (usually called nodal expansion methods), by approximating the transverse integrated flux with the help of a truncated polynomial expansion, the transverse integrated equations are solved. While in the analytic nodal methods, the analytic solution of the one-dimensional neutron diffusion equation is used to solve the transverse-integrated equations. Despite the superior computational accuracy of the analytic nodal methods, the nodal expansion methods have been more often employed in light water reactor kinetics codes. This is primarily because of the superior computer efficiency of the nodal expansion methods. A thorough review of various available

variations of these approximation methods has been carried out by Lawrence (1985) and Sutton and Aviles (1996).

Once the approximations for the time derivative and transverse leakage terms have been specified, the one-dimensional transverse equations are solved to obtain the relationships between the node-average fluxes and the interface-average currents. Consequently, nodal equations with a structure similar to finite-difference equations can be constructed and solved.

One of the essential differences between coarse-mesh and nodal methods is that the calculation of the multi-dimensional intra-nodal flux distribution is not a part of the solution procedures in the nodal methods. Therefore, the nodal methods lead to algebraic systems that are sparse and well-structured, like finite-difference methods. Furthermore, efficient reconstruction methods have been developed that allow determination of the detailed flux distribution within a node from the nodal method solution (for example: Koebke and Wagner, 1977; Koebke and Hetzelt, 1985).
Recently, Koclas (1998) proved that in the analytic nodal method, applying approximations such as zero transverse leakage and truncation of the matrix exponentials leads to the mesh-centered finite difference approximation. He thus concluded that the standard mesh-centered finite difference is actually the lowest order of all nodal methods.

1.2.2 Space-Time Factorization Methods

Space-time factorization methods are based on the direct factorization of the neutron flux into a time-dependent amplitude function describing the time behavior of the overall neutron flux level and a space- and time-dependent shape function describing the local adjustment of the neutron flux distribution. The main idea of this factorization is that the shape function in many situations is weakly time dependent, thus it can be

considered to be constant for relatively large time steps. Hence, the behavior of the reactor during these large time steps can be adequately described by the amplitude function. The space-time factorization methods can be categorized based on the type of approximation used to re-evaluate the shape function after each of these large time steps. In the point kinetics model (Henry, 1958), the shape function is considered to be constant for all $t \geq 0$ and therefore the dynamic behavior of the reactor is merely described by the point kinetics model. The adiabatic method (Henry and Curlee, 1958) considers that the time retardation in the shape of the neutron precursor distribution may be ignored so that the neutron flux immediately reaches its equilibrium, thus the shape functions are the solution of the static diffusion equations at various times during a transient. The quasi-static method (Ott, 1966) takes into account only the source of delayed neutrons while in the improved quasi-static method (Ott and Meneley 1969) all terms obtained from the factorization procedure are taken into account. The generalized quasi-static method (Devooght and Mund 1980) introduces energy-dependent amplitude functions. This method is mathematically preferable to the improved quasi-static method, however the gain in the accuracy of the solution is not significant in comparison to those obtained from the improved quasi-static method (Monier, 1991; Koclas *et al.*, 1997). In modern reactor kinetics, due to the type of approximations employed in the factorization methods, the use of any factorization method except the improved or generalized quasi-static procedure for real reactor simulations cannot be justified. Recently, Kaveh *et al.* (1999) concluded that for realistic CANDU-6 transient calculations which involves all reactivity devices and the reactor regulating system, a well-optimized direct method is superior to the improved quasi-static method in both the speed of calculations and precision of the results.

1.2.3 Modal and Synthesis Methods

In the family of synthesis methods (modal expansion, space-time synthesis, etc.), the flux is approximated by an expansion in terms of pre-computed functions (Stacey,

1969). In the synthesis method, the expansion functions are generally obtained by solving the static problem for different conditions that are expected during the transient (for example the core conditions related to beginning and end of the transient). A weighted residual procedure is then employed to obtain the expressions for the expansion coefficients. These methods offer the largest reduction in the number of spatial unknowns. The major drawback of the synthesis methods is that there is no clear procedure for choosing the expansion functions and it mostly depends on the experience of the user. In the modal methods, the expansion functions are rather the eigenfunctions of the diffusion equations. The lack of a rigorous way to estimate the amount of error produced in the solution is a serious limitation of these methods.

1.3 Time Integration Methods

Once the spatial discretization is completed, the space-time kinetics problem reduces to an initial value problem expressed by a set of ordinary differential equations, as follows:

$$\frac{d}{dt}[\Psi] = [H][\Psi] \tag{1.6}$$

where

$$[\Psi] = \begin{bmatrix} \Phi \\ C \end{bmatrix}, \quad [H] = \begin{bmatrix} H_{11} & H_{12} \\ H_{21} & H_{22} \end{bmatrix} \tag{1.7}$$

the initial conditions are given by:

$$[\Psi_0] = \begin{bmatrix} \Phi \\ C \end{bmatrix}_{t=0} \tag{1.8}$$

The time constants involved in this system differ very widely, resulting in a *stiff* problem. Numerous numerical methods are available to deal with this stiff problem. Among them are the finite-difference (θ-method), alternating-direction implicit procedure, stiffness confinement method, and the family of Runge-Kutta methods, which are the most widely used.

1.3.1 θ-method

The θ-method is an efficient and accurate method, which has been successfully applied to the time reactor kinetics problems (Nakamura, 1977):

$$[\Psi]^{n+1} - [\Psi]^n = \Delta t[\Theta][H]^{n+1}[\Psi]^{n+1} + \Delta t[H]^n (I - [\Theta])[\Psi]^n \tag{1.9}$$

where the matrix $[\Theta] = [\theta_{ij}]$ is a weighting operator and $0 \le \theta_{ij} \le 1$. It can be observed that setting all θ_{ij} equal to 1, 0.5, and 0, result in the fully implicit, Crank-Nicholson, and fully explicit schemes respectively. The most important advantage of this method is that its stability and accuracy are well known.

1.3.2 Alternating Direction Implicit Method

The procedure of the alternating-direction methods consists of first breaking the unknown coefficient matrix of equation (1.6) into three one-dimensional operators and one direction-independent term (Nakamura, 1977; Werner, 1977; and Langenbuch, *et al.*, 1977a):

$$[H] = [H_x] + [H_y] + [H_z] + [\Pi] \tag{1.10}$$

and then solving resulting simplified equations one at a time. The time step from n to $n+1$ is performed in three steps: the first step treats the x-direction implicitly and the y- and z- directions explicitly. The directions are then permuted in the second and third steps. The advantage of this method is that the structure of the matrix to be inverted in each smaller time step, i.e. $[H_u]$, is simpler and consequently less time consuming. Each of these steps is only conditionally stable; therefore, a careful choice of time steps is necessary to guarantee stability of the scheme. The major disadvantage of this method is that the convergence of the method is not generally proven. However, its convergence rate is one of the fastest among the time integration schemes.

1.3.3 Family of Runge-Kutta Methods

The Runge-Kutta methods have been very popular for solving normal and stiff linear ordinary differential equations. The principal reasons for their success are, first, high accuracy and, second, proven stability. In reactor kinetics, the Kaps Rentrop Generalized Runge-Kutta method (GRK), which belongs to the family of Rosenbrock-Wanner methods, has been more popular than the others. This method is an implicit Runge-Kutta method, originally developed by Kaps and Rentrop (1977). A thorough description of the method is carried out by Press *et al.* (1992). To solve initial value problem given by equation (1.6), this method suggests a solution in the following form:

$$[\Psi]^{n+1} = [\Psi]^{n} + \sum_{a=1}^{s} A_i [\xi_i]^{n+1} \tag{1.11}$$

where s is the number of stages, A_i is a set of fixed expansion constants, and $[\xi_i]^{n+1}$ is the vector of unknown expansion coefficients. Sánchez (1989) used this method to solve point-kinetics equations based on automatic time-step control and later, Aviles (1993) successfully adopted this method to carry out realistic three-dimensional space-time kinetics calculations, where the coefficient matrix $[H]$ changes due to control-rod motion and thermal hydraulic feedback. Koclas *et al.* (1997) utilized this method to compare the performance of multigroup improved and generalized quasi-static methods for different numbers of energy groups.

1.3.4 Stiffness Confinement Method

To confine the stiffness of the system (1.6), Chao *et al.* (1985, 1989) have developed a special procedure. They introduce space- and time- dependent dynamic frequencies as follows:

$$\frac{\partial}{\partial t}\Phi_g(\bar{r},t) \equiv \omega_g^{\Phi}(\bar{r},t)\Phi_g(\bar{r},t) \tag{1.12}$$

and

$$\frac{\partial}{\partial t} C_d(\bar{r},t) \equiv \omega^d(\bar{r},t) C_d(\bar{r},t) \tag{1.13}$$

Applying these definitions to space-time kinetics equations (1.1) through (1.3), and eliminating space- and time-dependent delayed-neutron precursors would result in equations similar to the static diffusion equations with modified group constants. The resulting equation is an eigenvalue problem, hence it must converge to unity. The dynamic frequencies are introduced as additional unknowns that must be approximated (for example using a first-order estimate) and iterated upon. During the iteration procedure, the spatial distribution of the dynamic frequencies is updated by the eigenvector changes while the deviation of the eigenvalue from unity is taken into account by a set of group-dependent constant correction terms applied to the dynamic frequencies. The advantage of this method is that numerous available static diffusion codes can be slightly modified to perform dynamic calculations using the stiffness confinement method.

1.4 Spatial Homogenization Methods in Reactor Kinetics

It has been assumed that the reactor volume can be divided into relatively large, non–overlapping homogeneous nodes. These nodes are either truly homogeneous from a physical point of view or they are forced to be homogeneous by using node-averaged, flux-weighted values of cross sections and diffusion coefficients. Due to the inherent heterogeneity in the reactor core, the first assumption is not realistic and the second one could lead to substantial errors in the flux calculations. Therefore, the answer to the following question is of a major importance:

"How can equivalent diffusion parameters be defined or approximated for all regions of the reactor such that applying them results in a minimum error in the transient flux calculations?"

The answer to this question is fundamentally similar to the solution of the transport-to-diffusion homogenization problem (also known as assembly or cell homogenization problem), that is defining the assembly-equivalent diffusion parameters permitting to reproduce the assembly-transport calculations (Henry, 1975; Smith, 1986). This similarity would permit advanced assembly-homogenization techniques to be adapted for transient reactor calculations. Among these techniques, Nodal Equivalence Theory (NET) is the most well suited procedure for the time-dependent reactor calculations. Two varieties of nodal equivalence theory have been developed: equivalence theory (ET) (Koebke, 1978), and generalized equivalence theory (GET) (Smith, 1980). A detailed description of the NET in a time-dependent formulation will be presented in chapter 2.

1.5 Non-Linear Nodal Methods in Reactor Kinetics

The nonlinear iteration procedure is a direct result of the use of the advanced spatial homogenization technique (NET) in reactor kinetics. This method was originally proposed by Smith (1984) in order to improve the efficiency of the traditional nodal methods (Lawrence, 1986). In this approach, the nodal equations are only solved for the *two-node problems*, which contain two adjacent nodes with common interfaces. The global solution procedure is subsequently defined based on the coarse-mesh finite-difference method. The coupling coefficients for the finite-difference model are obtained from the condition that the finite-difference model reproduce the same interface-averaged current as the nodal method. Therefore, the solution procedure consists of two parts: the local solution of the nodal equations for two-node problems, and the outer iterations for solving the global finite difference model of the reactor. This procedure results in an essential reduction in computer memory requirements since there is no need to save the neutron flux expansion coefficients (Smith, 1984). Moreover, employing efficient iterative methods developed for the finite-difference procedure leads to a significant reduction in the overall computing cost of the transient

simulation. Another significant advantage of this method is inherent decoupling between the two-node portion and the global finite-difference portions of the algorithm, that makes it very suitable for parallel or multiprocessor computers (Joo and Downar, 1996). This procedure has been widely used in many modern light-water-reactor kinetics codes using different varieties of nodal methods (for example: Al-Chalabi *et al.*, 1993; Aviles, 1993; Al-Chalabi and Turinsky, 1994; Zimin and Ninokata, 1997a; Zimin and Ninokata, 1997b).

1.6 Iterative Solution Methods

Once space and time discretization of the equations (1.1) through (1.3) is completed, a linear system of the following form will be obtained:

$$[A][\Psi]=[B], \qquad [\Psi]=\begin{bmatrix}\Phi\\ C\end{bmatrix} \tag{1.14}$$

Both stationary and non-stationary iterative methods have been used to solve these equations. Stationary methods such as Successive Over-Relaxation (SOR) and Red-Black Line SOR are older, but simpler to implement (Nakamura, 1977; Axelsson, 1994). They are accurate and efficient and can be combined with many acceleration techniques such as coarse-mesh rebalancing method (Nakamura, 1977; Al-Chalabi *et al.*, 1993). The only major drawback for SOR-type methods is that these methods are not particularly efficient in modern parallel computers (Zee *et al.*, 1989). The non-stationary methods differ from stationary methods in that the computations involve information, which changes at each iteration. Many varieties of the non-stationary methods have been successfully employed in reactor kinetics. Among them the family of Chebyshev iteration techniques (such as Cyclic Chebyshev Semi-Iterative and Semi-Analytic Methods) have been more popular than the others (Nakamura, 1977; Zimin and Ninokata, 1996). However, these methods, like SOR-type techniques cannot achieve good parallel efficiency. Recently, Krylov subspace methods and

preconditioning schemes have been employed in reactor kinetics problems (Yang *et al.*, 1993). They concluded that Krylov subspace methods have better performance in parallel computers. It is also expected that due to the substantial increase in the memory and speed of computers, the implementation of the direct matrix solution methods based on sparse-matrix techniques will become more popular in the near future (Sutton and Aviles, 1996).

CHAPTER 2

HIERARCHICAL NODAL KINETICS

The basis of the Hierarchical Nodal Kinetics (HNK) method is the use of nodal equivalence theory as the homogenization procedure. In this chapter, first a brief description of nodal equivalence theory will be presented. In the second part, the theoretical basis of hierarchical nodal kinetics will be discussed. Finally, in the last section, the implementation of HNK in the computer code NDF will be described.

2.1 Time-Dependent Nodal Equivalence Theory

Nodal equivalence theory (NET) (Koebke, 1978; Smith, 1980) is an homogenization procedure which is well-suited for reactor kinetics calculations. This method has been successfully implemented for most types of light-water reactors (Smith, 1986). To present a brief description of the NET in a time-dependent formulation, first we define the heterogeneous and homogeneous representations of a reactor.

The heterogeneous or fine-mesh flux is a detailed solution of the reactor that satisfies the group space-time kinetics equations defined for small regions of the reactor, called fine nodes (figure 2.1):

$$\frac{1}{v_g}\frac{\partial}{\partial t}\Phi_g(\vec{r},t) = -\vec{\nabla}\cdot D_g(\vec{r},t)\vec{\nabla}\Phi_g(\vec{r},t) - \Sigma_{tg}(\vec{r},t)\Phi_g(\vec{r},t) + \sum_{g'=1}^{G}\Sigma_{sgg'}(\vec{r},t)\Phi_{g'}(\vec{r},t) + \chi_g^p(1-\beta)\sum_{g'=1}^{G}\nu\Sigma_{fg'}(\vec{r},t)\Phi_{g'}(\vec{r},t) + \sum_{n=1}^{D}\chi_{ng}^d\,\lambda_n C_n(\vec{r},t) \qquad (2.1)$$

$$\frac{\partial C_n(\vec{r},t)}{\partial t} = -\lambda_n C_n(\vec{r},t) + \beta_n\sum_{g'=1}^{G}\nu\Sigma_{fg'}(\vec{r},t)\Phi_{g'}(\vec{r},t) \qquad (2.2)$$

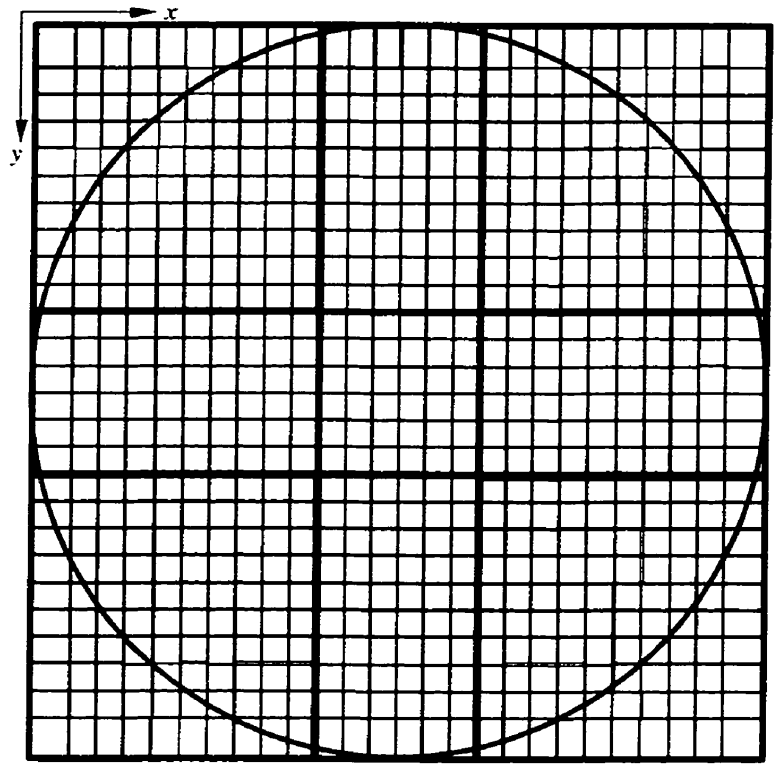

Figure 2.1: Fine and coarse representations of the reactor

The homogeneous representation of the reactor consists of large homogeneous regions of the reactor called supernodes or coarse nodes (figures 2.2 and 2.3). The homogeneous flux is the solution of space-time kinetics equations over these large regions of the reactor:

$$\frac{1}{v_g}\frac{\partial}{\partial t}\hat{\Phi}_g(\vec{r},t) = -\vec{\nabla}\cdot\hat{D}_g(\vec{r},t)\vec{\nabla}\hat{\Phi}_g(\vec{r},t) - \hat{\Sigma}_{tg}(\vec{r},t)\hat{\Phi}_g(\vec{r},t) + \sum_{g'=1}^{G}\hat{\Sigma}_{sgg'}(\vec{r},t)\hat{\Phi}_{g'}(\vec{r},t) + \chi_g^p(1-\beta)\sum_{g'=1}^{G}\nu\hat{\Sigma}_{fg'}(\vec{r},t)\hat{\Phi}_{g'}(\vec{r},t) + \sum_{n=1}^{D}\chi_{ng}^d\,\lambda_n\hat{C}_n(\vec{r},t) \qquad (2.3)$$

$$\frac{\partial\hat{C}_n(\vec{r},t)}{\partial t} = -\lambda_n\hat{C}_n(\vec{r},t) + \beta_n\sum_{g'=1}^{G}\nu\hat{\Sigma}_{fg'}(\vec{r},t)\hat{\Phi}_{g'}(\vec{r},t) \qquad (2.4)$$

where circumflexed variables stand for the homogenized parameters.

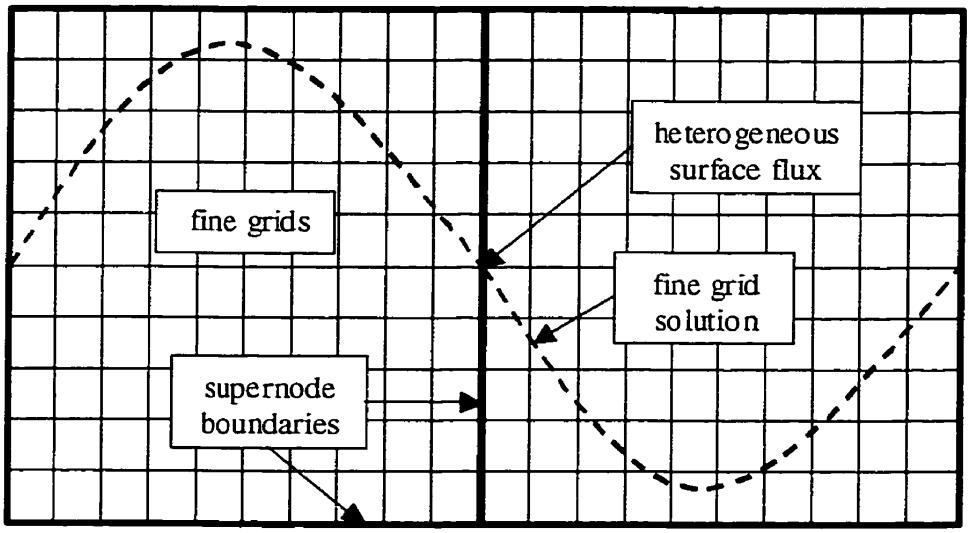

Figure 2.2: Heterogeneous representation of a supernode

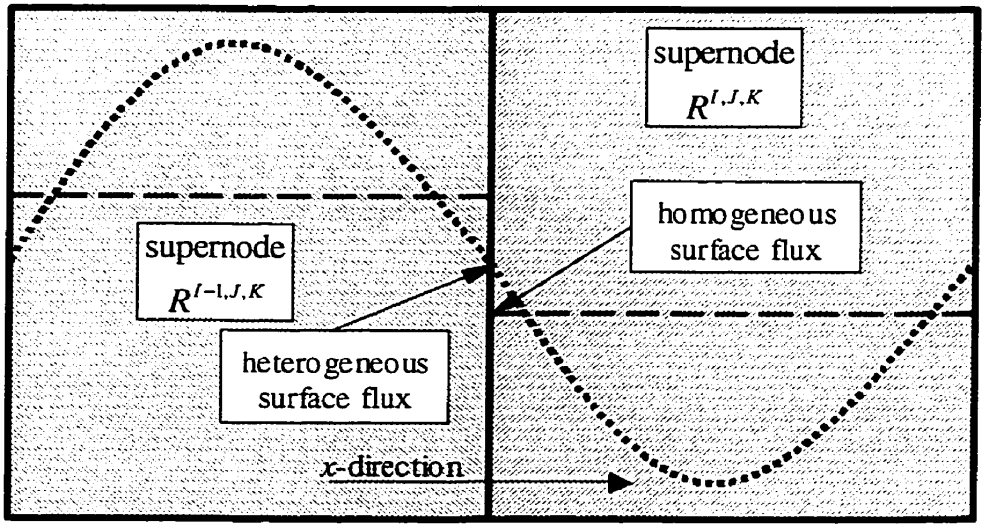

Figure 2.3: Homogeneous representation of a super node

The use of the homogenized model of a reactor leads to loss of certain information which is otherwise available if the reactor is analyzed by methods that do not involve the homogenization procedure. Therefore, it is necessary to determine after the

homogenization procedure which integral properties of the heterogeneous reactor should be preserved. Using the time-dependent formulation, these properties are:

- Preservation of the spatial integrals of supernode-average neutron reaction rates in each energy group for all $t \geq t_0$,

$$\int_{V_i} d\vec{r}\, \hat{\Sigma}_{\alpha g}(\vec{r},t)\hat{\Phi}(\vec{r},t) = \int_{V_i} d\vec{r}\, \Sigma_{\alpha g}(\vec{r},t)\Phi(\vec{r},t) \quad \alpha = t, gg', f \tag{2.5}$$

- Preservation of the integrals of the group currents on all surfaces of each supernode for all $t \geq t_0$,

$$\int_{\partial V_i} d\vec{S}\cdot\vec{\nabla}\hat{D}_g(\vec{r},t)\vec{\nabla}\hat{\Phi}_g(\vec{r},t) = \int_{\partial V_i} d\vec{S}\cdot\vec{\nabla}D_g(\vec{r},t)\vec{\nabla}\Phi_g(\vec{r},t) \tag{2.6}$$

- Preservation of the spatial integrals of supernode average concentration of the delayed neutron precursor in each family n for all $t \geq t_0$,

$$\int_{V_i} d\vec{r}\, \hat{C}_n(\vec{r},t) = \int_{V_i} d\vec{r}\, C_n(\vec{r},t) \tag{2.7}$$

- The initial reactor eigenvalue (critical reactor) is preserved at $t = t_0$

$$\hat{k}_{eff} = k_{eff} \tag{2.8}$$

It is common practice to consider that the homogenized parameters are spatially constant over each supernode. Hence, to assure preservation of the neutron reaction rates as well as delayed neutron precursors in each supernode, homogenized parameters (or nodal equivalence parameters) can be defined as follows:

$$\hat{\Phi}_g(t) \equiv \overline{\Phi}_g(t) = \frac{1}{V^{i,j,k}} \int_{V_i} d\vec{r}\, \Phi(\vec{r},t) \tag{2.9}$$

$$\hat{C}_n(t) \equiv \overline{C}_n(t) = \frac{1}{V^{i,j,k}} \int_{V_i} d\vec{r}\, C_n(\vec{r},t) \tag{2.10}$$

$$\hat{\Sigma}_{\alpha g}(t) \equiv \frac{1}{V_i \overline{\Phi}(t)} \int_{V_i} d\vec{r}\, \Sigma_{\alpha g}(\vec{r},t)\Phi(\vec{r},t) \tag{2.11}$$

where α stands for reaction type (fission, scattering, or absorption). To seek preservation of the integrals of the group currents on all surfaces, the first possible definition is to consider:

$$\hat{D}_g(t) \equiv \frac{1}{V_i \overline{\Phi}(t)} \int_{V_i} d\vec{r}\, D(\vec{r},t)\Phi(\vec{r},t) \tag{2.12}$$

which is probably the least accurate. It has been shown (Smith, 1980) that imposing both spatially constant flux-weighted diffusion coefficients and flux continuity conditions on the interfaces between the supernodes cannot simultaneously preserve the surface-integrated currents of all supernodes. Consequently, these definitions will give rise to relatively large errors in the flux calculations. To deal with this problem, either some of the homogenization criteria must be relaxed (which clearly is not desirable) or further homogenization parameters must be introduced. Nodal equivalence theory introduces six (in three dimensions) adjustable parameters per group and supernode that cause six interface-averaged currents per supernode and energy group to be preserved. Two varieties of nodal equivalence theory have been developed: equivalence theory (ET) (Koebke, 1978), and generalized equivalence theory (GET) (Smith, 1980). In both approaches, the transverse-integrated homogeneous flux is considered discontinuous at the supernode interfaces. The amount of discontinuity is measured by the definition of "heterogeneity factors" (ET) or "discontinuity factors" (GET). The values of discontinuity or heterogeneity factors are determined in such a way that interface-averaged homogeneous supernodal currents match the corresponding heterogeneous values. The difference between these two approaches is that in ET, diffusion coefficients and heterogeneity factors are adjusted simultaneously while in GET the diffusion coefficients are arbitrary and the discontinuity factors are the only adjustable parameters. In reactor kinetics, GET seems to be the more widely applied approach. In GET, the discontinuity factors are defined in terms of solutions to the one-dimensional transverse-integrated homogeneous nodal equations, given here for the x-direction:

$$\begin{aligned}\frac{1}{v_g}\frac{\partial}{\partial t}\hat{\Phi}_g^{i,j,k}(x,t) = &-\hat{D}_g^{i,j,k}\frac{\partial^2}{\partial x^2}\hat{\Phi}_g^{i,j,k}(x,t) - \hat{S}_{gx}^{i,j,k}(x,t) - \hat{\Sigma}_{tg}^{i,j,k}\hat{\Phi}_g^{i,j,k}(x,t) + \\ &\sum_{g'=1}^{G}\hat{\Sigma}_{sgg'}^{i,j,k}\hat{\Phi}_{g'}^{i,j,k}(x,t) + \chi_g^p(1-\beta)\sum_{g'=1}^{G}\nu\Sigma_{fg'}^{i,j,k}\hat{\Phi}_{g'}^{i,j,k}(x,t) + \\ &\sum_{n=1}^{D}\chi_{ng}^d\lambda_n\hat{C}_n^{i,j,k}(x,t)\end{aligned} \tag{2.13}$$

where the surface–averaged currents are forced to be equal to those of the heterogeneous problem (similar equations for the y- and z-directions). The resulting one-dimensional homogeneous surface-averaged fluxes will differ from those of heterogeneous solution hence; the time-dependent discontinuity factors are defined as the ratio of the heterogeneous and homogeneous interface-averaged fluxes:

$$
\begin{aligned}
f^{-}_{gx,i,j,k}(t) &\equiv \frac{\Phi^{i,j,k}_{gx}(x_i,t)}{\hat{\Phi}^{i,j,k}_{gx}(x_i,t)} \;,\; f^{+}_{gx,i,j,k}(t) \equiv \frac{\Phi^{i,j,k}_{gx}(x_{i+1},t)}{\hat{\Phi}^{i,j,k}_{gx}(x_{i+1},t)} \\
f^{-}_{gy,i,j,k}(t) &\equiv \frac{\Phi^{i,j,k}_{gy}(y_j,t)}{\hat{\Phi}^{i,j,k}_{gy}(y_j,t)} \;,\; f^{+}_{gy,i,j,k}(t) \equiv \frac{\Phi^{i,j,k}_{gy}(y_{j+1},t)}{\hat{\Phi}^{i,j,k}_{gy}(y_{j+1},t)} \\
f^{-}_{gz,i,j,k}(t) &\equiv \frac{\Phi^{i,j,k}_{gz}(z_k,t)}{\hat{\Phi}^{i,j,k}_{gz}(z_k,t)} \;,\; f^{+}_{gz,i,j,k}(t) \equiv \frac{\Phi^{i,j,k}_{gz}(z_{k+1},t)}{\hat{\Phi}^{i,j,k}_{gz}(z_{k+1},t)}
\end{aligned}
\tag{2.14}
$$

Consequently, the flux discontinuity conditions for each supernode in the x-direction can be written as:

$$
\begin{aligned}
f^{-}_{gx,i,j,k}(t)\cdot\hat{\Phi}^{i,j,k}_{gx}(x_i,t) &= f^{+}_{gx,i-1,j,k}(t)\cdot\hat{\Phi}^{i-1,j,k}_{gx}(x_i,t) \\
f^{+}_{gx,i,j,k}(t)\cdot\hat{\Phi}^{i,j,k}_{gx}(x_{i+1},t) &= f^{-}_{gx,i+1,j,k}(t)\cdot\hat{\Phi}^{i+1,j,k}_{gx}(x_{i+1},t)
\end{aligned}
\tag{2.15}
$$

y-direction:

$$
\begin{aligned}
f^{-}_{gy,i,j,k}(t)\cdot\hat{\Phi}^{i,j,k}_{gy}(y_j,t) &= f^{+}_{gy,i,j-1,k}(t)\cdot\hat{\Phi}^{i,j-1,k}_{gx}(y_j,t) \\
f^{+}_{gy,i,j,k}(t)\cdot\hat{\Phi}^{i,j,k}_{gy}(y_{j+1},t) &= f^{-}_{gy,i,j+1,k}(t)\cdot\hat{\Phi}^{i,j+1,k}_{gy}(y_{j+1},t)
\end{aligned}
\tag{2.16}
$$

z-direction:

$$
\begin{aligned}
f^{-}_{gz,i,j,k}(t)\cdot\hat{\Phi}^{i,j,k}_{gx}(z_k,t) &= f^{+}_{gz,i,j,k-1}(t)\cdot\hat{\Phi}^{i,j,k-1}_{gx}(z_k,t) \\
f^{+}_{gz,i,j,k}(t)\cdot\hat{\Phi}^{i,j,k}_{gz}(z_{k+1},t) &= f^{-}_{gz,i,j,k+1}(t)\cdot\hat{\Phi}^{i,j,k+1}_{gz}(z_{k+1},t)
\end{aligned}
\tag{2.17}
$$

Imposition of these discontinuity conditions and flux-weighted cross sections to global homogenized equations will guarantee the preservation of the heterogeneous time-dependent reaction rates and group surface currents (Smith, 1980).

In realistic situations, the solution of the time-dependent heterogeneous problem is not known a priori; hence, nodal equivalence parameters must be approximated. A common

procedure for approximating the nodal equivalence parameters is obtaining them from a sequence of static calculations for different reactivity device positions, temperatures, etc. To evaluate the values of nodal equivalence parameters, these tabulated static data are interpolated on the various independent variables during a transient simulation.

2.2 Description of Hierarchical Nodal Kinetics

It has been mentioned that the supernodes are very big regions of the reactor that are spatially homogenized using nodal equivalence theory. Each set of these supernodes forms a *grid level* and full space and time kinetics calculations can be performed over it. The grid levels form "time-level hierarchies" if they are used to perform the kinetics calculations corresponding to different time steps. Otherwise, if they are used to accelerate the iteration procedure of the finest grid level, they constitute "space-level hierarchies".

2.2.1 Time-Level Hierarchies

The concept of hierarchical nodal kinetics can be easily adapted to the different conventional approaches, such as the improved quasi-static method. This procedure is a well-known factorization method that uses a time hierarchy model to solve space-time kinetics equations. This method is based on the decomposition of the time-dependent neutron flux into the product of two functions: an amplitude function that depends only on time and a shape function that depends on space and energy as well as time (Ott and Meneley, 1969; Dodds, 1976):

$$\left[\Phi(\vec{r},t)\right]=\left[S(\vec{r},t)\right]T(t) \tag{2.18}$$

where $\left[S(\vec{r},t)\right]$ is the shape function and $T(t)$ is the amplitude function. Assuming that the transient is initiated from a steady state solution at time t_0 with $T(t)=T_0$ a constant for $t \le t_0$, the shape function is normalized by:

$$\int d\vec{r}\,[v]^{-1}\left[w(\vec{r},t)\right]^{T}\left[S(\vec{r},t)\right]=1 \tag{2.19}$$

for all $t \geq t_0$. Here $\left[w(\vec{r},t)\right]$ is an arbitrary weighting function that is usually selected to be the solution of the static adjoint diffusion equation corresponding to the initial state of the reactor, thereby minimizing the errors in reactivity. Applying relationships (2.18) and (2.19) into the space-time kinetics equations results in two sets of equations: first, the point-kinetics equations for the amplitude function expressed by (Henry, 1975):

$$\frac{d}{dt}T(t)=\left(\frac{\rho(t)-\bar{\beta}(t)}{\Lambda(t)}\right)T(t)+\sum_{n=1}^{D}\lambda_n C_n(t) \tag{2.20}$$

and

$$\frac{d}{dt}C_n(t)=\frac{\beta_n(t)}{\Lambda(t)}T(t)-\lambda_n C_n(t) \tag{2.21}$$

where $\rho(t),\bar{\beta}(t),\beta_n(t),$ and $\Lambda(t)$ are the classical point-kinetics parameters, and second, the space-time equations for the shape function as (dropping arguments of the shape function):

$$\begin{aligned}[v]^{-1}\frac{\partial}{\partial t}[S]+[v]^{-1}\frac{[S]}{T(t)}\frac{d}{dt}T(t)=-\vec{\nabla}\cdot[D]\vec{\nabla}[S]-[\Sigma][S]+\\ (1-\beta)[\chi_p]\left[\nu\Sigma_f\right]^{T}[S]+\frac{1}{T(t)}\sum_{n=1}^{D}[\chi_n^d]\lambda_n C_n\end{aligned} \tag{2.22}$$

Up to this point, the factorization procedure does not introduce any error in the solution of the equations. However, advantage may be gained if one assumes that the time-dependence of the shape function for relatively large time steps is weak enough that it can be considered constant. Hence, the behavior of the reactor during these large time steps can be adequately described by the point-kinetics equations that are solved more often on a smaller time scale (figure 2.4). In solving for the amplitude function, the point kinetics parameters must be updated as often as necessary to account for changes in the materials properties, device movement, and shape function. A practical algorithm used in the original implementation of the improved quasi-static scheme is to consider

that shape function varies linearly over the largest time interval. However, this consideration can lead to numerical difficulties in the neighborhood of prompt criticality (Ott and Meneley, 1969). To eliminate such difficulties, an additional layer of iterations has been introduced to yield a converged value of shape function which satisfies both relationships (2.19) and (2.22) (Dodds, 1976). Evidently, this additional iteration procedure makes the improved quasi-static method more time consuming and also more precise. The model of time-level hierarchy applied in the improved quasi-static procedure is normally an acceptable approximation for transients involving weak flux distortions. However, in cases where fast local shape distortions occur, the full core shape equations must be solved often during the transient, thus, the improved quasi-static method can become computationally as time-consuming as the conventional direct methods. To address this problem, Koclas (1993) proposed a modified improved quasi-static procedure involving a three-level rather than two-level time step hierarchy (figure 4.5).

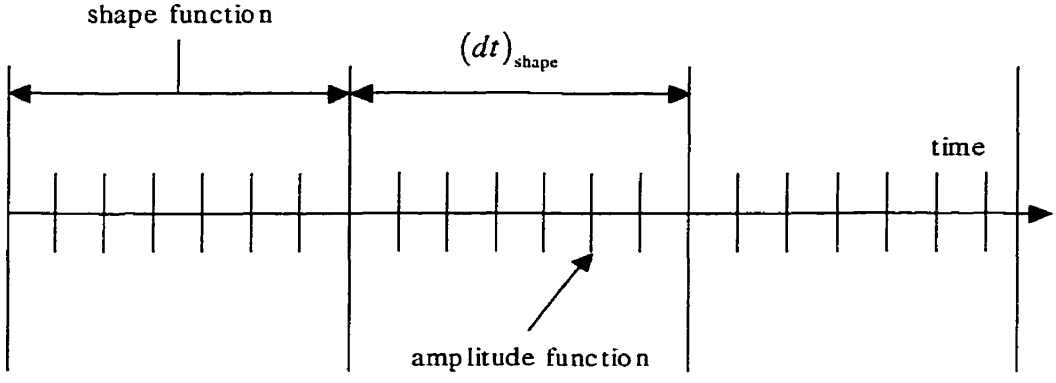

Figure 2.4: Time-level hierarchy employed in improved quasi-static method

According to this procedure, the quasi-static shape function can be calculated in two node size levels (fine and coarse) where each node size level corresponds to a time step hierarchy. It is supposed that the shape function in the coarser node size varies faster

than those of the finer nodes. Therefore, the shape function in the coarser node should be calculated more often. By using nodal equivalence theory, the preservation of all group reaction rates, all delayed-neutron precursor concentrations and all surface currents for each coarse mesh is guaranteed. The point-kinetics equations are solved on the smallest of these time hierarchies. The point kinetics parameters $\rho(t), \bar{\beta}(t), \beta_n(t)$, and $\Lambda(t)$ are all time dependent and defined by weighted integrals of the flux and cross sections over the coarse regions. Hence, these parameters must be updated at the end of each point kinetics time steps to reflect all possible cross section variations in the core. Since the number of coarse regions is small, these calculations are much less time consuming compared to the classical improved quasi-static method. On the intermediate time step the shape function is integrated over coarse nodes. Finally, after many coarse mesh calculations, the full-core fine-mesh shape function is recalculated using the full multigroup shape equations.

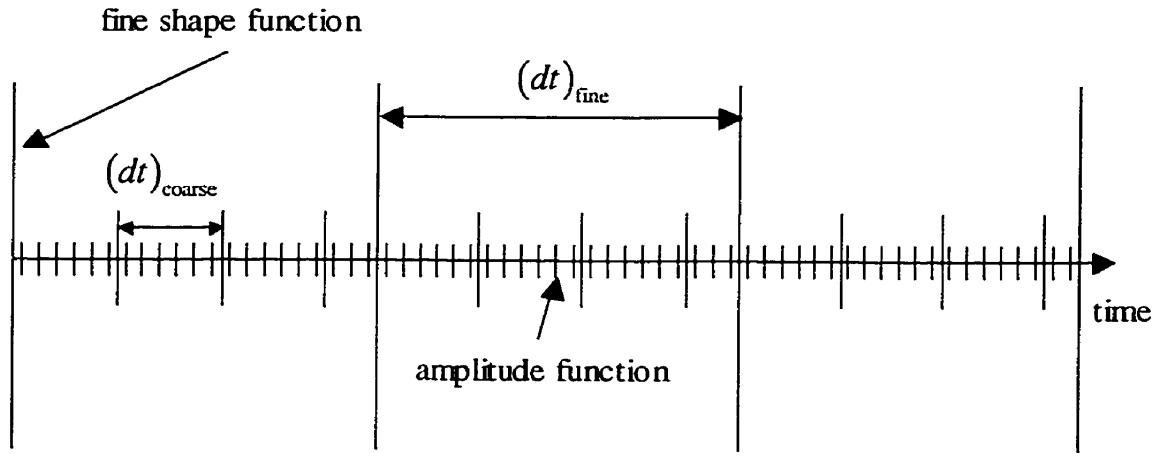

Figure 2.5: Three-level space and time kinetics calculations

The solution of the fine-mesh level is considered as the heterogeneous solution of the reactor and is used to update average cross sections, diffusion coefficients and

discontinuity factors for coarse regions. This three-level time hierarchy is successfully adopted for realistic CANDU-6 transient simulations involving all reactivity and safety devices (Kaveh *et al.* 1998, 1999a, 1999b).

One of the advantages of using time-level hierarchies is that independent space and time integration methods can be incorporated into each of the time levels, while the transition between the time levels is performed by nodal equivalence theory. For example, one can simply use a two-time-level hierarchy to evaluate the neutron flux distribution of the core: a fine level and a coarse level. On the smaller time step, full multigroup diffusion equations (not shape equations) are solved over supernodes where the supernodes are the spatially homogenized representation of the fine nodes. After many or few coarse calculations (depending on the severity of transient), the multigroup diffusion equations are solved over fine grids. The solution of this fine level is then used to re-homogenize the supernodes. Depending upon the nature of the transient even further time-level hierarchies can be introduced to calculate the neutron flux distribution.

2.2.2 Space-Level Hierarchies

The classical relaxation methods such as Gauss-Seidel and successive over-relaxation (SOR) are effective in reducing the amplitude of high-frequency components of errors while more iterations are necessary to reduce the amplitude of the low-frequency components of the error. To address this problem, a great deal of effort has been devoted to the development of different convergence acceleration techniques such as the family of cyclic Chebyshev polynomial methods (Nakamura, 1977; Axelsson, 1994) and multigrid acceleration techniques (Brandt, 1977). The multigrid acceleration techniques (also known as *coarse-mesh rebalancing*) are the convergence acceleration procedures that operate on a sequence of *space-level hierarchies* (levels of coarser nodes) to solve the finest node level problem. In reactor physics, the multigrid

acceleration techniques have been implemented by several authors (Nakamura, 1977; Finnemann and Volkert, 1988; Al-Chalabi and Turinsky, 1994), nevertheless, all of these reports are restricted to the reactor eigenvalue problem.

2.2.3 Multigrid Methods: Basic Theory and Definitions

The philosophy of the multigrid acceleration techniques is that the rapid convergence can be sustained by mapping a fine-grid problem to an equivalent coarser-grid problem and thus transforming the low-frequency error component of the fine-level problem to high-frequency component for coarse-grid. This high-frequency component can then be rapidly damped using an efficient iterative solution method such as point or line successive over-relaxation. This cycle can be repeated until the amplitude of the whole error is reduced. In most cases, the multigrid methods consist of three steps:

1. The process of collapsing the fine-grid data on a coarser grid is called "restriction or pre-smoothing" and is represented by $I_h^{\omega h}$, where ω is an integer greater than unity and h is the order of the mesh size.
2. The "smoothing" process where the high-frequency components of error are partially or completely damped (in the coarse-grid levels) using a *smoothing* operator.
3. Finally, the third step is the process of mapping the coarse-grid solution to fine-grids and is known as "interpolation, prolongation, or post-smoothing" and is represented by $I_{\omega h}^{h}$.

Based on the way that the coarse grids are formed, the multigrid procedures can be categorized into two groups: *algebraic multigrid* and *geometric multigrid* methods. In algebraic multigrid methods, only the finest grid is generated (or known). The coarse-grids are constructed by algebraic means, usually through Schur complement approaches, or their equivalent (Ruge and Stüben, 1987). Thus, the construction of a hierarchy of coarser levels, including the corresponding transfer operators, is part of the

algorithm. In general, the algebraic multigrid method takes into account coefficient values as well as geometry information. A coefficient is said to be strong if its absolute value is close to the maximum absolute value of all coefficients of that node. Multigrid theory proves that the error components in the direction of strong coefficients are rapidly reduced by the smoothing operators. Therefore, interpolation should follow the strong coefficient direction. In some algebraic multigrid procedures, the geometry information is not used at all to build coarse grids and operators. Thus, coarse-grids and the operators are determined in the way that the error, which is not reduced by relaxation in the range of the restriction operator, can be reduced in the coarse grid level during the smoothing process. The information required for an automatic coarsening is thus taken only from the given finest-level matrix. For various types of matrices, this approach has proven to be robust, efficient and very flexible. In particular, algebraic multigrid methods can directly be applied to a wide range of discretized elliptic partial differential equations on unstructured grids, both in 2D and 3D. The algebraic multigrid methods are very popular in computational fluid dynamics where unstructured-grids as well as automatically defined grids are of major importance.

In geometric multigrid methods (also known as classical multigrid methods, standard multigrid methods), the coarse grids are first determined using only geometry information (such as grid spacing). Suitable restriction, interpolation and smoothing operators are then adopted for these pre-defined coarse grids (Brandt, 1977). In geometric multigrid methods, different grid structures (finite difference, finite elements, different mesh size, etc) can be freely employed. In solving a discretized linear system, the multigrid method is tied to the underlying partial differential equations and the discretization strategies. In contrast to the algebraic multigrid method, to know where the linear system comes from is not necessary. There are some methods between the purely algebraic and purely geometric, the so-called matrix-dependent interpolation and coarse grid operator approaches. The multigrid methods applied in reactor physics are normally based on the geometric multigrid philosophy.

There exist two approaches to the use of geometric multigrid techniques: first the "coarse-grid correction" approach and, second, "full multigrid" approach. In the coarse-grid approach, the iterations start with some arbitrary initial guess for the fine-grid and continues using appropriate computational cycles over coarser grids such as V-cycles, W-cycles, etc. A typical algorithm for the coarse-grid approach applied to solving the linear problem $A\psi = B$, can be written as:

- Perform relaxation on the finest grid level $A^h\psi^h = B^h$ until error is smooth.
- Compute residual (defect) $r^h = B^h - A^h\psi^h$ and restrict to coarse grid $r^{\alpha h} = I_h^{\alpha h} r^h$.
- Solve the coarse-grid residual equation to obtain the error: $A^{\alpha h} e^{\alpha h} = r^{\alpha h}$.
- Interpolate the error to the fine grid and correct the fine-grid solution by: $\psi^h \leftarrow \psi^h + I_{\alpha h}^h e^{\alpha h}$.

A variant of the coarse-grid approach is the *full approximation scheme* that is more efficient in solving nonlinear equations. The full approximation scheme solves the equations for an approximation to the solution rather than for the correction at each grid. The interpolation can be written as:

- Perform relaxation on the finest grid level $A^h\psi^h = B^h$ until error is smooth.
- Solve the equivalent coarse-grid problem: $A^{\alpha h}\psi^{\alpha h} = B^{\alpha h}$.
- Interpolate the error to the fine grid and correct the fine-grid solution by: $\psi^h \leftarrow \psi^h + I_{\alpha h}^h\left(\psi^{\alpha h} - I_h^{\alpha h}\psi^h\right)$.

It can be observed that the interpolation error comes only from the correction and not from the full solution. In the coarse-grid approach, the definition of the coarser nodes can be considered as a temporary computational attachment that is a means of accelerating the process of relaxation of a fine-grid problem. To determine the coarse-grid operator, two methods can be used:

- First full discretization of equation over coarse-grid,
- Second, Galerkin approximation defined by $A^{\alpha h} = I_h^{\alpha h} A^h I_{\alpha h}^h$.

In the full multigrid method (also known as nested iterations) instead of starting with an arbitrary approximation on the finest grid, the first approximation is rather obtained by interpolating from an exact coarse-grid solution to the fine-grid problem. Hence, the full multigrid scheme starts on the coarsest discretization with an exact solver. These results are interpolated to the next finer grid, where a few cycles (V or W) of the multigrid method are applied. The result is again interpolated to the next finer grid, where again a few cycles of multigrid suffice to produce a solution whose algebraic accuracy and differential accuracy match. Special care must be taken to maintain the required accuracy in all components of this approach, in particular in the initial interpolation operations to the current finest grid.

2.2.4 A Geometric Full Multigrid Scheme Based on NET

Nodal equivalence theory accurately solves the homogenization problem provided that accurate enough local fine-mesh heterogeneous solutions are known or approximated within each node. The nodal equivalence parameters obtained from these local fine solutions account for all inherent heterogeneities of the supernodes. Hence, the flux distribution in the supernodes can be used to provide the approximate local solutions of the fine nodes. Consequently, nodal equivalence theory can be used as a restriction operator in a multigrid acceleration method for any classical relaxation method. Based on these observations, a new geometric full multigrid procedure is proposed. This scheme consists of the following steps:

1) Coarse-grid geometry selection: Any coarse-grid (supernode) structure can be defined as far as nodes can be spatially homogenized using nodal equivalence theory. Special treatment is necessary for exterior supernodes where empty fine nodes are

present. In practice, the same coarse-level defined in time-level hierarchies can be used for the multigrid procedure.

2) Restriction (pre-smoothing) procedure): The restriction operator $R_h^{\omega h}$ is defined by generalized equivalence theory (GET). Hence, the exact equivalent coarse-grid problem for $t \in [t_n, t_{n+1}]$ can be defined by:

$$\overline{\Phi}_g^{\text{coarse}} \equiv \frac{1}{(t_{n+1}-t_n)V_{\text{coarse}}} \int_{t_n}^{t_{n+1}} dt \int_{V_{\text{coarse}}} d\vec{r}\, \Phi(\vec{r},t) \tag{2.23}$$

$$\overline{C}_d^{\text{coarse}} \equiv \frac{1}{(t_{n+1}-t_n)V_{\text{coarse}}} \int_{t_n}^{t_{n+1}} dt \int_{V_{\text{coarse}}} d\vec{r}\, C(\vec{r},t) \tag{2.24}$$

$$\overline{\Sigma}_{\alpha g}^{\text{coarse}} \equiv \frac{1}{(t_{n+1}-t_n)V_{\text{coarse}}\overline{\Phi}_g^{\text{coarse}}} \int_{t_n}^{t_{n+1}} dt \int_{V_{\text{coarse}}} d\vec{r}\, \Sigma_{\alpha g}(\vec{r},t)\Phi(\vec{r},t) \tag{2.25}$$

where α stands for reaction type (fission, scattering, or absorption). Furthermore, the discontinuity factors are expressed by (given for the x-direction):

$$\bar{f}^{-}_{gx,\text{coarse}} \equiv \frac{\Phi_{gx}^{\text{fine}}}{\overline{\Phi}_{gx}^{\text{coarse}}} \quad , \quad \bar{f}^{+}_{gx,\text{coarse}} \equiv \frac{\Phi_{gx}^{\text{fine}}}{\overline{\Phi}_{gx}^{\text{coarse}}} \tag{2.26}$$

where Φ_{gx}^{fine} and $\overline{\Phi}_{gx}^{\text{coarse}}$ are time-averaged surface fluxes over the coarse grids. Using these exact equivalence parameters guarantees the best definition of the restricted problem in the coarse-grids. However, calculation of the exact restriction operator requires that one know the exact flux distribution for time interval $t \in [t_n, t_n + \Delta t]$. This is clearly not the case, because if the fine-level solution for that time interval were already known, the multigrid algorithm would be superfluous. To handle this problem, a restriction operator can be approximated by the flux values at present time t_n (which is known). Consequently, the coarse-grid parameters are expressed as follows:

$$\overline{\Phi}_g^{\text{coarse}} \equiv \frac{1}{V_{\text{coarse}}} \int_{V_{\text{coarse}}} d\vec{r}\, \Phi(\vec{r},t_n) \tag{2.27}$$

$$\overline{C}_d^{\text{coarse}} \equiv \frac{1}{V_{\text{coarse}}} \int_{V_{\text{coarse}}} d\bar{r}\, C(\bar{r}, t_n) \tag{2.28}$$

$$\overline{\Sigma}_{dg}^{\text{coarse}} \equiv \frac{1}{V_{\text{coarse}} \overline{\Phi}_g^{\text{coarse}}} \int_{V_{\text{coarse}}} d\bar{r}\, \Sigma_{dg}(\bar{r}, t_n) \Phi(\bar{r}, t_n) \tag{2.29}$$

The discontinuity factors are also approximated (given for the x-direction):

$$\bar{f}^{-}_{gx,\text{coarse}} \equiv \frac{\left(\Phi^{\text{het}}_{gx}\right)_{t_n}}{\left(\overline{\Phi}^{\text{hom}}_{gx}\right)_{t_n}} \quad , \quad \bar{f}^{+}_{gx,\text{coarse}} \equiv \frac{\left(\Phi^{\text{het}}_{gx}\right)_{t_n}}{\left(\overline{\Phi}^{\text{hom}}_{gx}\right)_{t_n}} \tag{2.30}$$

3) Smoothing Procedure: Based on relationships (2.27) through (2.30), the space-time kinetics equations for the coarse grids can be defined and solved. Since the number of coarse regions is small, the CPU time for this step is negligible. The solution of the coarse problem almost represents the spatial integrals of coarse-node-averaged neutron reaction rates in each energy group as well as the integrals of the group currents on all surfaces of each coarse node for the next time step. The small errors in the coarse-mesh calculations are due to the use of the flux distribution at the present time step (rather than time-averaged values) for calculating the coarse-region parameters (cross sections, diffusion coefficients, and discontinuity factors).

4) Interpolation (post-smoothing) procedure: In this step the solution must be interpolated over the fine nodes. To get the best result from the interpolation operator$\left(I^h_{\omega h}\right)$ three considerations must be taken into account: first, the operator should not amplify the low-frequency error component, second, it should use a maximum amount of information obtained from the coarse-level solution, and, third it should be inexpensive from a computational point of view. The choice of interpolation operator strongly depends on the way that space discretization is performed. For example, in nodal methods, the "pin-power reconstruction" method (Koebke and Wagner, 1977; Koebke and Hetzelt, 1985) is a good candidate. The "form function" concept employed in this method represents a fine grid correction and, hence, a high-frequency component

that can be damped rapidly using a conventional iterative method (Al-Chalabi and Turinsky, 1994). However, for a finer method such as the mesh-centered finite-difference method, the interpolation operator can be rather defined by:

$$\left(\Phi_g^{\text{fine}}\right)_{t_{n+1}} \equiv \left(r_g^{\text{fine}}\right)_{t_n} \left(\Phi_g^{\text{coarse}}\right)_{t_{n+1}} \tag{2.31}$$

where r_g^{fine} represents space- and energy-dependent local correction factors. The values of r_g^{fine} must be determined in the way that at least both the total group reaction rates and surface currents of the supernode solutions are preserved. It should be mentioned that this interpolation operator only initializes the solution for the fine-grid iteration procedure. As a result, the behavior of this multigrid scheme is similar to the full multigrid scheme rather than full approximation storage algorithm.

5) Fine-grid iteration: Once the interpolation procedure is completed the original fine-level problem can be solved using the interpolated flux as an initial guess. The savings on fine-grid iterations usually compensate for the cost of obtaining the initial solution for the fine-grid. One advantage of this multigrid procedure is that even additional convergence acceleration techniques can be implemented for the fine-grid iterations.

2.3 Code Implementation of Hierarchical Nodal Kinetics

Based on the aforementioned solution procedure, a new computer code named NDF has been developed (Kaveh *et al.* 1998, 1999a, 1999b). The computer code NDF consists of three major modules: fine-mesh, coarse-mesh and point-kinetics modules. Using procedure control language CLE-2000 (Roy and Hébert, 2000), the NDF is able to perform core static and dynamic calculations based on different varieties of hierarchical nodal kinetics. All time-averaged diffusion coefficients and macroscopic cross sections for the unit cells (fine level) are pre-calculated using the transport code DRAGON (Marleau *et al.* 1996). Furthermore, by taking advantage of a full representation of all moving devices in the computer code DONJON (Varin *et al.* 1996) the NDF code is

able to carry out complicated static and dynamic calculations related to control and safety devices in a CANDU reactor. In this section, a description of NDF will be presented.

2.3.1 Fine Level-Module

It has been proven that, among many available methods, the mesh-centered finite difference method, which is the lowest order of all nodal approximations, is sufficient for the study of CANDU reactors with one mesh per unit cell (Koclas, 1998). The higher-order approximations in the nodal method would only produce a marginal improvement in the flux solution. Eliminating the surface fluxes by enforcing continuity of the net current and flux across each interface leads to equations involving only the node-averaged fluxes. Based on these facts, a mesh-centered finite-difference method is applied to produce the fine-level or heterogeneous solution of a model of a reactor. Reproducing this exact solution at a lower computational cost is the ultimate motivation behind the hierarchical nodal kinetics scheme. The derivation of mesh-centered finite-difference equations is straightforward and has been carried out by several authors (Nakamura, 1977; Adams, 1977; Koclas, 1998):

$$\begin{aligned}\frac{V^{i,j,k}}{v_g}\frac{d}{dt}\Phi_g^{i,j,k} = {} & B_{gx+}^{i,j,k}\,\Phi_g^{i+1,j,k} + B_{gx-}^{i,j,k}\,\Phi_g^{i-1,j,k} + B_{gy+}^{i,j,k}\,\Phi_g^{i,j+1,k} + \\ & B_{gy-}^{i,j,k}\,\Phi_g^{i,j-1,k} + B_{gz+}^{i,j,k}\,\Phi_g^{i,j,k+1} + B_{gz-}^{i,j,k}\,\Phi_g^{i,j,k-1} - \\ & \left[B_{gx+}^{i,j,k} + B_{gx-}^{i,j,k} + B_{gy+}^{i,j,k} + B_{gy-}^{i,j,k} + B_{gz+}^{i,j,k} + B_{gz-}^{i,j,k} + V^{i,j,k}\Sigma_{tg}^{i,j,k}\right]\Phi_g^{i,j,k} \\ & V^{i,j,k}\sum_{g'=1}^{G}\Sigma_{sgg'}^{i,j,k}\,\Phi_g^{i,j,k} + V^{i,j,k}\chi_g^{p}(1-\beta)\sum_{g'=1}^{G}\nu\Sigma_{fg'}^{i,j,k}\,\Phi_{g'}^{i,j,k} + \\ & V^{i,j,k}\sum_{n=1}^{D}\chi_{ng}^{d}\,\lambda_n\,C_n^{i,j,k}\end{aligned} \tag{2.32}$$

The coupling coefficients are (x-direction):

$$B_{gx+}^{i,j,k} = h_y^j\, h_z^k \left(\frac{h_x^{i+1}}{2\,D_g^{i+1,j,k}} + \frac{h_x^i}{2\,D_g^{i,j,k}} \right)^{-1} , \quad B_{gx-}^{i,j,k} = h_y^j\, h_z^k \left(\frac{h_x^i}{2\,D_g^{i,j,k}} + \frac{h_x^{i-1}}{2\,D_g^{i-1,j,k}} \right)^{-1} \tag{2.33}$$

y-direction:

$$B_{gy+}^{i,j,k} = h_x^i\, h_z^k \left(\frac{h_y^{j+1}}{2\,D_g^{i,j+1,k}} + \frac{h_y^j}{2\,D_g^{i,j,k}} \right)^{-1} , \quad B_{gy-}^{i,j,k} = h_x^i\, h_z^k \left(\frac{h_y^j}{2\,D_g^{i,j,k}} + \frac{h_y^{j-1}}{2\,D_g^{i,j-1,k}} \right)^{-1} \tag{2.34}$$

and for z-direction:

$$B_{gz+}^{i,j,k} = h_x^i\, h_y^j \left(\frac{h_z^{k+1}}{2\,D_g^{i,j,k+1}} + \frac{h_z^k}{2\,D_g^{i,j,k}} \right)^{-1} , \quad B_{gz-}^{i,j,k} = h_x^i\, h_y^j \left(\frac{h_z^k}{2\,D_g^{i,j,k}} + \frac{h_z^{k-1}}{2\,D_g^{i,j,k-1}} \right)^{-1} \tag{2.35}$$

The nodal average precursor concentration group n is also given by:

$$\frac{d}{dt}\overline{C}_n^{i,j,k} = \beta_n \sum_{g'=1}^{G} \nu\Sigma_{fg'}^{i,j,k}\, \Phi_{g'}^{i,j,k} - \lambda_n \overline{C}_n^{i,j,k} \tag{2.36}$$

The static equations are obtained by setting the time derivatives to zero, substituting the resulting expression for the static precursor concentrations into the grid balance equation, and dividing the average number of neutrons produced per fission by k_{eff} .

2.3.2 Coarse-Level Module

The procedure of supernode homogenization is carried out in the context of the mesh-centered finite-difference scheme because of its simple nature, having only one unknown per node per energy group. Moreover, the coupling terms are not dependent on fluxes or currents, and, therefore, do not require any further iteration. The coarse-level module consists of two sub-modules: In the first sub-module, the solution obtained from the fine level is used to homogenize all supernodes based on nodal equivalence theory in the context of the mesh-centered finite-difference method. The second sub-module solves the space-time kinetics equations over these homogenized supernodes by applying a modified mesh-centered finite-difference algorithm.

2.3.2.1 Supernode Homogenization

To evaluate the nodal equivalence parameters, first the reactor core is partitioned into a small number of rectangular parallelepipeds coarse subregions (supernodes) where each of the supernodes includes many fine regions (figures 2.1 and 2.6). The relationships between the fine mesh and the supernode dimensions and volumes are thus written as:

$$\begin{aligned} H_x^I &= \sum_{i\in R} h_x^i \ , \ H_y^J = \sum_{j\in R} h_y^j \ , \ H_z^K = \sum_{k\in R} h_z^k \\ V^{i,j,k} &= h_x^i h_y^j h_z^k \ , \ V^{I,J,K} = \sum_{i,j,k\in R} h_x^i h_y^j h_z^k \end{aligned} \tag{2.37}$$

where I, J, and K refer to the index numbering of an arbitrary supernode R. According to nodal equivalence theory, the following definitions can be implemented:

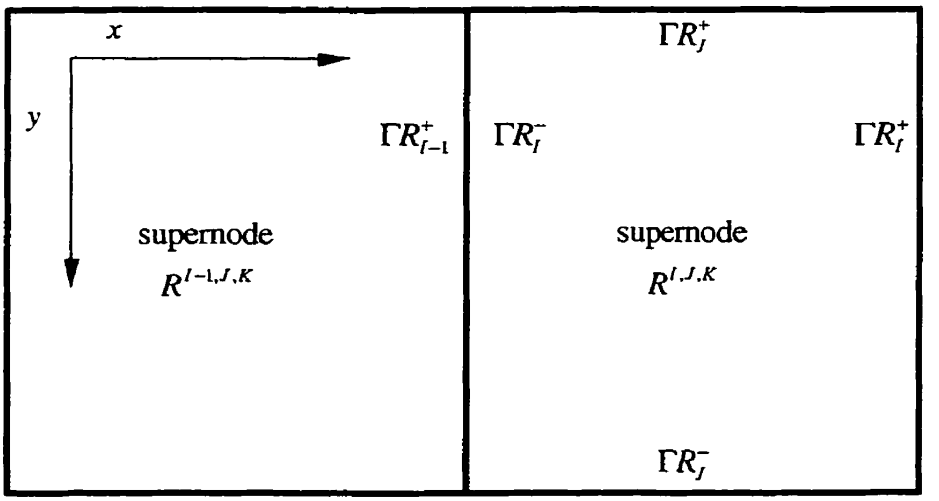

Figure 2.6: Projection onto xy-plane of two adjacent supernodes

1) Average supernode flux:

$$\overline{\Phi}_g^{I,J,K} = \frac{\sum_{i,j,k\in R} \Phi_g^{i,j,k} V^{i,j,k}}{V^{I,J,K}} \tag{2.38}$$

2) Average supernode precursor:

$$\overline{C}_n^{I,J,K} = \frac{\sum_{i,j,k \in R} C_n^{i,j,k} V^{i,j,k}}{V^{I,J,K}} \tag{2.39}$$

3) Average piecewise-constant flux-weighted cross sections for reaction type α:

$$\overline{\Sigma}_{\alpha g}^{I,J,K} = \frac{\sum_{i,j,k \subseteq R} \Sigma_{\alpha g}^{i,j,k} \Phi_g^{i,j,k} V^{i,j,k}}{\overline{\Phi}_g^{I,J,K} V^{I,J,K}} \tag{2.40}$$

4) Average piecewise-constant flux-weighted diffusion coefficients:

$$\overline{D}_{\alpha g}^{I,J,K} = \frac{\sum_{i,j,k \subseteq R} D_{\alpha g}^{i,j,k} \Phi_g^{i,j,k} V^{i,j,k}}{\overline{\Phi}_g^{I,J,K} V^{I,J,K}} \tag{2.41}$$

5) Discontinuity factors: In mesh-centered finite-difference (Koclas, 1998), one-dimensional transverse-integrated supernodal equations reduce to the following relationships between surface average fluxes and currents (for the x-direction):

$$\Phi_{gx}^{i,j,k}(x_i,t) = \Phi_g^{i,j,k} + \frac{h_x^i}{2D_g^{i,j,k}} J_{gx}^{i,j,k}(x_i,t) \tag{2.42}$$

and

$$\Phi_{gx}^{i,j,k}(x_{i+1},t) = \Phi_g^{i,j,k} - \frac{h_x^i}{2D_g^{i,j,k}} J_{gx}^{i,j,k}(x_{i+1},t) \tag{2.43}$$

Furthermore, the relationships between average fluxes and currents are:

$$J_{gx}^{i,j,k}(x_i,t) = \frac{2D_g^{i,j,k} D_g^{i-1,j,k} \left(\Phi_g^{i-1,j,k} - \Phi_g^{i,j,k}\right)}{h_x^i D_g^{i-1,j,k} + h_x^{i-1} D_g^{i,j,k}} \tag{2.44}$$

and

$$J_{gx}^{i,j,k}(x_{i+1},t) = \frac{2D_g^{i,j,k} D_g^{i+1,j,k} \left(\Phi_g^{i+1,j,k} - \Phi_g^{i,j,k}\right)}{h_x^i D_g^{i+1,j,k} + h_x^{i+1} D_g^{i,j,k}} \tag{2.45}$$

The relationships between surface flux and average fluxes are thus:

$$\Phi_{gx}^{i,j,k}(x_i,t) = \frac{h_x^{i-1} \Phi_g^{i,j,k} D_g^{i,j,k} + h_x^i \Phi_g^{i-1,j,k} D_g^{i-1,j,k}}{h_x^{i-1} D_g^{i,j,k} + h_x^i D_g^{i-1,j,k}} \tag{2.46}$$

and

$$\Phi_{gx}^{i,j,k}(x_{i+1},t)=\frac{h_x^{i+1}\Phi_g^{i,j,k}D_g^{i,j,k}+h_x^{i}\Phi_g^{i+1,j,k}D_g^{i+1,j,k}}{h_x^{i+1}D_g^{i,j,k}+h_x^{i}D_g^{i+1,j,k}} \tag{2.47}$$

Hence, the average supernode surface fluxes based on the fine-mesh distribution is simply given by:

$$\Phi_{gx}^{I,J,K}(x_I,t)=\frac{\sum_{\Gamma R_I^-}\left(\frac{h_x^{i-1}\Phi_g^{i,j,k}D_g^{i,j,k}+h_x^{i}\Phi_g^{i-1,j,k}D_g^{i-1,j,k}}{h_x^{i-1}D_g^{i,j,k}+h_x^{i}D_g^{i-1,j,k}}\right)h_y^j h_z^k}{\sum h_y^j h_z^k} \tag{2.48}$$

where $\Gamma R_I^{\pm}$ stand for opposite surfaces of the supernode R in x-direction, $i,j,k\in\Gamma R_I^-$,and $i-1,j,k\in\Gamma R_{I-1}^+$. Moreover,

$$\Phi_{gx}^{I,J,K}(x_{I+1},t)=\frac{\sum_{\Gamma R_I^+}\left(\frac{h_x^{i+1}\Phi_g^{i,j,k}D_g^{i,j,k}+h_x^{i}\Phi_g^{i+1,j,k}D_g^{i+1,j,k}}{h_x^{i+1}D_g^{i,j,k}+h_x^{i}D_g^{i+1,j,k}}\right)h_y^j h_z^k}{\sum h_y^j h_z^k} \tag{2.49}$$

where $i,j,k\in\Gamma R_I^+$ and $i+1,j,k\in\Gamma R_{I+1}^-$. Using relationship (2.42) and (2.43), the homogeneous supernode surface fluxes are written as:

$$\overline{\Phi}_{gx}^{I,J,K}(x_I,t)=\overline{\Phi}_g^{I,J,K}+\frac{h_x^I}{2\overline{D}_g^{I,J,K}}\overline{J}_{gx}^{I,J,K}(x_I,t) \tag{2.50}$$

and

$$\overline{\Phi}_{gx}^{I,J,K}(x_{I+1},t)=\overline{\Phi}_g^{I,J,K}-\frac{h_x^I}{2\overline{D}_g^{I,J,K}}\overline{J}_{gx}^{I,J,K}(x_{I+1},t) \tag{2.51}$$

According to nodal equivalence theory, the surface–averaged currents, $\overline{J}_{gx}^{I,J,K}(x_I,t)$ and $\overline{J}_{gx}^{I,J,K}(x_{I+1},t)$, must be equal to those obtained from the fine (heterogeneous) problem. Thus,

$$\overline{\Phi}_{gx}^{I,J,K}(x_I,t)=\overline{\Phi}_g^{I,J,K}+\frac{h_x^I}{\overline{D}_g^{I,J,K}}\sum_{\Gamma R_I^-}\frac{D_g^{i,j,k}D_g^{i-1,j,k}\left(\Phi_g^{i-1,j,k}-\Phi_g^{i,j,k}\right)}{h_x^{i}D_g^{i-1,j,k}+h_x^{i-1}D_g^{i,j,k}} \tag{2.52}$$

and

$$\overline{\Phi}_{gx}^{I,J,K}(x_{I+1},t)=\overline{\Phi}_g^{I,J,K}-\frac{h_x^I}{\overline{D}_g^{I,J,K}}\sum_{\Gamma R_I^+}\frac{D_g^{i,j,k}D_g^{i+1,j,k}\left(\Phi_g^{i+1,j,k}-\Phi_g^{i,j,k}\right)}{h_x^{i}D_g^{i+1,j,k}+h_x^{i+1}D_g^{i,j,k}} \tag{2.53}$$

where again the surface currents are evaluated in all fine regions forming the boundaries $\left(\Gamma R_I^{\pm}\right)$ of two adjacent supernodes in the x-direction. Using relationships (2.48), (2.49), (2.52), and (2.53), the discontinuity factors are:

$$f^{-}_{gx,I,J,K}(x_I,t) \equiv \frac{\Phi^{I,J,K}_{gx}(x_I,t)}{\overline{\Phi}^{I,J,K}_{gx}(x_I,t)} \;,\; f^{+}_{gx,I,J,K}(x_{I+1},t) \equiv \frac{\Phi^{I,J,K}_{gx}(x_{I+1},t)}{\overline{\Phi}^{I,J,K}_{gx}(x_{I+1},t)} \tag{2.54}$$

Similar expressions for the y- and z-directions are obtained:

$$f^{-}_{gy,I,J,K}(y_J,t) \equiv \frac{\Phi^{I,J,K}_{gy}(y_J,t)}{\overline{\Phi}^{I,J,K}_{gy}(y_J,t)} \;,\; f^{+}_{gy,I,J,K}(y_{J+1},t) \equiv \frac{\Phi^{I,J,K}_{gy}(y_{J+1},t)}{\overline{\Phi}^{I,J,K}_{gy}(y_{J+1},t)} \tag{2.55}$$

and

$$f^{-}_{gz,I,J,K}(z_K,t) \equiv \frac{\Phi^{I,J,K}_{gz}(z_K,t)}{\overline{\Phi}^{I,J,K}_{gz}(z_K,t)} \;,\; f^{+}_{gz,I,J,K}(z_{K+1},t) \equiv \frac{\Phi^{I,J,K}_{gz}(z_{K+1},t)}{\overline{\Phi}^{I,J,K}_{gz}(z_{K+1},t)} \tag{2.56}$$

In general, the discontinuity factors can be calculated using any transverse-integrated nodal method such as the nodal expansion or analytical nodal methods. However, higher-order solutions will result in expressions for discontinuity factors that are more complicated, for example the three-dimensional quadratic nodal expansion method has five unknowns per node per energy group. The important point is that identical approximations must be made both in determining the discontinuity factors and in solving the homogenized reactor (supernode) equations. Close examination of relationships (2.54) through (2.56) shows that the discontinuity factors depend only on the local spatial flux shape. Hence, it is expected that the discontinuity factors change slightly during mild transients. This would probably allow the use of constant discontinuity factors available from the initial criticality calculations. However, transients involving larger spatial flux changes (resulting perhaps from control-rod motions) are expected to require updating of the discontinuity factors. Moreover, it seems that updating discontinuity factors in the mesh-centered finite-difference method is of more importance than in the other transverse-integrated nodal methods, since all information due to an important spatial flux distortion will be transferred to the coarse-

mesh level only by the average fluxes. It can also be observed that the discontinuity factors account for both mesh-centered finite difference approximation and Fick's law with some arbitrary value of $\overline{D}_g^{I,J,K}$.

2.3.2.2 Supernode Equations

Once nodal equivalence parameters are evaluated, the global reactor problem represented by supernodes must be obtained and solved. The procedure is straightforward: the relationships between surface fluxes and currents for a given supernode R at surface ΓR^- is:

$$\overline{\Phi}_{gx}^{I,J,K}(x_I,t)=\overline{\Phi}_g^{I,J,K}+\frac{h_x^I}{2\overline{D}_g^{I,J,K}}\overline{J}_{gx}^{I,J,K}(x_I,t) \tag{2.57}$$

Moreover, for the neighboring mesh R_{I-1}, we have:

$$\overline{\Phi}_{gx}^{I-1,J,K}(x_I,t)=\overline{\Phi}_g^{I-1,J,K}-\frac{h_x^{I-1}}{2\overline{D}_g^{I-1,J,K}}\overline{J}_{gx}^{I-1,J,K}(x_I,t) \tag{2.58}$$

Multiplying equation (2.57) by $f_{gx,I,J,K}^-(x_I,t)$ and equation (2.58) by $f_{gx,I-1,J,K}^+(x_{I-1},t)$ and subtracting the results, gives:

$$\begin{aligned}&f_{gx,I,J,K}^-(x_I,t)\overline{\Phi}_{gx}^{I,J,K}(x_I,t)-f_{gx,I-1,J,K}^+(x_{I-1},t)\overline{\Phi}_{gx}^{I-1,J,K}(x_I,t)=\\&f_{gx,I,J,K}^-(x_I,t)\overline{\Phi}_g^{I,J,K}+\frac{f_{gx,I,J,K}^-(x_I,t)h_x^I}{2\overline{D}_g^{I,J,K}}\overline{J}_{gx}^{I,J,K}(x_I,t)-\\&f_{gx,I-1,J,K}^+(x_{I-1},t)\overline{\Phi}_g^{I-1,J,K}+\frac{f_{gx,I-1,J,K}^+(x_{I-1},t)h_x^{I-1}}{2\overline{D}_g^{I-1,J,K}}\overline{J}_{gx}^{I-1,J,K}(x_I,t)\end{aligned} \tag{2.59}$$

Considering the definition of the discontinuity factors (2.54) through (2.56) and imposing continuity of the supernode surface currents, we obtain:

$$\overline{J}_{gx}^{I,J,K}(x_I,t)=\frac{2\overline{D}_g^{I,J,K}\overline{D}_g^{I-1,J,K}\left[f_{gx,I-1,J,K}^+(x_{I-1},t)\overline{\Phi}_g^{I-1,J,K}-f_{gx,I,J,K}^-(x_I,t)\overline{\Phi}_g^{I,J,K}\right]}{f_{gx,I,J,K}^-(x_I,t)\overline{D}_g^{I-1,J,K}H_x^I+f_{gx,I-1,J,K}^+(x_{I-1},t)\overline{D}_g^{I,J,K}H_x^{I-1}} \tag{2.60}$$

Using the same procedure, the relationship between surface fluxes and currents for a given supernode R at the opposite surface ΓR^+ is:

$$\bar{J}_{gx}^{I,J,K}(x_{I+1},t)=\frac{2\bar{D}_g^{I,J,K}\bar{D}_g^{I+1,J,K}\left[f_{gx,I,J,K}^{+}(x_{I+1},t)\bar{\Phi}_g^{I,J,K}-f_{gx,I+1,J,K}^{-}(x_{I+1},t)\bar{\Phi}_g^{I+1,J,K}\right]}{f_{gx,I+1,J,K}^{-}(x_{I+1},t)\bar{D}_g^{I+1,J,K}H_x^{I+1}+f_{gx,I,J,K}^{+}(x_{I+1},t)\bar{D}_g^{I,J,K}H_x^{I}} \quad (2.61)$$

The expressions for the y- and z-directions are similar. Thus, the seven-point mesh-centered finite-difference approximation for supernodes modified by discontinuity factors can be written as:

$$\begin{aligned}\frac{V^{I,J,K}}{v_g}\frac{d}{dt}\bar{\Phi}_g^{I,J,K} &= E_{gx+}^{I,J,K}\bar{\Phi}_g^{I+1,J,K}+E_{gx-}^{I,J,K}\bar{\Phi}_g^{I-1,J,K}+E_{gy+}^{I,J,K}\bar{\Phi}_g^{I,J+1,K}+\\ &E_{gy-}^{I,J,K}\bar{\Phi}_g^{I,J-1,K}+E_{gz+}^{I,J,K}\bar{\Phi}_g^{I,J,K+1}+E_{gz-}^{I,J,K}\bar{\Phi}_g^{I,J,K-1}-\\ &\left[\begin{matrix}E_{gx+}^{I,J,K}+E_{gx-}^{I,J,K}+E_{gy+}^{I,J,K}+E_{gy-}^{I,J,K}+\\ E_{gz+}^{I,J,K}+E_{gz-}^{I,J,K}+V^{I,J,K}\Sigma_{tg}^{I,J,K}\end{matrix}\right]\bar{\Phi}_g^{I,J,K}+\\ &V^{I,J,K}\sum_{g'=1}^{G}\bar{\Sigma}_{sgg'}^{I,J,K}\bar{\Phi}_g^{I,J,K}+V^{I,J,K}\chi_g^{p}(1-\beta)\sum_{g'=1}^{G}\nu\bar{\Sigma}_{fg'}^{I,J,K}\bar{\Phi}_{g'}^{I,J,K}+\\ &V^{I,J,K}\sum_{n=1}^{D}\chi_{ng}^{d}\lambda_n\bar{C}_n^{I,J,K}\end{aligned} \quad (2.62)$$

The coupling coefficients are defined by (x-direction):

$$E_{gx+}^{I,J,K}=\frac{H_y^J H_z^K f_{gx,I+1,J,K}^{-}}{2}\left(\frac{H_x^I f_{gx,I,J,K}^{+}}{\bar{D}_g^{I,J,K}}+\frac{H_x^{I+1}f_{gx,I+1,J,K}^{-}}{\bar{D}_g^{I+1,J,K}}\right)^{-1} \quad (2.63)$$

and

$$E_{gx-}^{I,J,K}=\frac{H_y^J H_z^K f_{gx,I-1,J,K}^{+}}{2}\left(\frac{H_x^I f_{gx,I,J,K}^{-}}{\bar{D}_g^{I,J,K}}+\frac{H_x^{I-1}f_{gx,I-1,J,K}^{+}}{\bar{D}_g^{I-1,J,K}}\right)^{-1} \quad (2.64)$$

y-direction:

$$E_{gy+}^{I,J,K}=\frac{H_x^I H_z^K f_{gy,I,J+1,K}^{-}}{2}\left(\frac{H_y^J f_{gy,I,J,K}^{+}}{\bar{D}_g^{I,J,K}}+\frac{H_y^{J+1}f_{gy,I,J+1,K}^{-}}{\bar{D}_g^{I,J+1,K}}\right)^{-1} \quad (2.65)$$

and

$$E_{gy-}^{I,J,K}=\frac{H_x^I H_z^K f_{gy,I,J-1,K}^{+}}{2}\left(\frac{H_y^J f_{gy,I,J,K}^{-}}{\bar{D}_g^{I,J,K}}+\frac{H_y^{J-1}f_{gy,I,J-1,K}^{+}}{\bar{D}_g^{I,J-1,K}}\right)^{-1} \quad (2.66)$$

z-direction:

$$E_{gz+}^{I,J,K} = \frac{H_x^I H_y^J f_{gz,I,J,K+1}^-}{2}\left(\frac{H_z^K f_{gz,I,J,K}^+}{\overline{D}_g^{I,J,K}} + \frac{H_z^{K+1} f_{gz,I,J,K+1}^-}{\overline{D}_g^{I,J,K+1}}\right)^{-1} \tag{2.67}$$

and

$$E_{gz-}^{I,J,K} = \frac{H_x^I H_y^J f_{gz,I,J,K-1}^+}{2}\left(\frac{H_z^K f_{gz,I,J,K}^-}{\overline{D}_g^{I,J,K}} + \frac{H_y^{K-1} f_{gz,I,J,K-1}^+}{\overline{D}_g^{I,J,K-1}}\right)^{-1} \tag{2.68}$$

The supernodal average precursor concentration group n is also given by:

$$\frac{d}{dt}\overline{C}_n^{I,J,K} = \beta_n \sum_{g'=1}^{G} \nu\overline{\Sigma}_{fg'}^{I,J,K} \Phi_{g'}^{I,J,K} - \lambda_n \overline{C}_n^{I,J,K} \tag{2.69}$$

Equations (2.62) and (2.69) constitute the set of difference equations modified by nodal equivalence theory. Close examination of these equations demonstrates an essential difference between the structure of mesh-centered finite-difference modified and non-modified by nodal equivalence theory. In the cases that are not modified by equivalence theory, the coupling between surface currents and nodal average fluxes can be done by just one storage per node-interface per energy group (due to the symmetry of the coupling matrix). The cases modified by nodal equivalence theory require storage of two coefficients per supernode-interface per energy group. This is significant in that most mesh-centered finite difference codes store symmetric coupling parameters.

2.3.2.3 Partially Empty Supernodes

Difficulties arise in defining exact supernode cross sections and discontinuity factors when empty nodes from the fine mesh model are present in the supernodes. A usual treatment of boundary conditions for the supernodes on the exterior boundary of the core is simply to fill in the empty nodes with extra reflector material. Nevertheless, this approach can result in large errors in the flux calculations. A superior approach, implemented in NDF, is to apply proper neutron flux and current balances over these partially empty supernodes. An equivalent albedo boundary condition over the outside surfaces of supernodes is then calculated by averaging both the surface fluxes and

currents on these surfaces. Considering a supernode R with some empty fine nodes (figure 2.6), we can write:

$$R = R_f \cup R_e \quad \text{and} \quad V_R = V_{R_f} + V_{R_e} \tag{2.70}$$

where R_f consists of the fine mesh inside the reactor core and R_e consists of the empty fine nodes.

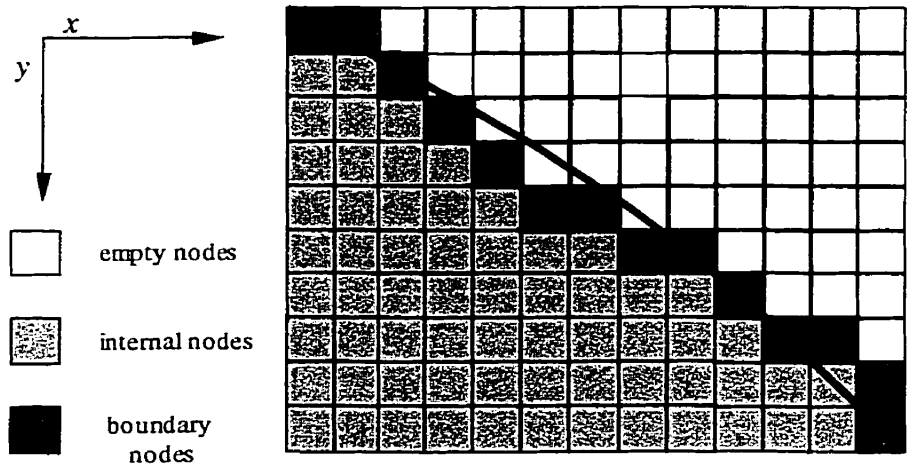

Figure 2.7: Partially empty supernode

The nodal equivalence parameters for this partially empty supernode are defined by:

1) Average supernode flux:

$$\overline{\Phi}_g^{I,J,K} = \frac{\sum_{i,j,k \in R_f} \Phi_g^{i,j,k} V^{i,j,k}}{V_{R_f} + V_{R_e}} \tag{2.71}$$

2) Average supernode precursor:

$$\overline{C}_n^{I,J,K} = \frac{\sum_{i,j,k \in R_f} C_n^{i,j,k} V^{i,j,k}}{V_{R_f} + V_{R_e}} \tag{2.72}$$

3) Average piecewise-constant flux-weighted cross sections for reaction type α:

$$\overline{\Sigma}_{\alpha g}^{I,J,K} = \frac{\sum_{i,j,k \in R_f} \Sigma_{\alpha g}^{i,j,k} \Phi_g^{i,j,k} V^{i,j,k}}{\left(V_{R_f} + V_{R_e}\right) \overline{\Phi}_g^{I,J,K}} \tag{2.73}$$

4) Average piecewise-constant flux-weighted diffusion coefficients:

$$\overline{D}_{\alpha g}^{I,J,K} = \frac{\sum_{i,j,k \in R_f} D_{\alpha g}^{i,j,k} \Phi_g^{i,j,k} V^{i,j,k}}{\left(V_{R_f} + V_{R_e}\right) \overline{\Phi}_g^{I,J,K}} \tag{2.74}$$

For the boundaries representing free surfaces, the total leakage must be preserved; hence, the equivalent $\overline{\alpha}$ - albedo is defined by (for x-direction):

$$\overline{\alpha}_{gx} = \frac{\overline{\Phi}_{gx}^{I,J,K}(x,t)}{\overline{J}_{gx}^{I,J,K}(x,t)} \tag{2.75}$$

where, $\overline{\Phi}_{gx}^{I,J,K}(x,t)$ and $\overline{J}_{gx}^{I,J,K}(x,t)$ are averaged over the external surfaces (normal to x-direction) of the fine grids forming the boundaries of the reactor core.

2.3.3 Point-Kinetics Module

The major difficulty in this step comes from the stiffness of the point-reactor kinetics equations. To address this problem, the generalized Runge-Kutta (GRK4A) method of the Kaps-Rentrop family (Sánchez, 1989) is chosen and implemented. In this step, the time-dependent cross sections and time-dependent flux represent the effects of perturbations to the core during the transient. Since the shape function is assumed constant between two shape calculations, the point kinetics parameters are not exact, and result in a certain amount of error being introduced into the solution.

2.3.4 Time Integration Method

After discretization of the space domain, an initial-value problem for a coupled system of ordinary differential equations is obtained. In order to manage stability and convergence of the time-dependent solution, the θ-finite difference scheme (Nakamura,

1977) is one of the most well-established procedures. Therefore, a full implementation of the θ-method on both fine and supernode levels has been carried out. In the present version of the NDF, the values of θ can be different for flux and delayed neutron precursors, and are independent of space.

2.3.5 Restriction Operator

Previously, it has been mentioned that the restriction operator $I_h^{\omega h}$ in the space-level hierarchy is defined by generalized equivalence theory (GET). Hence, in the computer code NDF, the restricted coarse-grid problem for $t \in [t_n, t_{n+1}]$ is approximated by:

1) Average piecewise-constant flux-weighted cross sections for reaction type α:

$$\overline{\Sigma}_{\alpha g}^{\text{coarse}} \equiv \frac{\sum_{i,j,k \in V_{\text{coarse}}} \left(\Sigma_{\alpha g}^{i,j,k} \Phi_g^{i,j,k}\right)_{t_n} V^{i,j,k}}{\sum_{i,j,k \in V_{\text{coarse}}} \left(\Phi_g^{i,j,k}\right)_{t_n} V^{i,j,k}} \tag{2.76}$$

2) Average piecewise-constant flux-weighted diffusion coefficients:

$$\overline{D}_g^{\text{coarse}} \equiv \frac{\sum_{i,j,k \in V_{\text{coarse}}} \left(D_g^{i,j,k} \Phi_g^{i,j,k}\right)_{t_n} V^{i,j,k}}{\sum_{i,j,k \in V_{\text{coarse}}} \left(\Phi_g^{i,j,k}\right)_{t_n} V^{i,j,k}} \tag{2.77}$$

2) Discontinuity factors, here given for x-direction:

$$f_{gx}^{-} \equiv \frac{\left[\Phi_{gx}^{\text{coarse}}(x_l)\right]_{t_n}}{\left[\overline{\Phi}_{gx}^{\text{coarse}}(x_l)\right]_{t_n}}, \quad f_{gx}^{+} \equiv \frac{\left[\Phi_{gx}^{\text{coarse}}(x_{l+1})\right]_{t_n}}{\left[\overline{\Phi}_{gx}^{\text{coarse}}(x_{l+1})\right]_{t_n}} \tag{2.78}$$

The restriction operator defined by these equations guarantees the proper definition of the restricted problem in context of the mesh-centered finite difference approximation.

2.3.6 Interpolation Operator

It has been mentioned that for the mesh-centered finite-difference method, the interpolation operator can be defined by:

$$\left(\Phi_g^{\text{fine}}\right)_{t_{n+1}} \cong \left(r_g^{\text{fine}}\right)\left(\Phi_g^{\text{coarse}}\right)_{t_{n+1}} \tag{2.79}$$

where r_g^{fine} represents space- and energy-dependent correction factors. In the computer code NDF, the interpolation operator is defined by:

$$\left(r_g^{\text{i,j,k}}\right)_{t_n} \cong \left(\frac{\Phi_g^{i,j,k}}{\overline{\Phi}_g^{\text{coarse}}}\right)_{t_n} \tag{2.80}$$

This interpolation operator preserves both total group reaction rates and surface currents obtained from the smoothing procedure.

2.3.7 Approximation of Nodal Equivalence Parameters

In realistic reactor calculations, it is not practical to perform too many fine mesh calculations for the sole purpose of updating the equivalence parameters. The precision of the coarse-level calculations thus depends on how the equivalence parameters can be approximated to correctly reflect reactivity-device movements in the core. In this section, descriptions of the different approximation methods employed in the computer code NDF are presented.

2.3.7.1 Equivalence Parameter Database

The first method is to establish an equivalence parameter database using *off-line* static fine-level calculations. All devices are initially set to a reference position. Each device is then moved and set to a new position independent of other devices. Based on the resulting static fine-mesh calculation, all equivalence parameters are then calculated and saved in the database. These tabulated data are then interpolated on the various independent variables (such as device position) to approximate the values of nodal equivalence parameters during a transient involving complicated device movements. This procedure would permit fewer fine-level calculations on long transients such as those involving xenon. However, numerous tests show that when many devices are present in the core, simple superposition or linear interpolation of the tabulated values

of cross sections and discontinuity factors result in large errors. These errors are mostly due to device interference effects that are not considered in the database generation. Moreover, the use of the steady-state flux distribution to generate equivalence parameters (instead of dynamic flux) causes an additional source of inaccuracy.

2.3.7.2 Correction Terms

Another approach is to define correction terms that are the differences between the exact values of the equivalence parameters at the end of the fine mesh calculation and those which are tabulated. These correction terms would then be added to tabulated values of the equivalence parameters during the next fine time step, thus:

$$f_{gu}^{\pm} \cong \left(f_{gu}^{\pm}\right)_{\text{database}}^{t} + \left[\left(f_{gu}^{\pm}\right)_{\text{exact}}^{t_f} - \left(f_{gu}^{\pm}\right)_{\text{database}}^{t_f}\right] \tag{2.81}$$

where t_f corresponds to the last fine-level calculation and t stands for present supernode calculations. In this approach, the data interpolation procedure at the end of a fine-level calculation can be replaced by an off-line static calculation resulting in a more precise correction term for the next fine-level time step. This method sounds promising, especially for benchmark problem solving. A similar approach is to consider that equivalence parameters are a linear combination of the exact values obtained at the end of fine-level calculations and those obtained from database interpolation:

$$f_{gu}^{\pm} \cong \varepsilon\left(f_{gu}^{\pm}\right)_{\text{exact}} + (1-\varepsilon)\left(f_{gu}^{\pm}\right)_{\text{database}} \tag{2.82}$$

where ε is a constant or a time-dependent weighting parameter. In this procedure, the data interpolation can also be replaced by off-line static calculation at the end of fine-level calculation. However, the procedure becomes more time consuming.

2.3.7.3 Piecewise Constant Discontinuity Factors

Using an interpolation procedure for discontinuity factors can give rise to a considerable amount of error in the flux calculations. The errors are mostly attributable to the

sensitivity of flux calculations to values of discontinuity factors. A very efficient way to deal with this problem is to consider that the discontinuity factors are constant between two fine-level calculations while flux-weighted diffusion coefficients and cross sections are updated after each lower-level time step by using a simple reconstruction procedure. The time intervals during which discontinuity factors are constant (fine-level time step) can be adjusted by considering the nature of the transient. For transients involving important spatial changes, the time intervals are much shorter than those involving small spatial flux changes. The fine-flux distribution is reconstructed using the last average coarse node flux and the intranodal distribution calculated after each fine-level time step. This method is the default option in the computer code NDF.

CHAPTER 3

NUMERICAL RESULTS: STATIC CASES

This chapter essentially deals with different aspects of applying nodal equivalence theory for steady-state calculations in a typical CANDU-6 reactor. Even though the use of equivalence theory in static diffusion calculations is not the primary interest of this research, the resulting conclusions can be to some extent useful for the purpose of dynamic calculations. Emphasis will be on practical aspects such as the effect of the number of coarse nodes on the precision of the coarse-level calculations, the sensitivity of the equivalence parameters to the device position and the error in the flux calculations due to the use of a set of reference equivalence parameters.

3.1 Reference Static Calculations

To perform numerical tests, a three-dimensional model of a CANDU-6 reactor has been developed. The model introduces a 26 x 26 x 12 grid for the x-, y- and z-directions to represent the fine regions of the reactor based on the one-mesh-per-cell approach. The fuel model consists of two fuel types and uses two neutron energy groups and six delayed-neutron precursor groups for dynamic calculations. The details of this model, such as region-material assignments, nuclear properties of fuel and reflector, reactivity devices properties, coarse-region description and other necessary information are described in appendix I.

The static reference solution of the reactor consists of both the reactor eigenvalue $\left(k_{eff}\right)$ and the group flux distribution for the critical reactor, which is the normal working condition of the reactor. In the reference critical reactor:

- All liquid zone controllers are 50% full,
- All adjuster banks are fully inserted,

- All mechanical control absorber rods are fully withdrawn.

Figure 3.1 shows the thermal neutron reference flux distribution for the critical reactor at a total reactor power of 2.164 x 10^9 Watts. The reference reactor eigenvalue for both cases with and without xenon load are shown in Table 3.1. The finer model (52 x 52 x 24) is obtained by splitting each cell into two equal subparts for the *x*-, *y*-, and *z*-directions representing eight nodes per fuel cell. It can be observed that the differences between reactor eigenvalues with xenon and without xenon are less than 0.04 mk.

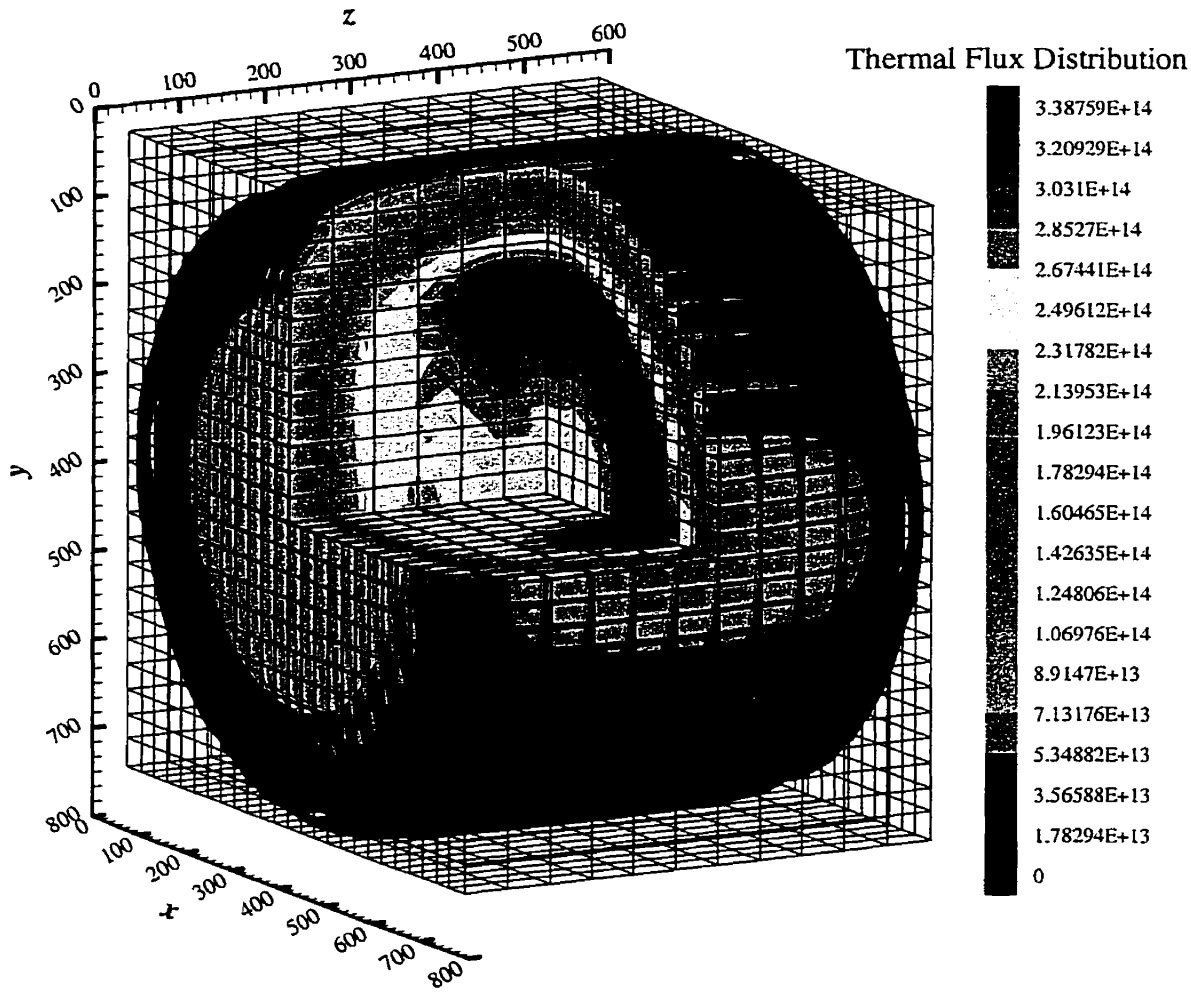

Figure 3.1: Thermal flux distribution for the reactor reference (26 x 26 x 12)

Table 3.1: k_{eff} for reference case

Number of mesh grids	$(k_{eff})_{\text{without xenon}}$	$(k_{eff})_{\text{with xenon}}$	Xenon load
26 x 26 x 12 (Ref.)	1.030670	1.002754	≈ -27.83 mk
52 x 52 x 24	1.030711	1.002774	≈ -27.85 mk

3.1.1 Comparison of Static Results

The comparison of two given sets of static results (with different mesh numbers) involves, first the comparison of the reactor eigenvalues and, second the comparison of the fluxes using the following definitions:

- Relative nodal group flux error:

$$e_g^{i,j,k} = \left(\frac{\Phi_g^{i,j,k} - \overline{\Phi}_g^{i,j,k}}{\overline{\Phi}_g^{i,j,k}} \right) * 100 \tag{3.1}$$

  where $\Phi_g^{i,j,k}$ is the nodal group flux from the coarser-grid calculation and $\overline{\Phi}_g^{i,j,k}$ is the collapsed nodal average group flux calculated from the finer flux distribution and is given by relationship (2.38).

- Maximum nodal flux error defined by:

$$e_{g,\max}^{i,j,k} = \max\left[\text{abs}\left(e_g^{i,j,k}\right)\right],\ g = 1,\ldots,G \tag{3.2}$$

- Average total nodal flux error defined by:

$$\overline{e} = \frac{\sum_{g=1}^{G}\sum_{n=1}^{N} \text{abs}\left(e_g^{i,j,k}\right)}{N} \tag{3.3}$$

where N is the number of coarse nodes.

3.1.2 More Realistic Calculations

It is essential to mention that obtaining more realistic results requires both a more detailed fuel model and a finer representation of the reactor core. However, a more

detailed fuel model and/or a finer representation of the reactor will result in a more accurate reactor calculation and will not affect the validity of the hierarchical nodal kinetics procedure.

To present a more detailed fuel model, further parameters, such as cell-to-cell variable burn-ups and local effects (temperatures and densities), must be taken into account. A finer representation of the reactor normally can be realized by defining more meshes for each unit cell (for example 8 meshes per unit cell). This mesh splitting procedure could result in a more precise reactor calculation. However, it may also bring certain features that complicate the comparison of the results. For example, how the reactivity devices (and their movement for dynamic calculations) are treated can significantly affect the accuracy of the results, thus making it difficult to assess the correctness of the underlying comparison procedure.

Figure 3.2 shows that depending on which procedure is performed first, device-modeling procedure or mesh-splitting procedure, two different mathematical problems can be obtained (A' and A"). If device cross sections are added to a given mesh (as a part of the device modeling procedure) before splitting the mesh, the resulting equivalent problem will consist of four finer grids with equal cross sections (A'). Otherwise if mesh splitting is performed before adding the device cross sections, the resulting equivalent problem will consist of four finer grids with different cross sections (A"). For the purpose of the static calculations, a correct approach would be the comparison of the resulting group fluxes for the grids A and A' (which is used in the present work) not those obtained for the grids A and A". Another correct but less convenient mesh-splitting method (also for static calculations) is to coincide the coarser mesh boundaries with the reactivity-device boundaries at their reference position and then split the resulting mesh to obtain a finer model. This approach would also guarantee that the group-flux errors are uniquely due to the spatial truncation error.

The assessment of the results from two sets of calculations, one from (26 x 26 x 12) and other from a finer representation of the reactor (52 x 52 x 24), show that while the eigenvalues are almost identical (Table 3.1), the relative nodal flux errors are not negligible (figure 3.3).

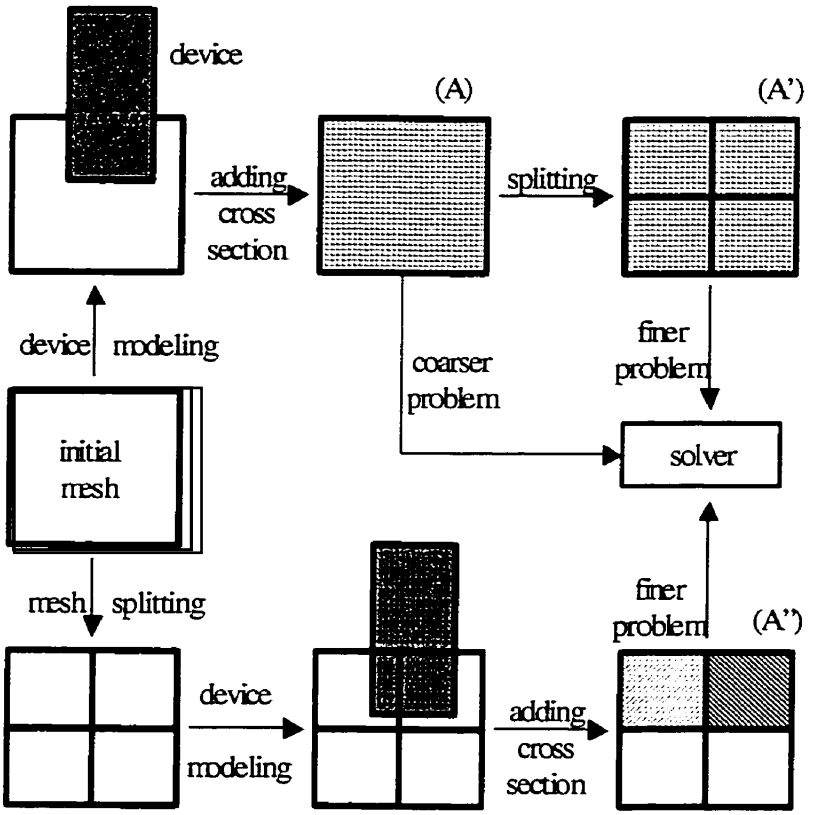

Figure 3.2: Effect of device modeling on the finer representation of a coarse mesh

It is also worthy to note that the computer code NDF permits definition of arbitrary configurations of fine and coarse regions, application of few neutron energy groups as well as the possibility of implementing a more detailed fuel model. However, for the sake of the validation procedure in the present work, a 26 x 26 x 12 model is sufficient.

3.2 Number of Coarse Regions

It is expected that using the exact values of equivalence parameters in the coarse-mesh calculations will lead to an almost perfect reproduction of the reactor eigenvalue and the collapsed nodal-average fluxes. To verify this, various coarse-mesh configurations (Appendix I) have been selected. For each of these coarse configurations, the reactor eigenvalue as well as the coarse-flux distribution are calculated.

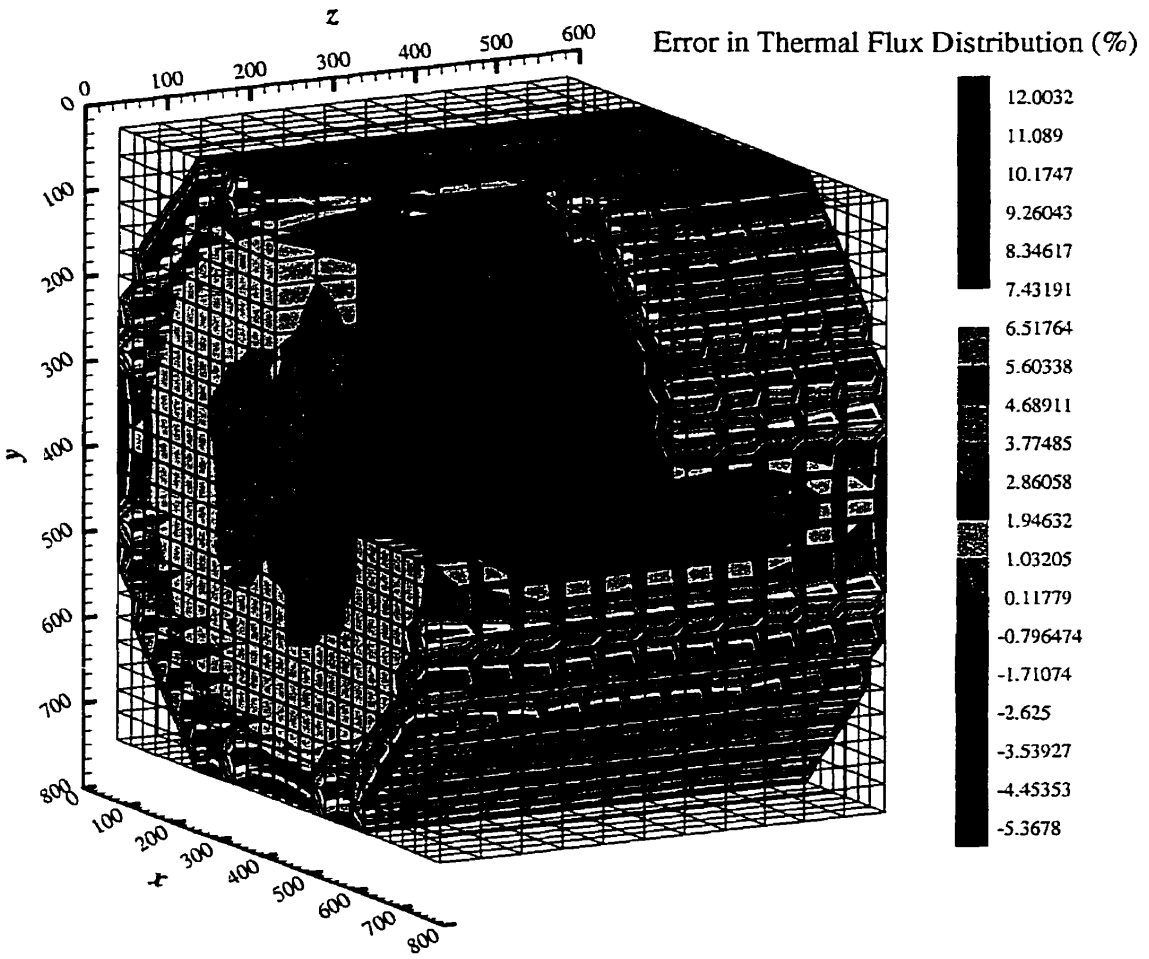

Figure 3.3: Thermal flux error distribution for a 26 x 26 x 12 reference model.

Comparisons between the results and the reference solution (Table 3.2) show that the reactor eigenvalue and average fluxes for all coarse configurations are well predicted. One interesting point is that the maximum and the average flux error for the cases with the bigger coarse meshes are greater than for those with smaller coarse meshes. This is primarily due to the inherent errors produced by the floating-point calculations. Bigger coarse nodes cover more fine regions, thus round-off errors in the evaluation of equivalence parameters are more significant. To reduce these errors, one solution is the use of higher precision variables in the floating-point calculations. However, the use of higher precision variables cannot be justified since it would result in a significant increase in the calculation time.

Table 3.2: Results for different numbers of coarse regions

Number of Coarse Regions	Maximum Error (%)	Average Error (%)	k_{eff}	Error in k_{eff} (%)
1 x 1 x 1	4.8e-04	4.4e-05	1.002845	9.9e-3
2 x 2 x 2	9.8e-01	4.4e-03	1.002556	1.9e-2
3 x 3 x 2	7.4e-01	2.2e-03	1.002757	2.9e-4
5 x 5 x 4	1.7e-01	6.5e-04	1.002746	7.9e-4
10 x 10 x 4	2.6e-02	1.6e-04	1.002756	1.9e-4
26 x 26 x 12 (Ref.)	----	-----	1.002754	----
5 x 5 x 4 (DFs=1)[1]	1.03e+2	3.3e+1	1.008978	6.2e-1

[1] All discontinuity factors (DFs) are forced to be equal unity.

Moreover, implementation of smaller coarse meshes can easily compensate for these kinds of errors without introducing any considerable penalty in the calculation time. In contrast to the static calculations, the errors due to the floating-point calculations play

an important role in dynamic calculations and this will be discussed in more detail in the next chapter.

One interesting case is the modeling of the reactor by only one coarse grid (1 x 1 x 1). In this case, the maximum and the average group flux errors are minimum. The coarse average group fluxes (calculated from the fine solution) are actually the solution of the coarse flux distribution problem. Hence, no inner iterations are necessary to obtain them and therefore no iteration round-off error is induced in the coarse solution. Consequently, the reactor problem defined by this big region is reduced to the determination of k_{eff} (outer iteration). It can also be observed that the average flux error for this special case is on the order of $10^{-5}\%$. This is the intrinsic floating-point error for single-precision calculations and is produced during the outer iterations on the coarse level. The results shown in Table 3.2 indicate that the reactor eigenvalue and the coarse flux distribution are always well predicted and changing the number of coarse grids would not lead to a significant amount of error in the coarse-flux calculations.

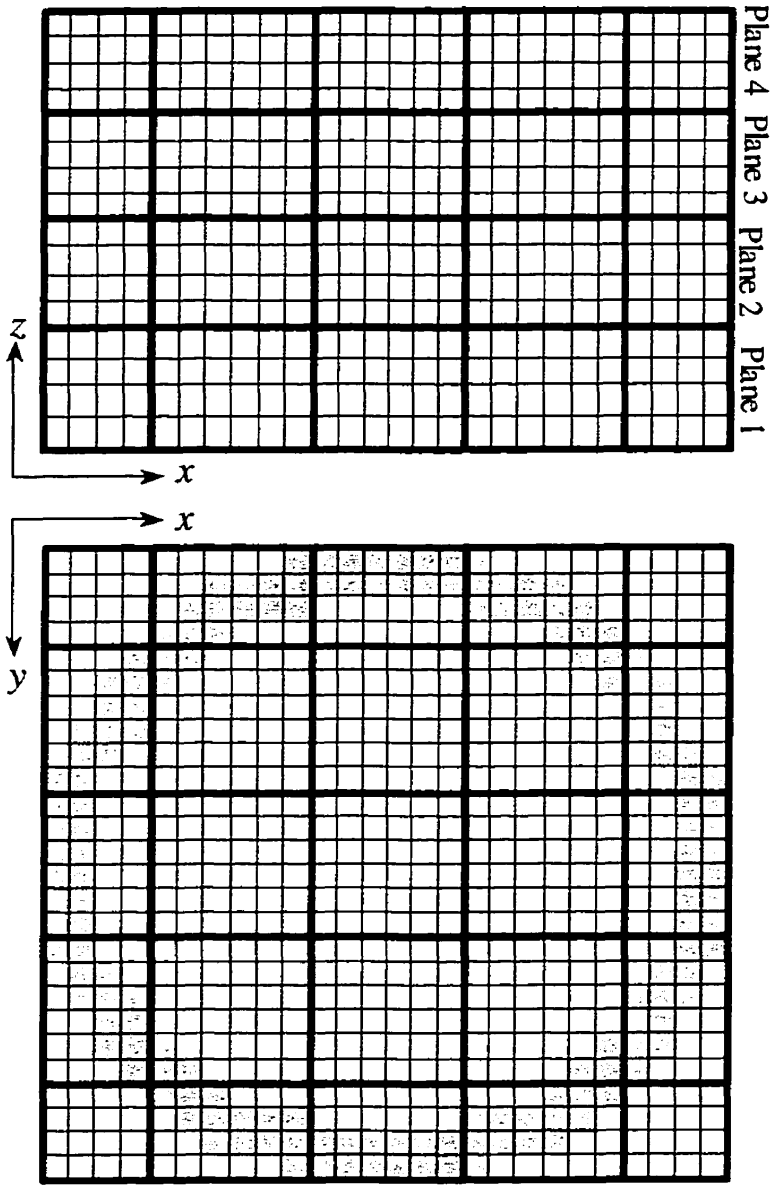

Figure 3.4: Coarse representation of reactor with 5 x 5 x 4 grids

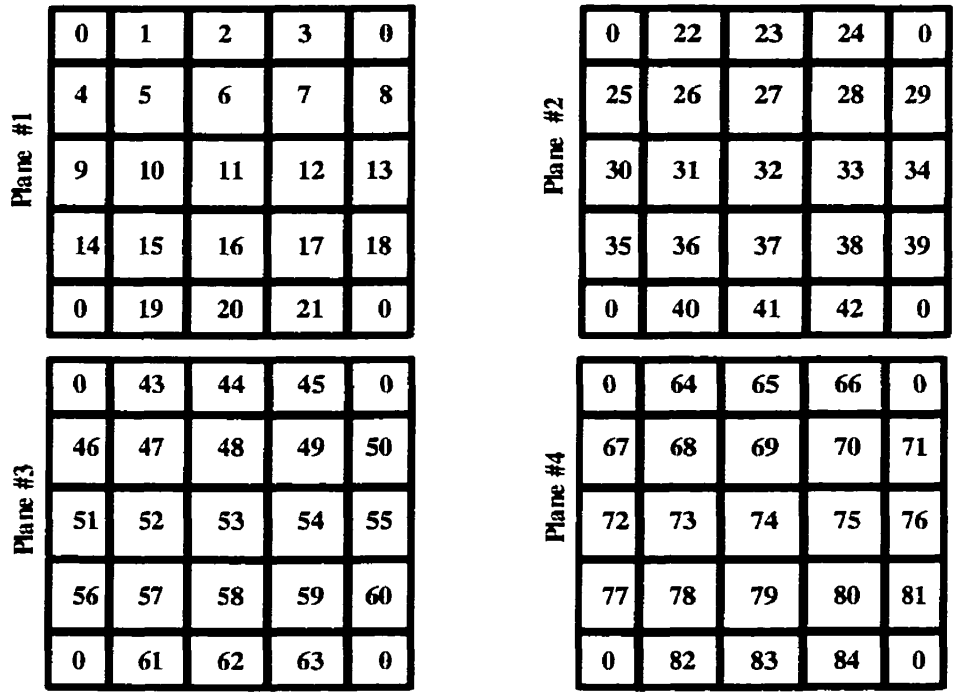

Figure 3.5: Region assignments for the case with 5 x 5 x 4 coarse grids

Thus during the remainder of this chapter, all numerical tests will be performed only for one case, that is, the default coarse configuration with 5 x 5 x 4 grids in the *x*-, *y*- and *z*-directions (figure 3.4). Region assignments for the default case are shown in figure 3.5. Using other coarse configurations with different numbers of coarse grids would lead to conclusions similar to those obtained from this default coarse configuration.

3.3 Importance of Discontinuity Factors

One simple way to demonstrate the importance of the discontinuity factors is to force all of them to be equal to unity. Considering relationships (2.9) through (2.12) and (2.15) through (2.17), this actually means that only the spatial integrals of the coarse average neutron reaction rates (fission, scattering, or absorption) are preserved and surface fluxes are continuous at the interfaces of the coarse nodes. The errors due this

hypothesis can be very significant (Figure 3.6, Table 3.2). The reason is that imposing spatially constant flux-weighted diffusion coefficients and cross sections as well as the flux continuity conditions on the interfaces between the coarse nodes cannot preserve the surface integrated currents of all the supernodes (leakage terms are not preserved). Consequently, very large errors in the flux calculations are produced.

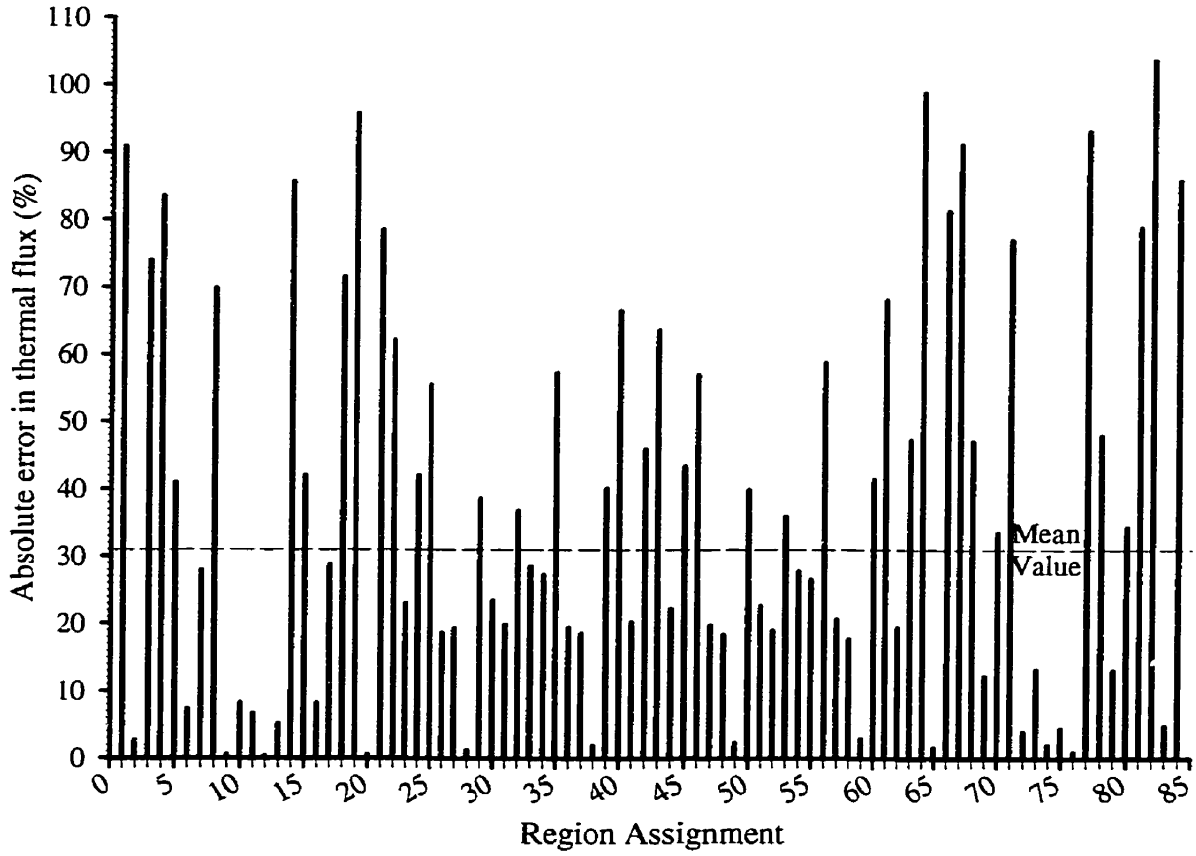

Figure 3.6: Absolute error in thermal flux for different regions of the reactor

3.4 Effect of Device Positions on Equivalence Parameters

In this section, the dependence of equivalence parameters on the device positions will be examined. This would be essential for establishing an equivalence parameter

database (if any). In order to study the dependence of the equivalence parameters on the device positions, the following approach is applied. This procedure can also be used to establish a full static database corresponding to a given coarse grid representation of the reactor core.

- All devices are initially set to their related reference positions,
- The static fine-mesh calculation is performed and the equivalence parameters for the default case (5 x 5 x 4 coarse grids) are calculated and saved,
- The selected device is moved separately and set to a new position,
- The static fine mesh calculation is again performed and the resulting equivalence parameters are recalculated and saved.
- The change in equivalence parameters for all coarse regions is evaluated using following relationship (here given for discontinuity factors):

$$df_{gu}^{\pm}(\%) = \frac{\left(f_{gu}^{\pm}\right)_{\text{new position}} - \left(f_{gu}^{\pm}\right)_{\text{reference position}}}{\left(f_{gu}^{\pm}\right)_{\text{reference position}}} \text{ x } 100 \qquad (3.4)$$

- The results for selected coarse regions are presented and visualized.

It should be noted that the physical interpretation of the results obtained from this procedure is not obvious and does not necessarily lead to a clear and general conclusion. Discontinuity factors are defined as a set of local adjustable parameters to achieve a better homogenization. Their values strongly depend on the fine-flux shape, fine- and coarse-mesh geometry as well as the numerical method used for the solution. It must be noted that discontinuity factors are not representing any physical property (local or integral) of the underlying problem. Thus, trying to find a physical interpretation for the way they are changing is somewhat irrelevant. Nevertheless, a sensitivity analysis for discontinuity factors can be useful from both practical and computational points of view.

3.4.1 Case Study for Adjuster Rods

To carry out numerical tests, adjuster bank #1 (including the center rod and the 4 corner rods, figure 3.7) is selected. Applying the aforementioned procedure, adjuster bank #1 is set to 20 different positions ranging from 95% to 0% of full insertion. For each of the bank positions a full fine calculation is performed. Applying the equivalence theory, all equivalence parameters are evaluated and then the reactor eigenvalue and the coarse flux distribution are calculated. Comparison of the fine and the coarse flux distribution shows that the maximum flux error never exceeds 0.2%. Moreover, using equation (3.4), the resulting equivalence parameters are compared to those of the reference position (100% of full insertion). It can be observed that the maximum changes for different equivalence parameters occur at the different coarse regions, with no predictable pattern. For example, the maximum change in f_{1x}^{-} is located at coarse mesh #26 (figure 3.5), while the maximum change in f_{2x}^{-} takes place at coarse mesh #24 (figure 3.5). Furthermore, maximum changes for other discontinuity factors and cross sections (for different energy groups) take place at different coarse regions. The results for coarse region #33 (figure 3.5) will be presented. Figure 3.8 shows how fast and thermal neutron fluxes are changed due to the gradual withdrawal of adjuster bank #1. Figures 3.9, 3.10 and 3.11 demonstrate the dependence of group discontinuity factors on the position of adjuster bank #1. It can be noted that discontinuity factors of both energy groups have similar tendencies. This is not a general observation for all coarse grids. Figure 3.12 shows the dependence of different cross sections on the device position. Mild changes in the total absorption cross sections (dSIGT1, dSIGT2) as well as a very slight increase in the fast and thermal neutron fluxes (figure 3.8) presumably stand for the fact that none of the adjuster rods passes through coarse region #33. For the coarse regions that are directly affected by passing adjuster rods, the changes are much more significant (for example coarse region #30, #34 etc.). The dependence of diffusion coefficients on the device position is of no importance due to the nature of generalized

equivalence theory. In GET the values of diffusion coefficients are rather arbitrary and discontinuity factors are evaluated to cover for the leakage terms.

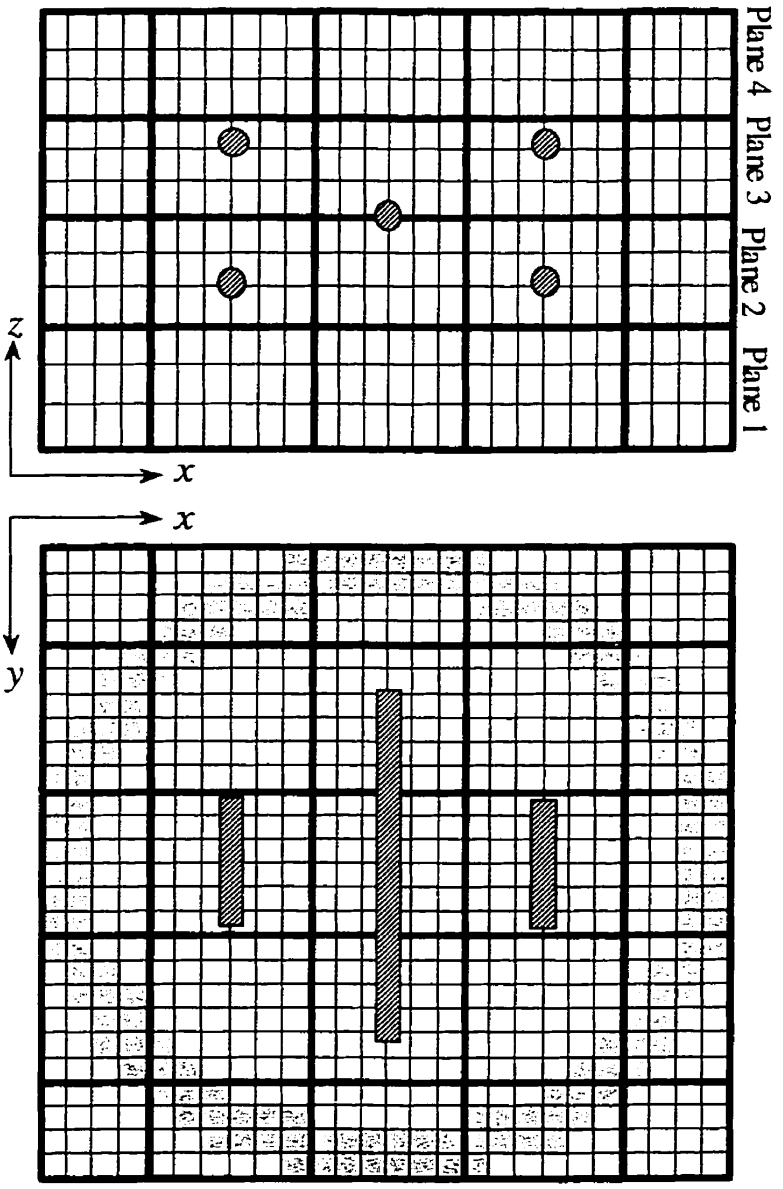

Figure 3.7: Position of adjuster bank #1

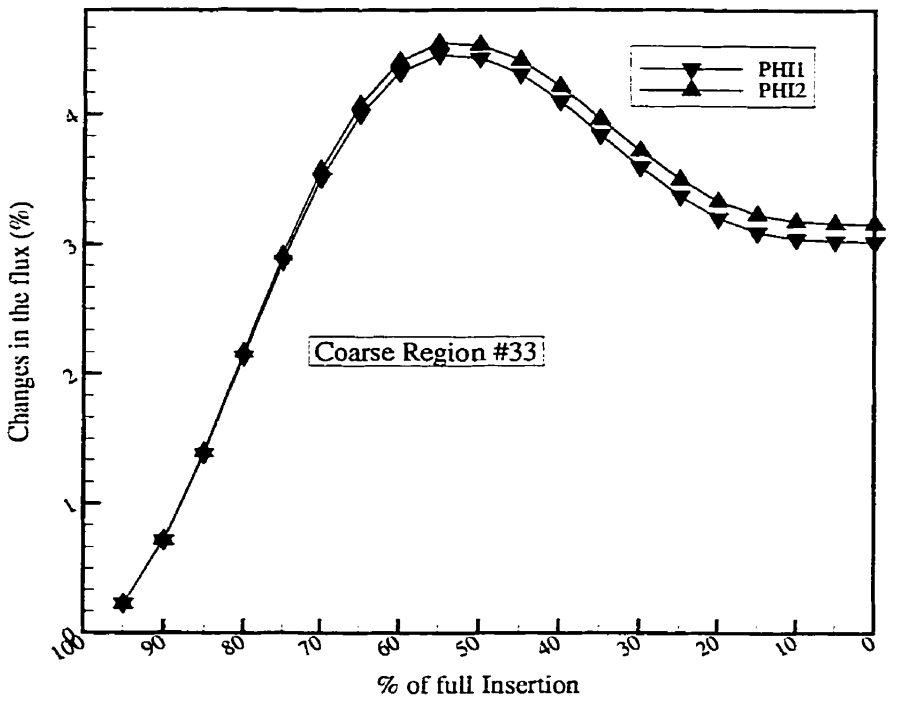

Figure 3.8: Changes in fast and thermal neutron flux, case study AB#1

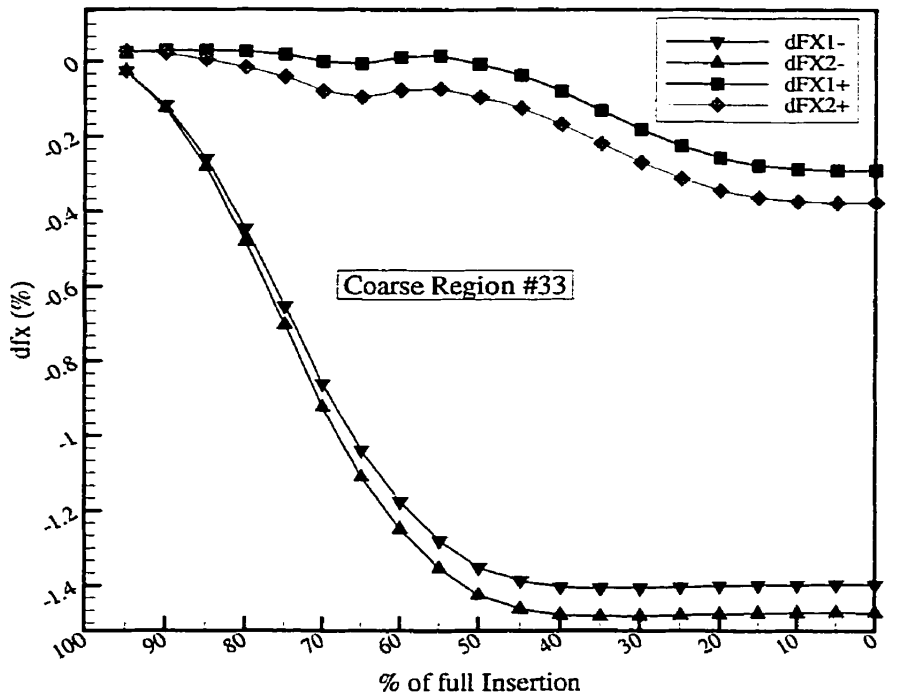

Figure 3.9: Changes in discontinuity factors (direction x), case study: AB#1

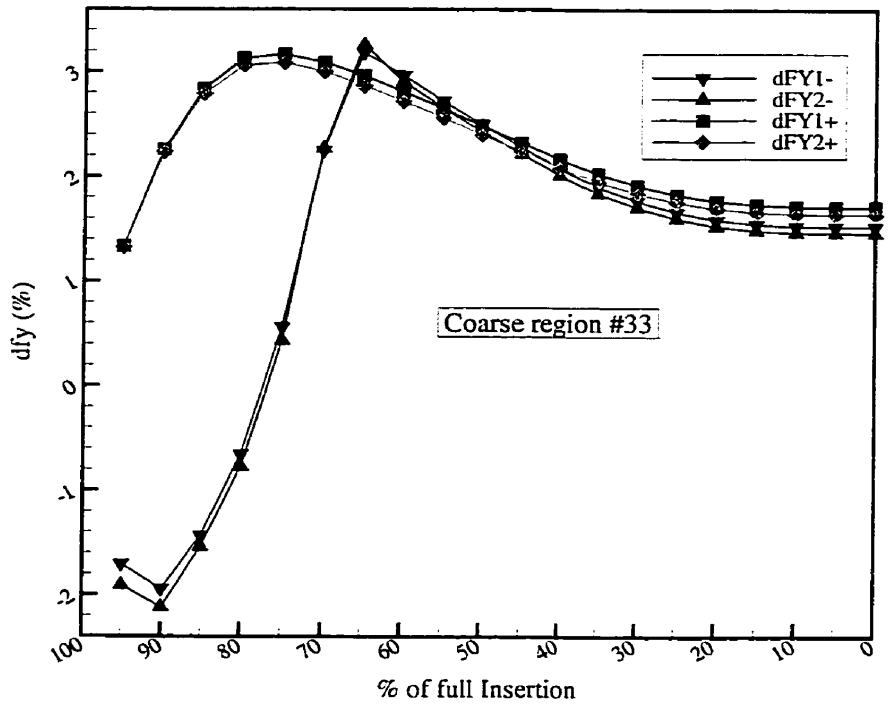

Figure 3.10: Changes in discontinuity factors (direction *y*), case study AB#1

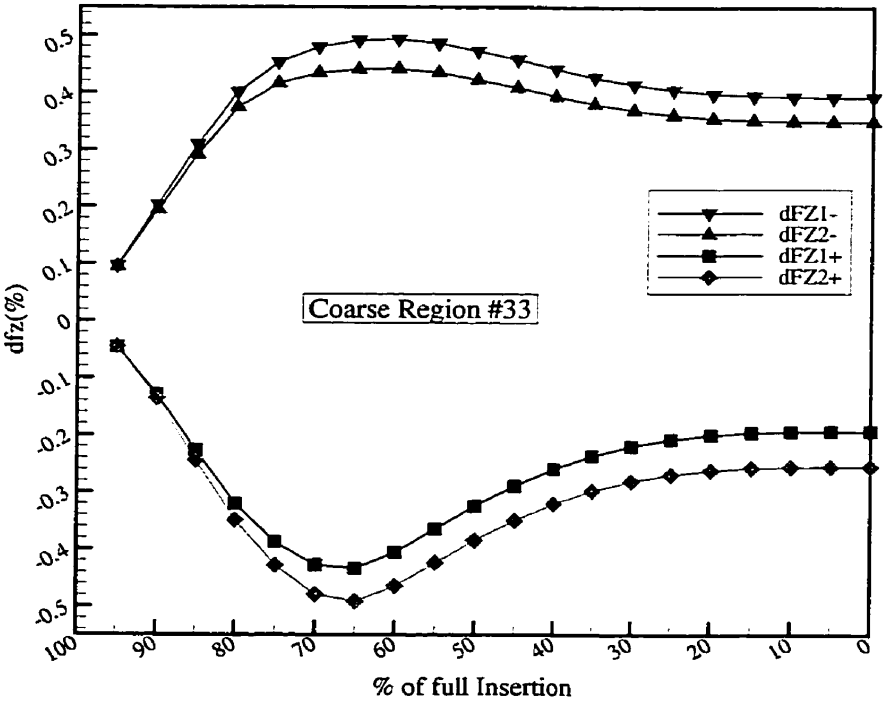

Figure 3.11: Changes in discontinuity factors (direction *z*), case study AB#1

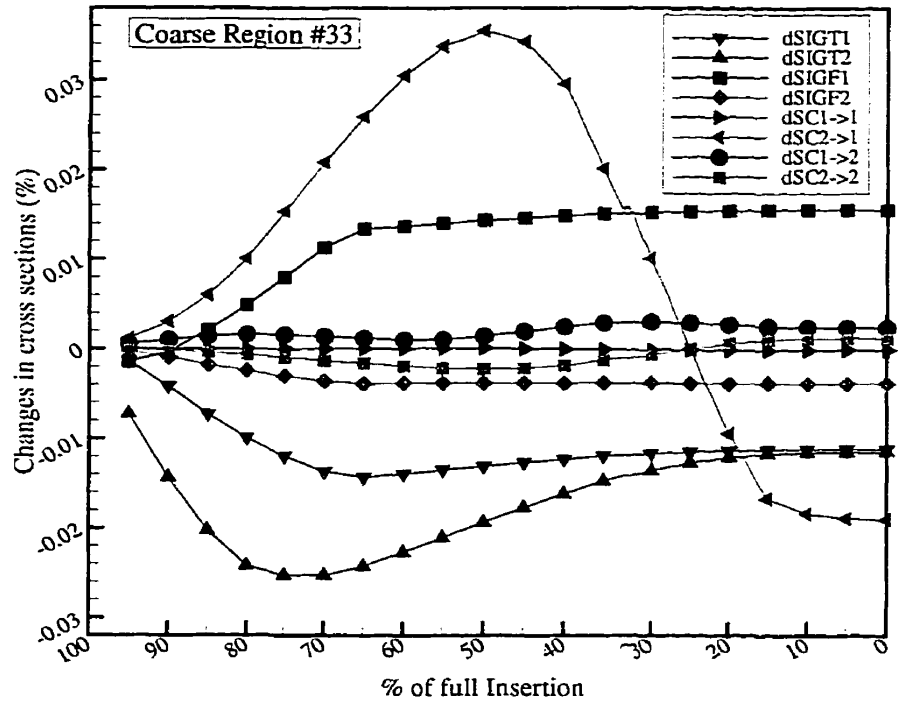

Figure 3.12: Changes in cross sections, case study AB#1

3.4.2 Case Study for Mechanical Control Absorbers

For this section, mechanical-control-absorber bank #1 (two rods in opposite corners, figure 3.13) is selected and set to 20 different positions from 5% to 100% of full insertion. For each position, a fine calculation is performed and then all equivalence parameters are calculated. Comparing the resulting equivalence parameters to those of the reference position (0% of full insertion) once more demonstrates that maximum changes for discontinuity factors and cross sections (for different energy groups) take place at different coarse regions. Here, the results for coarse region #5 (figure 3.5) are presented and visualized. Figure 3.14 shows the dependence of the fast and thermal neutron fluxes on the position of mechanical-control-absorber bank #1. Figures 3.15, 3.16 and 3.17 demonstrate the dependence of the group discontinuity factors on the position of the named device. Finally, figure 3.18 shows how cross sections are

changing with the position of the device. Extensive numerical tests have again demonstrated that no pattern for the dependence of the equivalence parameters on the device position could be found.

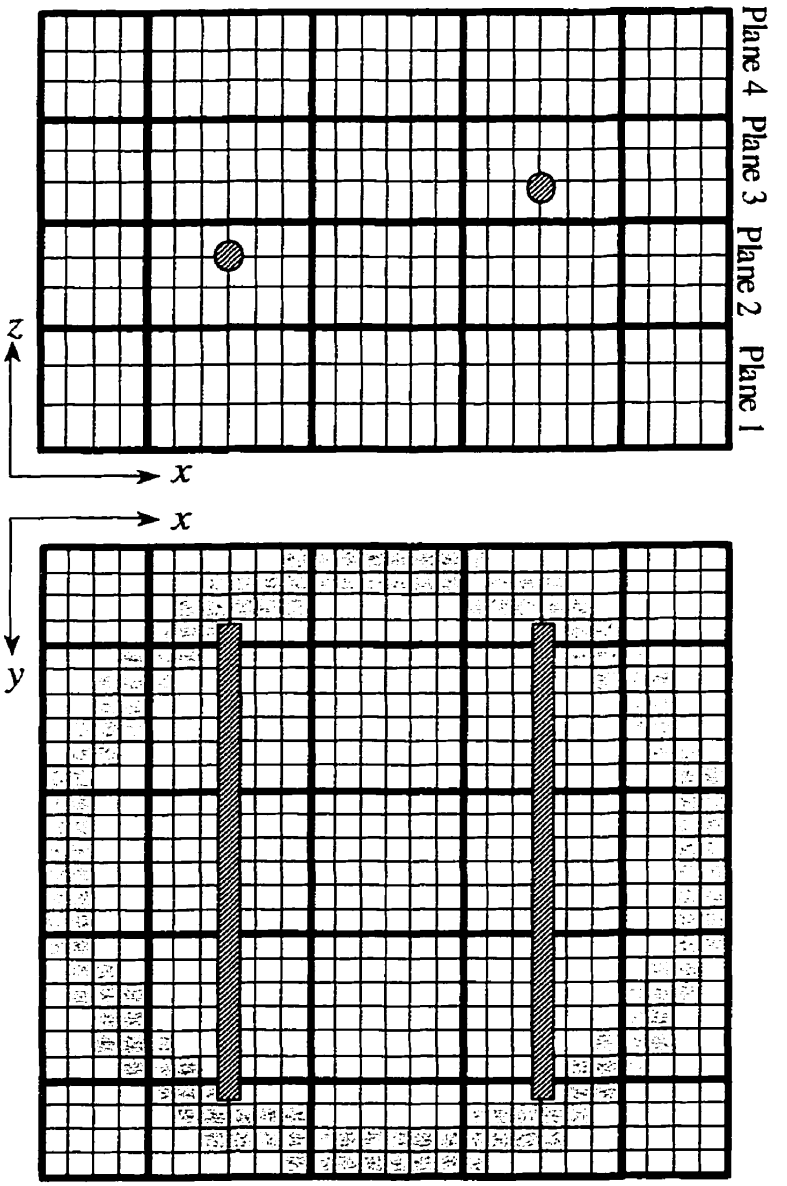

Figure 3.13: Position of mechanical control absorber bank #1

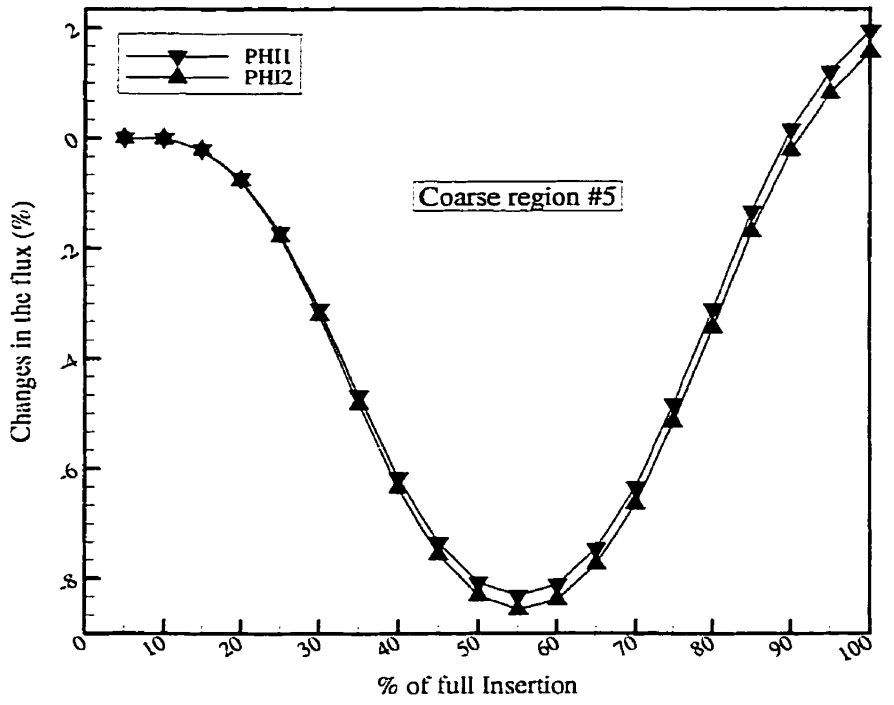

Figure 3.14: Changes in fast and thermal neutron flux, case study MCAB#1

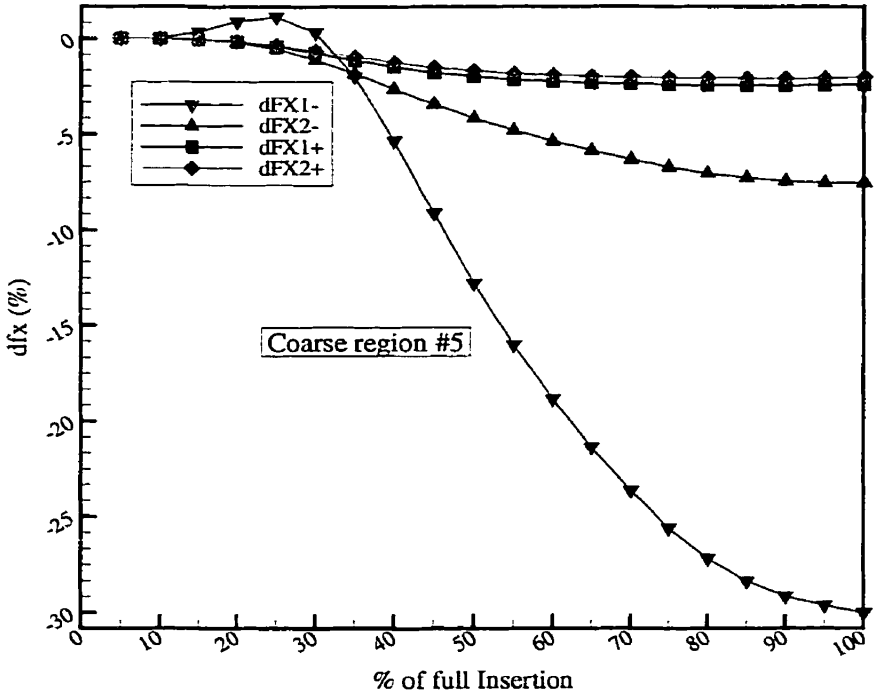

Figure 3.15: Changes in discontinuity factors (direction *x*), case study MCAB#1

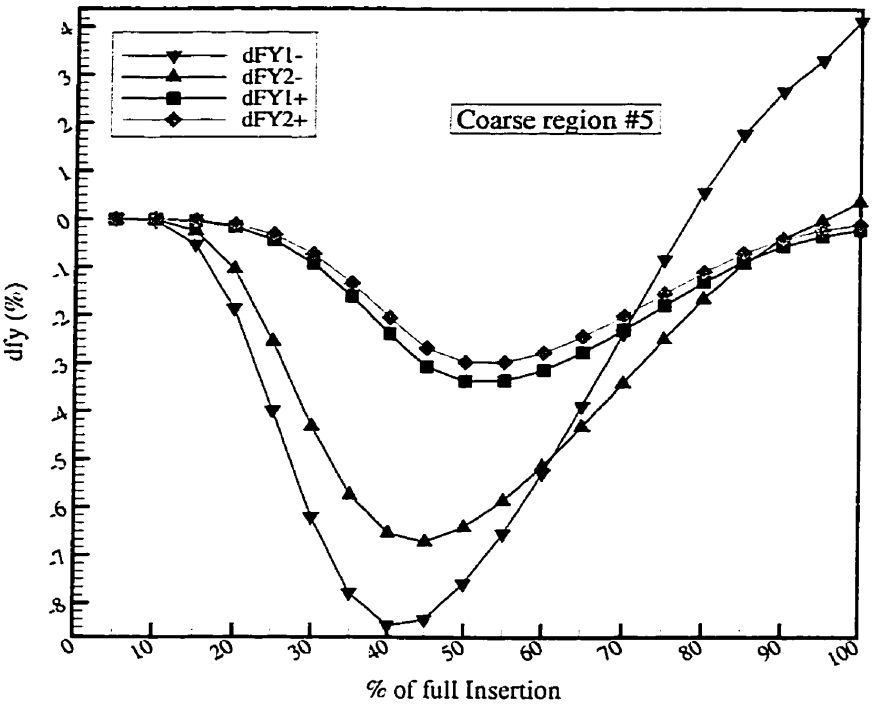

Figure 3.16: Changes in discontinuity factors (direction *y*), case study MCAB#1

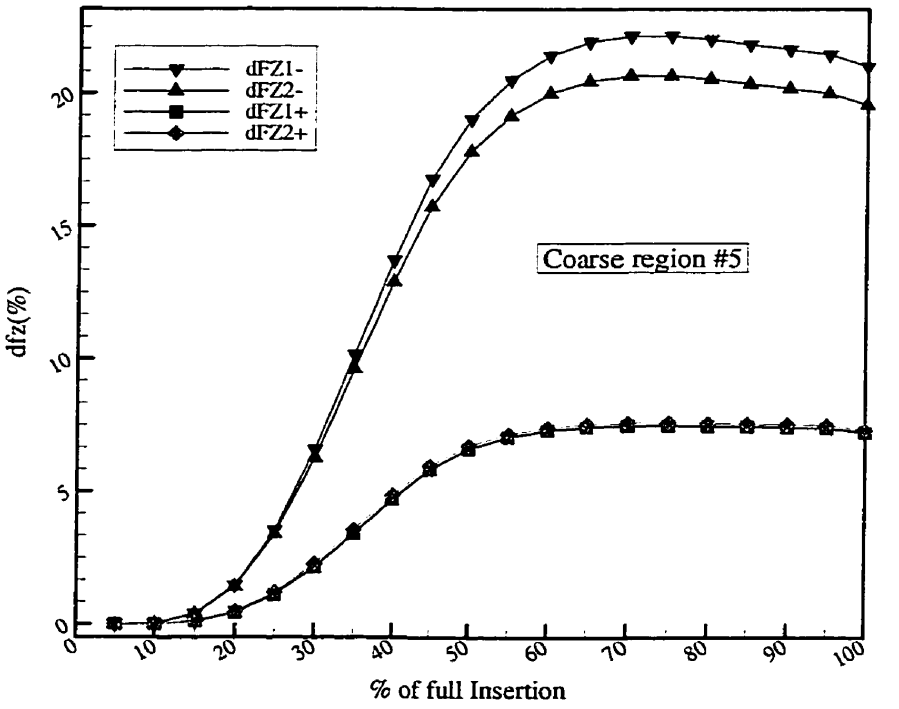

Figure 3.17: Changes in discontinuity factors (direction *z*), case study MCAB#1

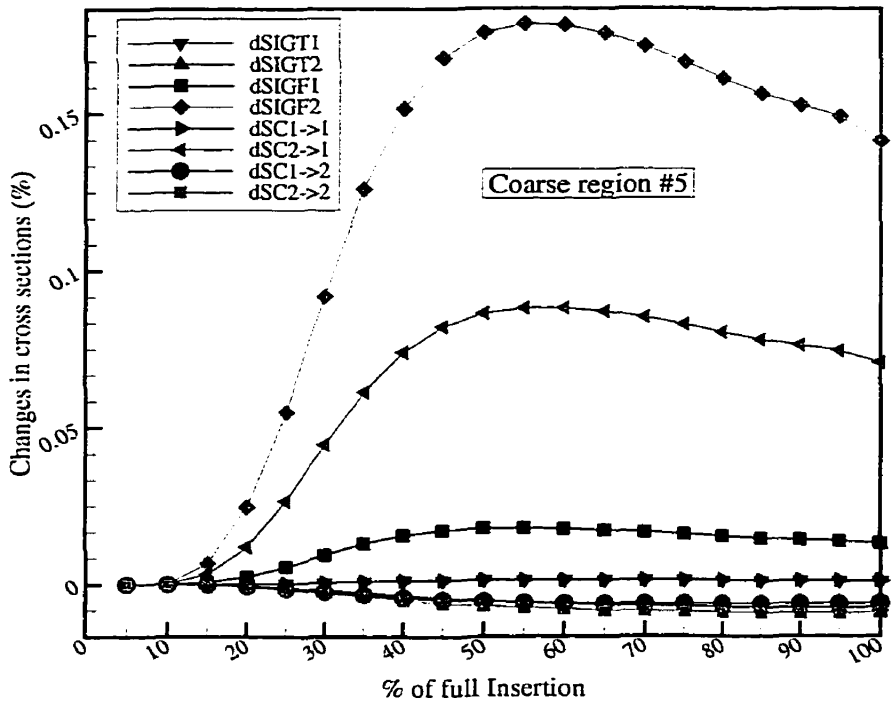

Figure 3.18: Changes in cross sections, case study MCAB#1

3.4.3 Case Study for Liquid Zone Controllers

The case study for liquid zone controller is similar to those for the adjuster rods and the mechanical control absorbers. The liquid zone controller #5 (located at power zone 5, figure 3.19) is chosen and set to 20 different positions from 5% to 100% of full level. For each level, a full fine calculation is performed and then all equivalence parameters are calculated. Comparing the resulting equivalence parameters to those of the reference position (50% of full level) again confirms that maximum changes for discontinuity factors and cross sections (for different energy groups) take place at different coarse regions. Figures 3.20 through 3.24 show the dependence of neutron fluxes, discontinuity factors, and cross sections (coarse region #5, figure 3.5) on the level of the liquid zone controller. Further numerical simulations again demonstrate that no straightforward relationship between the equivalence parameters and the position of the reactivity devices (or mesh cross sections) can be found.

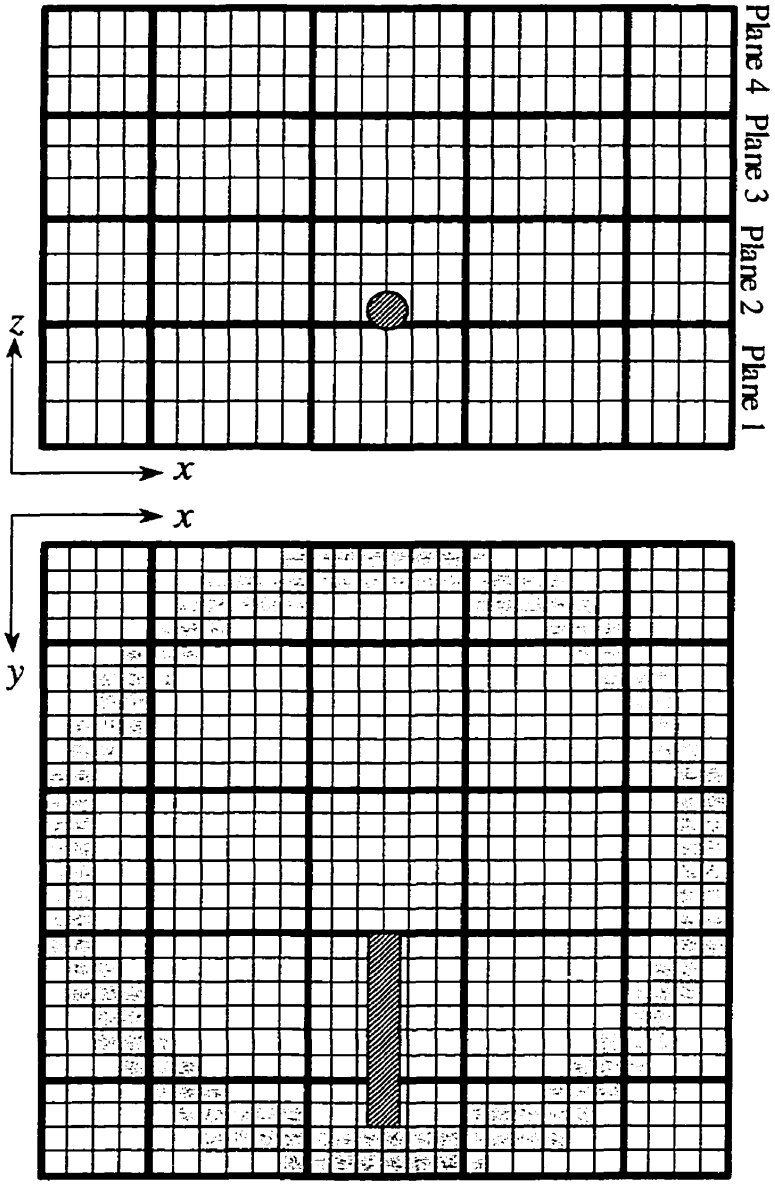

Figure 3.19: Position of liquid zone controller #5

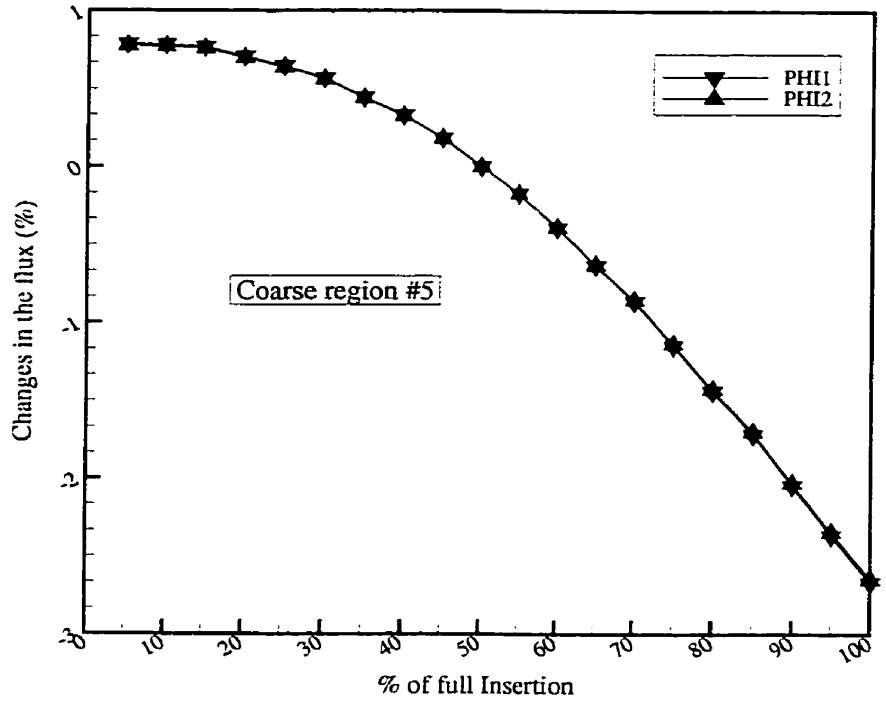

Figure 3.20: Changes in fast and thermal neutron flux, case study LZC

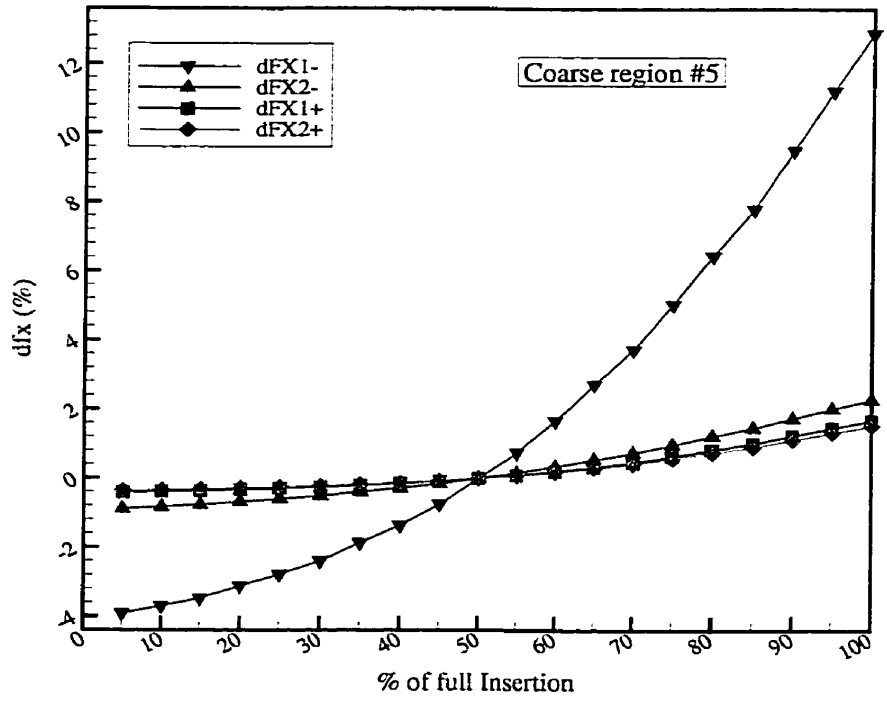

Figure 3.21: Changes in discontinuity factors (direction x), case study LZC

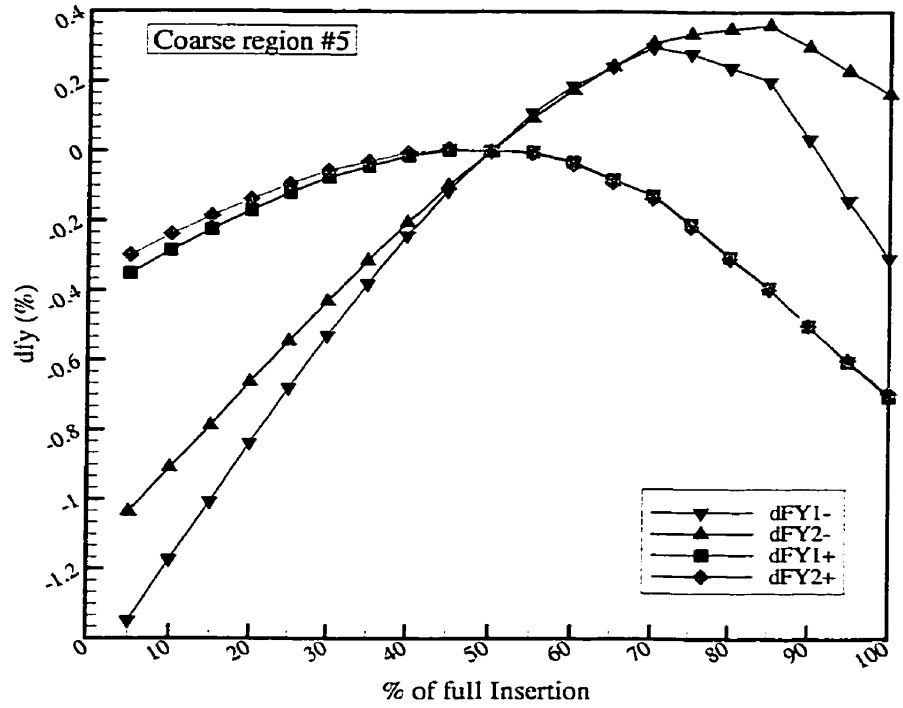

Figure 3.22: Changes in discontinuity factors (direction *y*), case study LZC

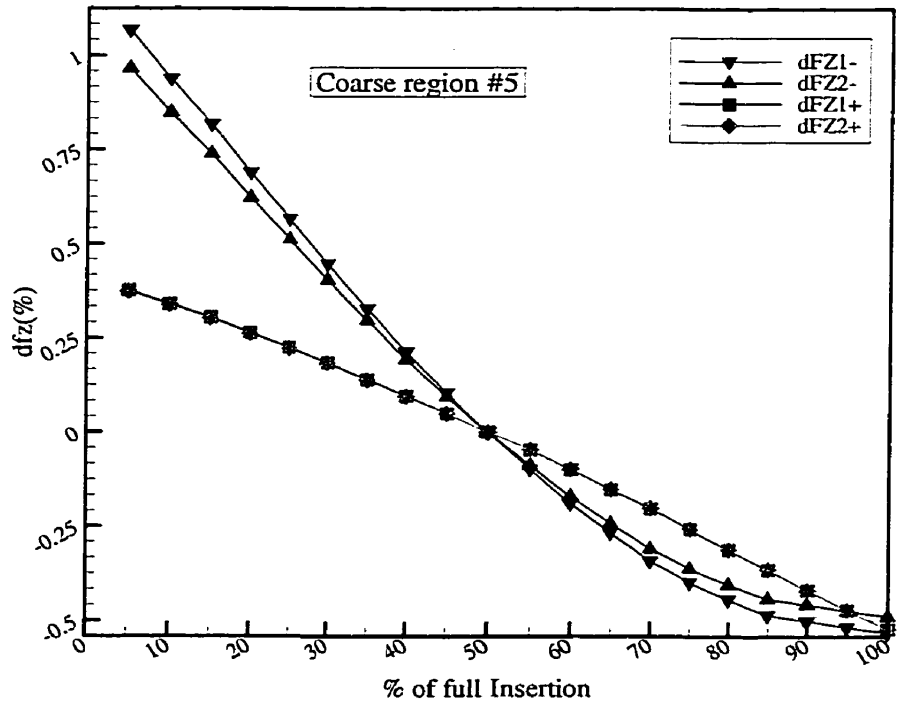

Figure 3.23: Changes in discontinuity factors (direction *z*), case study LZC

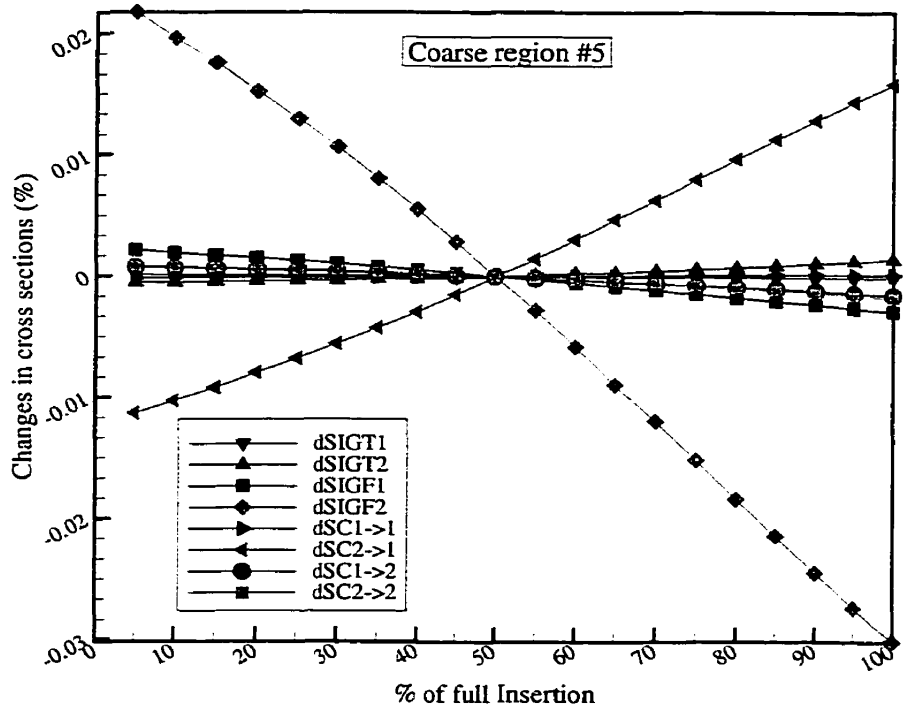

Figure 3.24: Changes in cross sections, case study LZC

3.5 Flux Error Due to the Use of Reference Equivalence Parameters

In the previous section, it has been concluded that: A reusable pattern for the dependence of equivalence parameters on reactivity device positions cannot be established. This fact immediately gives rise to the question: how important will be the errors due to the use of a set of reference equivalence parameters for different device positions? To answer this question a set of numerical simulations based on the following procedure is performed:

- All devices are initially set to their related reference positions,
- The reference equivalence parameters for the default case (5 x 5 x 4 coarse grids) are calculated and saved.
- The selected device is moved separately and set to a new position,
- The static fine mesh calculation for this new position is performed,

- The exact equivalence parameters are calculated and saved,
- The coarse mesh calculation is performed using exact values of cross sections, diffusion coefficients and discontinuity factors,
- The coarse mesh calculation is performed using exact values of discontinuity factors but reference values of cross sections and diffusion coefficients
- The coarse mesh calculation is performed using exact values of cross sections and diffusion coefficients but reference values of discontinuity factors,
- The coarse mesh calculation is performed using reference values of cross sections, diffusion coefficients and discontinuity factors,
- Using relationship (3.3), the average flux error for all cases are calculated

The results for three selected cases are visualized in figure 3.25 through 3.28. Figure 3.25 shows the results for one adjuster rod located in power zones 5 and 6. It is clear that using exact values of the equivalence parameters will result in perfect reproduction of the average coarse fluxes. However, using reference values of the diffusion coefficients, cross sections and discontinuity factors yields a maximum absolute average error equal to 6%, which can be considered as a significant error. Moreover, it can be observed that by the use of reference discontinuity factors and exact diffusion coefficients and cross sections, the error can be limited to only 2%. On the other hand, the combination of exact discontinuity factors and reference cross sections results in the highest flux error (almost 7%). This is naturally due to the fact that in the latter case the adjuster rod displacement is not taken into account, thus the cross sections of the coarse regions do not correspond to the adjuster rod position. In the former case due to the use of exact coarse cross sections, total neutron reaction rates are preserved and only leakage terms are approximated.

The results for the two mechanical-control-absorber cases studied are shown in figures 3.26 and 3.27. In the first case, only one mechanical control absorber (the one passing through power zone 1) is selected to study the error due to the use of reference

equivalence parameters (figure 3.26). While in the second case, two mechanical control absorbers (passing through power zones 1 and 13) are selected (figure 3.27). Finally, figure 3.28 shows the results for a zone liquid controller located at the corner of the reactor. The behavior of the flux error for these cases is similar to those for adjuster rod. Based on these case studies and other numerical tests, which for the sake of brevity are not presented here, the following conclusions are obtained:

1. Using exact values of equivalence parameters would always result in a perfect reproduction of the coarse fluxes.
2. Using the reference equivalence parameters for adjuster rods and mechanical control absorbers would yield considerable amounts of errors in the coarse flux calculations. These errors are much smaller for the liquid zone controllers since their absorption cross sections are much smaller than those of rod adjusters and mechanical control absorbers.
3. Forcing preservations of the total neutron reaction rates (using only exact cross sections for coarse nodes) would significantly reduce the average error in the coarse flux calculations. Nevertheless, for the adjuster rods and mechanical control absorbers, the errors in the coarse flux calculations are still far from being acceptable for practical uses.
4. Using only exact discontinuity factors would give rise to the considerable amounts of error in the coarse flux calculations. This is not surprising since using exact vales of discontinuity factors only preserves the coarse surface currents without actually preserving total neutron reaction rates.
5. No special pattern for the dependence of the average flux error on the device(s) position(s) can be established.
6. The errors in the flux calculations also depend on the coarse grid configuration. Smaller coarse grids will give rise to smaller errors in the flux calculations.

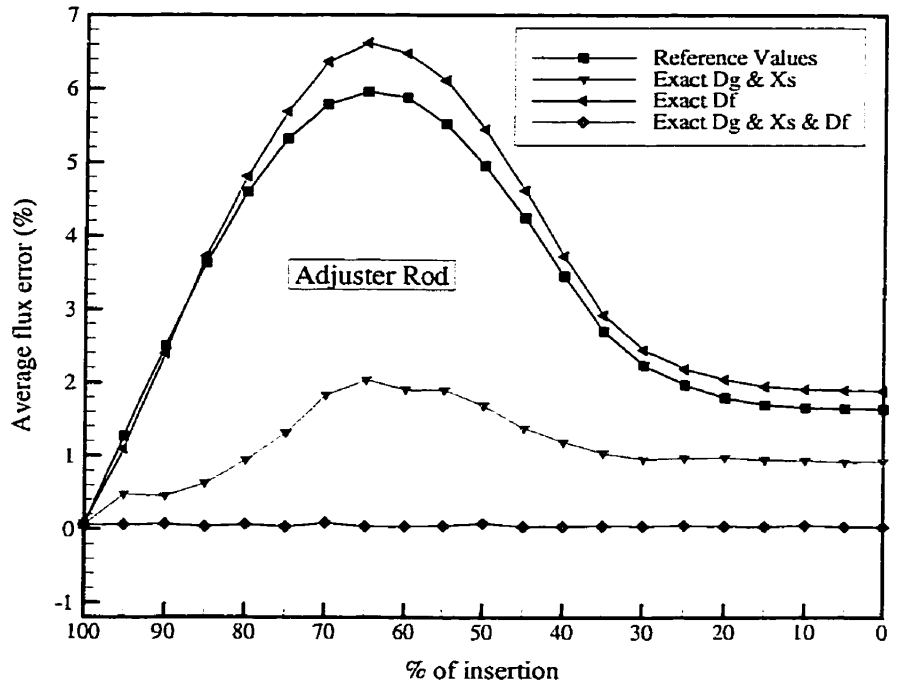

Figure 3.25: Flux error for a rod adjuster

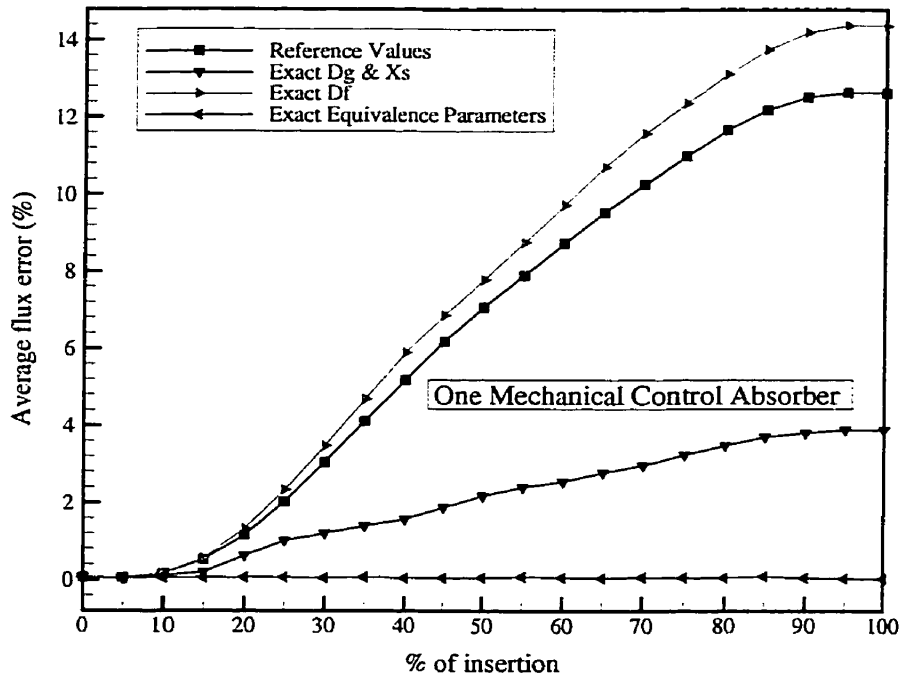

Figure 3.26: Flux error for a mechanical control absorber

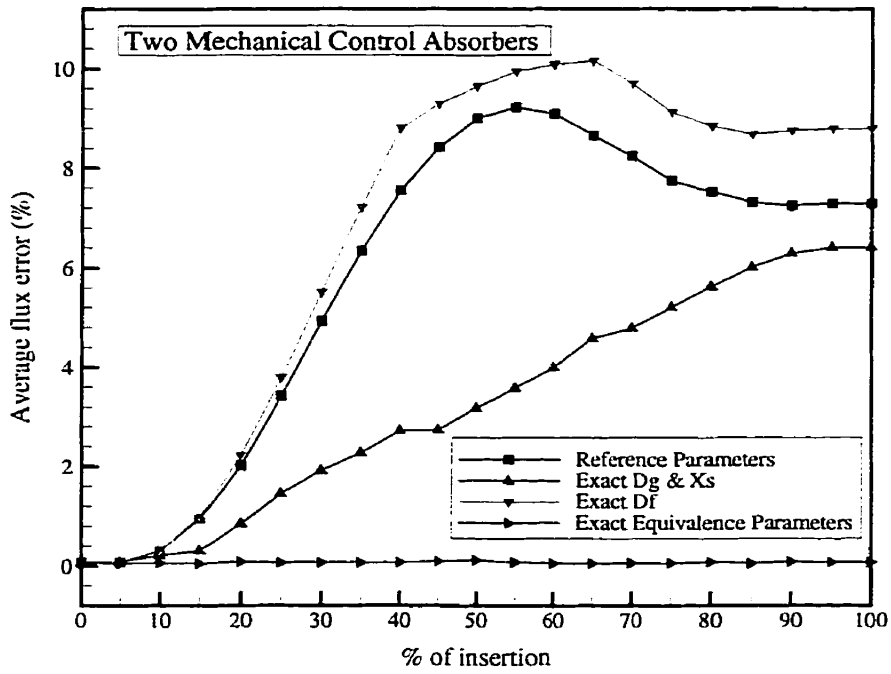

Figure 3.27: Flux error for two mechanical control absorbers

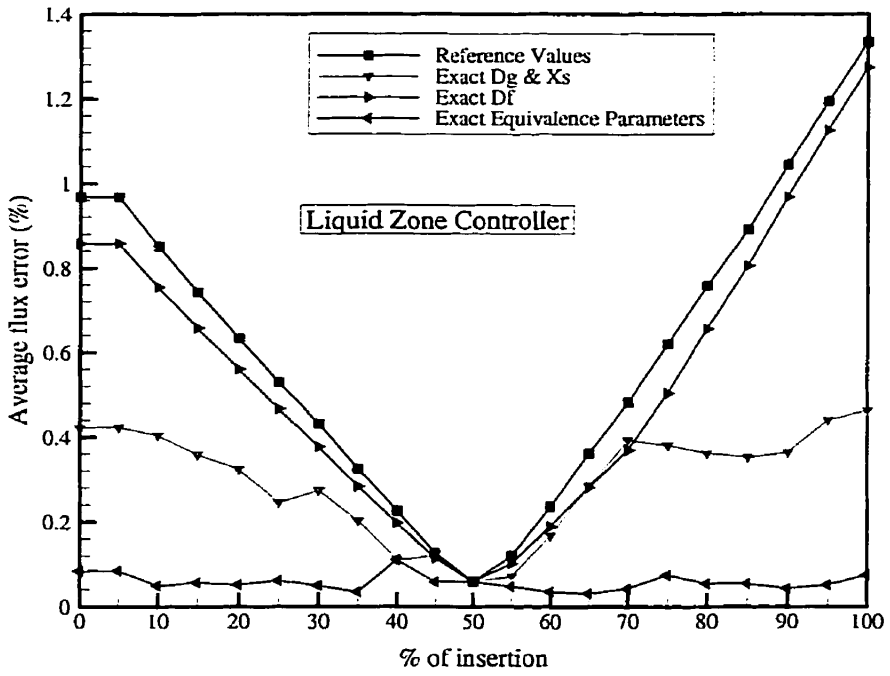

Figure 3.28: Flux error for a liquid zone controller

3.6 Interference Effect

In order to decrease the required number of fine calculations in both static and dynamic calculations, the usual procedure is to establish an equivalence parameter database for each of the reactivity devices (section 2.3.7.1). When more than one reactivity device are present in the reactor core, these tabulated data are interpolated upon the various independent variables to approximate nodal equivalence parameters. To examine the performance of this procedure, the following numerical test has been carried out:

1. The reference equivalence parameters for the default case (5 x 5 x 4 coarse grids) are calculated and saved.
2. Two mechanical control absorbers (two rods in opposite corners) are selected,
3. Each of these rods is moved separately and set to a new position. A static fine mesh calculation is then performed, and exact equivalence parameters are calculated and saved,
4. Now, both rods are simultaneously moved and set to the new positions. The static fine mesh calculation is performed, and exact equivalence parameters are calculated and saved,
5. The coarse-mesh calculation is performed using interpolated values of equivalence parameters (obtained from step 3),
6. The coarse-mesh calculation is performed using exact values of equivalence parameters, (obtained from step 4)
7. The results from steps 5 and 6 (for selected coarse regions) are compared and visualized.

Figure 3.29 shows the significant errors in the thermal flux calculations due to the use of interpolated values of discontinuity factors and/or cross sections for coarse region #36 (figure 3.5). These are predictable results since the values of equivalence parameters strongly depend on the flux shape and the presence of more than one reactivity device in the reactor core causes complicated flux distortions, which are not

considered during the database generation (here step 3). Thus, these flux distortions (known as interference effect) cannot be taken into account by interpolation or superposition of the database values. As a result, the interpolated equivalence parameters are inexact and using them results in the significant errors observed in the flux calculations. Based on extensive numerical tests, the following conclusions are obtained:

1. Since the number of the reactivity devices is substantial, considering all possible cases of devices positions for generating database is not practical.
2. Since the values of equivalence parameters also depend on the coarse geometry configuration, producing a database for all possible coarse geometry configurations is not manageable.
3. The relationship between equivalence parameters and flux shape are strongly non-linear, thus simple interpolation or superposition of database values cannot produce acceptable estimates for the values of equivalence parameters.
4. The coarse flux calculations are very sensitive to the values of equivalence parameters, thus inexact values of equivalence parameters (obtained from a database) could yield significant errors in the flux calculations.

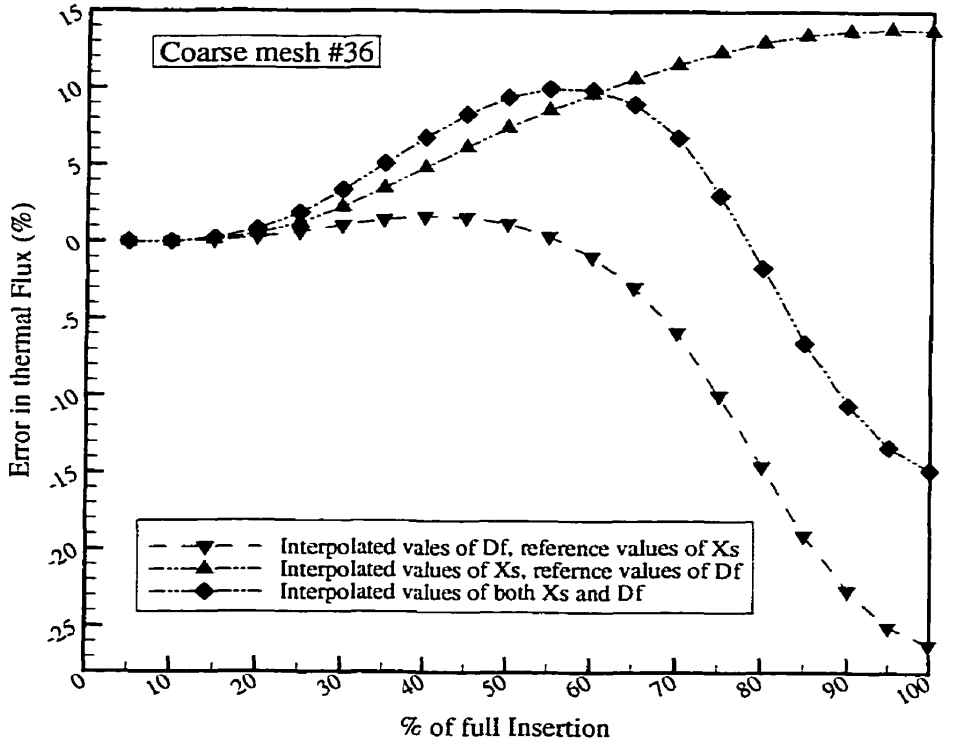

Figure 3.29: Error due to the use of interpolated values of equivalence parameters

3.7 Effect of Xenon Load on Equivalence Parameters

This section is aimed at the study of the effect of xenon load in the values of equivalence parameters. To study this effect, the following numerical simulation has been carried out:

1. All devices are initially set to their reference positions,
2. The static fine mesh calculation without xenon load is performed,
3. The reference equivalence parameters for this case (without xenon) are calculated and saved,
4. The static fine mesh calculation with xenon load is performed,
5. The reference equivalence parameters for this case (with xenon) are calculated and saved,
6. Two sets of discontinuity factors are compared using the following relationship:

$$df_{gu}^{\pm}(\%) = \mathrm{ABS}\left(\frac{\left(f_{gu}^{\pm}\right)_{\text{with xenon}} - \left(f_{gu}^{\pm}\right)_{\text{without xenon}}}{\left(f_{gu}^{\pm}\right)_{\text{without xenon}}} \right) \text{x } 100 \qquad (3.5)$$

Changes in the fast and thermal neutron fluxes due to the xenon load are visualized in figures 3.30 and 3.31. It can be observed that except for two regions (25 and 29) the change in thermal flux is less than 4%. Changes in the group discontinuity factors (in the x-direction) and thermal absorption cross section are presented in figures 3.32 through 3.36. The results for the other equivalence parameters are not presented here since they do not lead to a clear pattern for the changes in the equivalence parameters due to the presence of xenon. What is clear is the fact that due to the strong dependence of the equivalence parameters on the flux shape, the changes in the equivalence parameters due to xenon load are not negligible. Thus, it is expected that the use of constant equivalence parameters during long transients such as those involving xenon cannot guarantee the precision of the results. Consequently, they should be updated as often as necessary.

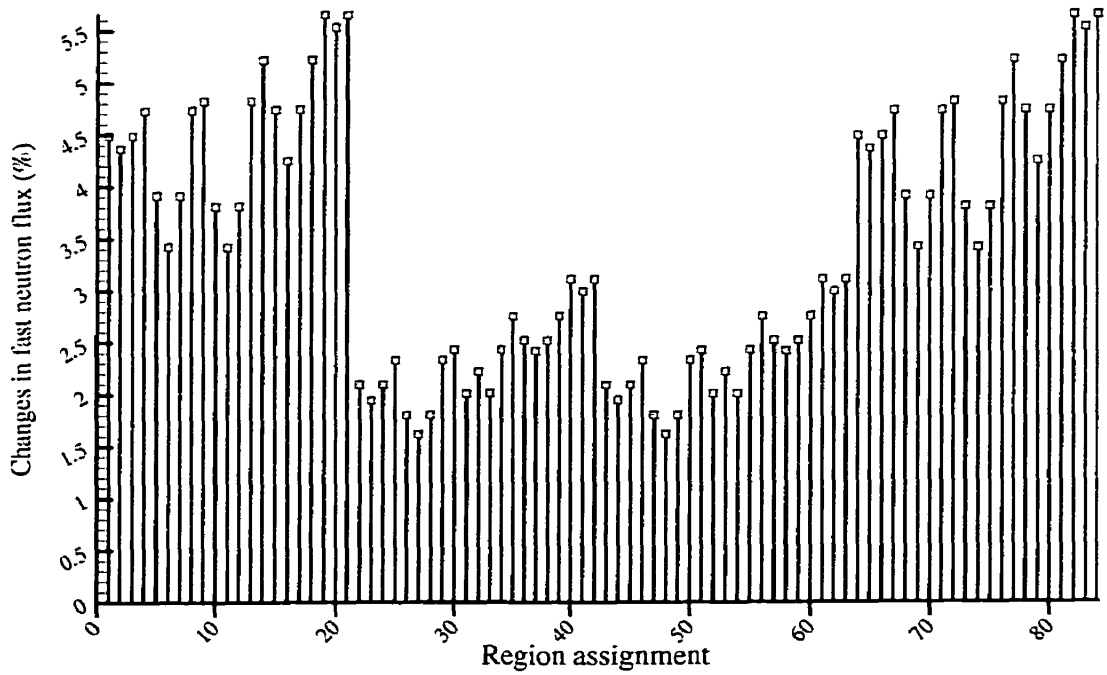

Figure 3.30: Changes in the fast neutron flux due to xenon load

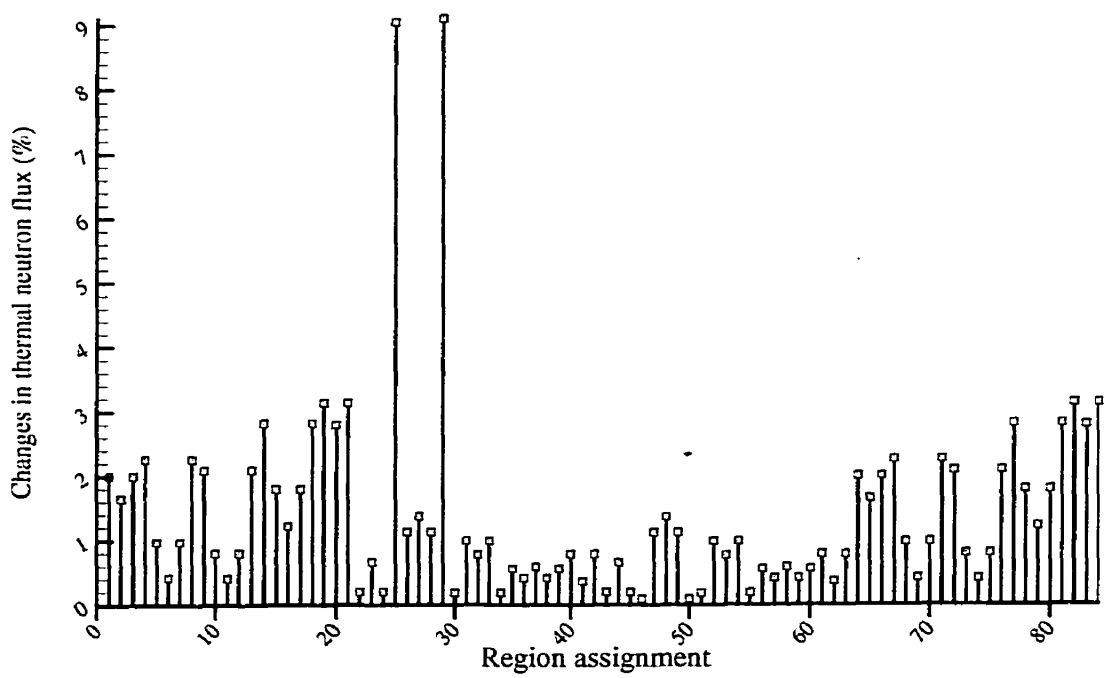

Figure 3.31: Changes in the thermal neutron flux due to xenon load

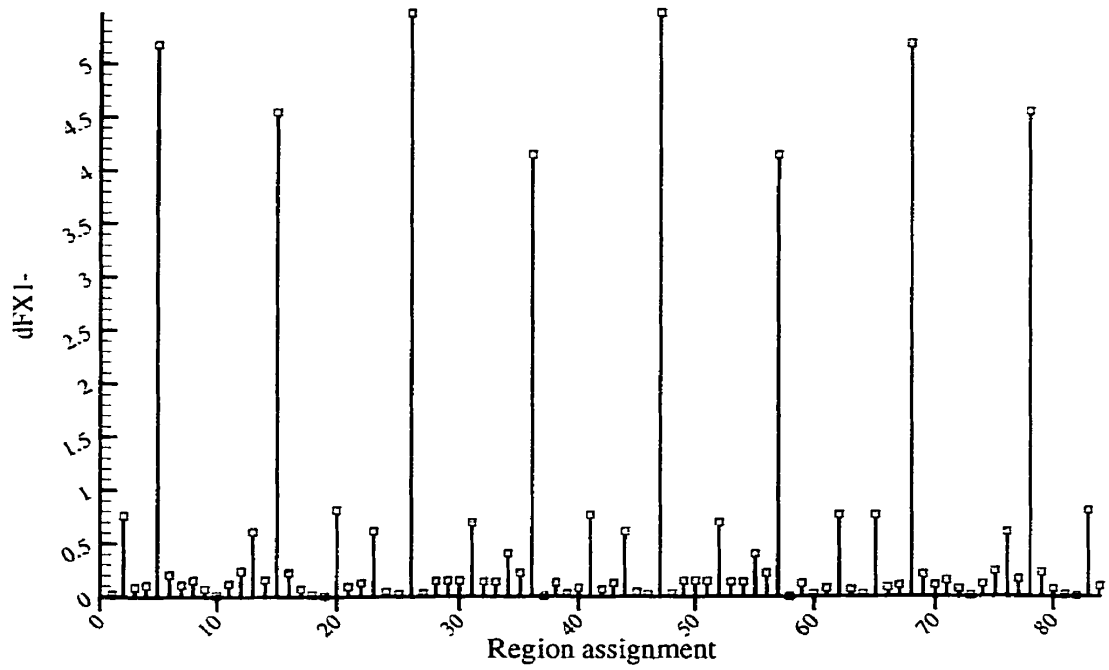

Figure 3.32: Changes in f_{x1}^{-} for different regions of the reactor due to xenon load

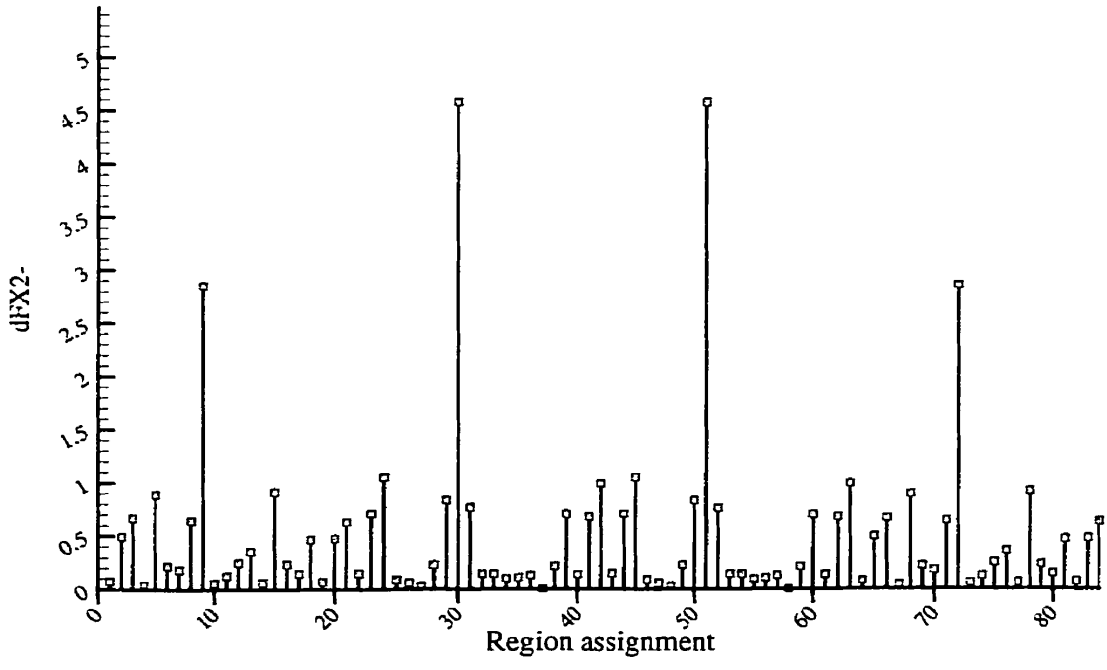

Figure 3.33: Changes in f_{x2}^{-} for different regions of the reactor due to xenon load

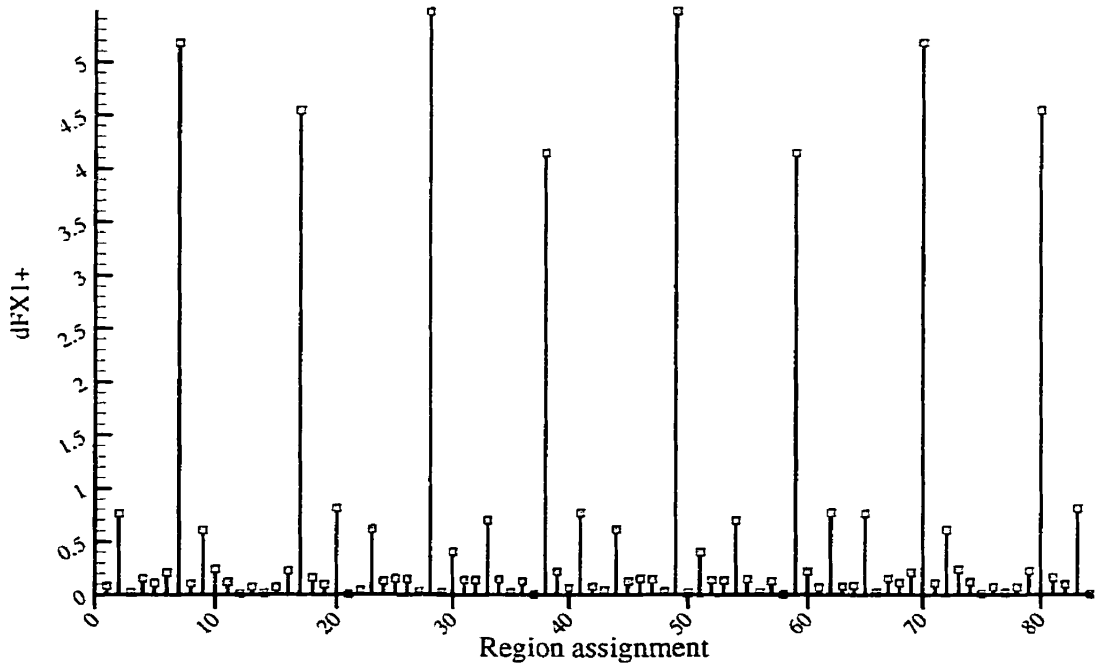

Figure 3.34: Changes in f_{x1}^{+} for different regions of the reactor due to xenon load

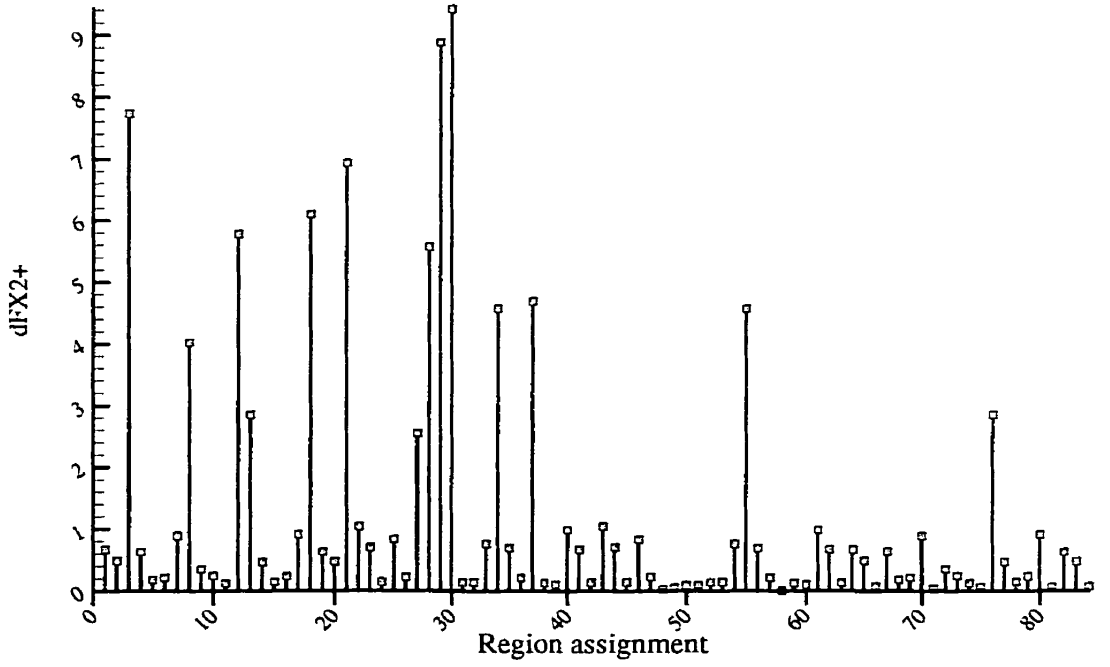

Figure 3.35: Changes in f_{x2}^{+} for different regions of the reactor due to xenon load

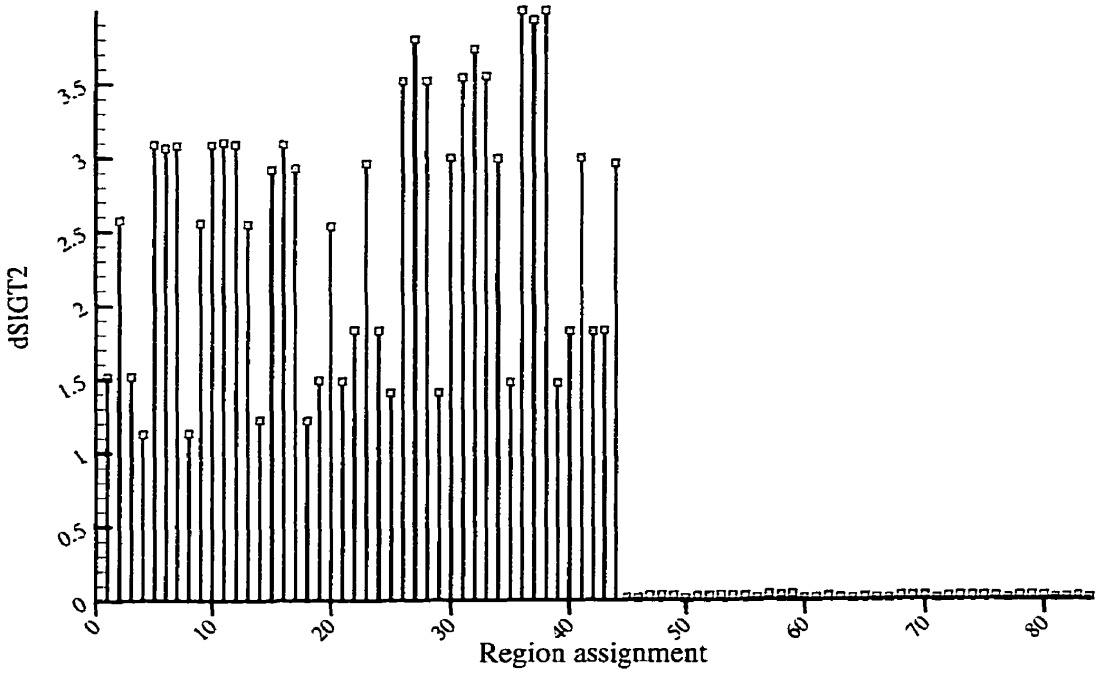

Figure 3.36: Changes in total thermal absorption cross section due to the xenon load

CHAPTER 4

NUMERICAL RESULTS: DYNAMIC CASES

In this chapter, the numerical results obtained from hierarchical nodal kinetics for transient simulations in a CANDU-6 reactor are presented. The results are compared to those obtained from direct and improved quasi-static methods. During the comparison procedure, emphasis will be placed on both the precision of the results and the speed of calculations. Three transient scenarios have been selected. In the first two, the responses of the reactor regulating system to substantial perturbations are simulated. The third scenario is a simplified simulation of a LOCA (Loss of Coolant Accident).

4.1 Methodology

To investigate the merits of a new numerical scheme, the first step is to define the set of parameters that will be used to quantify the performance of that method. The quantified parameters for a specific method will be compared to those obtained from the other methods, and consequently the performance of that method will be comparatively evaluated. In reactor kinetics, it is accepted that the performance of a numerical scheme essentially depends on two factors: first, the accuracy of the solution resulting from the implementation of that method and second, the speed of calculations involved in the simulation procedure. Additional factors, such as, the stability of the numerical scheme, must also be carefully taken into account. In this section, the criteria that will be used to evaluate the performance of hierarchical nodal kinetics will be identified.

4.1.1 Accuracy of the Solution

The accuracy of a numerical algorithm is defined as the difference between the true solution and the solution obtained from the implementation of that algorithm. Among other things, accuracy depends on both the space and the time truncation errors of the

numerical method. In the absence of the true solution, the accuracy of a method can be determined by comparison of the solution obtained from the underlying method to the reference solution. The reference solution is generally determined from a more precise numerical procedure with well-known truncation-error behavior. The comparison procedure requires definition of the error terms based on either local or integral properties of the solution.

In the present work, the comparison procedure primarily relies on the time-dependent error in the relative total power at time t, which is defined as follows:

$$\mathrm{E_P}(t) = \frac{p_{\mathrm{HNK}}(t) - p_{\mathrm{REF}}(t)}{p_{\mathrm{REF}}(t)} * 100 \tag{4.1}$$

where $p_{\mathrm{HNK}}(t)$ represents the relative total power obtained from the hierarchical nodal kinetics and $p_{\mathrm{REF}}(t)$ is the relative total power given by the reference solution. The relative total power is obtained with the help of the following relationship:

$$p_{\mathrm{Total}}(t) = \frac{\mathrm{P}(t)}{\mathrm{P_0}} = \frac{\sum_{g=1}^{G}\sum_{n=1}^{N} \Phi_g^{i,j,k}(t)(HF)_g^{i,j,k} V^{i,j,k}}{\sum_{g=1}^{G}\sum_{n=1}^{N} \Phi_g^{i,j,k}(0)(HF)_g^{i,j,k} V^{i,j,k}} \tag{4.2}$$

where $(HF)_g^{i,j,k}$ represent space- and energy-dependent conversion factors (Table I.2) and $\mathrm{P_0}$ stands for the total power of the critical reactor.

The comparison of two time-dependent solutions can also be carried out using time- and space- dependent error in the nodal group flux defined by:

$$e_g^{i,j,k}(t) = \frac{\left[\Phi_g^{i,j,k}(t)\right]_{\mathrm{HNK}} - \left[\Phi_g^{i,j,k}(t)\right]_{\mathrm{REF}}}{\left[\Phi_g^{i,j,k}(t)\right]_{\mathrm{REF}}} * 100 \tag{4.3}$$

where $e_g^{i,j,k}(t)$ is the space-, time- and energy-dependent error in the group flux and $\Phi_g^{i,j,k}(t)$ is the nodal group flux at time t. The comparison procedure based on this

definition is particularly enlightening for the type of transient involving very fast and severe changes in the flux shape.

Another integral property, which may be used for the comparison of the two time-dependent solutions, is the value of dynamic reactivity: however, the definition of the error based on the comparison of dynamic reactivity can result in erroneous conclusions. The main reason is the extreme sensitivity of the dynamic reactivity value (particularly for small perturbations) to inherent errors involved in the floating-point calculations. For example, if the value of the dynamic reactivity obtained from a given method is of the order of 10^{-6} and the one given by the reference solution is on the order of 10^{-7}, the resulting relative error is on the order of 1000%. This is clearly an incorrect conclusion since both values are actually representing a dynamic reactivity which is virtually equal to zero (non-perturbed condition). During the present work, no direct comparison based on the dynamic reactivity value is carried out. However, for some test cases, the values of dynamic reactivity are calculated and visualized to somehow quantify the intensity of the prescribed perturbations.

4.1.2 Speed of Calculation

The calculation speed is the second important factor, which is extensively used to evaluate the merits of a numerical scheme. The calculation speed primarily depends on the performance of the computer hardware. However, the speed of execution can also be considerably influenced by additional factors, such as the skill of the programmer, the quality of the compiler, the optimization level, etc. Even whether the corresponding computer code is part of a multi-purpose code or a stand-alone piece of software can significantly affect the speed of the calculations. In general, multi-functional codes involving many features and methods are slower than codes that are merely written to either test a specific method or solve a benchmark problem.

To be as fair as possible, in the present work all transient simulations are carried out using the same computer system, compiler and optimization level. Furthermore, all methods are taking advantage of the same supporting modules for the reactor geometry definition, device configuration, reactor regulating system, etc. Thus, any improvement (or deterioration) in the overall performance is almost solely due to the performance of the numerical scheme implemented in the solver module. In the present work, the improvement (or deterioration) in the speed of the calculations is primarily measured with the help of the following definition:

$$(TP)_{\text{HNK}} = \text{ABS}\left(\frac{(T_{total})_{\text{REF}}}{(T_{total})_{\text{HNK}}} - 1\right) * 100 \tag{4.4}$$

where $(TP)_{\text{HNK}}$ demonstrates the gain (or loss) in the overall performance of the hierarchical nodal kinetics (or any other method), $(T_{total})_{\text{HNK}}$ and $(T_{total})_{\text{REF}}$ are respectively the total CPU times corresponding to the hierarchical nodal kinetics and the reference methods.

An alternative way to compare the speed of calculations is to use only the CPU time related to the solver module. Consequently, the CPU time for the other supporting modules such as device movement, reactor regulating system, updating physical properties etc. are excluded:

$$(\text{PTP})_{\text{HNK}} = \left(\frac{(T_{solver})_{\text{REF}}}{(T_{solver})_{\text{HNK}}} - 1\right) * 100 \tag{4.5}$$

where $(PTP)_{\text{HNK}}$ is the gain (or loss) in the solver performance (for hierarchical nodal kinetics or any other method), $(T_{solver})_{\text{HNK}}$ and $(T_{solver})_{\text{REF}}$ are respectively the CPU times corresponding to the solver modules of the hierarchical nodal kinetics and the reference method. This is a less attractive method for comparing the speed of calculations since from a practical point of view the overall time performance is much more important. However, during the development of a computer code, time profiling of the modules

involved permits the more time-consuming parts of the computer code to be redesigned or optimized to a greater degree.

In the present work, whenever possible, the gain in the solver performance will be presented. Thus, emphasis will remain primarily on the gain (or loss) in the overall performance.

4.1.3 Stability of the Method

A numerical scheme is stable if small perturbations in the boundary conditions or computer round-off errors do not lead to significant changes in the solution. The stability properties of different numerical methods implemented in the hierarchical nodal kinetics (mesh-centered finite difference and Runge-Kutta methods) are individually well known. However, the stability of the combination of these methods forming the hierarchical nodal kinetics must also be investigated. The major reasons are the presence of homogenization/reconstruction procedures and xenon load that might affect the stability of the procedure as a whole. One practical way of studying the stability of a numerical scheme is to perform a *do-nothing* transient test. In this test, the space and time integrators are initiated by a steady-state solution. The solution advances in time without introducing any perturbation. Evidently after many seconds, no significant change in the solution must be observed. This test is adopted and performed using the following procedure:

- Different sets of values for fine, coarse, and point kinetics time steps are chosen. These values are similar to those which will be used for the principal transient simulations.
- The time and space integrators are initiated by the solution of the default reactor configuration given in chapter 3.
- The transient lasts for 900 seconds (the maximum simulation time for the principal transients presented in this work).
- For all test cases, the xenon load is taken into account.

- For each set of time steps, two simulations are performed. In the first one, the reactor regulating system is active, while in the second simulation the reactor regulating system is disabled. Furthermore, a minimum number of iterations (20 iterations) to both fine and coarse solvers is imposed to prevent an immediate convergence and consequently to allow for the introduction of round-off errors into the iteration procedures.

Figure 4.1 shows the results obtained for one of the test cases. In this case, the values of time steps for fine-, coarse- and point kinetics levels are respectively set to 5.0, 1.0, 0.25 seconds. The results corresponding to the do-nothing transient tests of the direct and improved quasi-static methods are also included. It can be observed that when the reactor regulating system is active, all three methods are perfectly stable. This means that either no bounded errors in the reactor solution are diffused or the errors are compensated by the reactor regulating system. To determine which one is the case, the reactor regulating system for the period of the do-nothing transient must be disabled.

The results obtained from disabling the reactor regulating system show that small amounts of error in the reactor solutions are actually propagated. For the hierarchical nodal kinetics, the amount of error propagated (~ 1.5%) is almost five times larger than those propagated in the direct and quasi-static methods (~ 0.3%). This difference can be largely attributed to significant sensitivity of the coarse mesh calculations to the values of equivalence parameters. The amount of floating-point error caused by the re-evaluation of equivalence parameters results in relatively larger amounts of error in the coarse flux distribution. Numerous additional tests also confirm that due to the utilization of homogenization and reconstruction procedures in the hierarchical nodal kinetics, the amount of bounded error produced by do-nothing transient tests is relatively greater than those produced by the direct and improved quasi-static methods. However, these errors normally remain within a reasonable tolerance range.

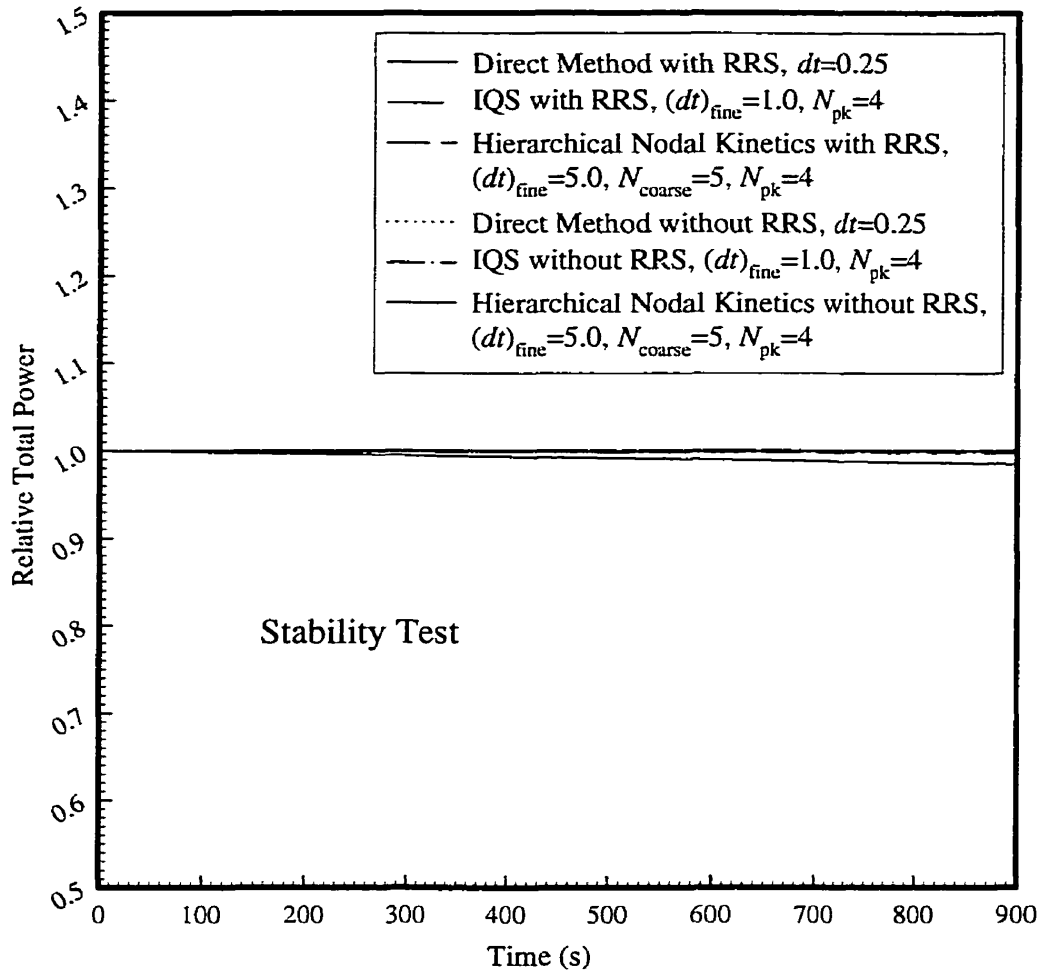

Figure 4.1: Stability test for hierarchical nodal kinetics

4.2 Input Parameters for Hierarchical Nodal Kinetics

Any transient simulation using hierarchical nodal kinetics is initially characterized by two sets of user-defined parameters: time steps and coarse-mesh configuration. The choice of these parameters can considerably affect the overall performance of the hierarchical nodal kinetics method, particularly for transient simulations involving the reactor regulating system. The main reason is that the reactor solutions obtained from the coarse-level calculations are average values over big regions of the reactor. Consequently, the correctness of the detector responses obtained and evidently reactor-

regulating-system reaction strongly depends on how well these average solutions are reconstructed over the fine regions.

In hierarchical nodal kinetics, better accuracy of detector responses can generally be achieved by three approaches: first, using smaller time steps for both fine and coarse levels, second, using more coarse regions and finally implementing a more precise reconstruction scheme. The decision for choosing one or many of these approaches must be carefully made considering the resulting impacts on the speed of calculation versus the improvement in the accuracy of solution.

In the present work, the improvement of the detector responses is primarily obtained by changing time steps. This is the simplest way to achieve better accuracy of the detector responses. The change in the number of coarse grids can also be used as a practical method to improve the accuracy of the reconstruction procedure and consequently detector responses. However, this approach requires re-evaluation of all static calculations and thus updating of databases (if necessary). The last approach for improving the accuracy of detector responses is the implementation of a more complex reconstruction method. In the framework of the present research, the use of another reconstruction method cannot be easily justified since these methods are generally more time consuming. Furthermore, changing the time steps and/or the number of coarse regions provides adequate adjustability in the accuracy of the reconstruction method. It should be kept in mind that the use of hierarchical nodal kinetics for transient simulations in other reactor types might bring about the necessity of a better reconstruction method that is outside of scope of the present work.

During the initialization of hierarchical nodal kinetics, another fact that must be carefully taken into account is the effect of the coarse configuration on the amount of floating-point error. To better understand this effect, the following test procedure was designed and performed:

- A set of coarse configurations i.e. 2 x 2 x 2, 3 x 3 x 2, 5 x 5 x 4, 10 x 10 x 4 and 10 x 10 x 12 are selected.
- Using the steady-state fine flux distribution of the reactor, the equivalence parameters for each of the coarse configurations are calculated.
- The time and space integrators of the coarse level are initiated, using the resulting values of equivalence parameters and steady-state coarse-flux distribution.
- The do-nothing transient test is performed using a one-level full coarse flux scheme (eliminating point kinetics and space-time factorization).
- The reactor regulating system is disabled and xenon load is taken into account.
- After each coarse flux calculation, the fine flux is reconstructed.
- The reconstructed fine flux is used to re-evaluate the equivalence parameters that will be used for the next time step.
- The simulation lasts for 100 seconds.

Table 4.1 shows the results obtained from this procedure for a typical test case. In this case, the value of the time step for the coarse calculation is set to 0.05 seconds. Theoretically, it is expected that the error in the relative total power remains in an acceptable range. However, it can be observed that the errors for the cases with bigger coarse nodes are much larger. After each of the coarse calculations, the homogenization and reconstruction procedures will introduce a certain amount of error affecting both the reactor solution and equivalence parameters. Depending on the volume of the coarse grids, these errors are then amplified when the reactor is solved over the coarse grids.

It is evident that in a real simulation, these errors would be much less important since they would be corrected by re-evaluating the equivalence parameters using an updated fine flux distribution. However, the aforementioned test shows that the floating-point errors in the coarse calculations involving bigger coarse regions propagate much faster than they propagate in the cases involving smaller coarse regions. Performing this test

can partially help to define an optimal number of coarse nodes for the implementation of the hierarchical nodal kinetics scheme.

Table 4.1:The effect of the number of coarse grids in dynamic calculations

NUMBER OF COARSE GRIDS	ERROR IN TOTAL POWER
2 x 2 x 2	-100 %
3 x 3 x 2	-100 %
5 x 5 x 4	-7.2%
10 x 10 x 4	-2.5%
10 x 10 x 12	-1.5%

4.3 Comments on Numerical Results

Prior to presenting the numerical results two practical points must be outlined:

1. It is widely accepted that the merits of any novel numerical scheme should be initially evaluated by the use of a set of well-known benchmark problems. Since the objective of the present work is originally aimed at the development of an industrial code, all presented transient scenarios are intended to be realistic cases for CANDU reactors. The improvement in this model can be easily carried out without actually changing the modules corresponding to the time and space integrators. To keep faith with the classical approach, the results obtained for the well-known 3D CANDU benchmark are also presented in appendix II.
2. Regardless of the solution method, all selected transient scenarios are initiated by perturbing a steady-state reactor (critical reactor) and thus when these perturbations occur the flux and precursor concentrations are considered to be at their corresponding steady-state values. These initial conditions are obtained directly from the static calculations presented in chapter 3. Since the reactor eigenvalue is not initially equal to unity, the fission cross sections in the flux and

precursor concentration equations are divided by the value of the corresponding critical reactor eigenvalue to obtain a correct initial condition.

4.4 Transient Scenario #1: Reactor Stepback

In this scenario, the response of the reactor regulating system to a substantial perturbation is simulated. This test can be considered as a relatively mild transient compared to the next two scenarios. A general description of the transient is outlined here:

- In the initial steady-state conditions (critical reactor), all reactivity devices are in their nominal positions.
- At t = 0.0, the adjuster rod bank #1, consisting of the center and four corner rods, is instantaneously withdrawn from the core (hypothetical).
- The xenon load is taken into account.
- The shutdown system is disabled.
- Geometric configurations of the standard CANDU-6 reactor models (non-uniform 26 x 26 x 12 fine regions and 5 x 5 x 4 coarse mesh) as well as reactivity devices are given in appendix I.
- All physical properties for the default reactor model as well as reactivity devices (a two-energy group and six groups of delayed neutron precursors) are given in appendix I.
- The transient lasts for 900 seconds.

The perturbation caused by this scenario can be quantified as an instantaneous injection of +1 mk at the beginning of the transient.

4.4.1 Direct Method

The starting point is to determine a reference solution to which the accuracy of the other solutions and their corresponding execution times will be compared. The reference

solution will be obtained using the mesh-centered finite-difference method since this algorithm is presently the only direct approach available in the computer code NDF. To choose suitable input parameters for the mesh-centered finite-difference method, two points must initially be taken into account. The first one is the limitation imposed by the fast part of the reactor regulating system. This part of the reactor regulating system is executed every half second, thus the time step used in the simulations should not exceed half a second. The second point to be considered is the choice of the time-integration procedure. In the present work, all transient simulations are performed using an implicit scheme, though the θ-method is available in the computer code NDF. Numerous tests demonstrate that using the θ-method brings only a small amount of improvement in the final solution. Furthermore, using a more precise time-integration scheme without improving other input parameters, especially fuel and device models, is somehow trivial.

Figures 4.2 and 4.3 show the results for three selected cases where the mesh-centered finite-difference method is used as the solution method. The time steps for these cases are respectively set to 0.050, 0.125 and 0.250 seconds (table 4.2). No time step longer than 0.250 seconds is chosen, to provide at least two flux evaluations per fast execution cycle of the reactor regulating system. For the first two cases (time steps equal to 0.050 and 0.125 seconds), the time steps after the first 120.0 seconds are automatically switched to 0.25 second to permit a further reduction in the total execution time. The reference solution here is set to be the solution of the problem with a time step equal to 0.05 second. However, for practical purposes, time steps longer than 0.05 (for example 0.25 seconds) can be comfortably used. Based on the results obtained (figures 4.2 and 4.3), it can be concluded that in the absence of the shutdown systems, the reactor regulating system is able to control the total power of the reactor. In fact, after a very short time, a reactor stepback will be engaged and all four mechanical control absorbers will be inserted into the reactor core. According to algorithms responsible for the reactor stepback, a new power endpoint will be established. After finishing the reactor

stepback, the power will be left at this new endpoint value, which is 0.983 of the initial total power.

Table 4.2: Input parameters for all selected test cases ($0.0 < t < 120.0$)

Method	$(dt)_{fine}$	Number of coarse calculations N_{coarse}	Number of point-kinetics calculations N_{pk}
Direct (Ref) [a]	0.050	--	--
Direct 0.125	0.125	--	--
Direct 0.250	0.250	--	--
IQS 1 [b]	0.250	--	5
IQS 2 [b]	0.500	--	10
IQS 3 [b]	1.000	--	20
Case 1 [c]	2.500	10	5
Case 2 [c]	2.500	5	10
Case 3 [c]	5.000	20	5
Case 4 [c]	1.000	5	4

a-for $t>120$, $dt=0.25$ s.

b-for $t>120$, $dt=1.00$ s, $N_{pk}=4$.

c-for $t>120$, $dt=5.00$ s, $N_{coarse}=10$, $N_{pk}=5$.

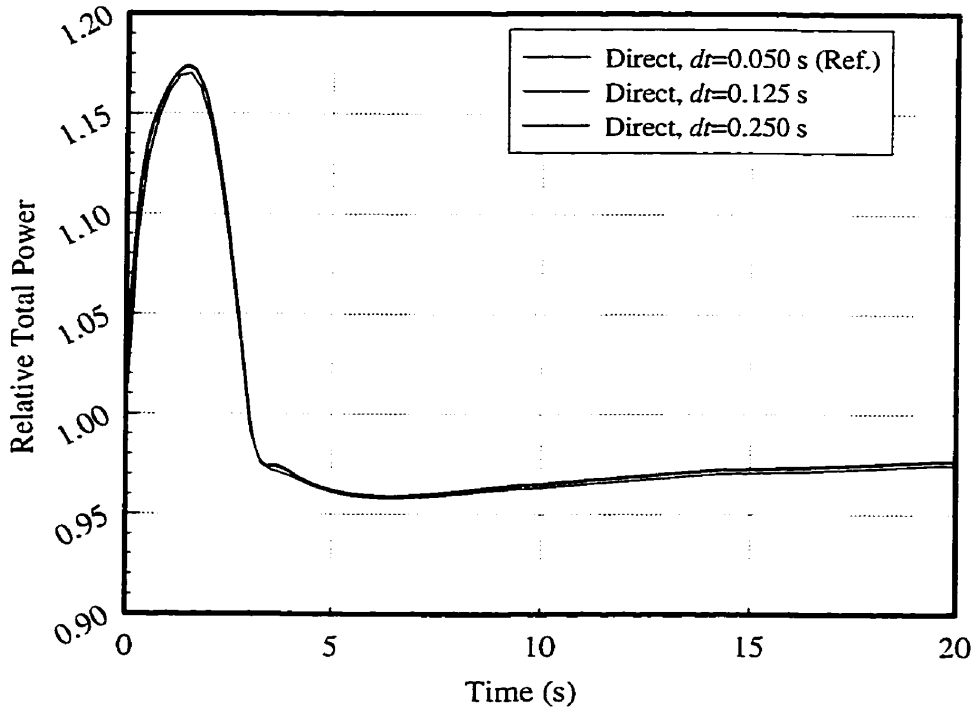

Figure 4.2: Relative total power obtained from direct method (0.0 to 20.0 seconds)

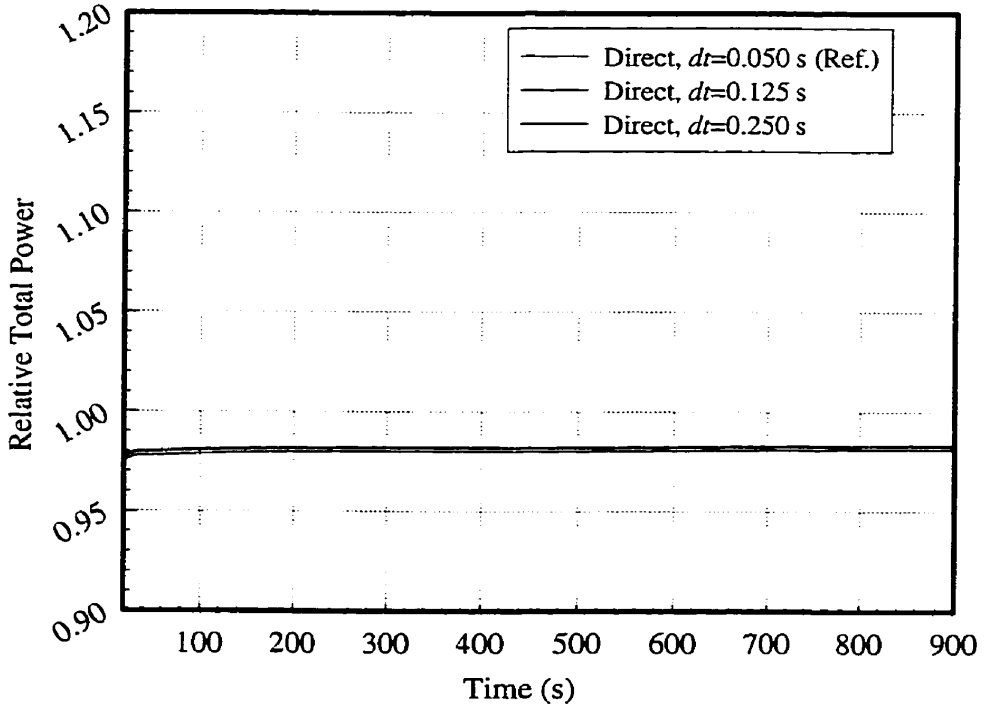

Figure 4.3: Relative total power obtained from direct method (20.0 to 900.0 seconds)

4.4.2 Classical Improved Quasi-Static Method

Prior to presenting the results obtained from the hierarchical nodal kinetics, it would be interesting to present those obtained from the improved quasi-static method. This method has been widely used to simulate CANDU reactor transients. To keep the improved quasi-static method less time consuming (from a computational point of view), no additional iterations over normalizing condition [equation (2.19)] are performed. The shape function rather has been re-normalized after each shape-function calculation. To consider this re-normalization, the amplitude is then re-adjusted to comply with relationship (2.18).

Figures 4.4 and 4.5 show the relative total power obtained from the selected cases where the improved quasi-static method is used as the solution method. The error in relative total power for the first 120 seconds is also presented in figure 4.6. The input parameters for these cases are described in table 4.2. It can be observed that the solutions obtained from two cases IQS1 ($dt_{\text{fine}} = 0.250$ s) and IQS2 ($dt_{\text{fine}} = 0.500$ s) are relatively in good agreement with the reference solution (except for the first five seconds). The first conclusion is that applying time steps longer than 0.50 seconds for the shape function calculation must be coupled with an additional layer of iteration over normalizing condition. This is due to the fast and considerable changes in the shape function during the first seconds of the transient. Thus, the hypothesis of considering a constant shape function during a fine-level step will quickly become inaccurate. The concept of using an additional layer of iteration over normalizing condition would permit the correction of these errors by returning in time and re-evaluating shape-function and point-kinetics parameters (Dodds, 1976). Consequently, using longer time steps for the shape calculations would be theoretically possible. However, the necessary CPU time would be proportionally increased and as a result, the scheme would become computationally more expensive.

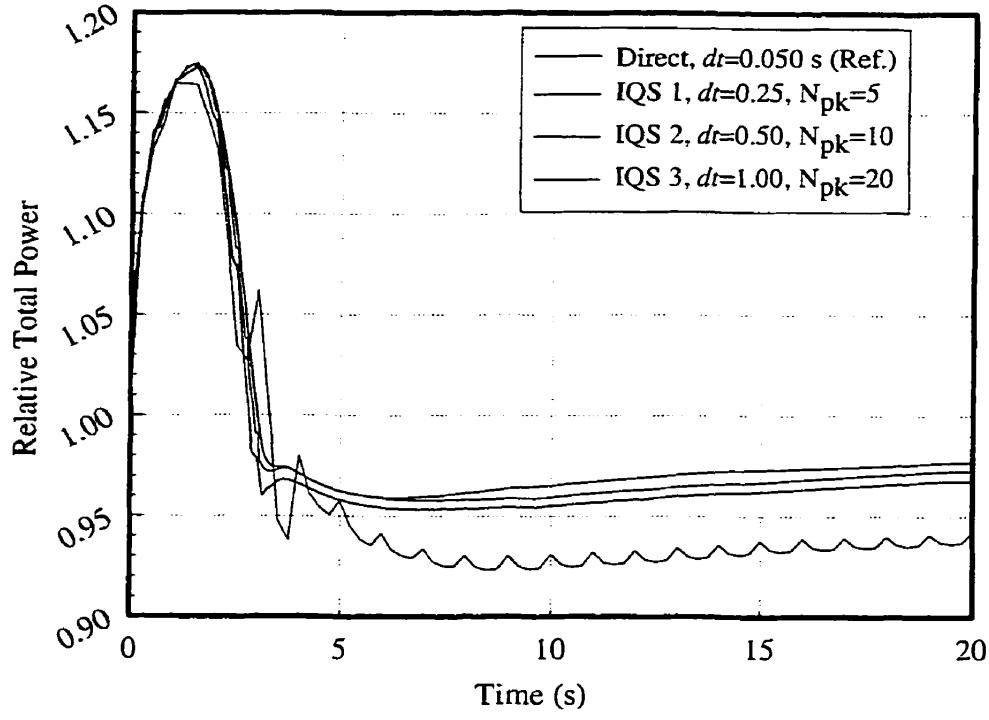

Figure 4.4: Relative total power obtained from IQS method (0.0 to 20.0 seconds)

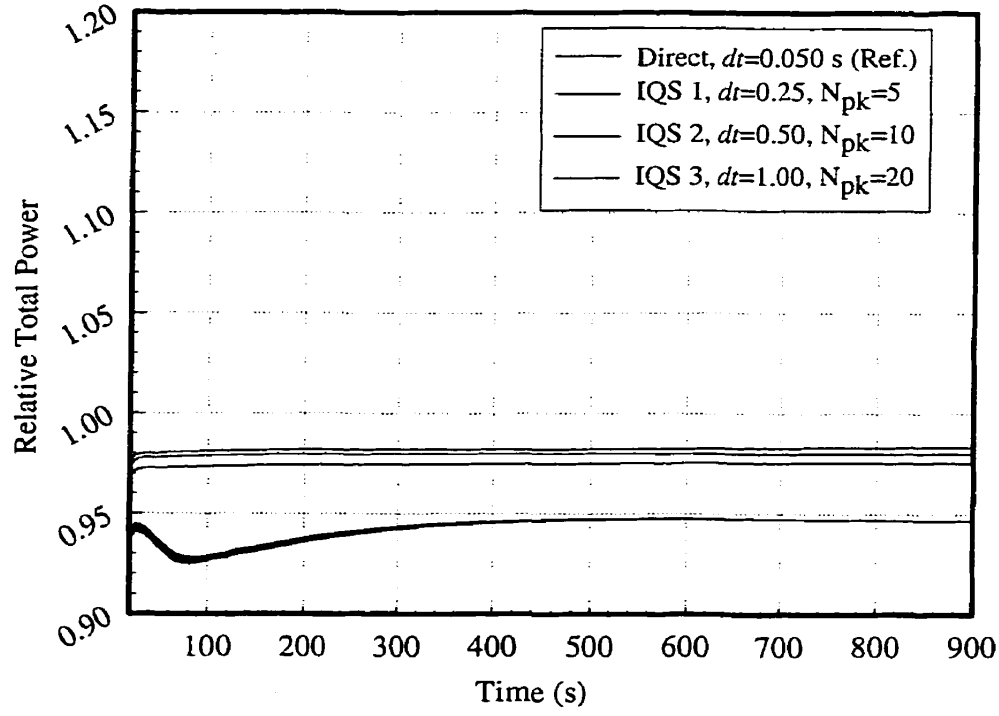

Figure 4.5: Relative total power obtained from IQS method (20.0 to 900.0 seconds)

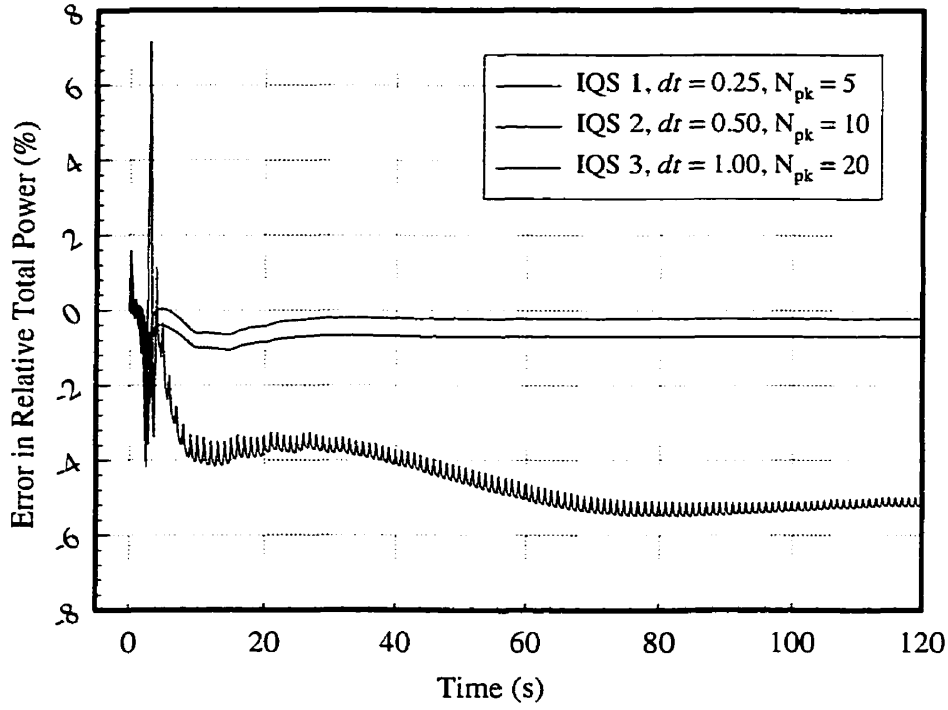

Figure 4.6: Error in relative total power, IQS (0.0 to 120.0 seconds)

Moreover, for the cases where the reactor regulating system is heavily involved, the implementation of an additional layer of iterations over normalizing condition might bring serious difficulties in the solution procedure. The concept of returning in time and using a linear combination of shape functions obtained at the beginning and the end of the corresponding time step and re-solving the point kinetics equations for that time step would not necessarily correct the reactor solution. In fact, the new "corrected amplitude functions" might cause a completely different response from the reactor regulating system and consequently result in completely different "reactor state". This method is useful for the cases where the changes in the cross sections are pre-determined.

4.4.3 Extended Quasi-Static Method as a Form of Hierarchical Nodal Kinetics

The hierarchical nodal kinetics method prescribes the implementation of an additional level of time-hierarchy permitting numerous updates of the shape-function over the

coarse representation of the reactor (section 2.2.1). Using this approach would permit the application of longer fine-shape time steps. To verify the capability of this approach, numerous numerical simulations have been carried out. A summary of the input parameters for the selected test cases is presented in table 4.2. The input parameters are: the fine-shape time step, represented by $(dt)_{fine}$, the number of coarse calculations during a fine-shape time step, represented by N_{coarse}, and the number of point-kinetics calculations during a coarse-shape time step, represented by N_{pk}.

For all cases, the discontinuity factors are considered constant between two fine-level calculations while flux-weighted diffusion coefficients and cross sections are updated after each point-kinetics time step (section 2.3.7.3). The fine-flux distribution is reconstructed using the last average coarse-node flux and the intranodal distribution calculated after each fine-level time step. This reconstruction scheme would provide the possibility of updating detector responses after each point-kinetics time step. Figures 4.7 through 4.10 present the results obtained for the selected cases. Based on these results, the first conclusion is that using very large time steps (case 3) results in a considerable amount of error in the total power. In this particular case, even numerous coarse-shape updatings cannot improve the final solution since both the hypothesis of considering constant discontinuity factors as well as the reconstruction procedure lose their efficiency. As expected, using smaller time steps generally gives better results. However, to obtain a better result, smaller fine-level time steps must be matched with an adequate number of coarse-shape updatings (case 1). If a sufficient number of coarse-shape updatings is not used (case 2), the error can be as large as those obtained for the cases with longer fine-shape time steps. The test case 4 uses a very small fine-shape time step with an adequate number of coarse-shape calculations. Consequently, the relative total power is very well predicted.

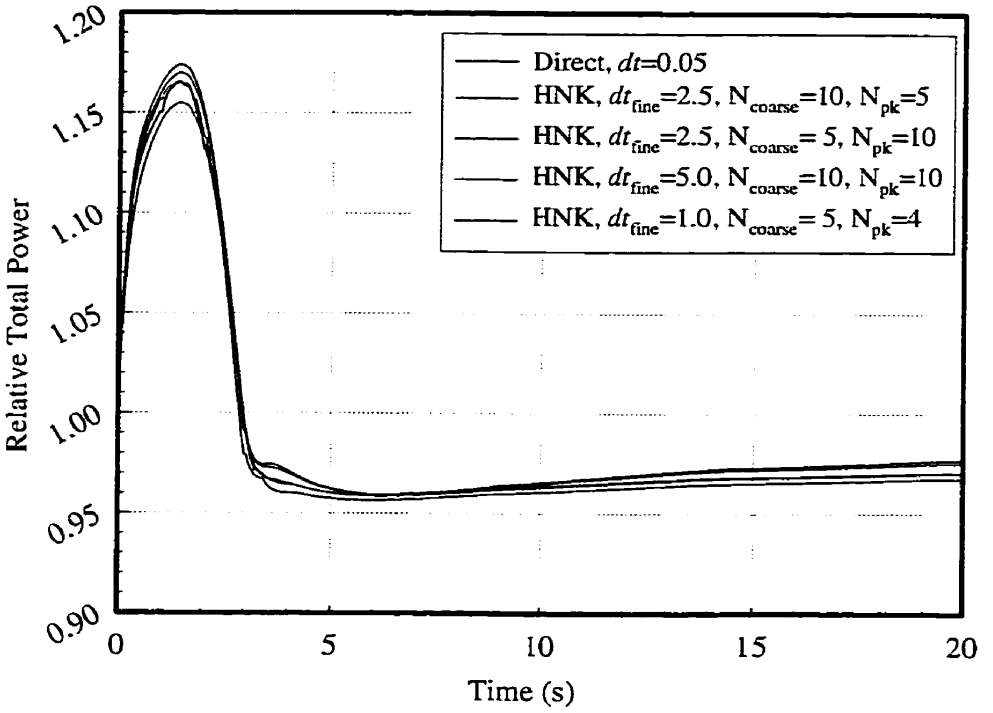

Figure 4.7: Relative total power obtained from HNK method (0.0 to 20.0 seconds)

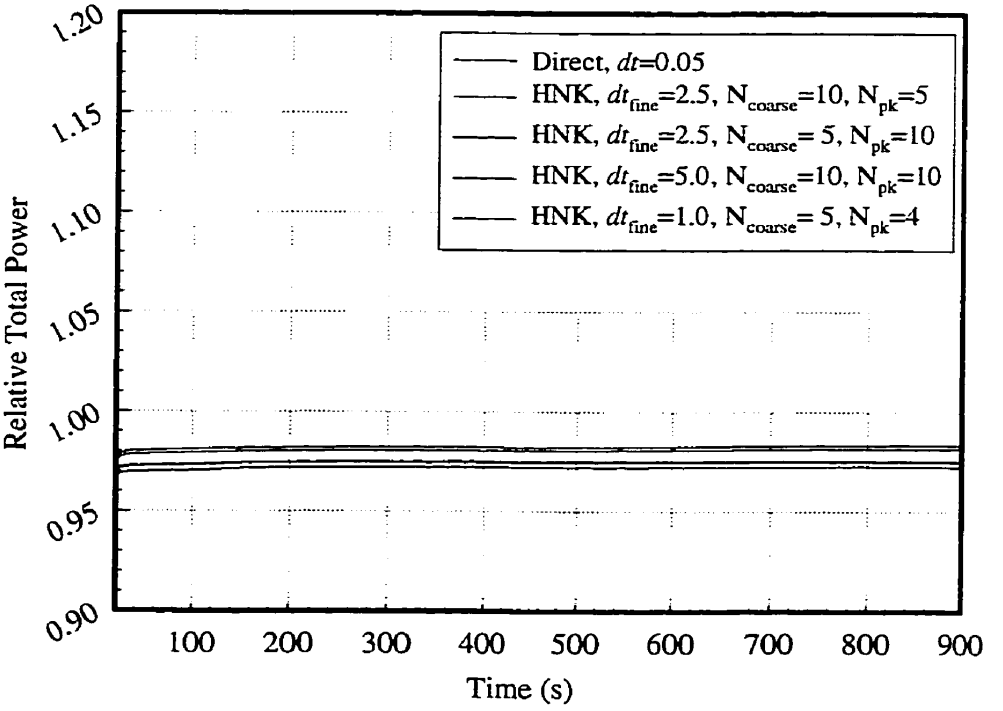

Figure 4.8: Relative total power obtained from HNK method (20.0 to 900.0 seconds)

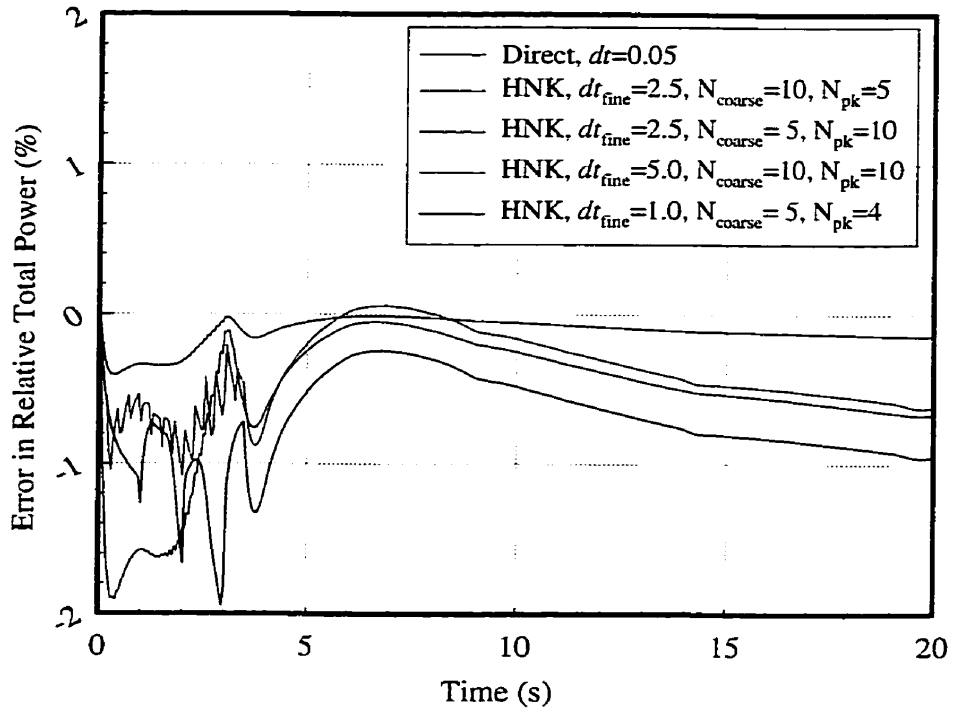

Figure 4.9: Error in relative total power for HNK method (0.0 to 20.0 seconds)

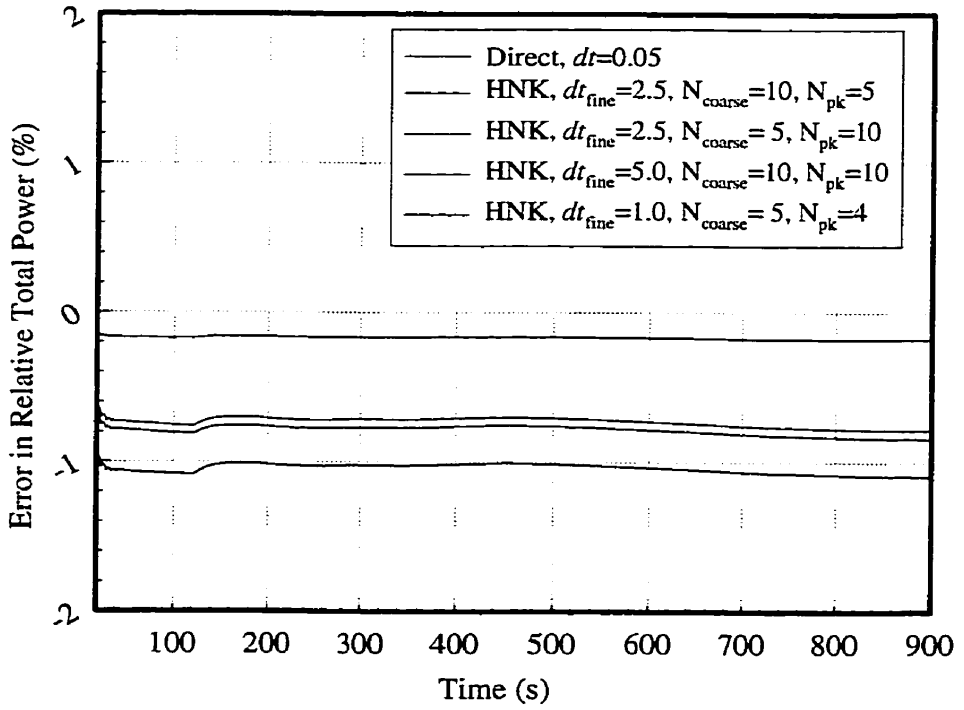

Figure 4.10: Error in relative total power for HNK method (20.0 to 900.0 seconds)

4.4.4 Time Performance Comparison

To evaluate the performance of the hierarchical nodal kinetics method, the next step is comparing the speed of the various calculations. Since the input parameters after the first 120 seconds are changed, the comparison is done based on the necessary CPU time for completing the first 120.0 seconds of the transient. Using relationship (4.4) and considering the total necessary CPU time for the reference case (almost 1710 seconds in this case), the gain in overall time performance of the different methods is calculated and presented in figure 4.11. The first interesting conclusion is that a well-optimized direct method is computationally superior to the improved quasi-static method. Thus, the improved quasi-static method cannot be suggested for this type of transient simulations.

Furthermore, close examination of these results shows that the overall performance gain for the hierarchical nodal kinetics method is at least 85%. Even if the number of fine-level calculations is considerably reduced (20 to 50 times for cases 1, 2, and 4), the gain in overall time performance does not exceed 150%. This is primarily due to the necessary CPU time for executing and moving data between supporting modules such as the reactor regulating system, detector responses, reactivity devices, and macro-library and point-kinetics parameters updating. It is expected that the amount of gain in the solver performance would be much greater compared to those of the overall performance. However, the quantification of the solver performance is not an easy task, since it requires a complete time profiling of the execution procedure. Hence, the comparison of the solver performance is left for the simpler test cases where the transient lasts for a shorter time or where a specially designed benchmark problem is solved.

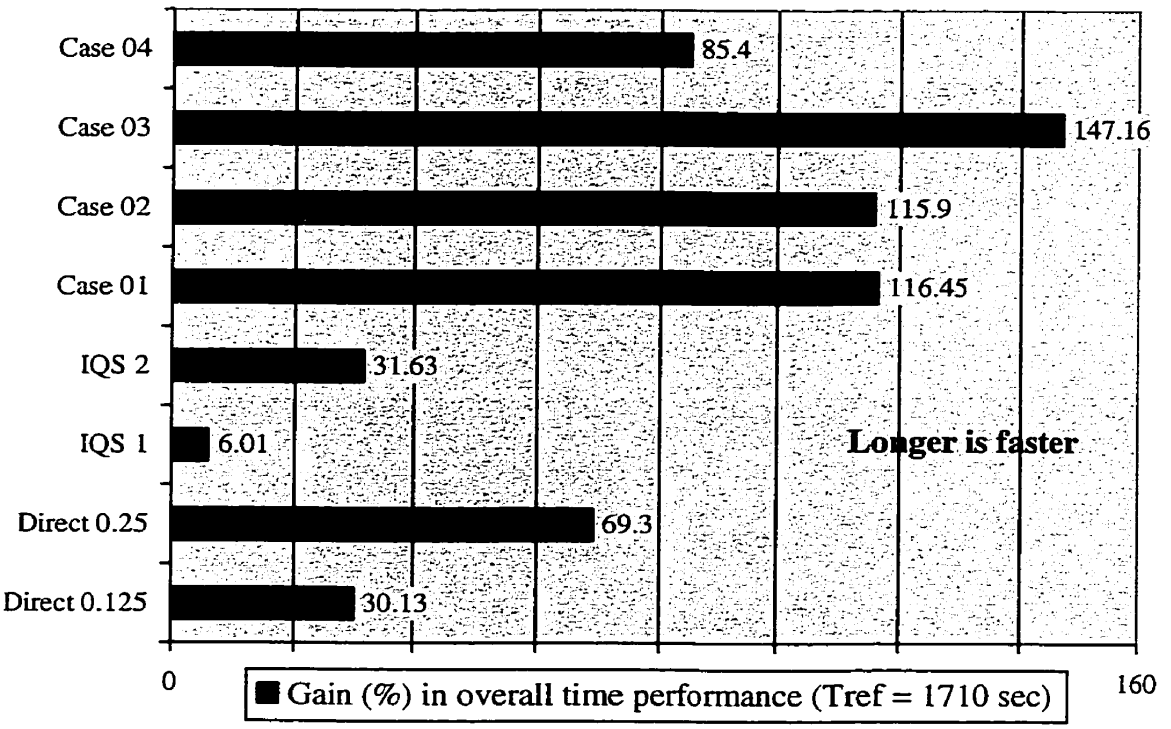

Figure 4.11: Gain (or loss) in overall time performance compared to the reference

4.5 Transient Scenario #2: MCA insertion

In this transient scenario, the response of the reactor regulating system to a very substantial perturbation is simulated. This test can be considered as a relatively more intense transient compared to the transient scenario #1. A general description of the transient is outlined here:

- In the initial steady-state conditions (critical reactor), all reactivity devices are in their nominal positions.
- At t=0.0, two mechanical control absorbers (opposite corners) are instantaneously inserted in the reactor core.
- The xenon load is taken into account.
- The shutdown system is disabled to permit the performance evaluation of the reactor regulating system.

- Geometric configurations of the default reactor model (non-uniform 26 x 26 x 12 fine regions and 5 x 5 x 4 coarse mesh) as well as reactivity devices are described in appendix I.
- All physical properties for the default reactor model as well as reactivity devices (a two-energy group and six groups of delayed neutron precursors) are described in appendix I.
- The transient lasts for 900 seconds.

The resulting perturbation is equivalent to a sudden insertion of –3.32 mk (dynamic reactivity).

4.5.1 Direct Method

As usual, the starting point is to determine the reference solution and its corresponding execution time. Once more, the mesh-centered finite-difference method and implicit time integration procedure are the chosen methods for determining the reference solution. Figures 4.12 and 4.13 show the relative total powers for three selected test cases where these methods are used as integration algorithms (see table 4.3 for input parameters). The case with a time step equal to 0.05 second is set to be the reference solution.

It should be kept in mind that the time steps equal to 0.125 or 0.25 seconds can also be adequately used for practical purposes. The essential observation is that the reactor regulating system is able to keep the reactor operational but at a lower total power. The error in power due to the sudden insertion of two mechanical control absorbers is more than –4%. The response of the reactor regulating system is the following: first, the immediate withdrawal of two adjuster rod banks, second, immediate withdrawal of the two inserted mechanical control absorbers, and third, immediate emptying of the liquid zone controllers all with maximum speed. After a while, a new power endpoint will be

established (almost 0.70 of initial total power) and reactor power will be left at this value.

Table 4.3: Input parameters for all selected test cases ($0.0 < t < 120.0$)

Method	$(dt)_{fine}$	Number of coarse calculations N_{coarse}	Number of point-kinetics calculations N_{pk}
Direct (Ref) [a]	0.050	--	--
Direct 0.125 [a]	0.125	--	--
Direct 0.250	0.250	--	--
IQS 1 [b]	0.250	--	5
IQS 2 [b]	0.500	--	10
IQS 3 [c]	1.000	--	20
Case 1 [d]	2.500	10	5
Case 2 [d]	2.000	8	5
Case 3 [c]	5.000	20	5
Case 4 [d]	0.750	5	3

a-for $t>120$, dt=0.25 s.

b-for $t>120$, dt=1.00 s, N_{pk}=4.

c- failed.

d-for $t>120$, dt=5.00 s, N_{coarse}=10, N_{pk}=4.

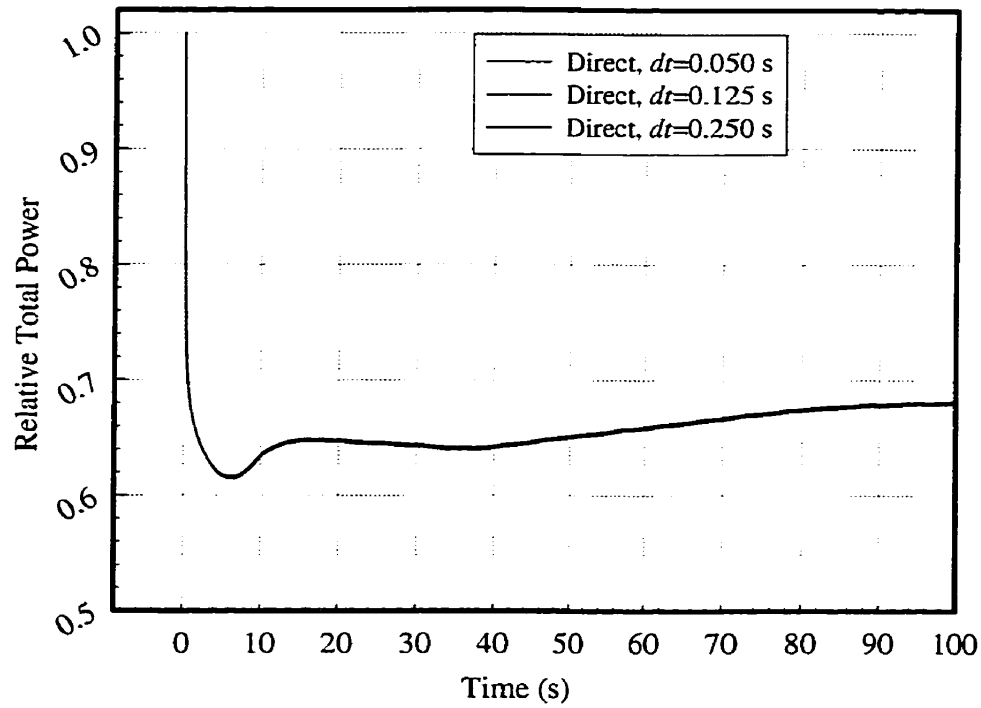

Figure 4.12: Relative total power obtained from direct method (0.0 to 100.0 seconds)

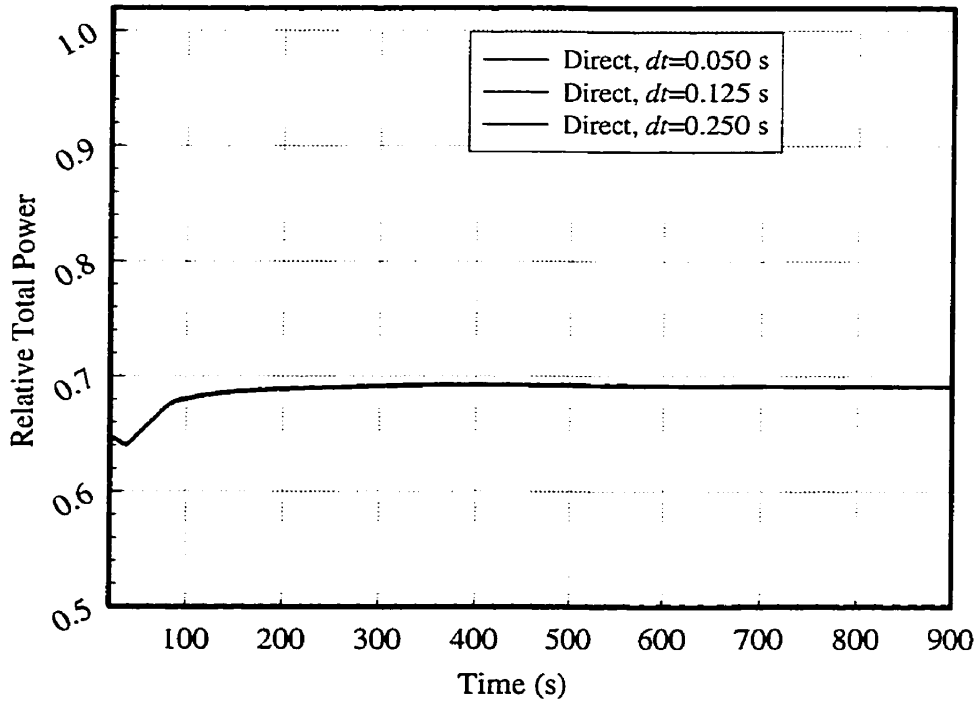

Figure 4.13: Relative total power obtained from direct method (100.0 to 900.0 seconds)

4.5.2 Classical Improved Quasi-Static Method

Before presenting the results obtained using the improved quasi-static method, it must be recalled that no additional layer of iterations over the normalizing condition [equation (2.19)] are performed. The shape function is re-normalized after each shape-function calculation and, consequently, the amplitude is re-adjusted to seek the relationship (2.18). This results in the fastest version of improved quasi-static method from a computational point of view.

Figures 4.14 and 4.15 show the relative total power obtained for the selected cases where the improved quasi-static method is used as the solution method. The input parameters for these cases are described in table 4.3. Once again, it can be concluded that the improved quasi-static method is not an efficient solution method for transients that involve considerable changes in the shape function. In the present scenario, the shape-function distortions are so significant that even during a time step equal to 0.25 seconds, it cannot be considered constant. Thus, using a constant shape-function results in a set of inaccurate point kinetics parameters. In turn, the detector responses are not correctly updated and the response of the reactor regulating system becomes considerably erroneous. Any attempt to improve the accuracy of this method would result in a computationally more expensive method. At the same time, a direct method with a similar time step (0.25 sec.) can efficiently produce an acceptable solution for the transient problem. Thus, using the improved quasi-static method for this type of transient again cannot be easily justified.

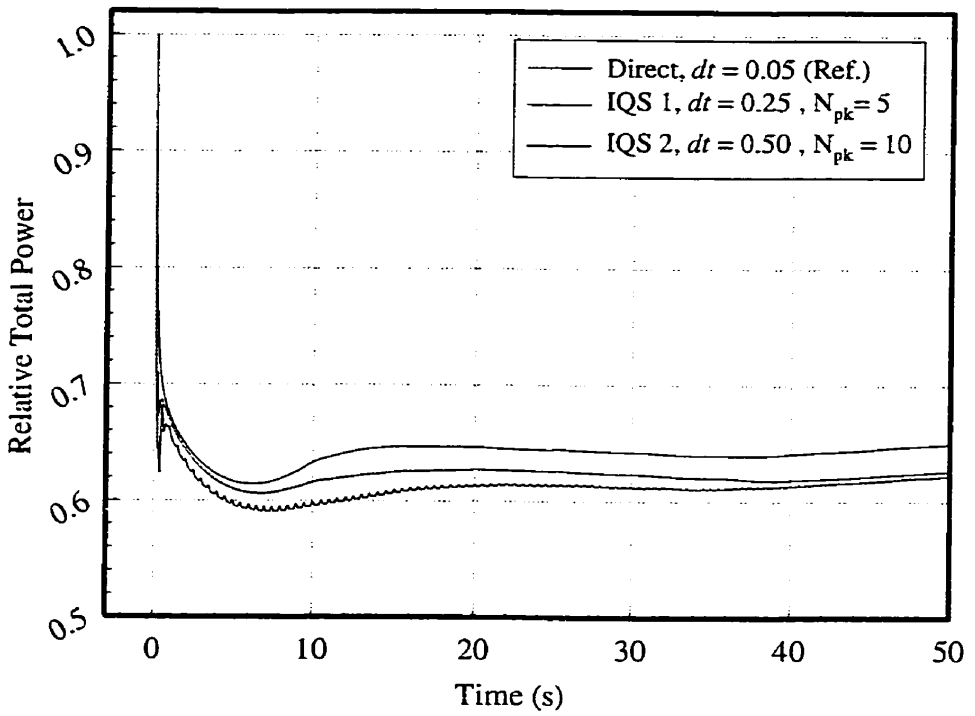

Figure 4.14: Relative total power obtained from IQS method (0.0 to 50.0 seconds)

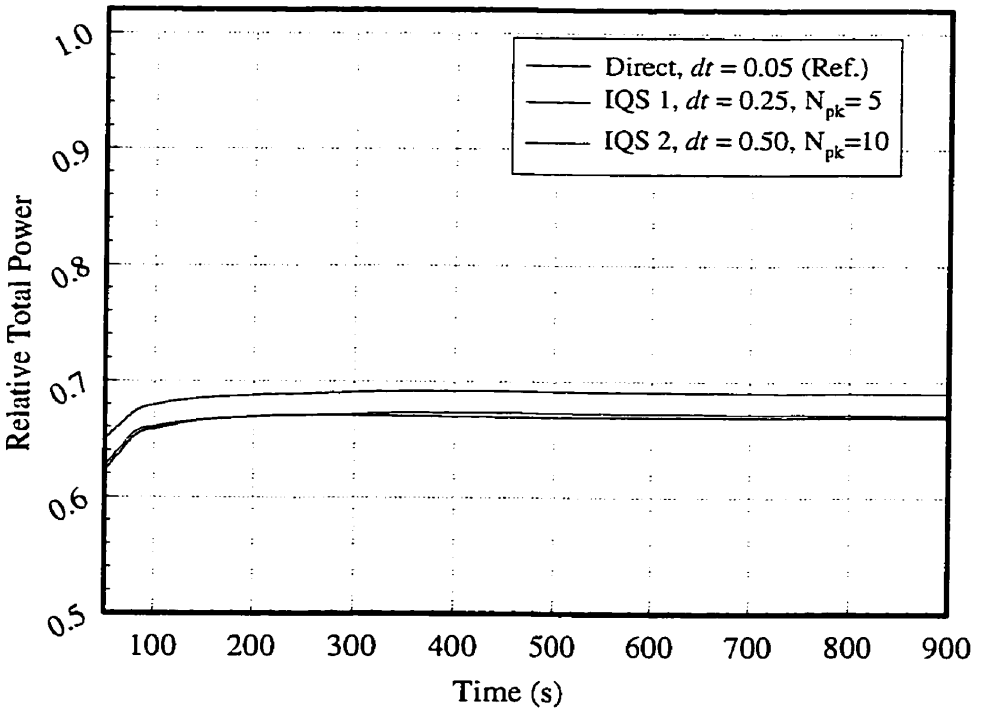

Figure 4.15: Relative total power obtained from IQS method (50.0 to 900.0 seconds)

4.5.3 Extended Quasi-Static Method as a Form of Hierarchical Nodal Kinetics

The success of the hierarchical nodal kinetics method essentially depends on two factors, first, how well the equivalence parameters are approximated during a fine-shape time step, and second, how well the coarse flux distribution is reconstructed over fine regions of the reactor. The second factor is especially important for transients involving the reactor regulating system. Numerous tests have shown that the total power obtained from the coarse level is in relatively good agreement with those obtained from a full fine calculation. However, the reconstruction of the coarse flux does not correctly reflect the flux distribution over the fine regions. These relatively inaccurate reconstructed fluxes in turn cause unexpected responses from the reactor regulating system. The transient scenario #2 is a typical example of these cases.

The input parameters for selected test cases are presented in table 4.3. Once more, for all cases, constant discontinuity factors are used between two fine-level calculations while flux-weighted diffusion coefficients and cross sections are updated after each point-kinetics time steps (section 2.3.7.3). The fine-flux distribution is reconstructed using the last average coarse node flux and the intranodal distribution calculated after each coarse-level time step. Figures 4.16 through 4.18 show the results for the selected cases. The interpretation of these results is similar to that of the previous transient scenario. It is evident that using very large time steps (case 1) again results in an inaccurate prediction of the total power. Performing numerous coarse-shape updatings cannot improve the final solution since either the hypothesis of considering constant discontinuity factors loses its efficiency or the reconstruction procedure causes erroneous responses from the reactor regulating system. As expected using enough smaller fine-level time steps generally gives a much better result (case 3). This particular case uses a very small fine-shape time step with an adequate number of coarse-shape calculations. Consequently, the resulting relative total power is relatively well predicted.

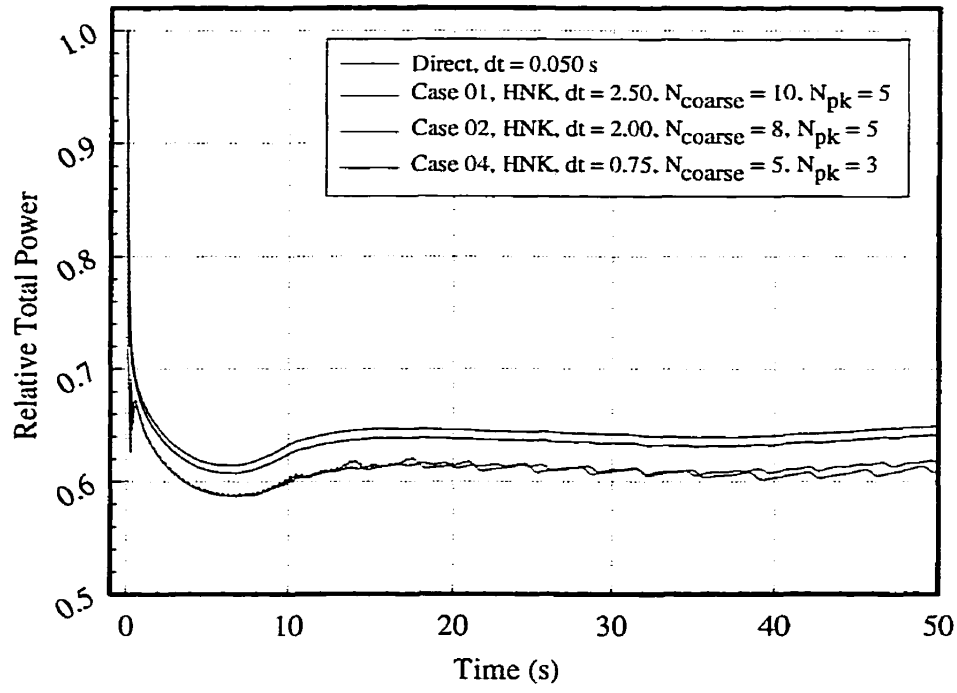

Figure 4.16: Relative total power obtained from HNK method (0.0 to 50.0 seconds)

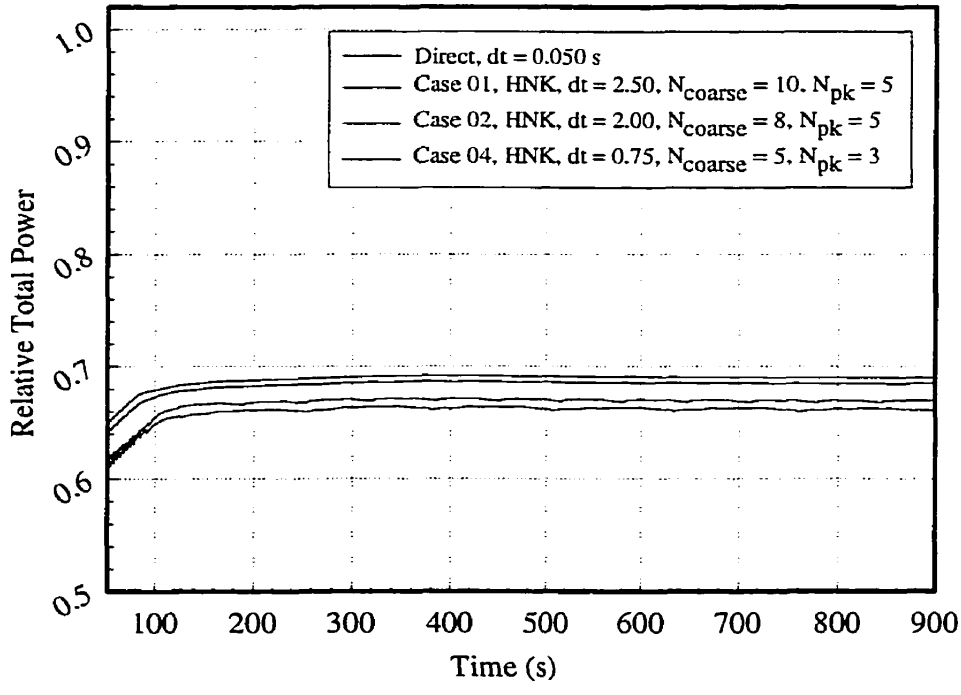

Figure 4.17: Relative total power obtained from HNK method (50.0 to 900.0 seconds)

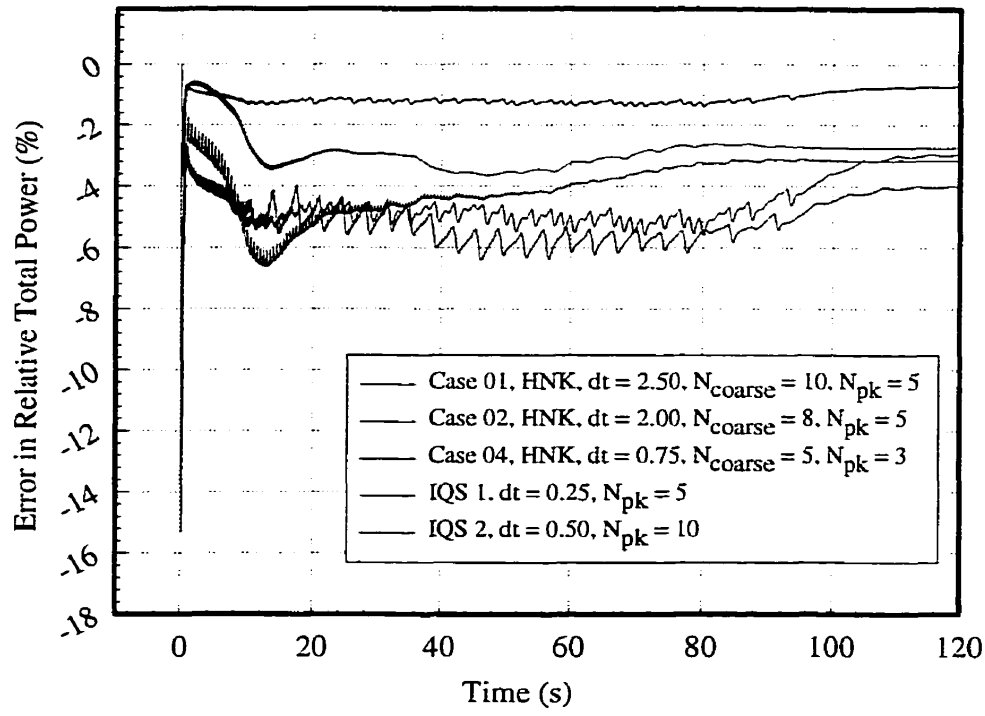

Figure 4.18: Error in relative total power for HNK method (0.0 to 120.0 seconds)

4.5.4 Time Performance Comparison

To complete the comparison procedure, the next step is comparing the speed of the calculations. Since the input parameters are changed after the first 120 seconds, the comparison is carried out only on the CPU time necessary for completing the first 120 seconds of transient. Once more, applying relationship (4.4) and considering, the total CPU time necessary for the reference case (almost 1810 seconds in this case) the gain in overall time performance of different methods is calculated and compared in figure 4.19. Close examination of these results once more shows that a well-optimized direct method is generally superior to the improved quasi-static method. Moreover, the overall performance gain for hierarchical nodal kinetics is at least 98%. Even when the number of fine-level calculations is considerably reduced, the gain in overall time performance does not exceed 126% (due to necessary CPU time for executing and moving data between supporting modules).

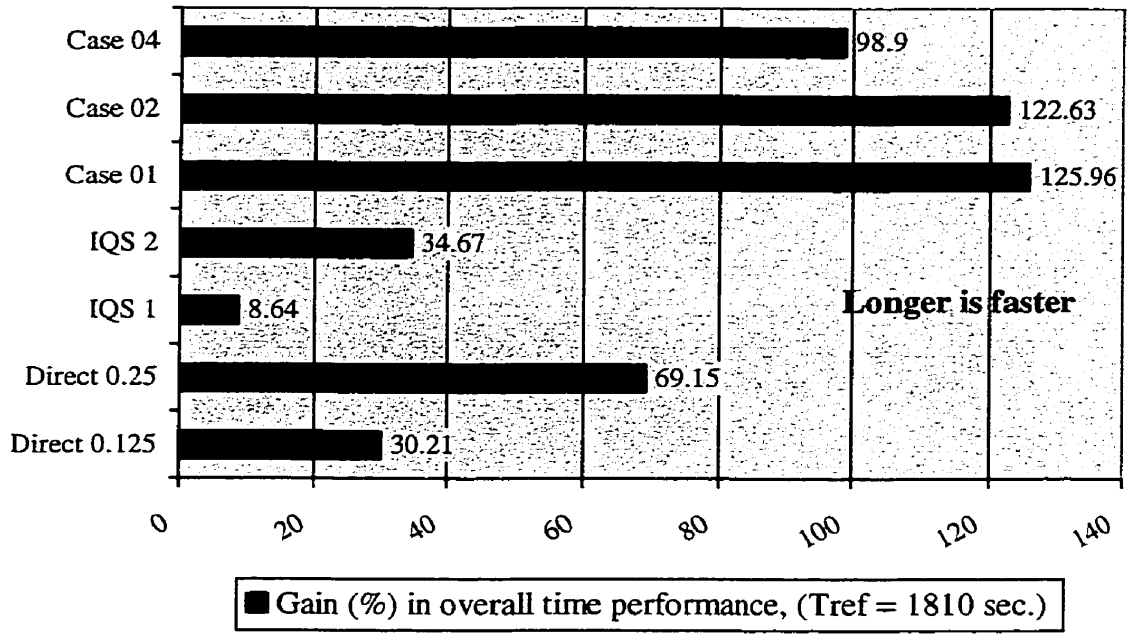

Figure 4.19: Gain (or loss) in overall time performance compared to the reference

4.6 Transient Scenario #3: LOCA

Following a hypothetical break in a primary circuit pipe, the mixture of steam and water would rapidly discharge into the containment. The resulting void in the primary circuit would then cause a significant decrease in the coolant density in corresponding fuel channels, especially in the channels downstream of the break. This effect would then introduce a considerable amount of positive reactivity at a rate that the reactor regulating system would not be able to compensate. The resulting rise in the reactor power would be followed by a significant increase in the fuel heat generation and consequently in the fuel temperature. How fast these events will happen depends directly on the break size and location. Within a fraction of second, the trip signals would cause the reactor to be shut down. After reactor trip, it is expected that the fission

power quickly drops within less than 3 seconds. This sequence of events is known as Loss of Coolant Accident (LOCA).

4.6.1 A Simplified Model

A complete analysis of this accident would require the coupling between neutronic and thermal-hydraulic models of the reactor. The neutronic model would take care of the space and time flux evolution while the thermal-hydraulic model would determine coolant density and temperature as well as fuel temperature. Additional models are necessary to quantify the local effects (temperature and density) on the physical properties of the fuel and possibly other materials. Supplementary models such as pressure-tube creep, fuel dry-out etc. would also be necessary to perform a realistic simulation of a LOCA.

It is noteworthy to mention that most of the aforementioned supplementary models require some proprietary information and thus are not readily available. Furthermore, the objective of the present simulation is primarily to evaluate the performance of the hierarchical nodal kinetics. Consequently, the choice of a simplified model of the accident is justified. A summary of the model used for the simulation procedure is outlined here:

- In the initial steady-state conditions (critical reactor), all reactivity devices are in their nominal positions.
- It is considered that the shutdown system #1 is the only available safety device in the reactor and all shutoff rods are initially parked out of the core.
- Different geometric configurations of the reactor model used during simulations (both coarse and fine) as well as reactivity and safety device locations are described in appendix I.
- All physical properties for the default reactor model as well as reactivity devices (a two-energy group and six groups of delayed neutron precursors) are given in

appendix I. The physical properties of the shutoff rods are the same as those of mechanical control absorbers.

- At t=0.0, a break in the primary circuit occurs. The resulting effect is translated by a uniform decrease in thermal-neutron absorption cross section in the affected zones (the affected zones are shown in figure 4.20):

$$\frac{\partial \Sigma_2}{\partial t} = \begin{cases} -1.0*10^{-4}\,(\mathrm{cm}\cdot\mathrm{s})^{-1}, & \text{for } t \le 0.4\,\mathrm{s} \\ -8.88889*10^{-6}\,(\mathrm{cm}\cdot\mathrm{s})^{-1}, & \text{for } t > 0.4\,\mathrm{s} \end{cases} \tag{4.6}$$

- The reactor regulating system is disabled to permit the evaluation of the shutdown system performance.
- The xenon load is not taken into account since it has a negligible effect during this short transient.
- The shutdown system #1 is fired at t=0.305 seconds after the beginning of the accident.
- Two most effective shutoff rods are disabled (#24 and #28).
- The following unified drop correlation for both short and long shutoff rods are applied:

$$x = -0.0014306788 + 0.61787386(t - t_{\mathrm{ins}}) - 0.1377489(t - t_{\mathrm{ins}})^2 + 0.20675315(t - t_{\mathrm{ins}})^3 - 0.066724897(t - t_{\mathrm{ins}})^4 \tag{4.7}$$

with $t_{\mathrm{ins}} < t < t_{\mathrm{final}}$, $0.0 \le x \le 1.0$, x is the fraction of full insertion and t_{ins} is the time of firing of the shutdown system.

- The transient lasts for 3 seconds.

Despite its simplicity, the aforementioned model can be adequately used to evaluate the performance of the hierarchical nodal kinetics method. Any improvement in different parts of this model would naturally result in a more realistic simulation. Depending on the complexity of the applied improvements, the overall performance might be proportionally changed. However, the solver performance would not be particularly affected by the implemented features. From the user's point of view, as long as the

comparison between different solution methods is performed using the same supporting modules, the conclusion can be considered as a fair one in that computational environment.

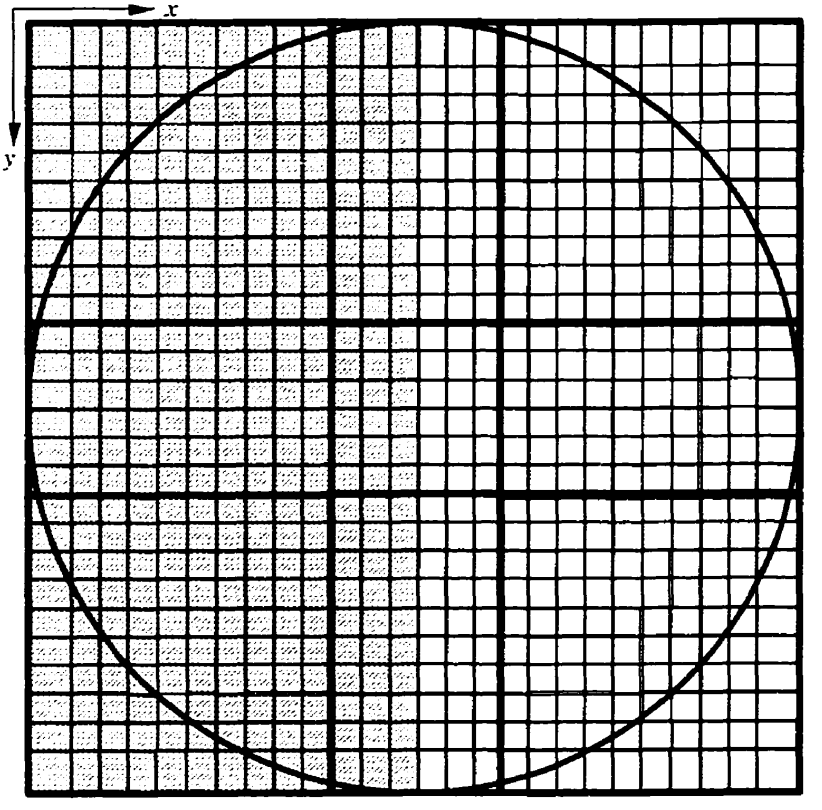

Figure 4.20: The zones affected by the break in heat transport system

4.6.2 Input Parameters

To better understand different aspects of the hierarchical nodal kinetics, numerous simulations have been carried out. Summaries of the input parameters for different test cases are presented in tables 4.4 and 4.5.

Table 4.4: Input parameters for all selected test cases

Method	dt_{fine}	N_{coarse}	N_{pk}	Coarse mesh	Const.
Direct	0.001	--	--	--	--
Direct	0.005	--	--	--	--
Direct	0.010	--	--	--	--
Direct	0.050	--	--	--	--
Direct	0.250	--	--	--	--
IQS 1	0.050	--	5	--	--
IQS 2	0.100	--	10	--	--
IQS 3	0.250	--	25	--	--
IQS 4	0.500	--	50	--	--
IQS 5	1.000	--	100	--	--
HNK 1	0.100	5	2	10x10x4	DFs
HNK 2	0.250	5	5	10x10x4	DFs
HNK 3	0.500	10	5	10x10x4	DFs
HNK 4	1.000	20	5	10x10x4	DFs
Case 01	0.500	50	--	10x10x4	DFs
Case 02	1.000	100	--	10x10x4	DFs
Case 03	0.250	25	--	10x10x4	DFs
Case 04	3.000	300	--	10x10x4	DFs
Case 05	3.000	300	--	5x5x4	DFs
Case 06	0.250	25	--	5x5x4	DFs

Table 4.5: Input parameters for all selected test cases (cont.)

Method	dt_{fine}	N_{coarse}	N_{pk}	Coarse mesh	Const.
Case 07	0.500	50	--	5x5x4	DFs
Case 08	1.000	100	--	5x5x4	DFs
Case 09	0.500	50	--	10x10x12	DFs
Case10	0.500	50	--	10x10x4	DFs (static)
Case11	0.500	50	--	10x10x4	DFs (weighed)
Case12	0.500	100	--	10x10x4	DFs

4.6.3 Direct Method

As usual, the starting point is to determine the reference solution and its corresponding execution time. Figure 4.21 shows the results obtained from different input parameters for the direct method.

It can be observed that the difference between the cases with time steps 0.001, 0.005, and 0.010 second is practically negligible. Here, the case with a time step equal to 0.010 is set to be the reference solution. It can be also concluded that for practical purposes, a longer time step 0.050 can be used. Nonetheless, in the real life simulations, the choice of time steps also depends on the time steps corresponding to the thermal-hydraulics and other supporting models.

To better understand the importance of the perturbation caused by a LOCA, it would be interesting to visualize the dynamic reactivity evolution. Figure 4.22 shows the evolution of dynamic reactivity during the transient period. It can be observed that in the absence of the two most effective shutoff rods, a dynamic reactivity almost equal to –42 mk is provided by all active shutoff rods resulting in a reactor shutdown in less than 2.0 seconds.

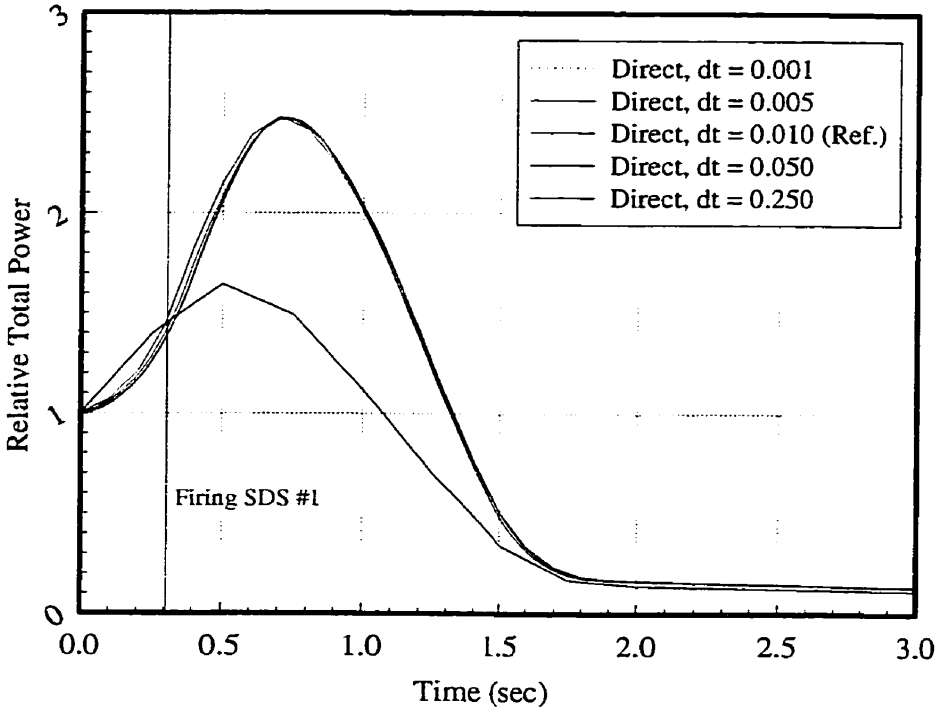

Figure 4.21: Relative total power obtained from direct methods (LOCA)

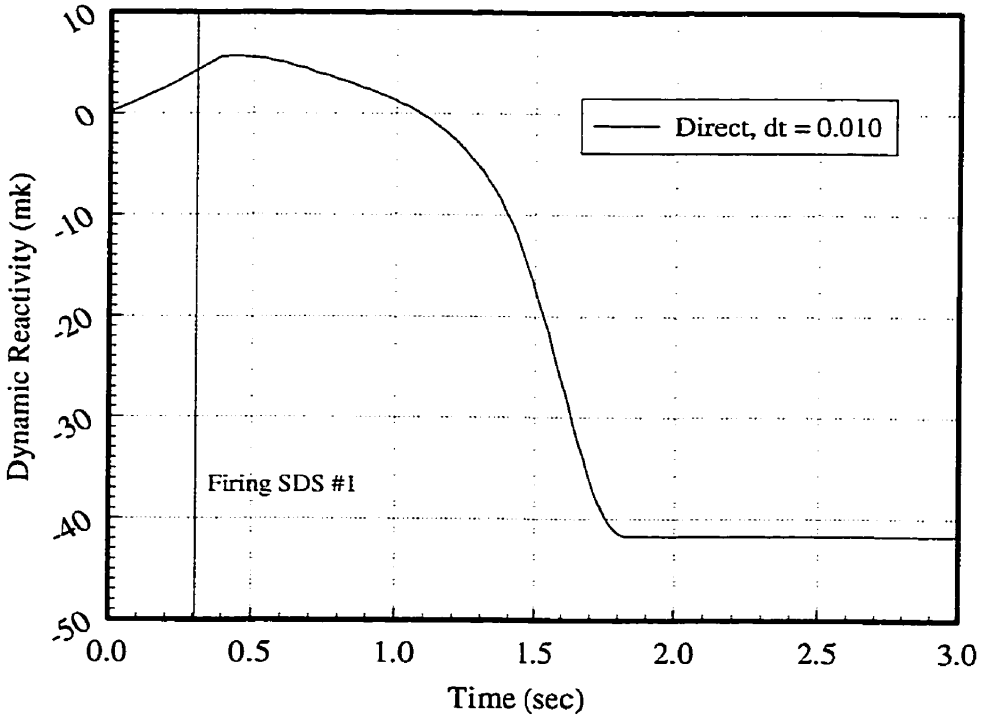

Figure 4.22: The evolution of dynamic reactivity for LOCA

4.6.4 Classical Improved Quasi-Static Method

Based on the results obtained for the previous transient cases (#1 and #2), it is normal to predict that the use of a simple version of the improved quasi-static method (without iteration over the normalizing condition) will not yield an acceptable solution for the LOCA simulation. To verify this, a set of tests has been performed. The input parameters for selected test cases are presented in table 4.4. The results obtained from the point kinetics method, as a special form of the improved quasi-static method, are also included. It can be observed that for all cases the relative total power is significantly underestimated (figure 4.23). This underestimation starts to appear when the shutoff rods pass through the reflector and start entering the reactor core. When the shutoff rods are still out of the core, the perturbation prescribed by the model is uniformly distributed over the left half of the reactor core. Thus, the improved quasi-static method, which is an efficient method for a uniformly distributed perturbation, produces an excellent prediction of the relative total power. Shutoff rods entering into the core cause a very strong local perturbation, which in turn yield a very considerable shape distortion. From this moment on, the hypothesis of a constant shape function cannot be considered valid anymore and the improved quasi-static method quickly loses its efficiency. At this moment, the additional layer of iteration over the normalizing condition must be included in the solution procedure, and it is not necessary to emphasize that this will result in an increase in the CPU time. The last point to mention is that all test cases which use time steps longer than 0.100, have failed even to predict the transient tendency and thus they are not included in figure 4.23.

4.6.5 Extended Quasi-Static Method as a Form of Hierarchical Nodal Kinetics

Close examination of previous results (cases #1 and #2) shows that the efficiency of the quasi-static approach can be substantially improved by frequent updating of the shape function over the coarse representation of the reactor. To examine the efficiency of this approach for LOCA analysis, a set of simulations has been performed. The input

parameters for these cases are presented in table 4.4 (cases HNK 1 through HNK 4). The last column stands for the choice of using piecewise constant discontinuity factors during a fine-level time step.

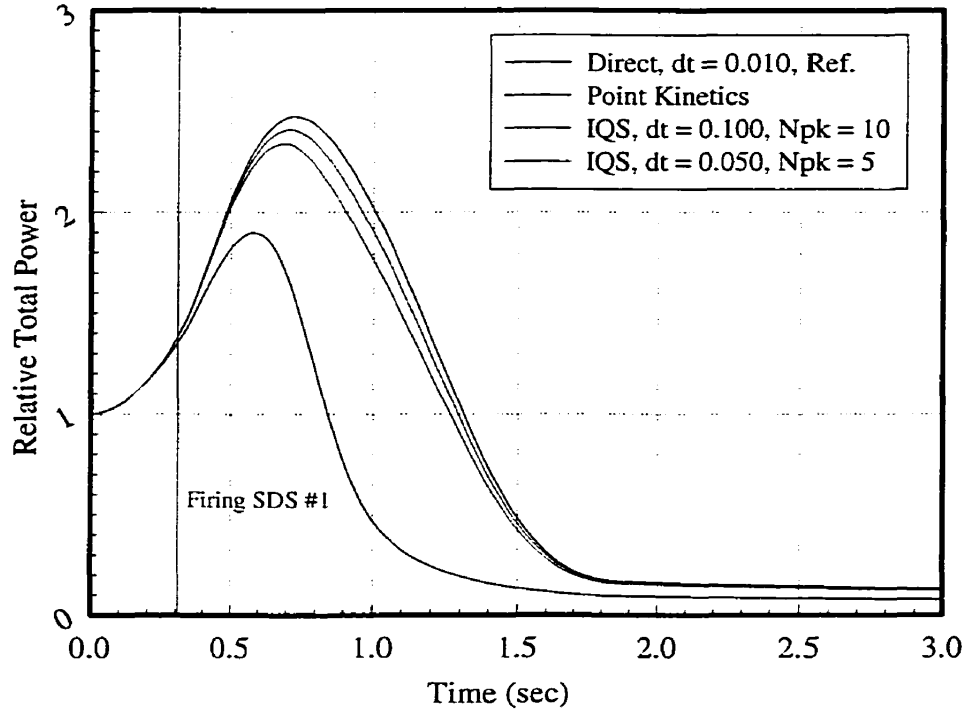

Figure 4.23: Relative total power obtained from IQS method

Figures 4.24 and 4.25 show the results obtained from these test cases. The first observation is that using fine-shape time steps longer than 0.25 second will result in a considerable amount of error in the total power (up to –7% for HNK 3). The test case HNK 4 (fine time step equal to 1.00) even failed to produce a presentable result. The considerable error can be attributed to one of the following factors:

1) The hypothesis of constant discontinuity factors quickly becomes inexact. The coarse shape functions are inaccurately calculated during coarse steps, leading to a considerable amount of error in relative total power.

2) The basic hypothesis of the quasi-static approach, which is to consider a constant shape function for a certain time, is not accurate for the transients involving intense shape distortions such as a LOCA. In other words, the solution procedure loses its efficiency during the point-kinetics calculations not the coarse shape calculations. This means that even using exact values of discontinuity factors cannot improve the precision of the results.

Various numerical tests can be designed and performed to clarify which of the aforementioned explanations is more accurate. For example, all exact equivalence parameters can be pre-calculated and then be used during the simulation period. A more interesting method is to eliminate the flux factorization procedure and consequently point-kinetics calculations. This would result in a different formalism of the hierarchical nodal kinetics that is the subject of the next section.

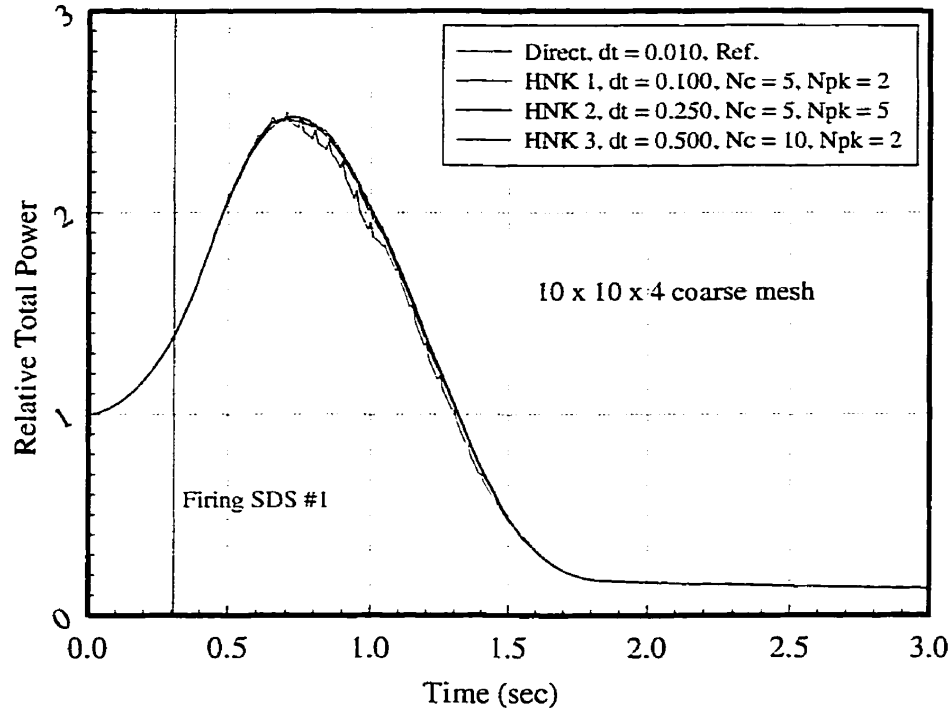

Figure 4.24: Relative total power obtained from HNK method

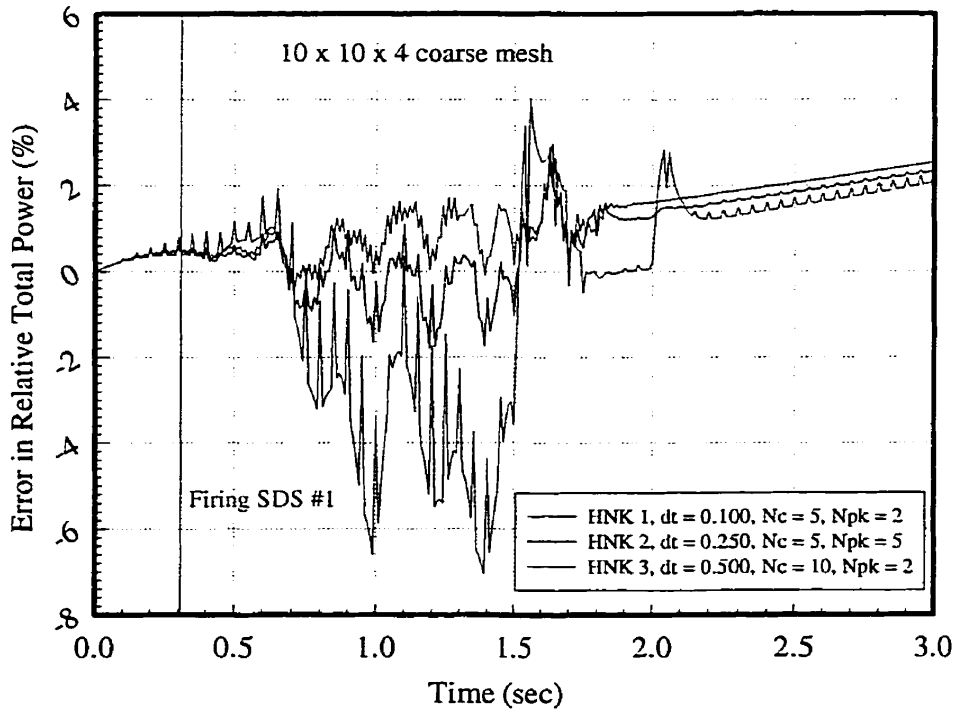

Figure 4.25: Error in relative total power obtained from HNK method

4.6.6 Two Time-Level Full Flux vs. Extended Quasi-Static Method

To eliminate the inherent errors caused by the use of quasi-static approach (extended or classical), one solution is to perform full flux calculations (instead of shape function calculations) over fine and coarse configurations of the reactor. After completing each coarse-level flux calculation, the fine flux will be reconstructed using the last available average coarse node flux and the intranodal fine-flux distribution. The reconstructed fluxes will be used to update all equivalence parameters except the discontinuity factors, which are considered constant during a fine-level time step. Hence, all prescribed perturbations including device movements will be projected to the coarse level by only cross sections and diffusion coefficients. This approach would establish a two-level time hierarchy rather than a three-level time hierarchy. The test cases 01 through 04 are designed to evaluate the performance of this specific formulation of hierarchical nodal kinetics. The input parameters for the test cases are presented in table 4.4. Figures 4.26 and 4.27 show the results obtained for these test cases. The first observation is that all test cases are able to produce a relatively acceptable solution. One interesting situation is test case 04, which for all periods of the transient uses constant discontinuity factors calculated at the beginning of the transient. It is not surprising that the resulting error in relative total power is relatively considerable (up to +9 %). This amount of error can be uniquely attributed to the use of constant discontinuity factors. As is expected, smaller fine-level time steps will result in a smaller amount of error in the solution (case 03 and 04). The conclusion is straightforward:

"For transients involving very intense perturbations such as a LOCA, a two-level (or a multi-level) full flux calculation is computationally superior to a multi-level shape function calculation based on the quasi-static approach."

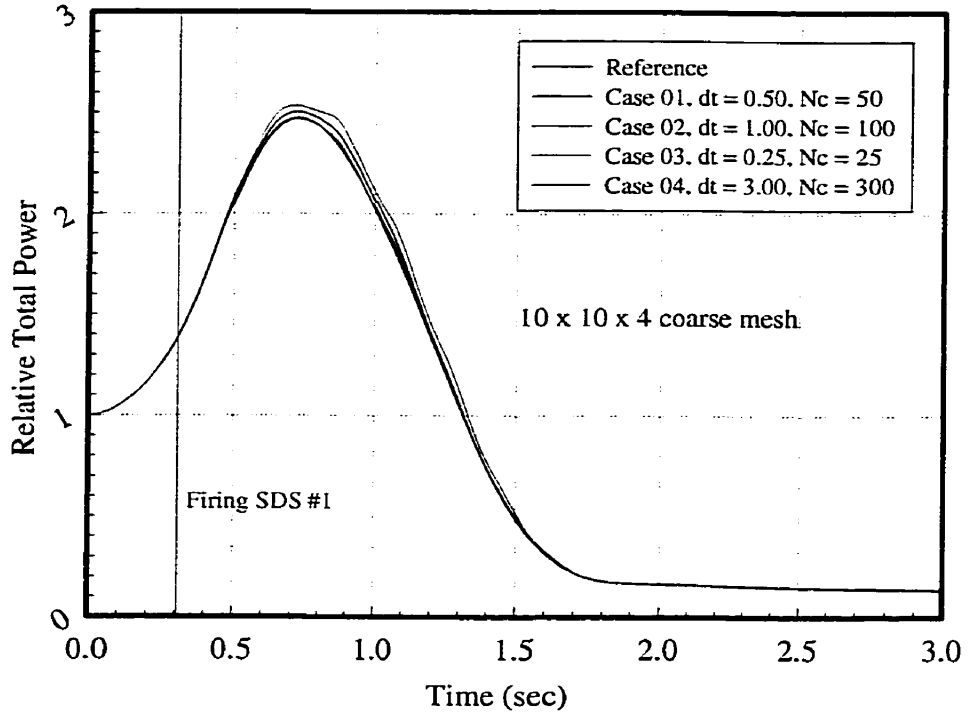

Figure 4.26: Relative total power case 01 to case 04

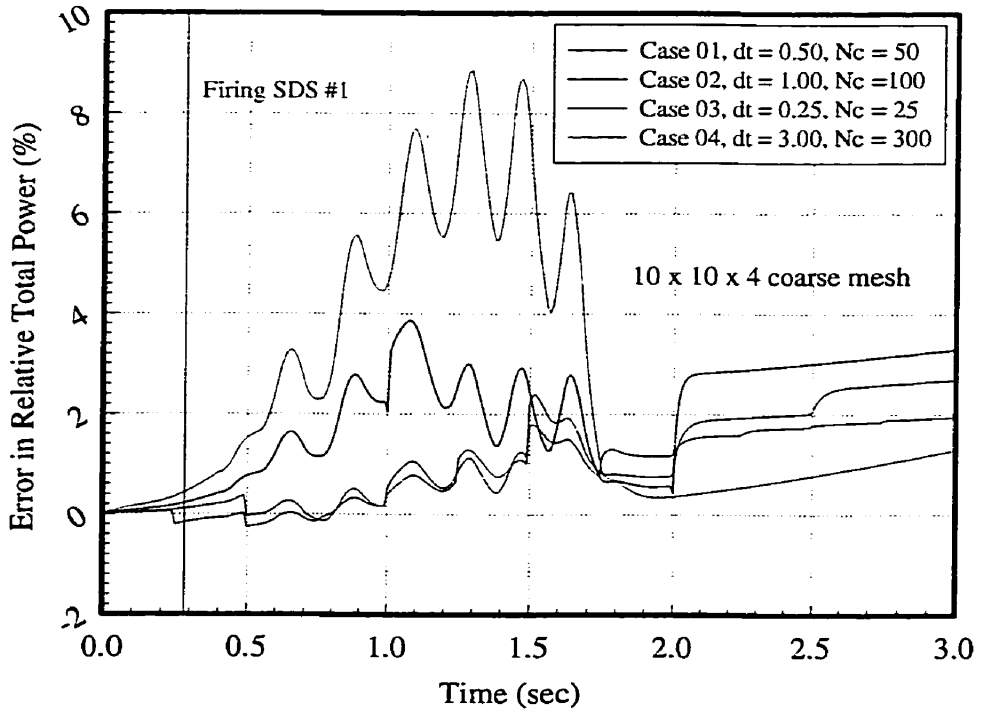

Figure 4.27: Error in Relative total power case 01 to case 04

4.6.7 The Effect of Number of Coarse Nodes

To analyze the effect of the number of coarse nodes on the accuracy of the final solution, a set of complementary test cases is designed and performed. The test cases 05 through 08 (tables 4.4 and 4.5) are similar to the test cases 01 through 04 except the number of coarse nodes is set to 5 x 5 x 4. The results obtained are shown in figures 4.28 and 4.29. It can be observed that regardless of the implied fine-level time step, the amount of error in relative total power is quite high (up to –30%). Moreover, the amount of error would not necessarily decrease using smaller fine-level time steps (for example case 05 vs. case 08). The resulting errors can be attributed to two factors: first, the reconstruction procedure and second, inherent floating point errors.

Reconstruction procedure: the comparison of reconstructed fluxes obtained from cases 01 and 07 showed that the prediction of the fine-node fluxes at a given time can differ by 30 %, though in both cases, the reconstructed fluxes preserve both total group reaction rates and surface currents obtained from the coarse nodes. The erroneous reconstructed fluxes will then be used to update the coarse node cross-sections and diffusion coefficients of the next time step causing unpredictable amount of error in the next coarse calculations.

Inherent floating point errors: in section 4.2, it is shown that the floating-point errors in the coarse calculations involving bigger coarse regions diffuse faster than those diffuse in the cases involving smaller coarse regions. One way to decrease the amount of error produced by floating point calculations is to implement higher precision variables for the period of simulation. However, the preparation of a higher-precision version of the computer code NDF requires a considerable amount of effort and time. Thus, using a simpler approach would be preferable. To overcome the errors due to effect of the number of coarse nodes, many solutions can be suggested. An efficient solution is to perform a do-nothing transient for different coarse configurations of the reactor and

then choosing the one that produces the minimum amount of error. Numerous tests demonstrate that the difference in the total CPU time for the cases with 5 x 5 x 4 and 10 x 10 x 4 is almost negligible. Thus, the smaller coarse nodes would be computationally a safer choice. Another criterion for the choice of coarse mesh configurations is the intensity of the prescribed perturbations. For transients involving very intense local perturbations smaller coarse configuration can be strongly suggested. For transient simulations of the CANDU-6 reactors involving very strong perturbations (LOCA), it has been demonstrated that the choice of 10 x 10 x 4 can be safely used. For the less intense transients such as reactor stepback due to rod ejection, bigger coarse nodes (5 x 5 x 4) can be comfortably used. It is necessary to mention that the use of a more complicated reconstruction procedure and consequently a more time-consuming procedure cannot be easily justified in the framework of the CANDU-6 reactors, because the use of smaller coarse nodes generally results in a significant improvement in the final solution without considerable penalty in the total CPU time.
The bottom line is: A minimum number of coarse nodes is required to maintain the efficiency of the two-level full flux algorithm.

4.6.8 Two Time-Level Full Flux: Additional Comments

Some additional test cases are necessary to complete the analysis of the time-hierarchy approach. Each of these test cases is aimed at a specific aspect of the two-level full flux approach.

Case 09: Test case 09 is designed to confirm the fact that using smaller coarse nodes can significantly improve the precision of the reconstruction method and consequently that of the final solution (see table 4.5 for input parameters). In this special test case, the coarsening of the fine nodes is performed in the x- and y- directions (10 x 10 x 12).

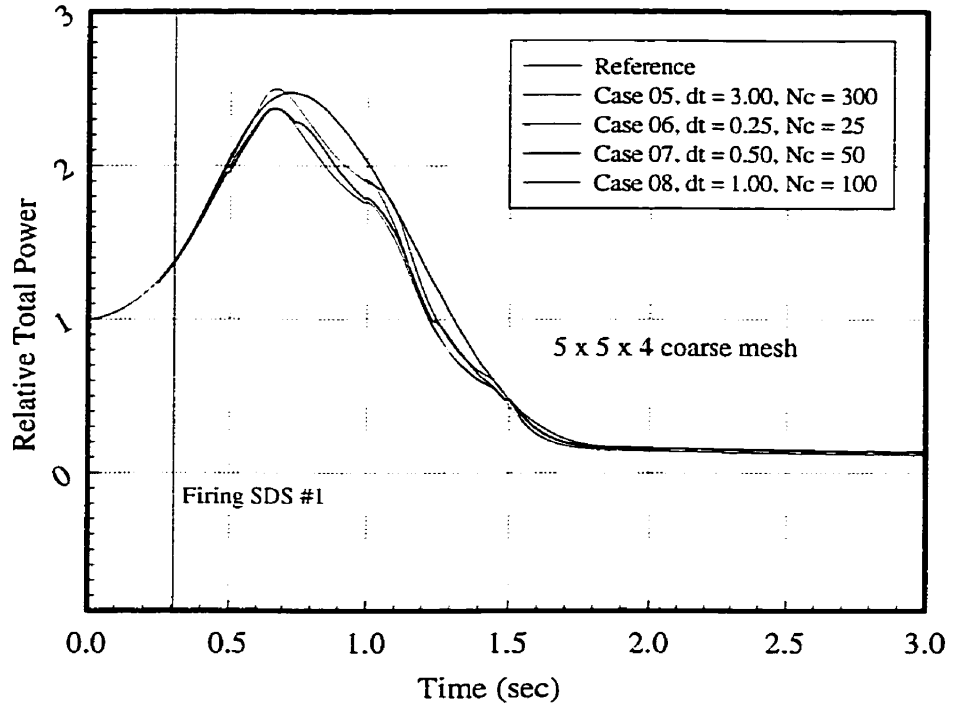

Figure 4.28: Relative total power case 05 to case 08

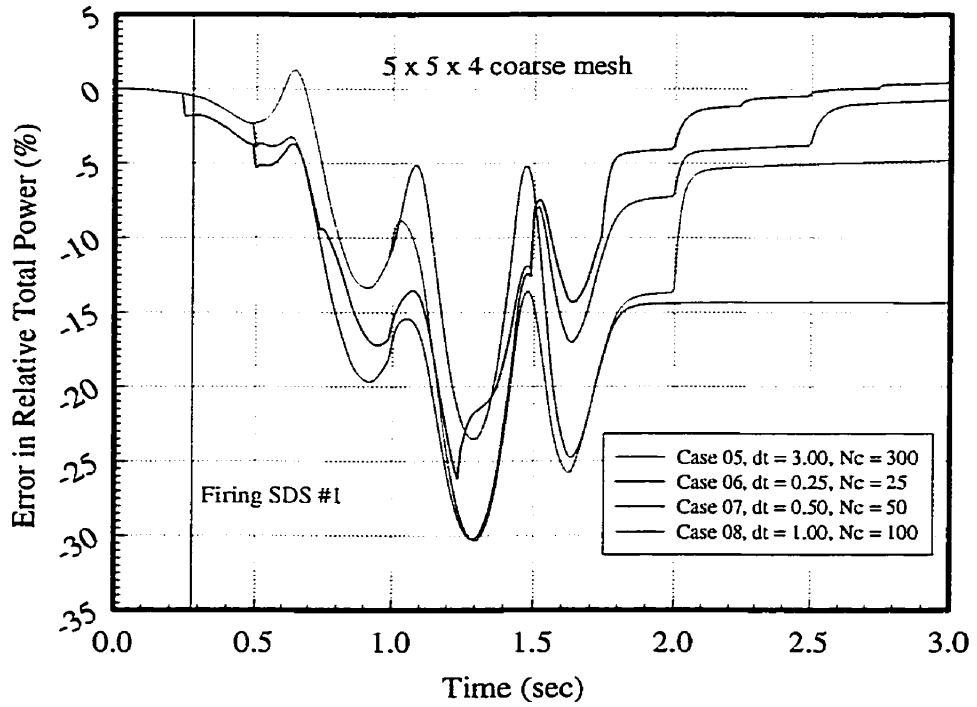

Figure 4.29: Error in Relative total power case 05 to case 08

Thus, in z-direction the number of coarse and fine nodes is equal (12 for both cases). Figures 4.30 and 4.31 show that the solution obtained from this test case is in good agreement with the reference solution (a maximum error of almost +1%).

Case 10 and 11: It is widely accepted that using tabulated values of equivalence parameters is a satisfying approach for approximating the values of discontinuity factors during a transient involving complicated device movements. To examine the validity of this approach, test case 10 was designed and performed. In this case, after each fine-level calculation, the position of safety and reactivity devices is scanned and used to initialize an off-line static calculation corresponding to that state of the reactor. The discontinuity factors obtained from these static calculations are then used for the coarse calculations during the next fine-level time step. These off-line static calculations would eliminate the necessity of performing well-known interpolation procedure for approximating the values of discontinuity factors. Figures 4.30 and 4.31 shows the results obtained from this test case. It can be observed that the use of static discontinuity factors results in a bigger amount of error in the reactor solution compared to the cases where the piecewise constant dynamic discontinuity factors are used (case 10 vs. case 01, figures 4.26 and 4.27). This difference can be attributed to the fact that the piecewise constant dynamic discontinuity factors covers for both device interference effects and dynamic flux distributions while the static discontinuity factors only covers the device interference effects. Numerous numerical simulations also showed that using the correction terms or a linear combination of static and dynamic discontinuity factors cannot give rise to a better solution compared to the cases where the piecewise-constant dynamic discontinuity factors are used. Test case 11 is a typical example of these approaches where a linear combination of static and dynamic discontinuity factors is used for the coarse node calculations, i.e., ε=0.5 in relationship 2.82. It can be observed that the results obtained for this test case is less accurate compared to the cases where only static or only piecewise constant discontinuity factors are used (case 11 vs. cases 10 and 01, figures 4.26 and 4.27).

Case 12: Test case 12 is aimed at the study of the effect of coarse-time steps in the precision of the solution. Figures 4.30 and 4.31 prove that using smaller coarse-level time steps does not lead to an improvement in the results. This is not surprising since the accuracy of the result depends primarily on the "fine-level" time steps not on the coarse-level time steps.

4.6.9 LOCA: Time Performance Comparison

The next step in the evaluation procedure is to compare the speed of the various calculations. The comparison is done based on the total CPU time necessary to complete the transient simulation. The results are presented only for the cases that produce accurate enough results. The case IQS 1 is also presented to give an idea of the CPU time necessary for the improved quasi-static methods. The direct method with a time step equal 0.05 second is excluded since for practical purposes, the time step equal to 0.05 is a very long time step due to the restrictions imposed by the thermalhydraulics model. Applying relationship (4.4) and considering the total necessary CPU time for the reference case (almost 380 seconds in this case), the gain in overall performance of different methods are calculated and compared in figure 4.32.

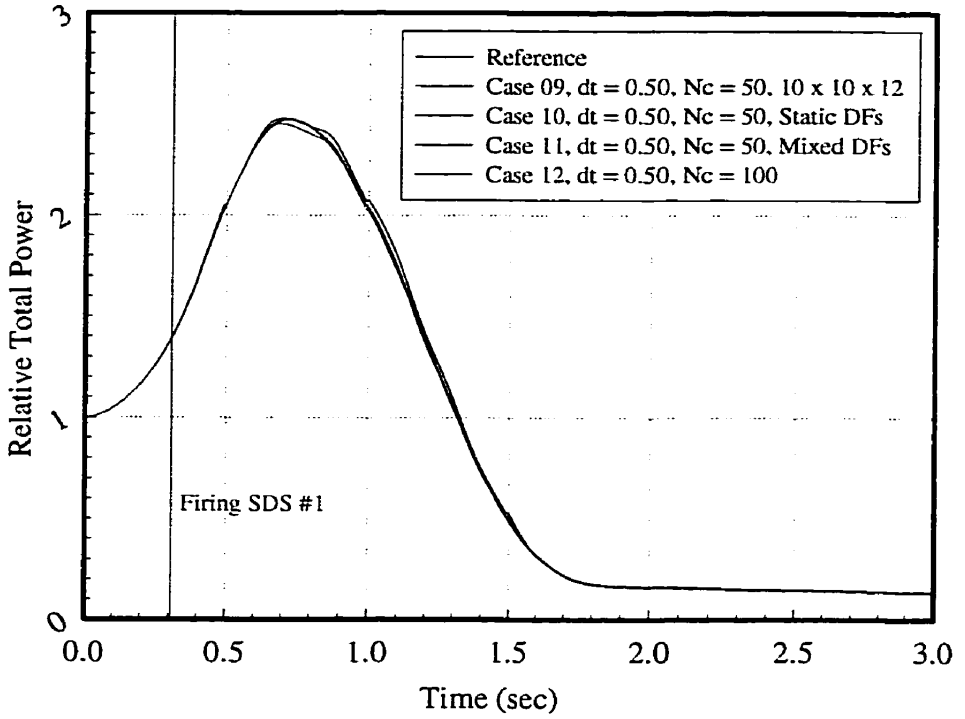

Figure 4.30: Relative total power case 09 to case 12

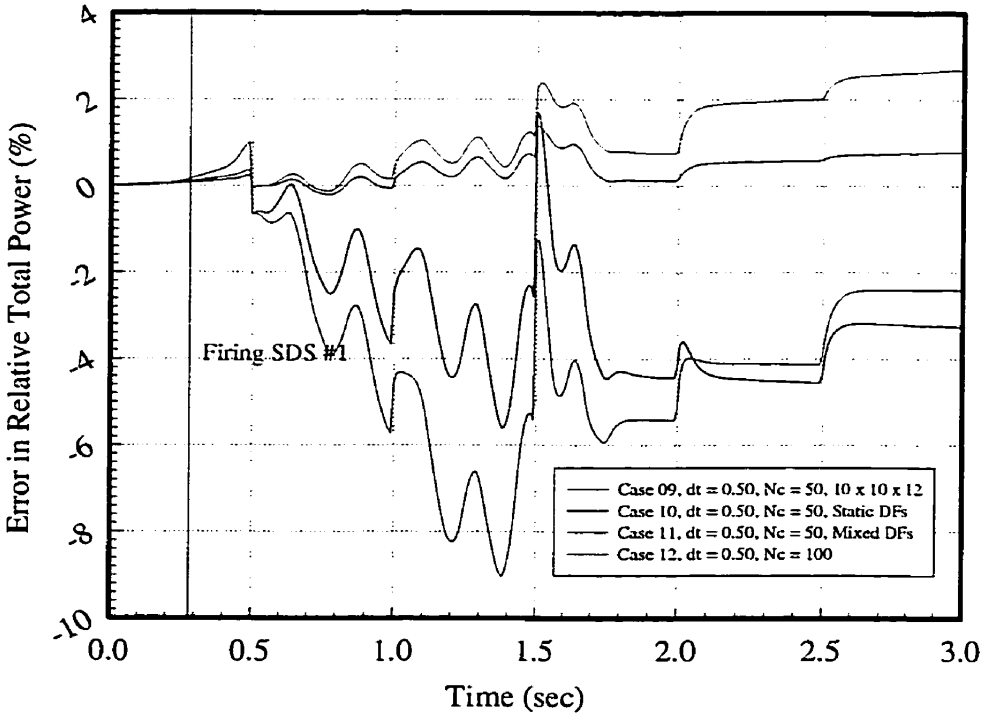

Figure 4.31: Error in relative total power case 09 to case 12

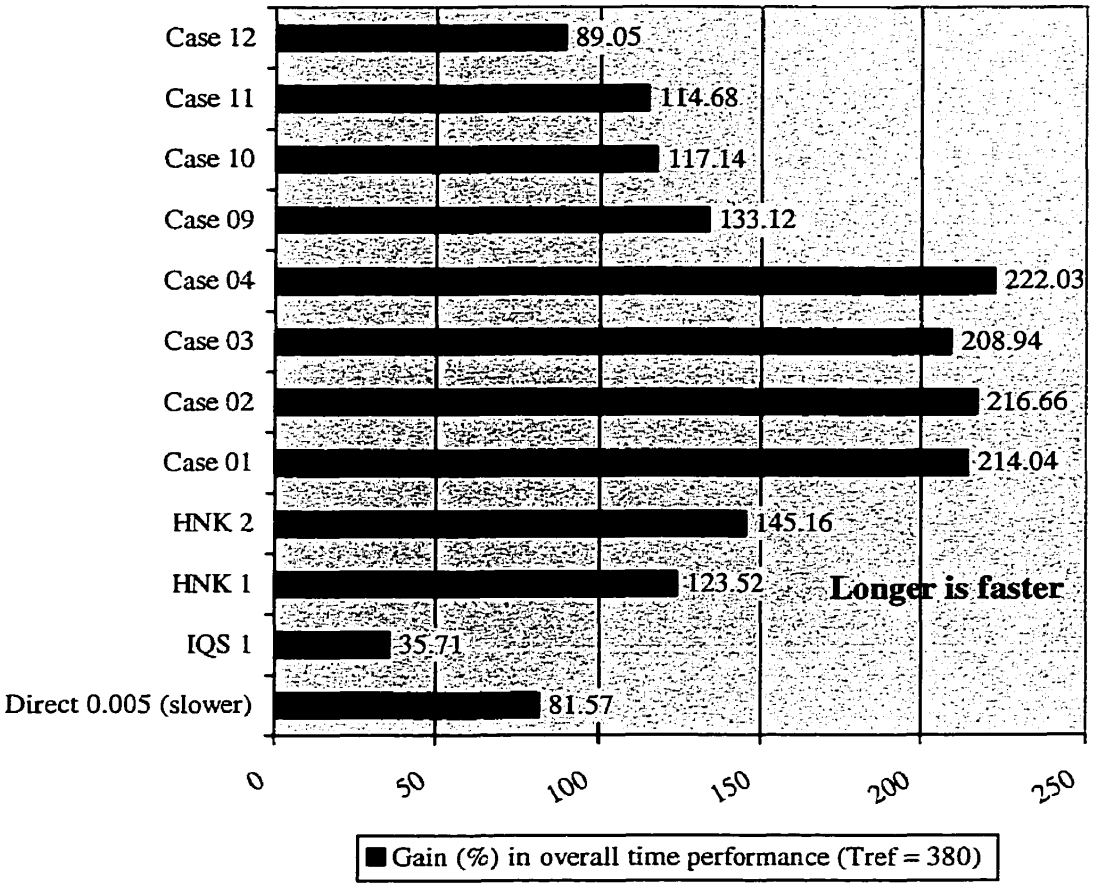

Figure 4.32: Gain (or loss) in overall time performance compared to the reference

The conclusion is straightforward: "the two-full flux approach is superior to all the quasi-static approaches (classical or extended) in both accuracy of the solution and speed of calculations." Thus, considering these two factors, from the user's point of view, the choice of a solution method is now an easy task.

4.6.10 Space Hierarchy: Multigrid Method

In some circumstances, such as those defined by regulatory organizations or those prescribed by design standards, the reactor calculations must be performed by using an accurate solution algorithm. In these situations, the implementation of various

simplifying hypotheses such as flux factorization is not allowed. Furthermore, the user might also be compelled to apply very fine time and space discretization for the reactor simulations. Consequently, the necessary CPU time for completing the reactor calculations will be considerably increased. For these situations, the use of acceleration techniques can be strongly recommended, since they are generally aimed at the reduction of the total CPU time necessary without compromising the accuracy of the resulting solution.

As explained in chapter 2, hierarchical nodal kinetics provides two formalisms: time hierarchies and space hierarchies. In the time hierarchies, the coarse-grid calculations are aimed at finding the flux distribution of the next time step. While in the space hierarchies, they are rather a means to accelerate the flux calculations for the present time. In this section, the performance of the space-hierarchy formalism will be examined. As usual, the evaluation procedure must be carried out based on both accuracy of the solution and speed of the calculations. The accuracy of the resulting solutions will be almost the same, since the algebraic equations to be solved are the same and only the iterative methods are different. Thus, the evaluation procedure will be restricted to the comparison of execution speeds.

4.6.10.1 Cases with 26 x 26 x 12 fine nodes

Based on space hierarchy algorithm, which is a multigrid approach, a set of test cases for LOCA analysis is designed and performed. The input parameters for the selected test cases are presented in table 4.6. The first group of simulations is performed over the default fine configuration of the reactor that is one mesh per fuel cell (26 x 26 x 12). The results are shown in the figure 4.33. These results confirm that by applying this multigrid acceleration technique the number of fine iterations can be reduced slightly (case 17 vs. case 16). Moreover, as it is expected, using smaller coarse grids results in a smaller number of iterations for converging to the solution (case 17 vs. case 18).

However, taking into account the necessary CPU time for the homogenization procedure, solving the resulting coarse problem and reconstructing procedure, this slight advantage can be immediately lost. This is not surprising since similar to all other acceleration techniques, a minimum number of grids is required to make the acceleration technique computationally useful. For the smaller problems, such as the test cases presented in this section, normally a well-optimized classical iterative method such as successive over-relaxation is sufficient. Since the problem is relatively fast convergent, in the present work, the optimal value of ω is determined based on a simple trial and error approach. The choice of optimal ω would be more precise if it was determined based on some auxiliary approaches (for example see Nakamura 1977).

Table 4.6: Input parameters for the selected test cases[1]

	Dt	Fine mesh	Coarse mesh	Iterative Solution Method
Case 13	0.01	26 x 26 x 12	--	Gauss-Seidel
Case 14	0.01	26 x 26 x 12	--	SOR, $\omega = 1.20$
Case 15	0.01	26 x 26 x 12	--	SOR, $\omega = 1.40$
Case 16	0.01	26 x 26 x 12	--	SOR, $\omega = 1.47$
Case 17	0.01	26 x 26 x 12	10 x 10 x 4	Multigrid-SOR, $\omega = 1.47$
Case 18	0.01	26 x 26 x 12	5 x 5 x 4	Multigrid SOR, $\omega = 1.47$
Case 19	0.01	52 x 52 x 24	--	SOR, $\omega = 1.42$
Case 20	0.01	52 x 52 x 24	10 x 10 x 4	Multigrid, SOR, $\omega = 1.42$
Case 21	0.01	52 x 52 x 24	5 x 5 x 4	Multigrid, SOR, $\omega = 1.42$

[1] Convergence criteria for all test cases set to 10^{-6}.

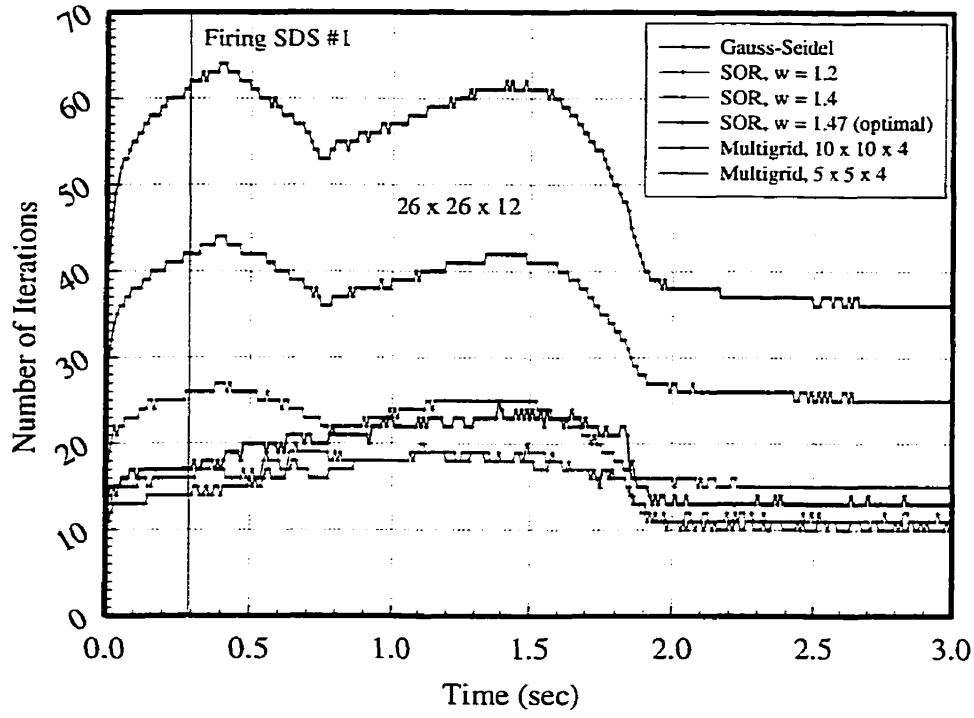

Figure 4.33: Number of iterations for different iterative methods (26 x 26 x 12)

In practice, however, implementation of an additional subprogram to calculate the optimal ω must be carefully evaluated to prevent any penalty in execution time.

4.6.10.2 Cases with 52 x 52 x 24 fine nodes

The test cases 19 through 21 are performed using a fine mesh configuration of 52 x 52 x 24 nodes representing eight nodes per fuel cell. The input parameters are presented in table 4.6. The results show that by applying the new multigrid technique (figure 4.34), the number of iterations required for the given convergence criterion (10^{-6}) is significantly reduced. Consequently, the corresponding total CPU time is reduced by almost the same amount (figure 4.35). For all cases, the CPU time consumed by the solver module is measured from the moment the module is initialized until the moment that the converged solution becomes available for the next modules. The total CPU time for the multigrid cases consist of the CPU time necessary for the homogenization

procedure, solving coarse grid problem, reconstruction procedure and solving the fine grid problem. Additional time profiling proves that for the multigrid cases, almost only 10% of the total CPU time is consumed by the multigrid part of the scheme. Moreover, additional tests demonstrated that this multigrid technique becomes more efficient when the number of fine grids increases. Examination of the results, once more, shows that using smaller coarse grids (which means a more precise flux reconstruction) result in a better convergence rate for the final solution.

One unique feature of this multigrid scheme is the way it accelerates the convergence rate of the iteration procedure. In the majority of geometric multigrid techniques, the smooth part of the error function is converted to a rapidly oscillating function by changing the mesh dimensions and using an appropriate restriction operator. In these cases, the restriction and interpolation operators as well as the coarse mesh dimensions are primarily determined based on a detailed analysis of the error function for the underlying iterative algorithms. In the new multigrid technique presented in this work, the acceleration is achieved by a completely different mechanism. First, a physically equivalent problem over an arbitrary coarse space is defined. Then this equivalent problem is solved over that arbitrary coarse grid. Finally, the equivalent solution, which in most cases is an excellent approximation of the real solution, is projected back to the fine grids preserving the physical properties of the equivalent solution (total group reaction rates and group surface currents). Hence, the connection between different space levels is done based on the physical properties of the problem not the mathematical behavior of the implemented iterative method. This feature permits a complete decoupling between the mathematical nature of iteration algorithm (the way its error function behaves) and the definition of restriction and interpolation operators as well as coarse mesh spacing. Thus, further acceleration techniques can be independently applied to each of the space hierarchies without being concerned about possible undesired consequences. Moreover, the definition of coarse grids becomes almost arbitrary and independent of the way the error function of the iterative methods

behaves. The only restriction is that the user must be certain that homogenization of the coarse grids based on generalized equivalence theory is possible.

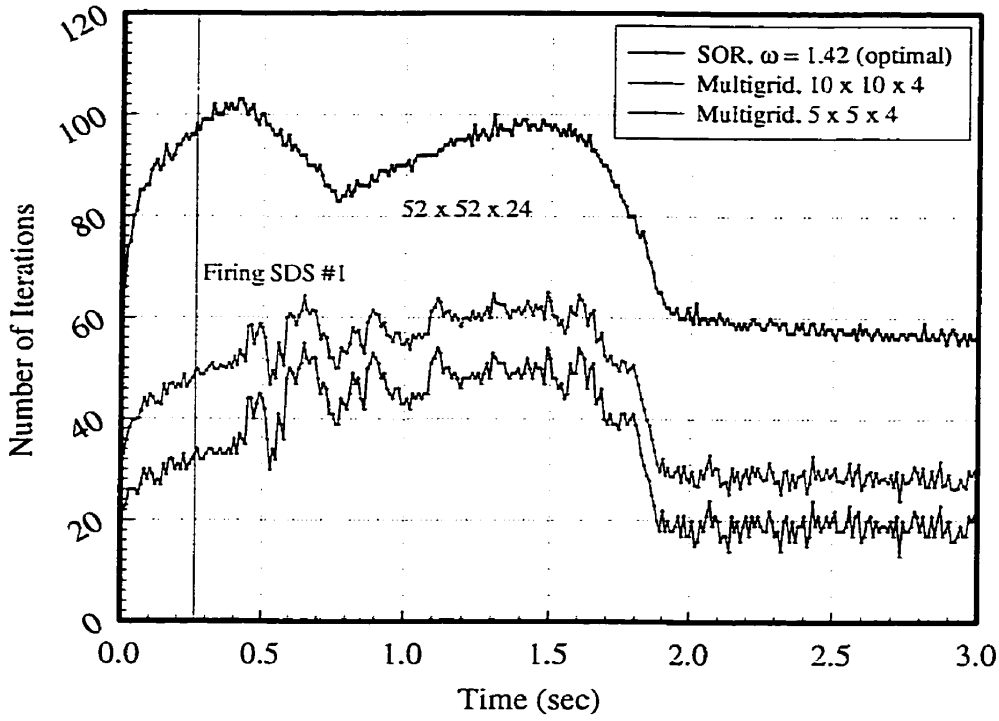

Figure 4.34: Number of iterations for different iterative methods (52 x 52 x 24)

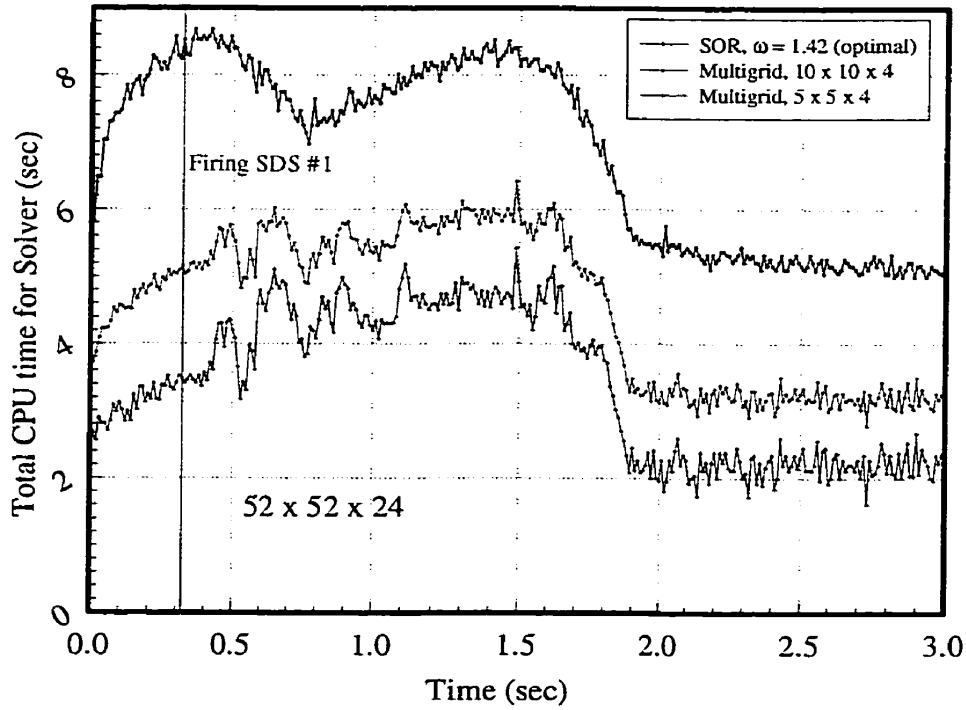

Figure 4.35: Total CPU time for the solver module (sec)

CONCLUSION

In an attempt to accurately predict the flux distribution and total power during a transient, a new numerical algorithm called hierarchical nodal kinetics has been developed. The essence of this method is the definition of one or more intermediate coarser grids over which the reactor problem is solved at a much lower computational cost. To maintain the accuracy of the coarse calculations, the projection of the reactor problem from the finer grids to the coarser grids is carried out using generalized equivalence theory and so-called discontinuity factors. Two formalisms of hierarchical nodal kinetics are established; these are the time-hierarchy and space-hierarchy approaches. In the time hierarchy formalism, the solution of the reactor over these coarse grids is treated as the reactor solution (or a part of the reactor solution) for the next time step. In the space hierarchy formalism, these intermediate solutions are rather used to accelerate the convergence rate of the fine-grid problem. It is clear that the success of this algorithm depends primarily on the quality of the intermediate coarse calculations, which in turn depends upon how well the equivalence parameters are estimated to correctly reflect the changes in the *reactor state*. In order to decrease the required number of fine calculations in both static and dynamic calculations, one treatment, which has been widely used in similar procedures, is to establish an equivalence parameter database for each of the reactivity devices. When more than one reactivity device is present in the reactor core, these tabulated data are interpolated upon the various independent variables to approximate the nodal equivalence parameters. The hierarchical nodal kinetics recommends rather the use of dynamic flux distribution to evaluate "piecewise-constant dynamic discontinuity factors".

Based on this new algorithm, a computer code called NDF has been developed. This code is primarily designed to handle static and dynamic calculations related to CANDU type reactors involving all reactivity and safety devices. Numerous simulations (for both static and dynamic calculations) were designed and performed to better understand

different aspects of using generalized equivalence theory and thus to correctly evaluate the performance of the hierarchical nodal kinetics. All test cases were performed for a relatively realistic model of a CANDU-6 reactor. Some of the important conclusions will be outlined here.

Static Calculations

Based on numerous static calculations, it was confirmed that no matter what the number of coarse grids is, using exact values of the equivalence parameters would always result in a very accurate reproduction of the reactor eigenvalue and the collapsed nodal average fluxes. However, the errors in collapsed nodal fluxes for the cases with larger coarse grids are greater than those obtained from smaller coarse grids. This behavior is primarily attributed to inherent errors in the floating-point calculations.

After that, to study the effect of device positions on the values of equivalence parameters (particularly discontinuity factors), a series of test cases for adjuster rods, liquid zone controllers and mechanical control absorbers were designed and performed. No reusable pattern for the dependence of equivalence parameters (especially discontinuity factors) on reactivity device positions could be established.

Then, the effect of using a set of reference equivalence parameters (instead of exact values) was studied. It was found that using the reference equivalence parameters for adjuster rods and mechanical control absorbers would result in significant errors in the coarse flux calculations. These errors were found to be much smaller for the liquid zone controllers since their absorption cross sections are much smaller than those of adjuster rods and mechanical control absorbers. Furthermore, it was shown that forcing preservation of the total neutron reaction rates (by using only exact cross sections for coarse nodes) would significantly reduce the average error in the coarse flux calculations. While using only exact discontinuity factors would give rise to the

significant errors in the coarse flux calculations. This was not surprising since using exact values of discontinuity factors only preserves the coarse surface currents without actually preserving the total neutron reaction rates. Another conclusion was that no special pattern for the dependence of the average flux error on the device(s) position(s) could be established.

The next step was to examine if interpolating the values of an equivalence parameter database to approximate their real values is an acceptable approach or not. Thus, additional tests were designed and carried out. From the beginning, some serious difficulties were encountered for this approach. For example, it was clear that due to the substantial number of the reactivity devices, considering all possible device positions for generating the database would not be practical. Furthermore, since the values of equivalence parameters depend upon the coarse geometry configuration, producing a database for all possible coarse geometry configurations would not be reasonable. The results obtained from test cases brought up further difficulties for this approach. It was shown that the relationship between equivalence parameters and flux shape are non-linear, thus simple interpolation or superposition of database values could not produce acceptable estimates for the values of equivalence parameters. Moreover, the coarse flux calculations are sensitive to the values of equivalence parameters thus inexact values of the equivalence parameters (obtained from database) could yield substantial errors in the flux calculations.

Finally, the effect of xenon load on the discontinuity factors was studied. It was found that due to the dependence of the equivalence parameters (particularly discontinuity factors) on the flux shape, the changes in the equivalence parameters due to xenon load were not negligible. Thus, it was concluded that the use of constant equivalence parameters during very long transients such as those involving xenon might deteriorate the precision of the results.

Dynamic Calculations

To evaluate the performance of the hierarchical nodal kinetics method in reactor transient simulations, three specific formalisms were selected. The first one was an extended version of the improved quasi-static method where an intermediate coarse level was used to allow for the frequent updates of the shape function (applied to scenario #1, #2). These frequent updates would maintain the validity of the basic hypothesis of the quasi-static approach, that is to consider a constant shape function for a long time step. The second formalism did not involve any flux factorization; thus, the intermediate level was used to perform the full flux calculations corresponding to the next time step (applied to LOCA analysis). Finally, in the third formalism, the calculations obtained from the intermediate level were used to accelerate the convergence rate of the fine problem (applied to LOCA analysis).

Once the formalisms had been selected, the next step was to determine how the performance of the hierarchical nodal kinetics or any other method would be evaluated. Two comparison criteria were selected and formulated: first accuracy of the method and second, corresponding calculation speed. After that, based on a set of do-nothing transients, the stability of the hierarchical nodal kinetics scheme for different input parameters was verified and confirmed. It was found that the accumulation of error in the solutions obtained from the hierarchical nodal kinetics is inherently greater than obtained by using the other methods and this error accumulation might bring up some difficulties during the transient simulation.

The first scenario was the simulation of a reactor stepback based on a hypothetical rod ejection. The results obtained from the use of hierarchical nodal kinetics resulted in a performance increase of between 85% and 150% as compared to the reference solution while maintaining the accuracy of the solution. The overall gain was less than expected, however, it was found that these differences were primarily due to the CPU time

necessary for executing and moving data between supporting modules. In the second scenario, it was also shown that the overall gain in the performance was around 98% to 125% over the reference solution.

In the third scenario, a simplified but efficient model of a LOCA was developed. After performing numerous tests, the first conclusion was that the quasi-static approaches (classical or extended) are not computationally efficient for these types of transients. The deficiency was attributed to the hypothesis of a constant shape function over a certain time. It was shown that the error for these cases was generated during point-kinetics calculations and frequent updating of shape functions over fine or coarse would not result in a significant improvement in the final solution. Thus, it was immediately expected that the use of the second formalism, which is a two-level full flux calculation, would be much more efficient for the LOCA analysis. It was observed that the accuracy of the results obtained using the full-flux approach was strongly dependent on the volume of the coarse grids and it was concluded that a minimum number of coarse grids was required to guarantee the accuracy of the two-full flux approach. The considerable error due to the use of bigger coarse grids was found to be generated during the reconstruction procedure. To deal with this effect, some practical remedies were suggested, among others defining a smaller coarse representation of the reactor. One very important conclusion supported by numerous tests was that the use of tabulated static discontinuity factors would result in a considerable error in the flux calculations. It was shown that the approach of hierarchical nodal kinetics method, which is to use piecewise-constant dynamic discontinuity factors, is superior to the use of interpolated static discontinuity factors (at least for CANDU-type reactors). In other words, using dynamic flux snapshots representing the actual state of the reactor is an intrinsic choice for calculating discontinuity factors, not off-state static flux distributions.

In the last part, the performance of the space hierarchy formalism, which is a multigrid approach, was evaluated. It was found that for the cases with a small number of fine

grids, the method would not produce significant saving in CPU time. However, when the number of nodes is increased, the method quickly becomes more efficient. In a LOCA analysis, it was verified that the number of iterations necessary for a given convergence criterion can be reduced by at least 50% resulting in a considerable saving in total CPU time.

Recommendations

The results obtained using hierarchical nodal kinetics confirmed that actual version of this method could be useful for realistic CANDU-type reactor simulations. However, many improvements can still be implemented.

The author believes that the first priority is to introduce an auto-switching (adaptive) mechanism into the scheme. Numerous spatial levels can be defined, from a very fine space to an ultra-coarse space. The ultra coarse space is actually the projection of the whole reactor into one very big node. When the flux distortions are significant, the problem would be solved over a very fine space by using space hierarchies to accelerate the convergence rate of the fine problem. As soon as the intensity of the perturbations decreases, the auto-switching mechanism would project the reactor problem onto a coarser grids and solve it by an appropriate time hierarchy approach. Even in a more advanced auto-switching model, the coarse levels are not pre-configured. They are rather built during the transient simulation permitting the definition of finer grids around moving devices and coarser grids for the zones far enough away from these devices. The initial tests using simple auto-switching criteria such as total power and dynamic reactivity were partially successful. However, the need for a better switching criterion was immediately felt. The possibility of implementing a variable time step algorithm inside the auto-switching module could also be a very interesting follow-up for the conventional hierarchical nodal kinetics method.

Another interesting case to be studied is the development of an embedded version of hierarchical nodal kinetics. In this embedded version, the algorithm and all other supporting modules would be uniquely re-programmed for a very specific reactor. Thus, the necessary CPU simulation times would be considerably reduced. Since the hierarchical approach results in a considerable economy in the number of fine-level calculations, it would be interesting to evaluate the performance of the method for real-time or near real-time simulations.

Since the definition of coarse grids in hierarchical nodal kinetics is somewhat arbitrary, the spatial mesh for neutronics and thermal-hydraulics codes could be overlaid. In other words, the hierarchical nodal kinetics could follow the spatial requirements of the thermal-hydraulics model. This advantage inherently permits a better coupling between the neutronic and thermal-hydraulics codes. It is clear that achieving a very tight coupling between the neutronic and thermal-hydraulics models is a very fertile field of research.

Another interesting area of the study is the possibility of using a more advanced reconstruction method especially for the multigrid approach. A better reconstruction method would lead to greater CPU time economy in the fine iterations. However, the performance of a new reconstruction method must be ultimately evaluated based on both its accuracy and its computational cost.

Finally, applying a higher-order direct method such as nodal method in the fine level calculations can be strongly recommended. A thorough performance evaluation based on the accuracy of the resulting solutions and the speed of corresponding calculations will evaluate the usefulness of those higher-order methods (at least for CANDU-type reactors).

BIBLIOGRAPHY

ABU-SHUMAYS, I. K. and HAGEMAN, L. A., (1975). *Development and Comparison of Practical Discretization Methods for the Neutron Diffusion Equations over General Quadrilateral Partitions.* Proc Conf. Computational Methods in Nuclear Engineering, CONF-750413, I, 117-165, Charleston.

ADAMS, C. H., (1977). *Current Trends in Methods for Neutron Diffusion Calculations.* Nuclear Science and Engineering, Vol. 64, 552-562.

AECL-6593, (1979). *Data Base for a CANDU-PHW Operating on a Once-Through Natural Uranium Cycle.* Atomic Energy of Canada Limited, AECL-6593, INFCE/WG 8/CAN/DOC 2.

AL-CHALABI, R. M., TURINSKY, P. J., FAURE, F. X., SARSOUR, H. N. and ENGRAND, P. R., (1993). *NESTLE: A Nodal Kinetics Code.* Transactions of American Nuclear Society, Vol. 68, 432.

AL-CHALABI, R. M. and TURINSKY, P. J., (1994). *Application of Multigrid Method to Solving the NEM form of Multigroup Neutron Diffusion Equation.* Transactions of American Nuclear Society, Vol. 71, 259.

ANL, (1985). *Benchmark Problem Book,* Argonne National Laboratory, ANL-7416, ID 17-A2.

AVILES, B. N., (1993). *Development of a Variable Time-Step Transient NEM Code: SPANDEX.* Trans. Am. Nucl. Soc., Vol. 68, 425-427.

AXELSSON, O., (1994). *Iterative Solution Methods.* Cambridge University Press.

BRANDT, A., (1977). *Multi-level Adaptive Solutions to Boundary Value Problems.* Mathematics of Computation, Vol.31, No. 138, 333-390.

CHAO, Y.-A. and ATTARD A., (1985). *A Resolution of the Stiffness Problem of Reactor Kinetics.*, Nuclear Science and Engineering, Vol. 90, 40-46.

CHAO, Y.-A. and HUANG P., (1988). *Theory and Performance of the Fast-Multidimensional Pressurized Water Reactor Kinetics Code SPNOVA-K.*, Nuclear Science and Engineering, Vol. 103, 415-419.

DEVOOGHT. J and MUNND, E. (1980). *Generalized Quasi-Static Method for Nuclear Reactor Space-Time Kinetics.* Nuclear Science and Engineering, Vol. 76, 10-17.

DODDS, H. L. Jr., (1976). *Accuracy of the Quasi-Static Method for Two-Dimensional Thermal Reactor Transients with Feedback.* Nuclear Science and Engineering, Vol. 59, 271-281.

FINNEMANN, H., VOLKERT, J. (1988). *Parallel Multigrid Algorithms implemented on Memory-Coupled Multiprocessors.* Nuclear Science and Engineering, Vol. 100, 226.

HENRY, ALAN, F. (1975). *Nuclear Reactor Analysis.* MIT Press, Cambridge, Mass.

HENRY, ALAN, F. (1958). *The application of Reactor Kinetics to the Analysis of Experiments.* Nuclear Science and Engineering, Vol. 3, 52-70.

HENRY, ALAN, F and CURLEE N. J., (1958). *The Verification of a Method for for Treating Neutron Space-Time Problems.* Nuclear Science and Engineering, Vol. 4, 727.

JOO, H. G. and DOWNAR, T. J., (1996). *An Incomplete Domain decomposition Preconditioning Method for Nonlinear Nodal Kinetics Calculations.* Nuclear Science and Engineering, Vol. 123, 403.

KANG, C. M. and HANSEN, K. F., (1973). *Finite Element Methods for Reactor Analysis,* Nuclear Science and Engineering, Vol. 51, 456-495.

KAPS, P. and RENTROP, P. (1979), *Generalized Runge-Kutta methods of order Four wit Stepsize Control for Ordinary Differential Equations.* Numer. Math., Vol.33, 55-68.

KAVEH, S., KOCLAS, J., and ROY, R., (1998). *Three-Level Space-Time Kinetics Based on Supernodal Analysis.* Proceedings, 19th Annual Conference, Canadian Nuclear Society, Vol. 2., Toronto, Canada.

KAVEH, S., KOCLAS, J., and ROY, R., (1999a). *Simulation of CANDU Reactor Transients Using Hierarchical Supernodal Analysis.* Proceedings, 20th Annual Conference, Canadian Nuclear Society, Montréal, Canada.

KAVEH, S., KOCLAS, J., and ROY, R., (1999b). *The Improved Quasi-Static Method vs the Direct Method: A Case Study for CANDU Reactor transients.* Proceedings, 20th Annual Conference, Canadian Nuclear Society, Montréal, Canada.

KAVEH, S., KOCLAS, J., and ROY, R., (1999c). *Reactor Kinetics Using Hierarchical Super Nodal Analysis.* Proceeding, International Conference on Mathematics and Computation, Reactor Physics and Environmental Analysis in Nuclear Applications Madrid.

KOCLAS, J., (1993). *Reactor Kinetics Using a Three Level Time Step Hierarchy Based on Super Nodal Analysis,* Proceedings of the joint international Conference on

Mathematical Methods and Supercomputing in Nuclear Applications, Vol. 1, 581-588, Karlsruhe.

KOCLAS, J., (1996). *Calcul Neutronique de Réacteur.* Lectures Note, École Polytechnique de Montréal, Montréal, Canada.

KOCLAS, J., (1997). *Reactor Control and Simulation.* Lectures Note, École Polytechnique de Montréal, Montréal, Canada.

KOCLAS, J., SISSAOUI, M. T. and MARLEAU, G., (1997). *Comparison between the Multi-Group Improved and Generalized Quasistatic Methods for Different Numbers of Energy Groups.* Ann. Nucl. Energy, Vol. 24, No. 15, 1223-1232.

KOCLAS, J., (1998). *Comparisons of the Different Approximations Leading to Mesh Centered Finite Differences Starting from Analytic Nodal Method.* Ann. Nucl. Energy, Vol. 25, No. 11, 821-838.

KOEBKE, K., and, WAGNER, M. R., (1977). *The Determination of the Pin Power Distribution in a Reactor Core on the Basis of Nodal Coarse Mesh Calculations.* Atomkernenerie, (ATKE), Vol. 30, No. 2, 136-142.

KOEBKE, K., (1978). *A New Approach to Homogenization and Group Condensation.* IAEA Technical Committee Meeting on Homogenization Methods in Reactor Physics, Lugano, 13-15 November.

KOEBKE, K., and, HETZELT, L., (1985). *On the Reconstruction of Local Homogeneous Neutron Flux and Current Distribution of Light Water Reactors from Nodal Schemes. Nuclear Science and Engineering.* Vol. 91, 123-131.

LANGENBUCH, S., MAURER, W., and WERNE, W. (1977a). *Coarse-Mesh Flux-Expansion method for the Analysis of Space-Time Effects in large Light Water Reactor Cores.* Nuclear Science and Engineering, Vol. 63, 437-456.

LANGENBUCH, S., MAURER, W., and WERNE, W. (1977b). *High-Order Schemes for Neutron Kinetics Calculations, Based on a Local Polynomial Approximation.* Nuclear Science and Engineering, Vol. 64, 508-5166.

LAWRENCE, R. D., (1986). *Progress in Nodal Methods for the Solution of the Neutron Diffusion and Transport Equations.* Progress in Nuclear Energy, Vol. 17, No. 3, 271-301./

MARLEAU, G., ROY, R., and HÉBERT, A., (1996). *DRAGON user's guide*, IGE-208, Institut de Génie Nucléaire, École Polytechnique de Montréal.

MONIER, A., (1991) *Application of the Collocation Technique to the Spatial Discretization of the Generalized Quasistatic Method for Nuclear Reactors.* Ph.D Thesis, École Polytechnique de Montréal.

NAKAMURA, S. (1977). *Computational Methods in Engineering and Science.* Wiely and Sons Inc.

NAVARRO, ARIAS Silvio H., (1996). *Étude Numérique des effets de Diffusion Directionnels dans le Coeaur du Réactor Gentilly-2.* Mémoire de Maîtrise, Institut de Génie Nucléaire, École Polytechnique de Montréal.

OTT, K, (1966), *Quasistatic Treatment of Spatial Phenomena in Reactor Dynamics.* Nucl. Sci. Eng., Vol. 26, 563.

OTT, K, and MENELEY D. A. (1969). *Accuracy of the Quasistatic Treatment of Spatial Reactor Kinetics.* Nuclear Science and Engineering, Vol. 36, 402.

PRESS, W. H., TEUKOLSKY, W. T., VETTERLING, W. T., and FLANNERY, B. P., *Numerical Recipes in Fortran. The Art of Scientific Computing, Second Edition.* Cambridge University Press, 731-735.

ROY, R., and HÉBERT, A., (2000). *The GAN Generalized Driver.* Institut de Génie Nucléaire, École Polytechnique de Montréal.

RUGE, J. W. and STÜBEN, K., (1987). *Multigrid Methods.* Frontiers in Appl. Math., SIAM publishing, Chapter 4.

SÁNCHEZ, J., (1989). *On the Numerical Solution of the Point Reactor Kinetics Equations by Generalized Runge-Kutta Methods.* Nuclear Science and Engineering, Vol. 103, 94-99.

SHOBER, R. A., SIMS, R. N., and HENRY A. F., (1977). *Two Nodal Methods for Solving Time-Dependent Group Diffusion Equations.* Nuclear Science and Engineering, Vol. 64, 582-592.

SMITH, K. S., (1980). *Spatial Homogenization Methods for Light Water Reactor Analysis.* PhD Thesis, Massachusetts Institute of Technology.

SMITH, K. S., (1984). *Nodal Method Storage Reduction by Nonlinear Iteration.* Transactions of American Nuclear Society, Vol. 44, 265.

SMITH, K. S., (1986). *Assembly Homogenization Techniques for Light Water Reactor Analysis.* Progress in Nuclear Energy, Vol. 17, No. 3, 303-335.

STACEY, W. M., (1969). *Space-Time Nuclear Reactor Kinetics.* Academic Press, New York.

SUTTON, T. M. and AVILES, B.N. (1996). *Diffusion Theory Methods for Spatial Kinetics Calculations.* Progress in Nuclear Energy, Vol. 30, No. 2, 119-182.

VARIN, E., HÉBERT, A., ROY, R., KOKLAS, J., (1996). *A user's guide for DONJON.* IGE-208, Institut de Génie Nucléaire, École Polytechnique de Montréal.

WACHSPRESS, E. L., BURGESS, R. D., BARON S. (1962). *Multichannel Flux Synthesis.* Nuclear Science and Engineering, Vol. 12, 381-389.

WERNER, W., (1977). *Solution Methods for Space-Time Dependent Neutron Diffusion Equation.* Advances in Nuclear Science and Technology, Vol. 10, 313-364.

YANG, D. Y., CHEN, G. S., and CHOU, H. P., (1993). *Application of Preconditioned Conjugate Gradient-Like Methods to Reactor Kinetics.* Annals of Nuclear Energy. Vol. 20. 9-33.

ZEE, S. K., TURINSKY, P. J, and SHAYER, Z.,(1989). *Vectorized and Multitasked Solution of the Few-Group Neutron Diffusion Equations.* Nuclear Science and Engineering, Vol. 101, 205.

ZIMIN, V. G. and NINOKATA, H., (1996). *Acceleration of the Outer Iterations of the Space-Dependent Neutron Kinetics Equations Solutions.* Annals of Nuclear Energy, Vol. 23, 17.

ZIMIN, V. G. and NINOKATA, H., (1997a). *Nonlinear Iteration Procedure Based on Legendre Polynomials.* Transactions of American Nuclear Society, Vol. 76, 162.

ZIMIN, V. G., and NINOKATA, H., (1997b). *Nodal Neutron Kinetics Model Based on Nonlinear Iteration Procedure For LWR Analysis.* Annals of Nuclear Energy, Vol. 25, No. 8, 507-528.

APPENDIX I: CANDU REACTOR MODELING

In this appendix, first a brief description of CANDU reactors will be presented. Emphasis is on a quick review of reactor regulating system that plays a major role in postulated transients of the present work. The characteristics of the CANDU-6 reactor model used in the numerical simulations of the present work will be discussed in detail. These characteristics are necessary and sufficient in order to reproduce the results presented in the previous chapters.

I.1 CANDU Reactor

The CANDU-type reactors consist of a large horizontally oriented calandria that contains the heavy water moderator, reactivity control mechanisms and fuel channel assemblies (380 for a typical CANDU-6 reactor). The fuel channels and heavy water coolant are contained in pressure tubes made of Zirconium alloy and they are surrounded by cold heavy water that acts as the moderator. The typical fuel channel of a CANDU-6 reactor contains a 37 pin fuel bundles of 50 cm length approximately. The fuel pins enclose natural Uranium in the form of Uranium oxide pellets that are surrounded by a Zircalloy sheath. A Calandria tube, also made of Zirconium alloy separates the fuel channel from the cold moderator. Between the calandria tubes and fuel channels CO_2 gas circulates. As in the case of the pressurized water reactor, reactor-cooling pumps circulate the pressurized, high temperature heavy water through the fuel channels, removing heat from the fuel, and then through heat exchangers to the steam generators in a closed loop. The moderator system has a separate heat exchanger with circulation system for cooling the moderator. The control of the reactor power is achieved by reactor regulating system that is a part of the overall plant control system. The CANDU reactors contain several special safety systems including fast reactor shutdown systems using shut-off rods (shutdown system #1) or liquid poison injection (shutdown system #2) into the moderator.

In-depth description of CANDU reactors can be found in documents published by Atomic Energy of Canada Limited (for example AECL-6593, 1979).

I.1.1 CANDU Reactor Regulating System

The brief description of the reactor regulating system presented here is directly taken from the *Reactor Control and Simulation course notes* (Koclas, 1997) where a much more detailed description of the reactor regulating system and its working logic are available. The reactor regulating system is aimed at many objectives, among them:

- Controlling the total reactor power to a specified setpoint that means maintaining the reactor critical. During the normal operation, the reactor power level is chosen by the boiler pressure controller to sustain steam pressure in the boilers.
- To adequately maintain the power distribution in the core. A typical CANDU-6 reactor is divided into fourteen control zones each with pre-specified zonal power.
- To determine and prevent (if possible) too fast variations of different parameters in order to prevent unnecessary shutdown system activation.
- To obtain information about the reactor by monitoring measured and calculated parameter values or by activating alarms when certain parameter are attained.

The reactor regulating system essentially consists of in-core flux detectors, out-core ion chambers, adjuster rods, light-water zone controllers, mechanical control absorbers:

- In-core flux detectors: The regulating system requires power measurements for the control of zone and total reactor power. These are obtained on short-time scale, from 28 self-powered (for a typical CANDU-6 reactor two per control zone), in-core platinum flux detectors. Moreover, 102 Vanadium in-core flux detectors are used to perform a slow correction of the zonal powers obtained by

the Platinum detector assemblies. Estimates of total reactor power derived from the platinum flux detectors are updated via thermal power measurements.

- Out-core flux detectors: In the low-power range, estimation of total reactor power is based on measurements from ion-chambers. Ion-chambers are characterized by fast response to any change or variation of power. However, they would not last long in the intense neutron fields found in the core. They are thus located near the periphery of the core by the external boundary of the reflector.
- Liquid zone controllers: The primary method of short-term reactivity control is by varying the levels in the 14 liquid zone controllers (one per zone). Their level is continually changing in order to keep both the total reactor power and zonal power at constant values. In normal condition the average zone level is between 20% and 70% full.
- Adjuster rods: Their major roles are to provide operating margin against Xenon and to flatten the spatial flux distribution. They are made from stainless steel (21 for a typical CANDU-6), sometimes of Cobalt 59 and they sit vertically in the core (perpendicular to the fuel channels). In normal condition, the adjuster rods are fully inserted.
- Mechanical absorber rods: They are made of stainless steel and Cadmium (4 in a typical CANDU-6 reactor), as very strong absorbers of thermal neutrons and they are normally fully withdrawn. They are used to control mostly extreme conditions. For example when power error is very large or when liquid zone controllers levels are very high.

In the long term, on-load refueling is used to control reactivity and flux shape.

I.1.2 CANDU Devices for Reactor Safety

It has been mentioned that two completely independent shutdown systems are presented in CANDU-type reactors:

- Shutdown system #1 (SDS1) that acts by quickly inserting 28 shutoff rods in the core (for a typical CANDU-6 reactor). The flux detectors connected to SDS1 are 3 ion chambers and 34 Platinum detectors (for a typical CANDU-6) reactor. The logarithmic rate of change of data obtained from ion chambers will activate SDS#1. The platinum detectors are uniformly distributed in the core and constitute the SDS1 part of Regional Overpower Protection system (ROP). ROP is designed to prevent any fuel channel to attain critical heat flux during postulated loss of regulation accidents.
- Shutdown system #2 (SDS2) that acts by adding liquid poison at high pressure in the moderator. This system connected to 3 out-core ion chambers (for a typical CANDU-6 reactor) and 23 in-core platinum detectors. The role of these in-core detectors is similar to those of SDS#1.

I.2 Reactor Modeling

It is obvious that solving even the lowest order approximations of the transport equations over the complete geometry of the CANDU reactor is still very far from being practical. To address this problem, the reactor core is considered as being made of a limited number of identical units known as *cells* where each of them consists of a fuel bundle, pressure tube, calandria tube and moderator (figure I.1). In the reactor core, the fuel elements are arranged periodically; hence, the spatial distribution of the neutron flux in the reactor can be separated into two components: first a periodic fine flux structure known as *microscopic flux* and second *macroscopic flux*. The microscopic flux is the local solution of transport equations over unit cells (for example using collision probability method). Each cell is supposed to be imbedded in an infinite lattice of identical cell that permits the use of reflection boundary conditions. These local flux calculations yield the space- and energy-dependent cross sections and diffusion coefficients for each unit cell. The cell calculations are then followed by both a spatial homogenization and energy condensation of these nuclear cross-sections and diffusion

coefficients. The spatial homogenization procedure results in the effective space-independent cross sections and diffusion coefficients for each unit cell (per energy group). The energy condensation generates these homogeneous properties for few energy groups, generally two for a typical thermal reactor.
The raw geometry of a CANDU-6 describing fuel unit cells and reflector region is shown in figure I.2.

I.2.1 Fine Model

Once homogeneous properties of cell units are determined, an appropriate mesh grid is required to form the discretized model of the reactor. This is normally achieved by extending the unit cell lines far enough to reach the external boundary of the reactor (figure I.3). The macroscopic flux is the solution of the obtained few-group diffusion equations over entire reactor represented by this mesh grid. The coordinates of the mesh grid used in the present work are shown on Table I.1. This mesh grid (26 x 26 x 12) is the coarsest representation of the unit cells of a CANDU-6 reactor that is one mesh per fuel cell.

Hierarchical nodal kinetics is aimed at the solution of the few-group diffusion model of the reactor, thus for the purpose of the present work all cross sections and diffusion coefficients of the unit cells are assumed to be known and pre-calculated. The goal of the present work is to verify the performance of the hierarchical nodal kinetics thus; a simple model involving only two fuel types (type 1 and 2 have the same nuclear properties) and one reflector type is used (figure I.3). The fuel and reflector properties for this model are given on Table I.2 and they are obtained using transport code DRAGON (Marleau, Roy, and Hébert, 1996). An important aspect of CANDU operation is the reactivity effect related to xenon concentration. To be as realistic as possible, a simple yet efficient Xenon model has been applied:

- Radioactive decay of ^{135}I, $\lambda_I = 2.85 \times 10^{-5}\ s^{-1}$,

- Radioactive decay of ^{135}Xe, $\lambda_X = 2.09 \times 10^{-5}\ s^{-1}$,
- Yield of ^{135}I in fission, $\gamma_I = 0.0631$,
- Yield of ^{135}Xe in fission, $\gamma_X = 0.0045$,
- Absorption cross sections for ^{135}Xe, $\sigma_{x1} = 1.3105$ b and $\sigma_{x2} = 1.1502 \times 10^{+6}$ b.

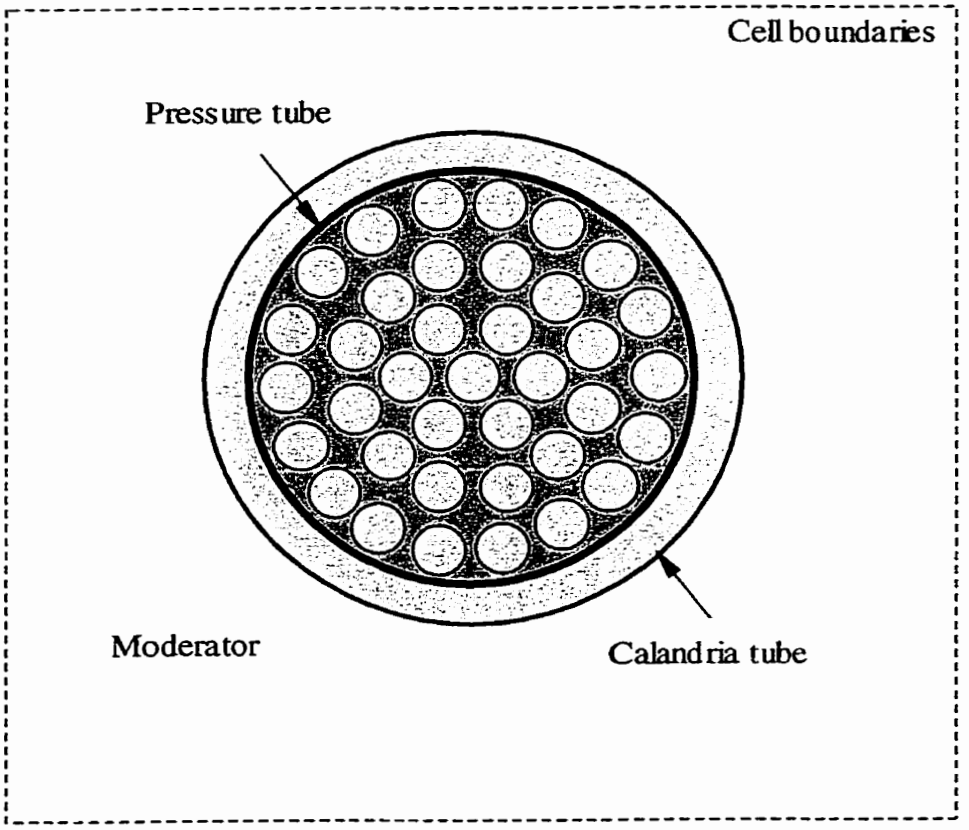

Figure I.1: Typical cell of a CANDU-6 with 37 elements

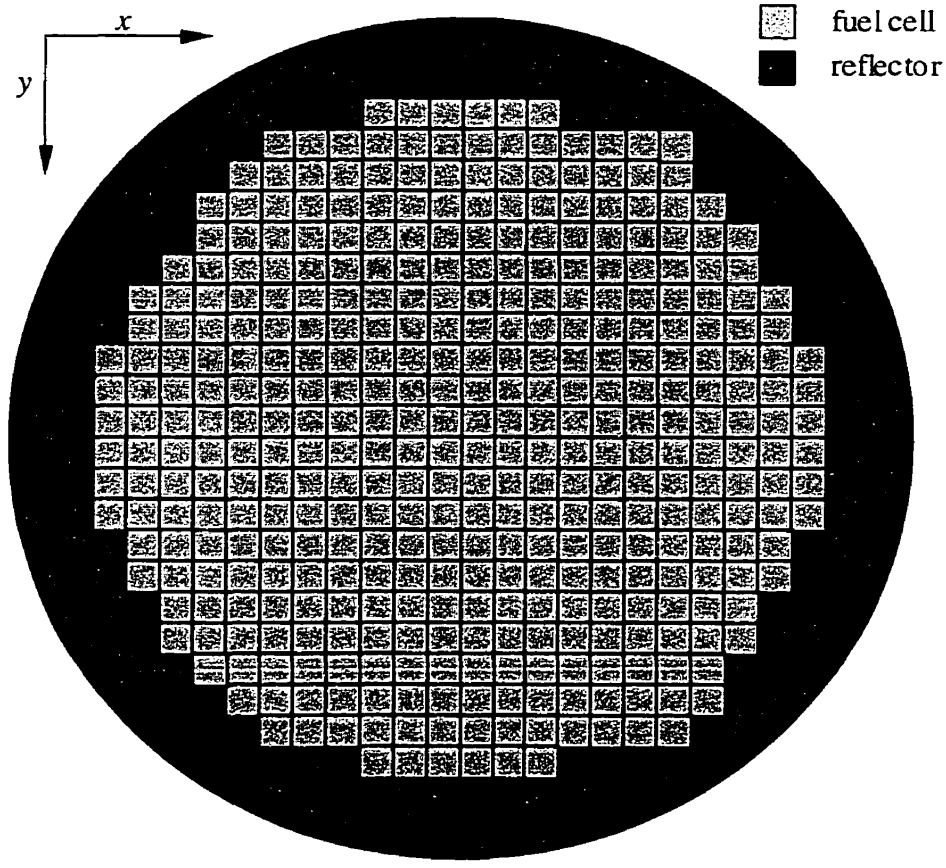

Figure I.2: Raw geometry of a CANDU-6

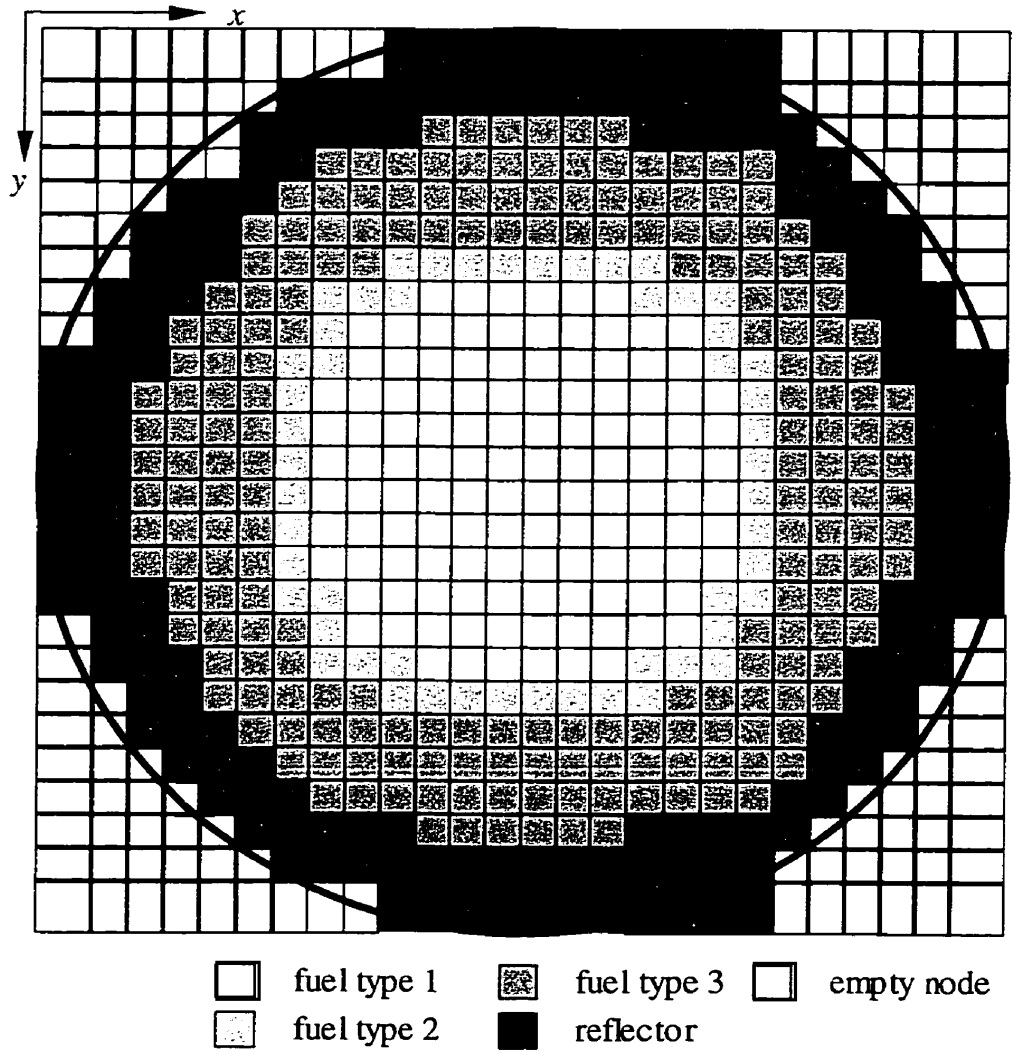

Figure I.3: Discretized model of a CANDU-6 reactor

Table I.1: Cell coordinates for a typical CANDU-6

No.	Pos. x	Δx	Pos. y	Δy	Pos. Z	Δz
1	3.150	41.900	3.150	41.900	3.94	49.53
2	45.050	23.475	45.050	23.475	53.47	49.53
3	68.525	28.575	68.525	28.575	103.00	49.53
4	97.100	28.575	97.100	28.575	152.53	49.53
5	125.675	28.575	125.675	28.575	202.06	49.53
6	154.250	28.575	154.250	28.575	251.59	49.53
7	182.825	28.575	182.825	28.575	301.12	49.53
8	211.400	28.575	211.400	28.575	350.65	49.53
9	239.975	28.575	239.975	28.575	400.18	49.53
10	268.550	28.575	268.550	28.575	449.71	49.53
11	297.125	28.575	297.125	28.575	499.24	49.53
12	325.700	28.575	325.700	28.575	548.77	49.53
13	354.275	28.575	354.275	28.575	598.30	--
14	382.850	28.575	382.850	28.575		
15	411.425	28.575	411.425	28.575		
16	440.000	28.575	440.000	28.575		
17	468.575	28.575	468.575	28.575		
18	497.150	28.575	497.150	28.575		
19	525.725	28.575	525.725	28.575		
20	554.300	28.575	554.300	28.575		
21	582.875	28.575	582.875	28.575		
22	611.450	28.575	611.450	28.575		
23	640.025	28.575	640.025	28.575		
24	668.600	28.575	668.600	28.575		
25	697.175	23.475	697.175	23.475		
26	720.625	41.900	720.625	41.900		
27	762.550	--	762.550	--		

Table I.2: Nuclear properties of fuel and reflector

TYPE	FUEL TYPE I	FUEL TYPE II	FUEL TYPE III	REFLECTOR
Σ_{t1}	2.6296^{E}-01	2.6298E-01	2.6298E-0	2.6238E-01
Σ_{t2}	3.6266^{E}-01	3.6264E-01	3.6264E-01	3.7532E-01
Σ_{f1}	3.4236^{E}-04	3.4408E-04	3.4408E-04	0.000E+00
Σ_{f2}	1.73999^{E}-03	1.7477E-03	1.7477E-03	0.000E+00
$\nu\Sigma_{f1}$	9.1408^{E}-04	9.1865E-04	9.1865E-04	0.000E+00
$\nu\Sigma_{f2}$	4.4642^{E}-03	4.4842E-03	4.4842E-0	0.000E+00
χ_1	1.000E+00	1.000E+00	1.000E+00	1.000E+00
χ_2	0.000E+00	0.000E+00	0.000E+00	0.000E+00
$1/v_1$	4.6082^{E}-08	4.6096E-08	4.6096E-08	5.3635E-08
$1/v_2$	3.7038^{E}-06	3.7044E-06	3.7044E-06	3.7621E-06
D_{g1}	1.0693^{E}+00	1.0692E+00	1.0692E+00	1.3025E+00
D_{g2}	7.9253^{E}-01	7.9261E-01	7.9261E-01	9.5088E-01
$(HF)_1$	1.0807^{E}-14	1.0883E-14	1.0883E-14	0.000E+00
$(HF)_2$	5.5748^{E}-14	5.6359E-14	5.6359E-14	0.000E+00
$\Sigma_{1\leftarrow1}$	2.5144^{E}-01	2.5146E-01	2.5146E-01	2.4967E-01
$\Sigma_{2\leftarrow1}$	9.7073^{E}-03	9.7108E-03	9.7108E-03	1.27138E-02
$\Sigma_{1\leftarrow2}$	1.9508^{E}-06	1.9387E-06	1.9387E-06	1.0060E-06
$\Sigma_{2\leftarrow2}$	3.5884^{E}-01	3.5884E-01	3.5884E-01	3.7527E-01

The boundary conditions on the external surfaces of the core model have to be specified in order to complete the model of the core. Many choices can be implemented such as zero flux, zero flux extrapolated or albedo conditions. In the present research for the purpose of numerical simulations, zero flux boundary condition is applied.
The geometric and nuclear properties of reactivity devices (mechanical rod absorbers, liquid zone controllers and adjuster rods) are directly taken from the previous work done by Navarro (1996) thus for the sake of briefness they are not tabulated here. The reactor regulating system logic for a typical CANDU-6 is represented by related modules available in the computer code DONJON (Varin, Hébert, Roy, and Koclas, 1996). These modules are inserted in the sequence of the performed numerical tests by the use of procedure control language CLE-2000 (Roy and Hébert, 2000).

I.2.2 Coarse Model

The coordinates of different coarse mesh grid representation of (for example figure I.4) a typical CANDU-6 used in the present work are shown on Table I.3. The evaluation procedure for diffusion parameters of coarse regions is thoroughly discussed in chapter 2.

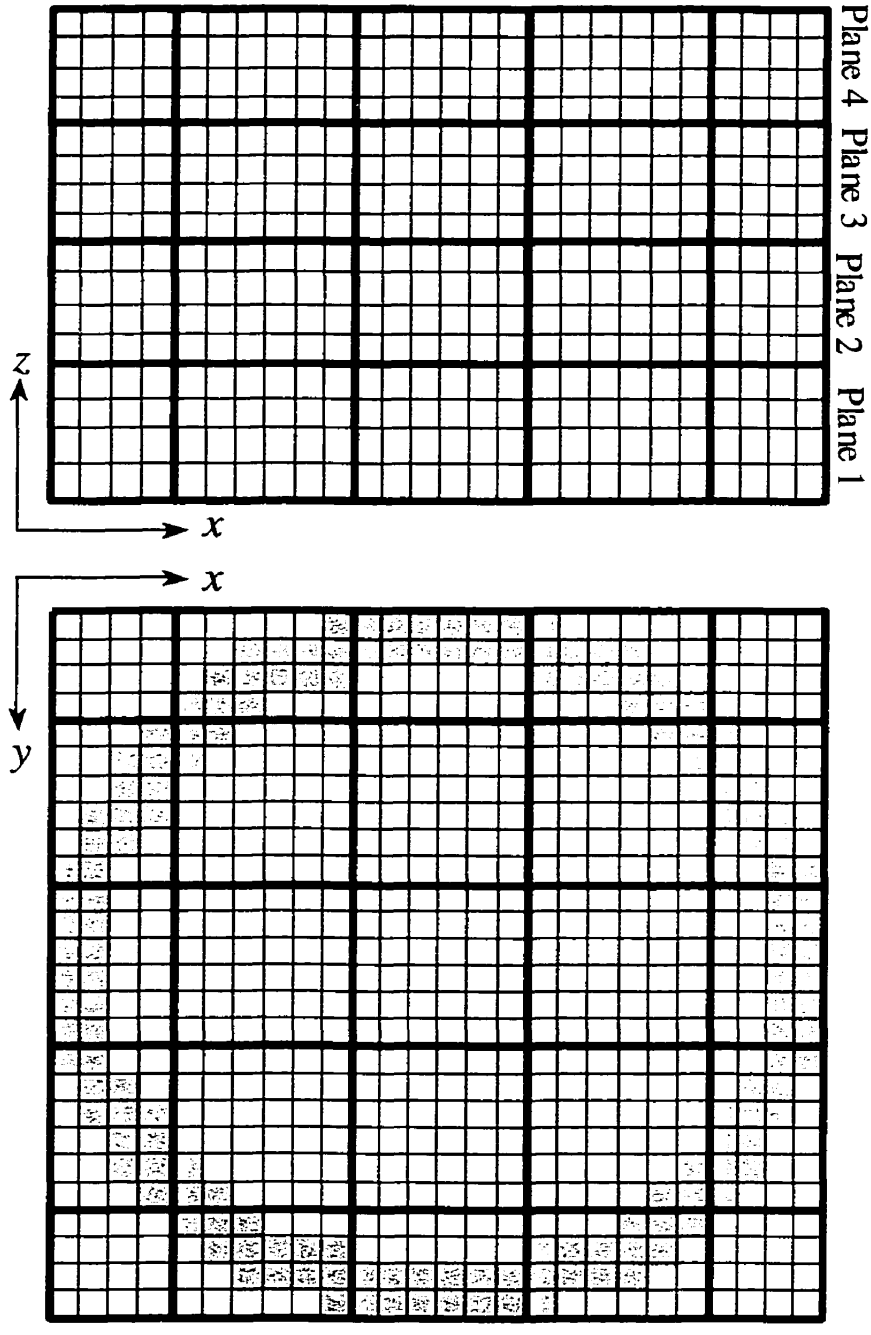

Figure I.4: A typical coarse model of a CANDU-6 reactor (5 x 5 x 4)

Table I.3: Coarse mesh coordinates for a typical CANDU-6

1 x 1 x 1	No.	Pos. x	Δx	Pos. y	Δy	Pos. z	Δz
	1	3.150	759.4	3.150	759.4	3.94	594.365
2 x 2 x 2	No.	Pos. x	Δx	Pos. y	Δy	Pos. z	Δz
	1	3.150	379.7	45.050	379.7	3.94	247.655
	2	382.85	379.7	382.85	379.7	251.595	346.71
3 x 3 x 2	No.	Pos. x	Δx	Pos. y	Δy	Pos. z	Δz
	1	3.150	293.975	3.150	293.975	3.94	247.655
	2	297.125	171.45	297.125	171.45	251.595	346.71
	3	468.575	293.975	468.575	293.975		
5 x 5 x 4	No.	Pos. x	Δx	Pos. y	Δy	Pos. z	Δz
	1	3.150	122.525	3.150	122.525	3.94	148.59
	2	125.675	171.45	125.675	171.45	152.53	148.59
	3	297.125	171.45	297.125	171.45	301.12	148.59
	4	468.575	171.45	468.575	171.45	449.71	148.59
	5	640.025	122.525	640.025	122.525		
10 x 10 x 4	No.	Pos. x	Δx	Pos. y	Δy	Pos. z	Δz
	1	3.150	65.375	3.150	65.375	3.94	148.59
	2	68.525	57.15	68.525	57.15	152.53	148.59
	3	125.675	57.15	125.675	57.15	301.12	148.59
	4	182.825	114.3	182.825	114.3	449.71	148.59
	5	297.125	85.725	297.125	85.725		
	6	382.850	85.725	382.850	85.725		
	7	468.575	114.3	468.575	114.3		
	8	582.875	57.15	640.025	57.15		
	9	640.025	57.15	640.025	57.15		
	10	697.175	65.375	697.175	65.375		

APPENDIX II: 3-D CANDU BENCHMARK

It is a common approach to evaluate the performance of a numerical scheme initially based on the well-known benchmark problems. In this appendix, the results obtained for the well-known 3D CANDU benchmark using hierarchical nodal kinetics will be presented.

II.1 Description

The CANDU benchmark (ANL, 1985) is a three-dimensional reactor kinetics problem in a heavy water reactor which originally consists of 24 regions. The layout of the reactor and region assignments are shown in figure II.1 through II.3.

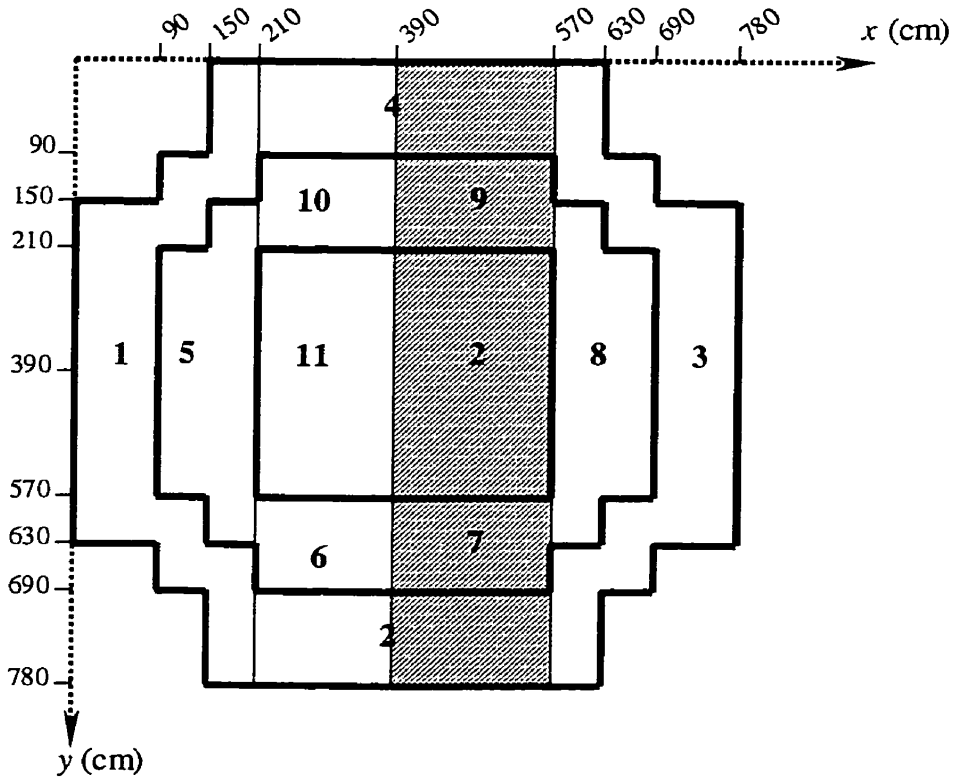

Figure II.1: xy projection showing region assignments for $0 < z < 300$ (cm)

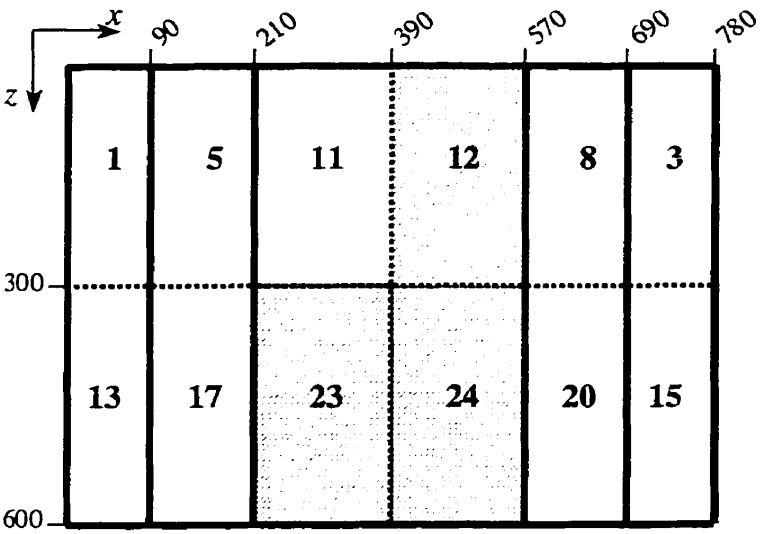

Figure II.2: xz projection showing region assignments at $y = 390$ (cm)

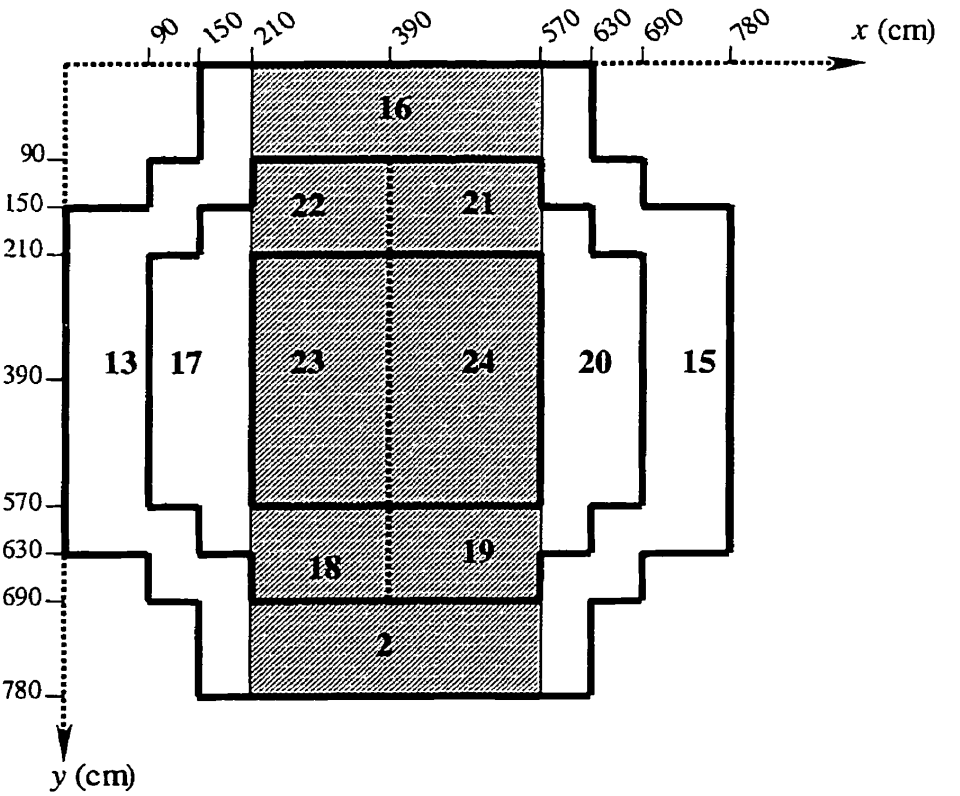

Figure II.3: xy projection showing region assignments for $300 < z < 600$ (cm)

Physical properties of different regions as well as delayed neutron data are presented in tables II.1 and II.2.

Table II.1: Physical properties for different regions of the reactor

Region [1]	Group	D_i (cm)	Σ_i (cm^{-1})	$\nu\Sigma_{fi}$ (cm^{-1})	$\Sigma_{1\to2}$ (cm^{-1})
1,2,3,4,13, 14,15,16	1	1.3100E+0	1.0180E-2	0.0000E0	1.0180E-2
	2	0.8695E+0	2.1170E-4	0.0000E0	1.0180E-2
5,6,7,8,9,10,17, 18,19,20,21,22	1	1.2640E+0	8.1540E-3	0.0000E0	7.3680E-3
	2	0.9328E+0	4.0140E-3	4.7230E-3	7.3680E-3
11,12,23,24	1	1.2640E+0	8.1540E-3	0.0000E0	7.3680E-3
	2	0.9328E+0	4.1000E-3	4.5620E-3	7.3680E-3

[1] for all regions, group neutron speeds are $v_1 = 10^7$ cm/s and $v_2 = 3 \times 10^5$ cm/s.

Table II.2: Delayed neutron data

Type	β_i	λ_i (s^{-1})	Type	β_i	λ_i (s^{-1})
1	4.170E-4	1.244E-2	4	3.339E-3	3.079E-1
2	1.457E03	3.063E-2	5	8.970E-4	1.198E+0
3	1.339E-3	1.139E-1	6	3.200E-4	3.212E+0

The transient starts by a decrease of the total thermal cross section in regions 5, 6, 10, 11, 17, 18, 22 and 23 based on the following linear correlation:

$$\frac{\partial \Sigma_2}{\partial t} = \begin{cases} -1.0*10^{-4}\,(\mathrm{cm}\cdot\mathrm{s})^{-1}, & \text{for } t \le 0.4\,\mathrm{s} \\ -8.88889*10^{-6}\,(\mathrm{cm}\cdot\mathrm{s})^{-1}, & \text{for } t > 0.4\,\mathrm{s} \end{cases}$$

At t = 0.6 sec, an incremental cross section, $\Delta\Sigma_2$ = 6.150 x 10^{-4} (cm^{-1}), is added to regions 2, 4, 7, 9, 12, 14, 16, 18, 19, 21, 22, 23 and 24 (hatched regions in figures II.1 through II.3) to simulate asymmetric insertion of absorbers. The absorbers are inserted at constant velocity of 520 cm/s in the y-direction. The moving absorber boundary is parallel to the xz plane. The transient lasts for 2.5 seconds. The initial configuration of reactor is made critical by dividing the fission cross-section by k_{eff}.

A non-uniform 18 x 18 x 10 grid for the x-, y-, and z directions respectively was used to represent fine regions. For the coarse representation of the reactor, various configurations were used: 3x3x2, 5x5x4 coarse nodes in x-, y- and z-directions. The cell coordinates for fine and coarse representations of the reactor are presented in tables II.3 and II.4. The steady-state results include the eigenvalue and the maximum error in the coarse mesh fluxes. The obtained results presented in table II.5 show that this error is less than 0.001%

Figure II.4 represents the plot of relative total power versus time obtained using direct method with the time step dt = 0.001 as well as the benchmark reference solution. The initial error in total power for the direct method comparing to the published results is also plotted in figure II.5. The amount of errors in total power can be attributed to the fact that the reference calculation was carried out using improved quasi-static method. Moreover, many details regarding to implementation of improved quasi-static method are ambiguous. For example it is not clear that in the reference calculations, how point kinetics parameters are updated to reflect changes in the cross sections or if additional layer of iterations over normalizing conditions was applied or not.

Table II.3: Cell coordinates for 3D CANDU benchmark

No.	Pos. x	Δx	Pos. Y	Δy	Pos. Z	Δz
1	0.0	60.0	0.0	60.0	0.0	60.0
2	60.0	30.0	60.0	30.0	60.0	60.0
3	90.0	30.0	90.0	30.0	120.0	60.0
4	120.0	30.0	120.0	30.0	180.0	60.0
5	150.0	30.0	150.0	30.0	240.0	60.0
6	180.0	30.0	180.0	30.0	300.0	60.0
7	210.0	30.0	210.0	30.0	360.0	60.0
8	270.0	60.0	270.0	60.0	420.0	60.0
9	330.0	60.0	330.0	60.0	480.0	60.0
10	390.0	60.0	390.0	60.0	540.0	60.0
11	450.0	60.0	450.0	60.0	600.0	--
12	510.0	60.0	510.0	60.0		
13	570.0	60.0	570.0	60.0		
14	600.0	30.0	600.0	30.0		
15	630.0	30.0	630.0	30.0		
16	660.0	30.0	660.0	30.0		
17	690.0	30.0	690.0	30.0		
18	720.0	30.0	720.0	30.0		
19	780.0	--	780.0	--		

Table II.4: Coarse mesh coordinates for 3D CANDU benchmark

3 x 3 x 2	No.	Pos. x	Δx	Pos. y	Δy	Pos. z	Δz
	1	0.0	210.0	0.0	210.0	0.0	300.0
	2	210.0	360.0	210.0	360.0	300.0	600.0
	3	570.0	310.0	570.0	310.0		
5 x 5 x 4	No.	Pos. X	Δx	Pos. y	Δy	Pos. z	Δz
	1	0.0	180.0	0.0	180.0	0.0	180.0
	2	180.0	150.0	180.0	150.0	180.0	120.0
	3	330.0	120.0	330.0	120.0	300.0	120.0
	4	450.0	150.0	450.0	150.0	420.0	180.0
	5	600.0	180.0	600.0	180.0		

Table II.5: Results of Steady-State Calculations for 3D CANDU benchmark

Case	k_{eff}	Max. flux error %
Reference (ANL, 1985)	1.00355	--
Fine (implicit)	1.00355	$\sim 10^{-4}$
3x3x2 Coarse node (implicit)	1.00355	$\sim 10^{-3}$
5x5x4 Coarse node (implicit)	1.00355	$\sim 10^{-4}$

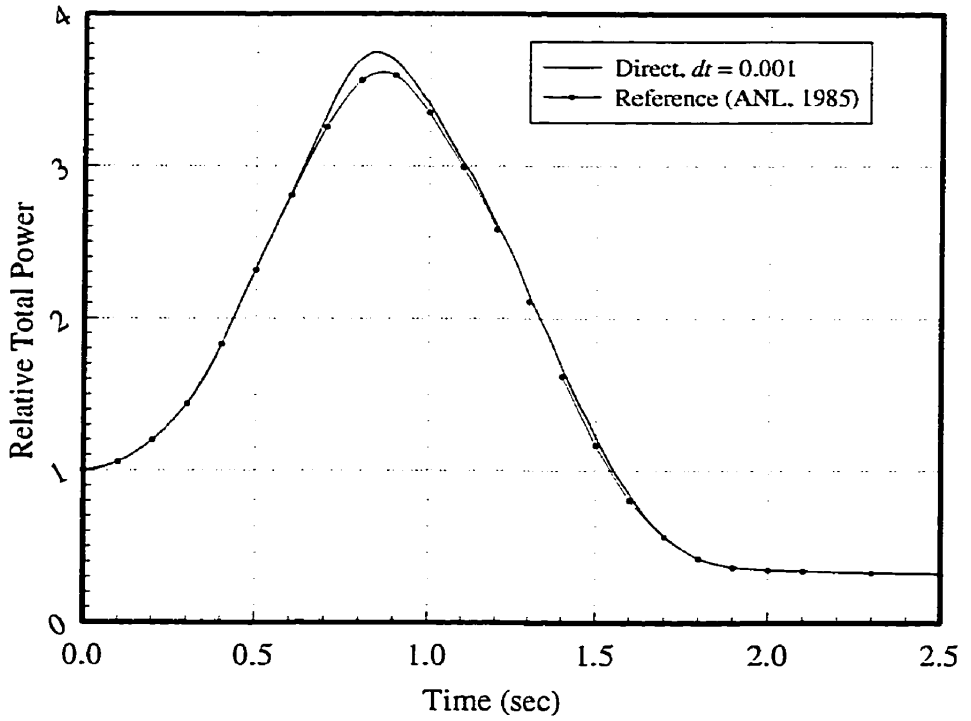

Figure II.4: Relative total power vs. time for direct method and reference solution

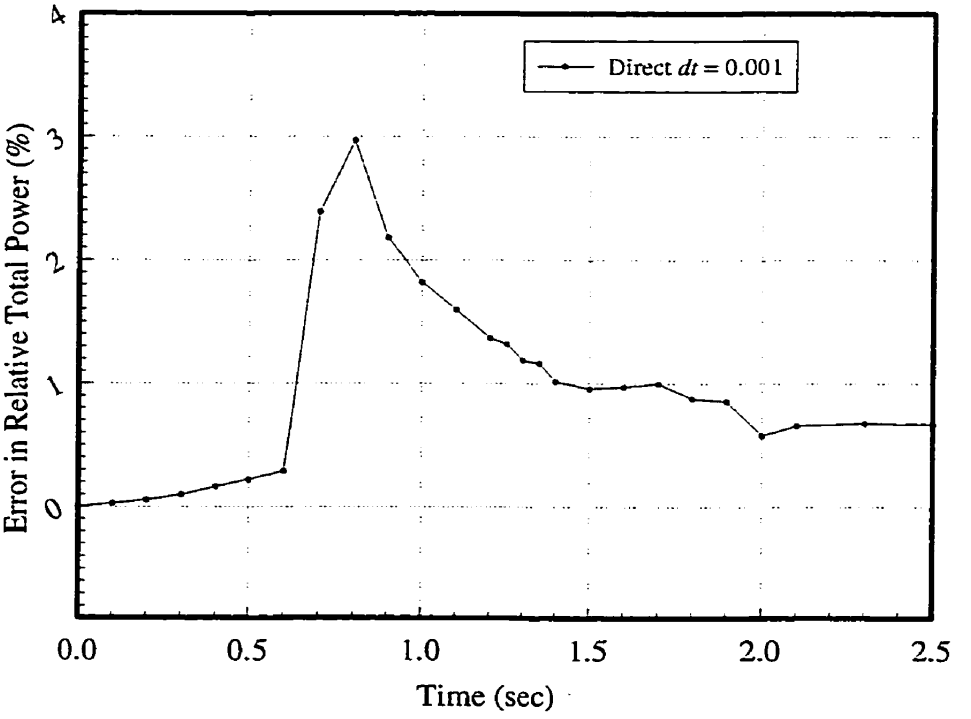

Figure II.5: Initial error in relative total power for direct method

To deal with these uncertainties, the exact solution obtained from the direct method with the time step $dt = 0.001$ is set to be the reference solution keeping in mind that an initial amount of error in total power does exist. To assess the merits of the hierarchical nodal kinetics, numerous tests were performed. Input parameters for some of the selected cases are described in Table II.6. The obtained results are visualized in figures II.6 through II.11. In these test cases, the chosen formalism of hierarchical nodal kinetics is the implementation of the intermediate coarse level calculations to extend the validity of classical improved quasi-static method. It is expected that this approach can correctly solve the benchmark problem since the prescribed perturbations result in a dynamic reactivity of the order of –7.5 mk. A close examination of the results, once more proves that using very big coarse nodes (case 3) can result in the substantial amount of errors in the flux calculations. These errors are possibly due to four major reasons: reconstruction procedure, intrinsic errors caused by the flux factorization in all forms of quasi-static approaches, the hypothesis of considering piecewise constant discontinuity factors, and finally inherent errors due to iterative procedures which are amplified in homogenized cross sections in the large volumes of reactor. However, in practice, by using smaller coarse nodes (case 3), these errors could be successfully limited to an acceptable range (case 3).

Table II.6: Description of selected test cases

Case	Number of nodes	dt_{fine}	N_{coarse}	N_{pk}	CPU time (sec)
Case 1	3 x 3 x 2	0.100	10	10	300-589
Case 2	5 x 5 x 4	0.100	10	10	380-590
Case 3	5 x 5 x 4	0.050	10	5	400-610
IQS	18 x 18 x 10	0.010	--	10	1200-1100
Direct	18 x 18 x 10	0.001	--	--	1500

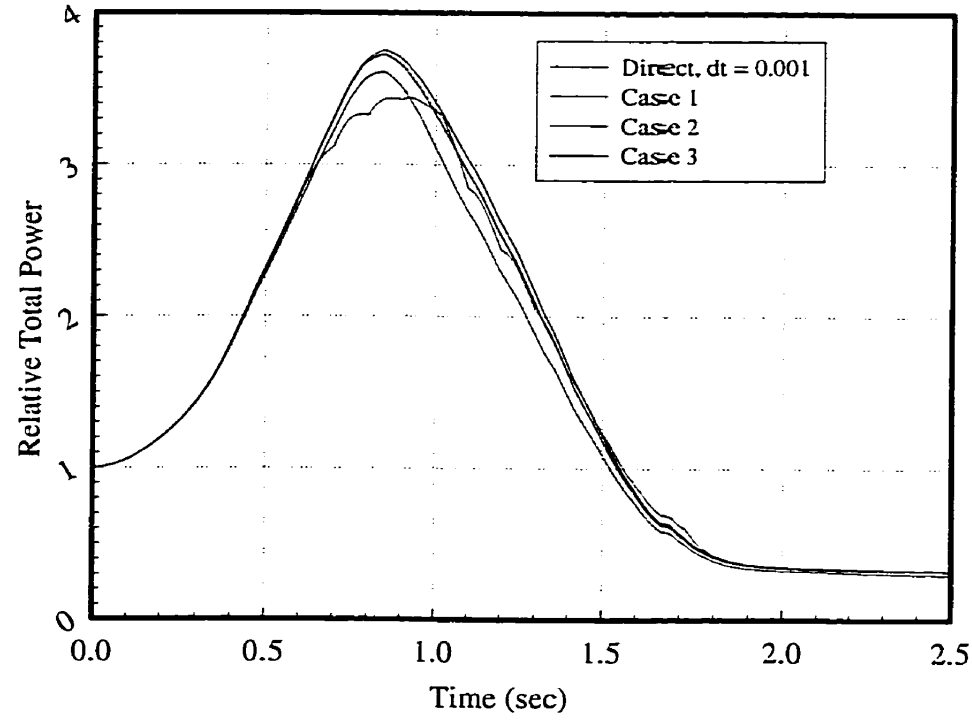

Figure II.6: Relative total power for selected test cases

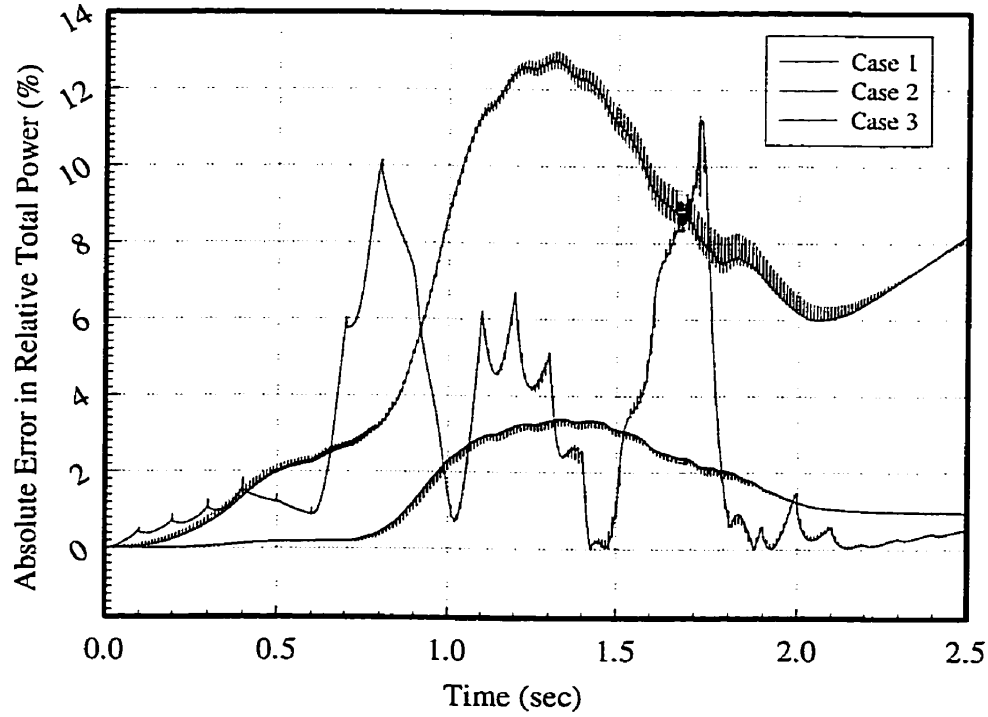

Figure II.7: Absolute error in relative total power for selected test cases

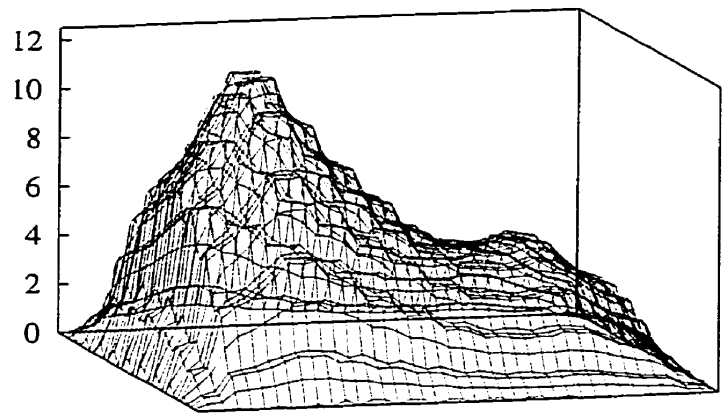

Figure II.8: Thermal flux distribution, xz-plane at $y = 360$ cm and $t = 0.9$ sec (Case 3)

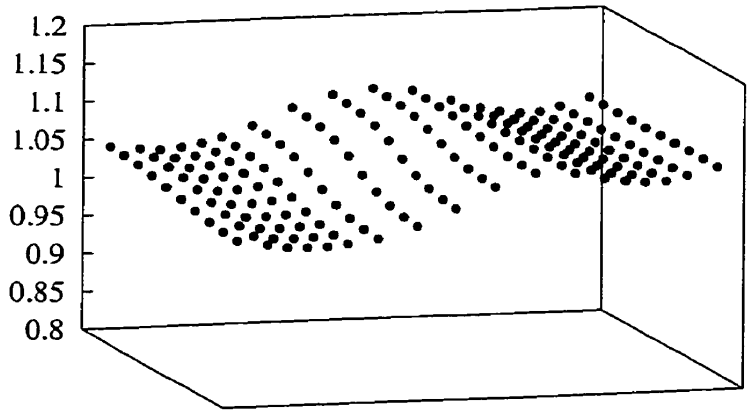

Figure II.9: Error in thermal flux, xz-plane at $y = 360$ cm and $t = 0.9$ sec (Case 3)

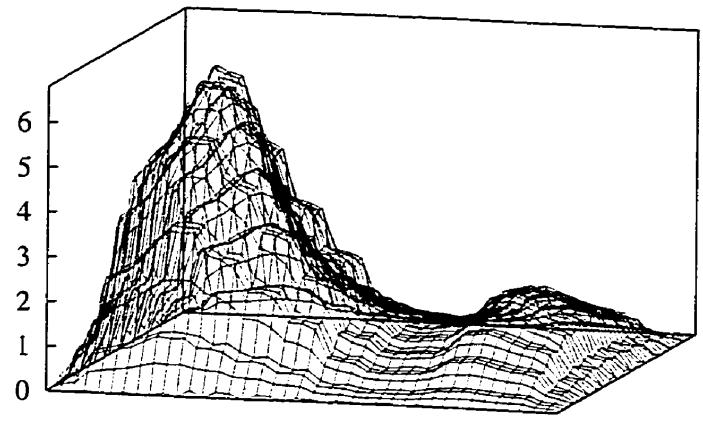

Figure II.10: Thermal flux distribution, xz-plane at $y = 360$ cm and $t = 1.35$ sec (Case 3)

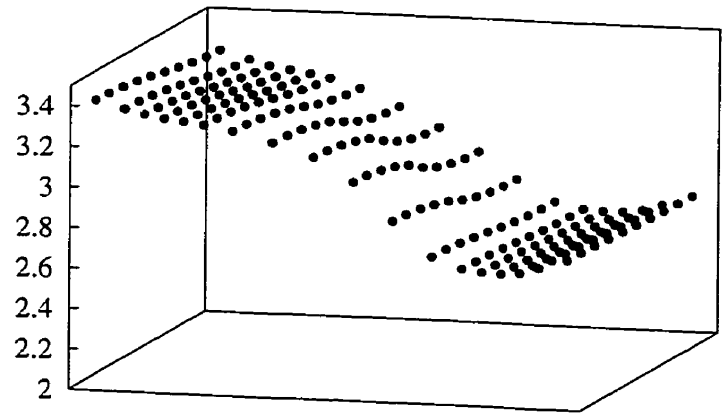

Figure II.11: Error in thermal flux, xz-plane at $y = 360$ cm and $t = 1.35$ sec (Case 3)

To complete this appendix, the results obtained using space hierarchy (multigrid acceleration technique) will be also presented. To be able to take advantage of the multigrid approach, a non-uniform 36 x 36 x 20 grid for the x-, y-, and z- directions respectively was used to represent the fine regions. This fine configuration was obtained by the mesh splitting procedure for all fine grids defined in table II.4. For the coarse-grid representation of the reactor, 5 x 5 x 4 coarse nodes in x-, y- and z-directions are established (see table II.4). As usual the emphasis is upon both computational efficiency and the accuracy of the solution (in comparison to a reference solution). Accuracy of the solution is guaranteed since algebraic equations to be solved are the same for all iterative methods. Thus, emphasis is rather on the computational efficiency. The obtained results show that by applying the aforementioned procedure the number of iteration can be considerably reduced (Figure II.12) depending on the number of the coarse nodes, Δt, and severity of the perturbation. Consequently, the CPU time will be reduced by almost the same amount. Figures II.13 through II.20 show dynamic evolution of the normalized thermal flux in this 3D CANDU geometry, quite similar to a realistic CANDU core. At the start of the transient, the flux shape is symmetric and smooth (see Figure II.13 and II.14). Then, as the transient goes on, the local perturbations (resembling to a LOCA) considerably increase both fast and thermal neutron fluxes (Figure II.15 through II.17). Finally, figures II.18 through II.20 show the effect of asymmetric insertion of the absorbers in the reactor core for the selected plane.

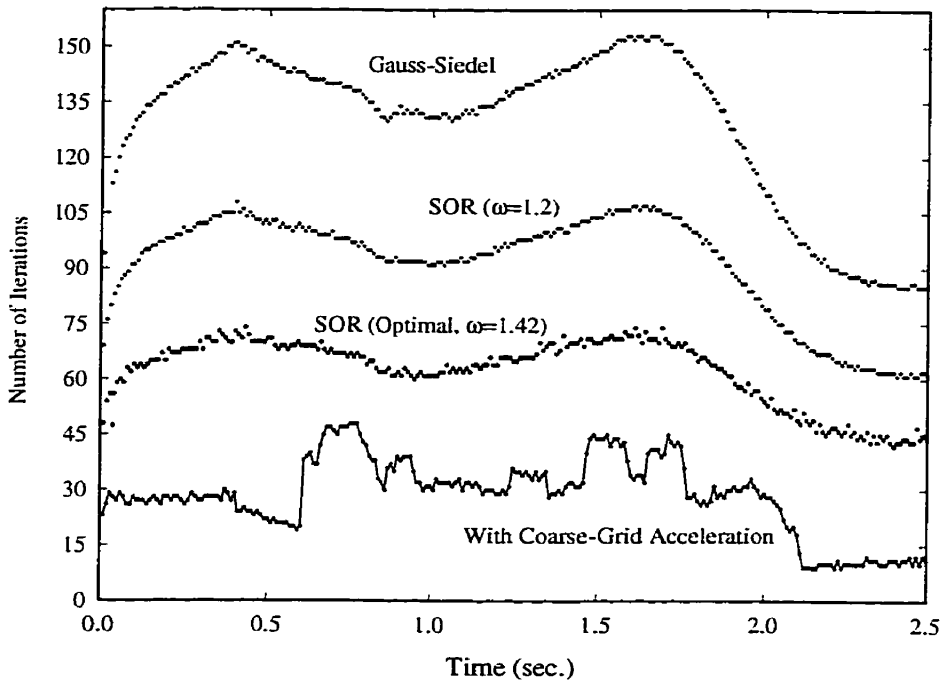

Figure II.12: Number of necessary iterations for different iterative methods

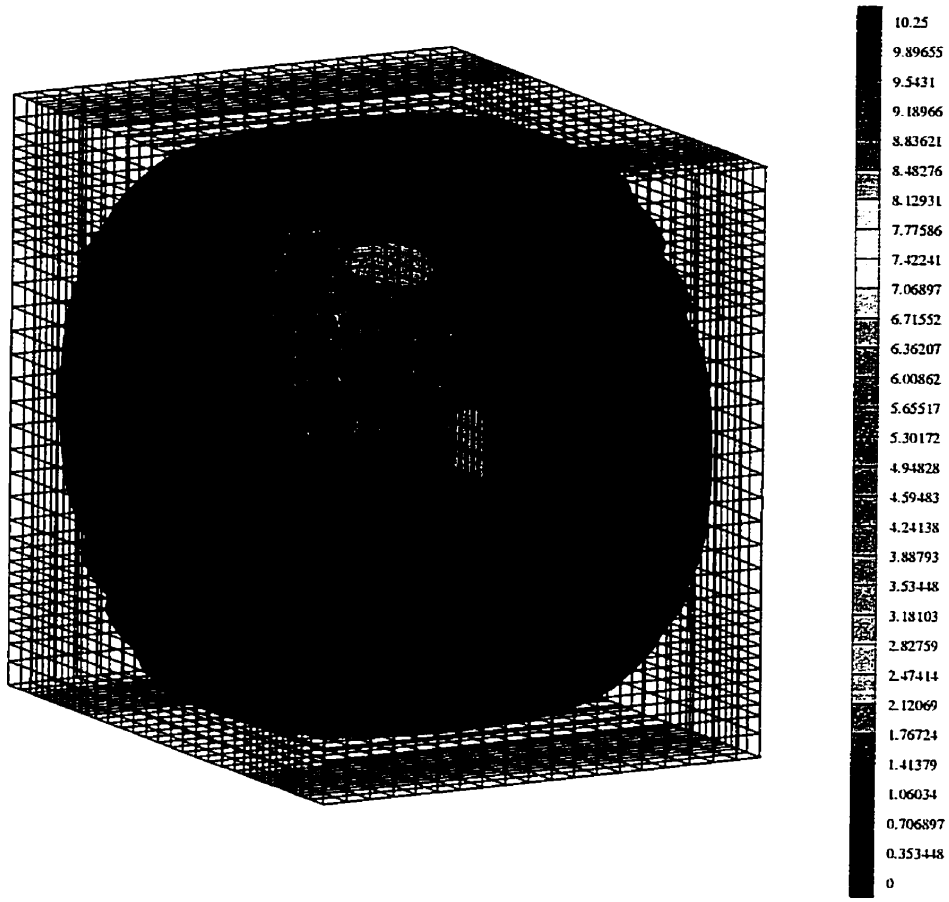

Figure II.13: Normalized thermal flux distribution at t=0 sec

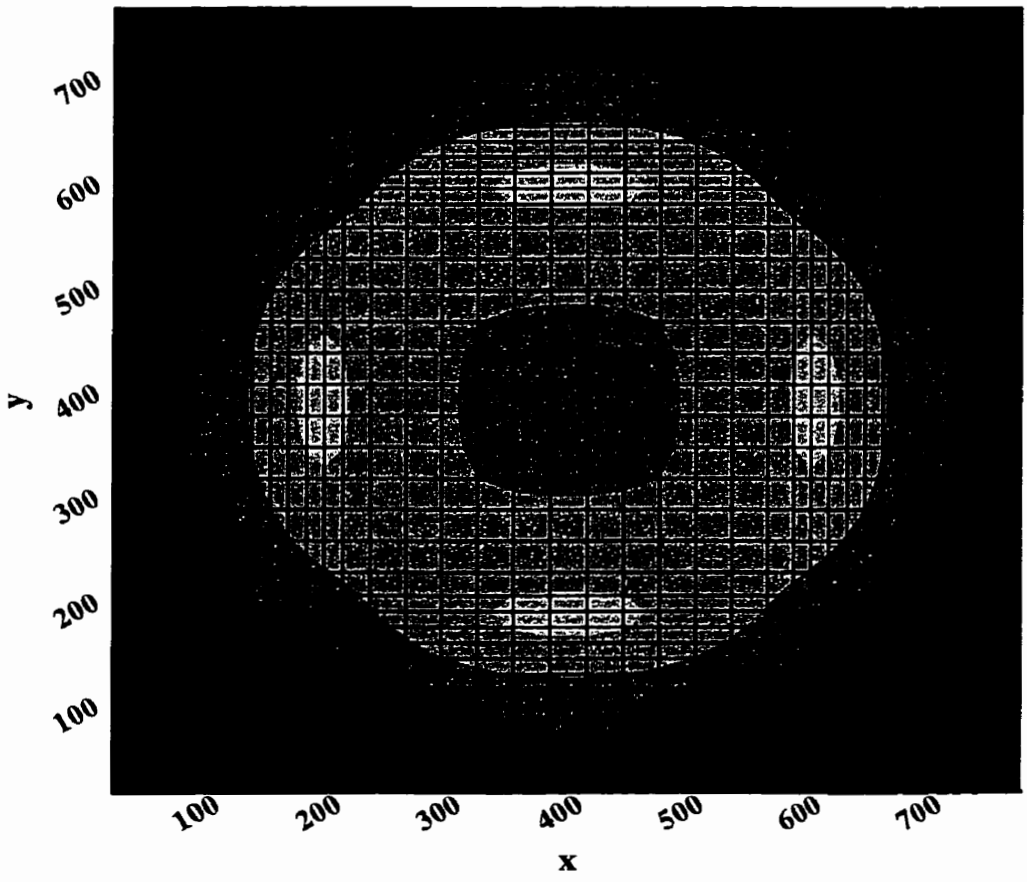

Figure II.14: Normalized thermal flux distribution at t=0 sec, z= 285 cm

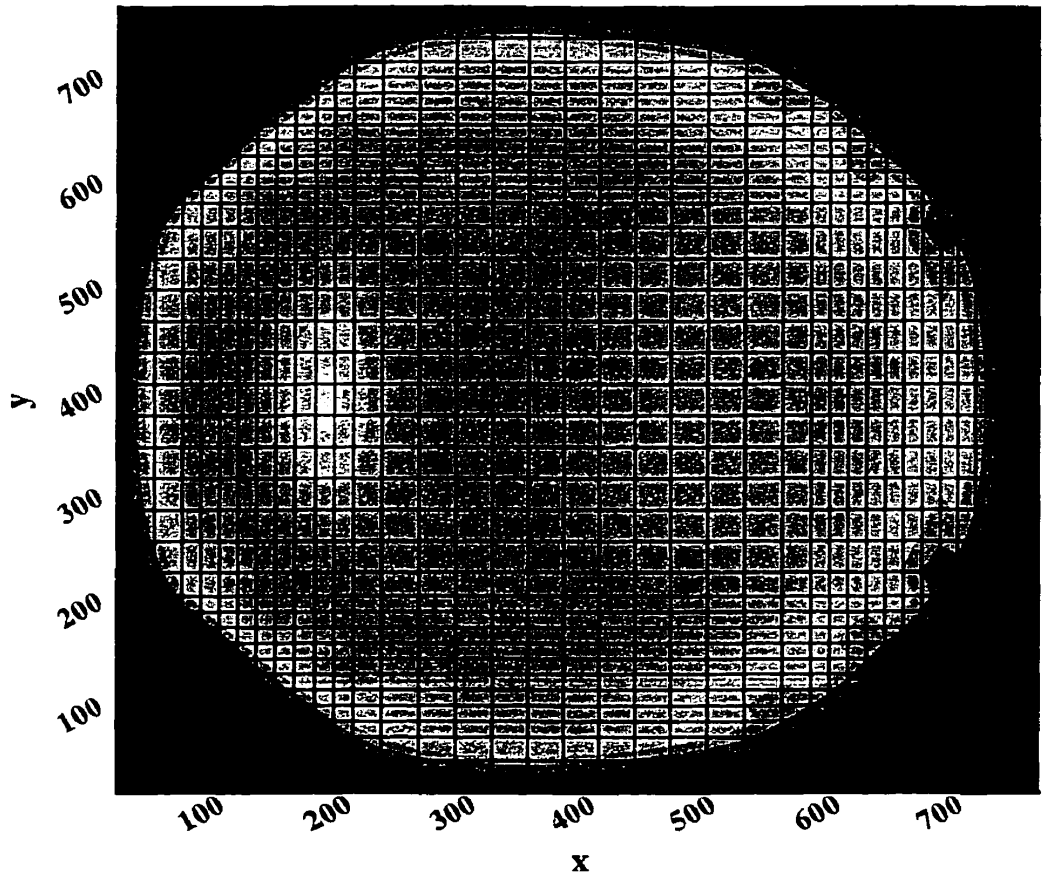

Figure II.15: Normalized thermal flux distribution at t=0.6 sec, z= 285 cm

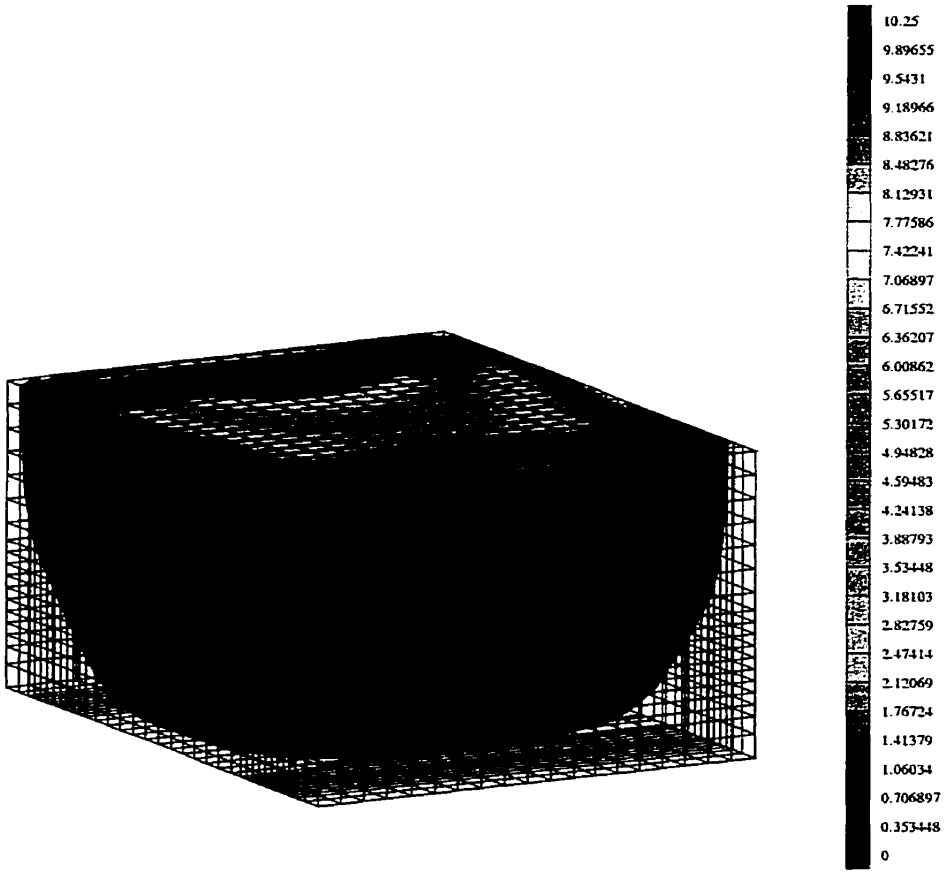

Figure II.16: Normalized thermal flux distribution at t=0.9 sec.

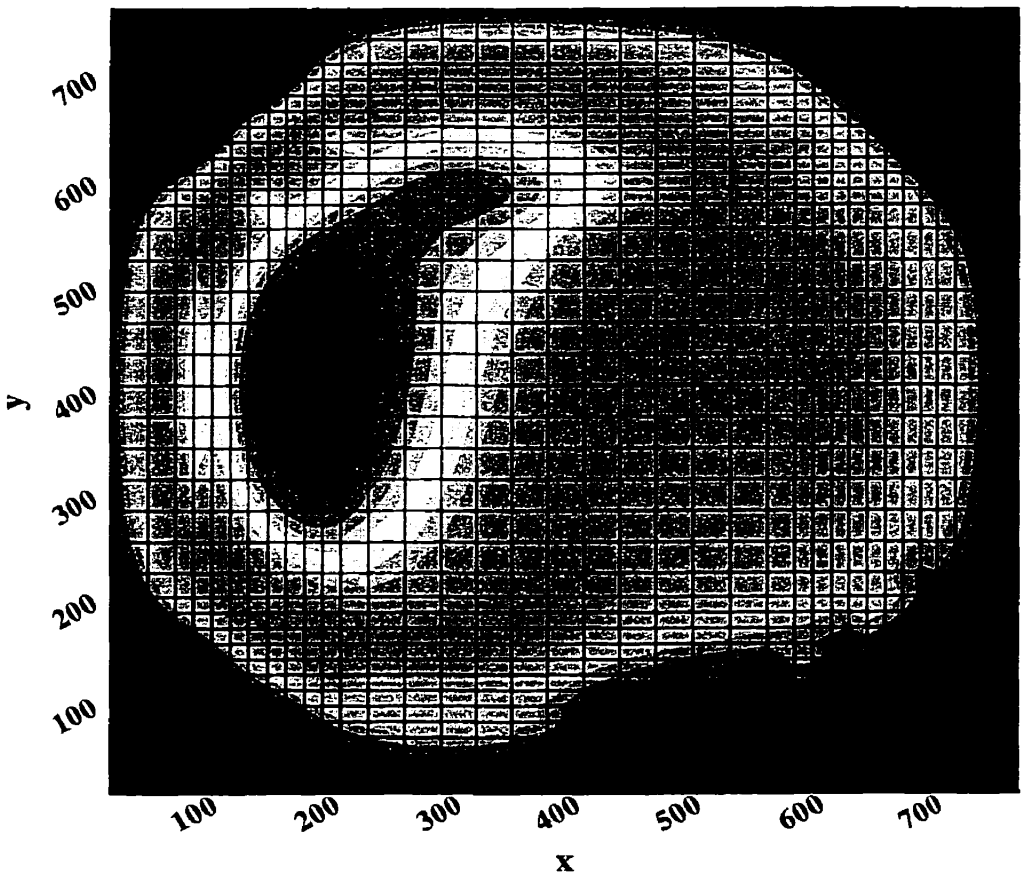

Figure II.17: Normalized thermal flux distribution at t=0.9 sec, z= 285 cm.

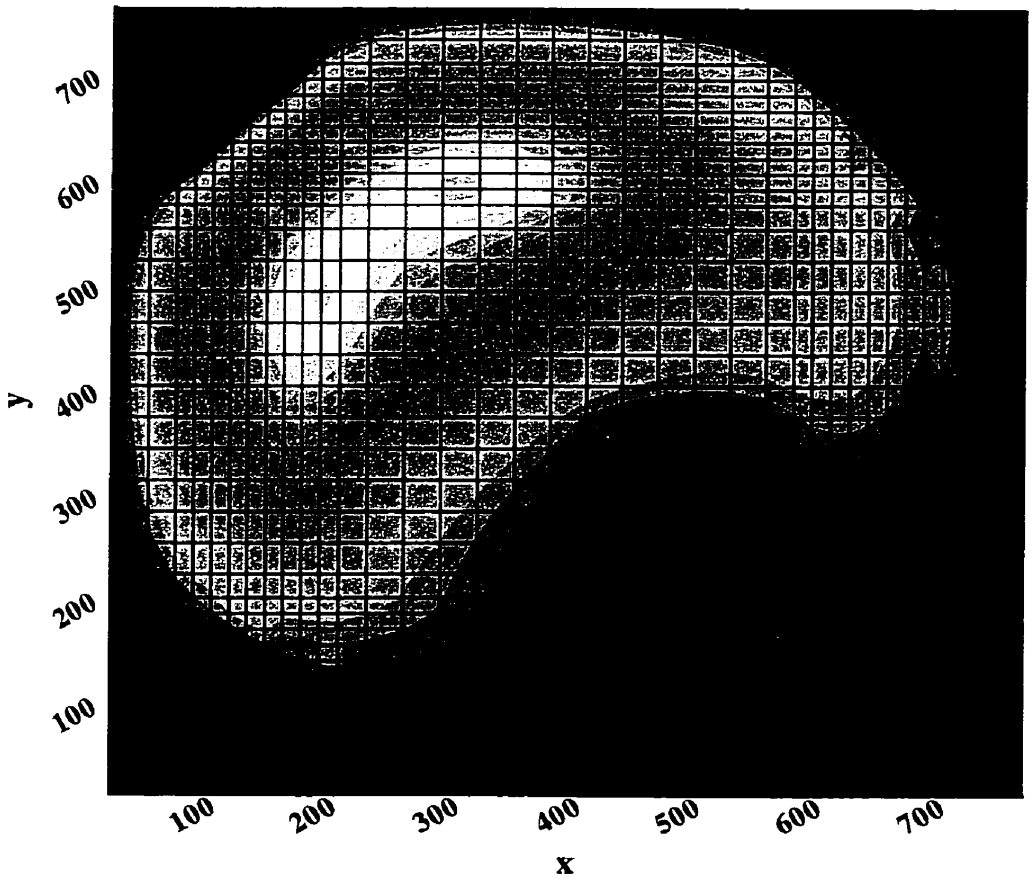

Figure II.18: Normalized thermal flux distribution at t=1.35 sec, z= 285 cm

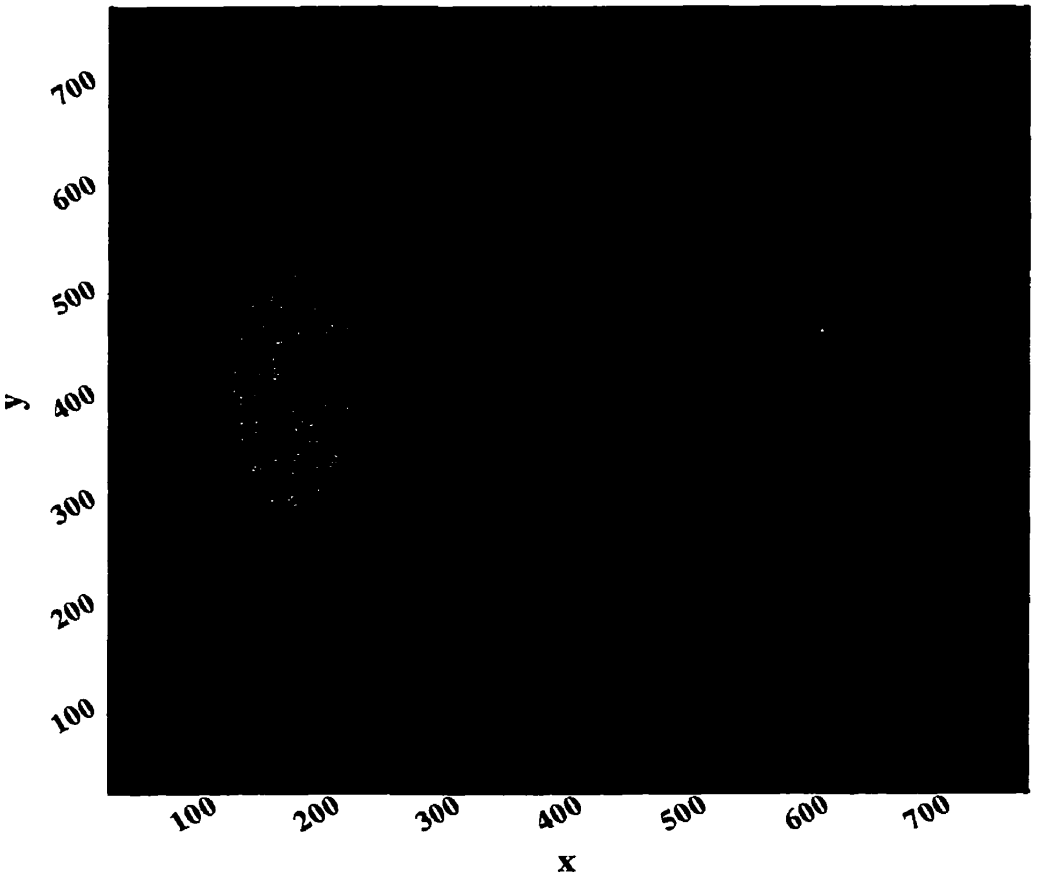

Figure II.19: Normalized thermal flux distribution at t=2.1 sec, z= 285 cm

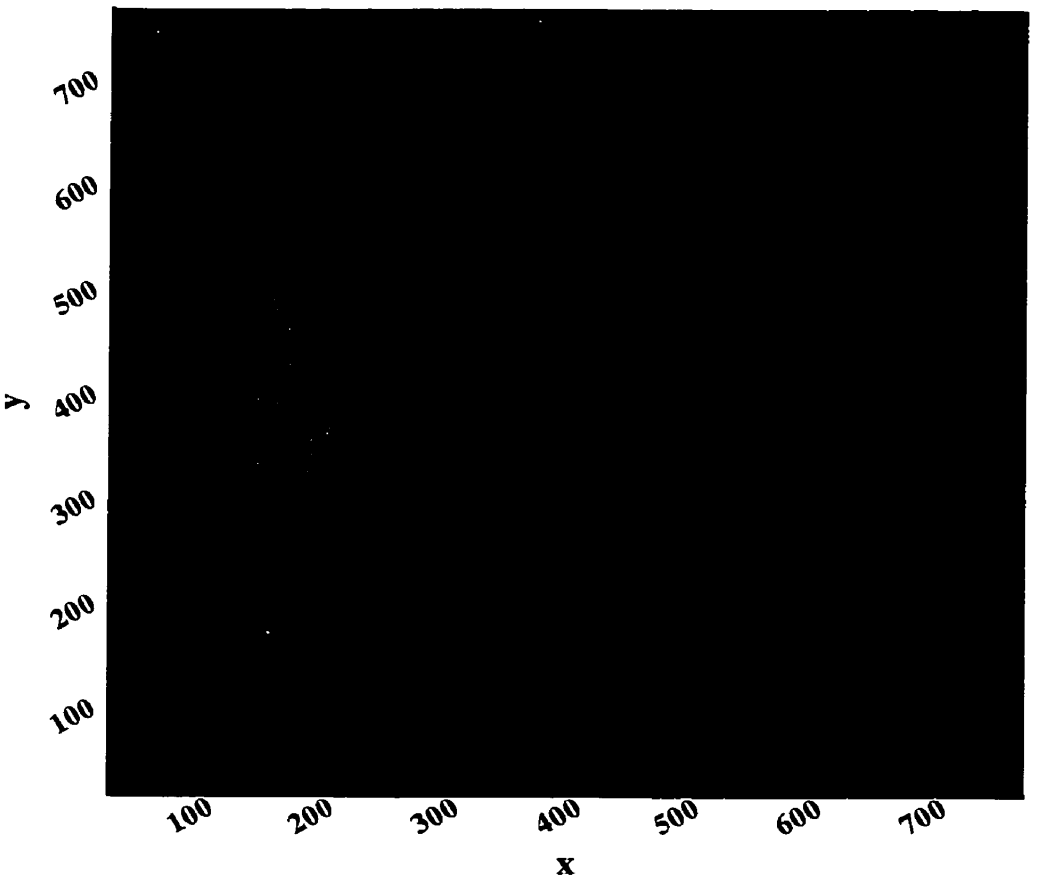

Figure II.20: Normalized thermal flux distribution at t=2.5 sec, z= 285 cm.

APPENDIX III: FLUX EVOLUTION DURING LOCA

The objective of this appendix is primarily to visualize the flux evolution during a hypothetical LOCA. The presented results are obtained using two time-level full flux approach identified by test case 01. The input parameters for this case are described in table 4.4. According to results presented in figures 4.24 and 4.25, the maximum amount of error in the relative total power does not exceed from 2.5%. It would also be interesting to visualize the distribution of time- and space- dependent errors in the nodal group flux defined by relationship 4.3. Hence, these local errors for the selected z-plane will be presented.

- Figure III.1 shows the thermal neutron flux distribution at t = 0.0 seconds. At this moment, flux distribution is symmetric.
- Figure III.2 presents the thermal neutron flux distribution at t = 0.3 shortly before firing the shutdown system #1. At this moment, the thermal neutron flux at left side of the reactor, where the loss of coolant is happening, attains to approximately 8×10^{14}.
- Figure III.3 demonstrates the thermal neutron flux distribution at t = 0.7. It can be observed that the thermal neutron flux continues to rise ($\sim 12.5 \times 10^{14}$). At this time, the shutoff rods are already passed through the reflector and their effect would start to be felt shortly (shutoff rods are inserted in the y-direction).
- Figure III.4 shows the thermal neutron flux distribution at t = 1.0 sec. In the upper side of the reactor, the effect of shout off rods can be observed.
- Figure III.5 presents the thermal neutron flux distribution at t = 1.3 sec. The upper side of the reactor is fully shutdown.
- Figure III.6 demonstrate the thermal neutron flux at t = 1.8, when all shutoff rods are fully inserted and consequently the reactor is completely shutdown.

As it was mentioned, the figures III.1 through III.6 are produced based on the results obtained from the test case 01. These results are compared to those obtained from the reference calculations (direct method, $dt = 0.01$ sec) and the errors in nodal group fluxes are calculated using relationship 4.3. For the selected z-plane ($k = 6$ representing the grids covering $251.59 < z < 301.12$), these errors are presented in figures III.7 through III.12.

- It is evident that at $t = 0.0$ sec, the amounts of local errors are null (figure III.7).
- Prior to the insertion of shutoff rods, the perturbation is uniformly distributed and the local errors are relatively small (figure III.8).
- Close examination of figure III.9 and III.10 shows that the local errors in the zones affected by shutoff rods are greater than the zones still far from shutoff rods.
- Figures III.11 and III.12 demonstrate that once the shut off rods are completely inserted, the local errors are distributed all across the reactor without any special pattern.

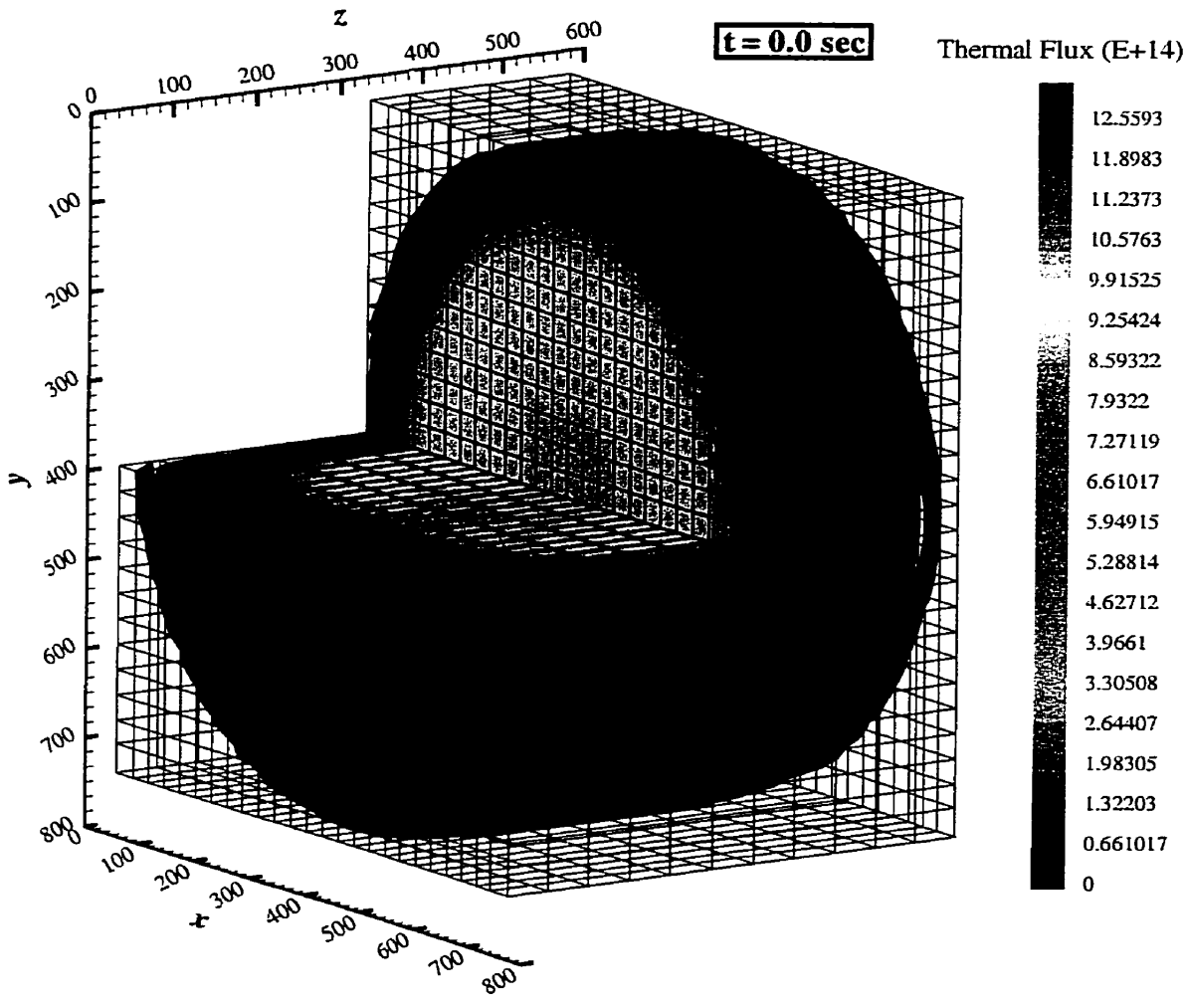

Figure III.1: Thermal neutron flux distribution at $t = 0.0$ s.

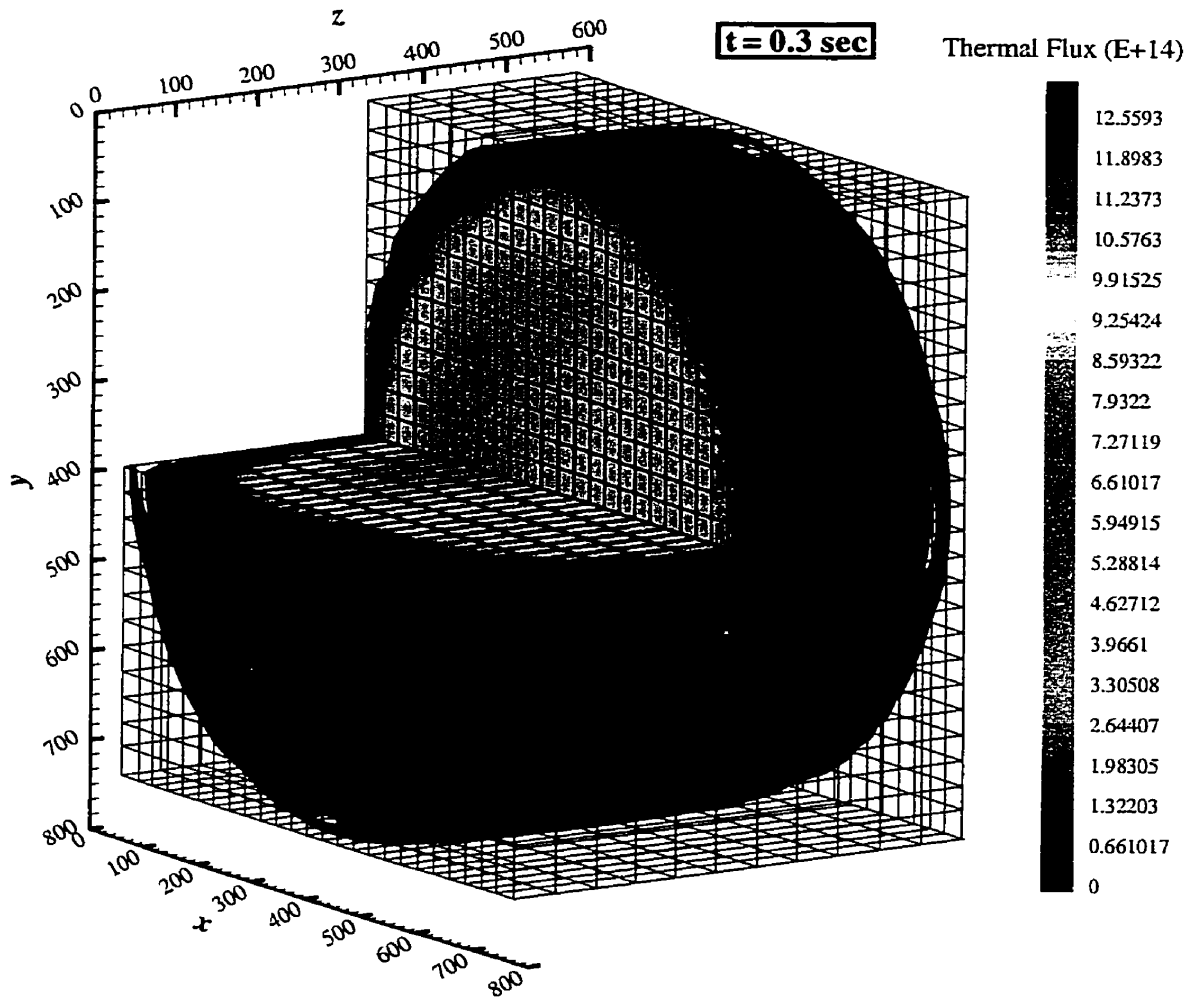

Figure III.2: Thermal neutron flux distribution at $t = 0.3$ s.

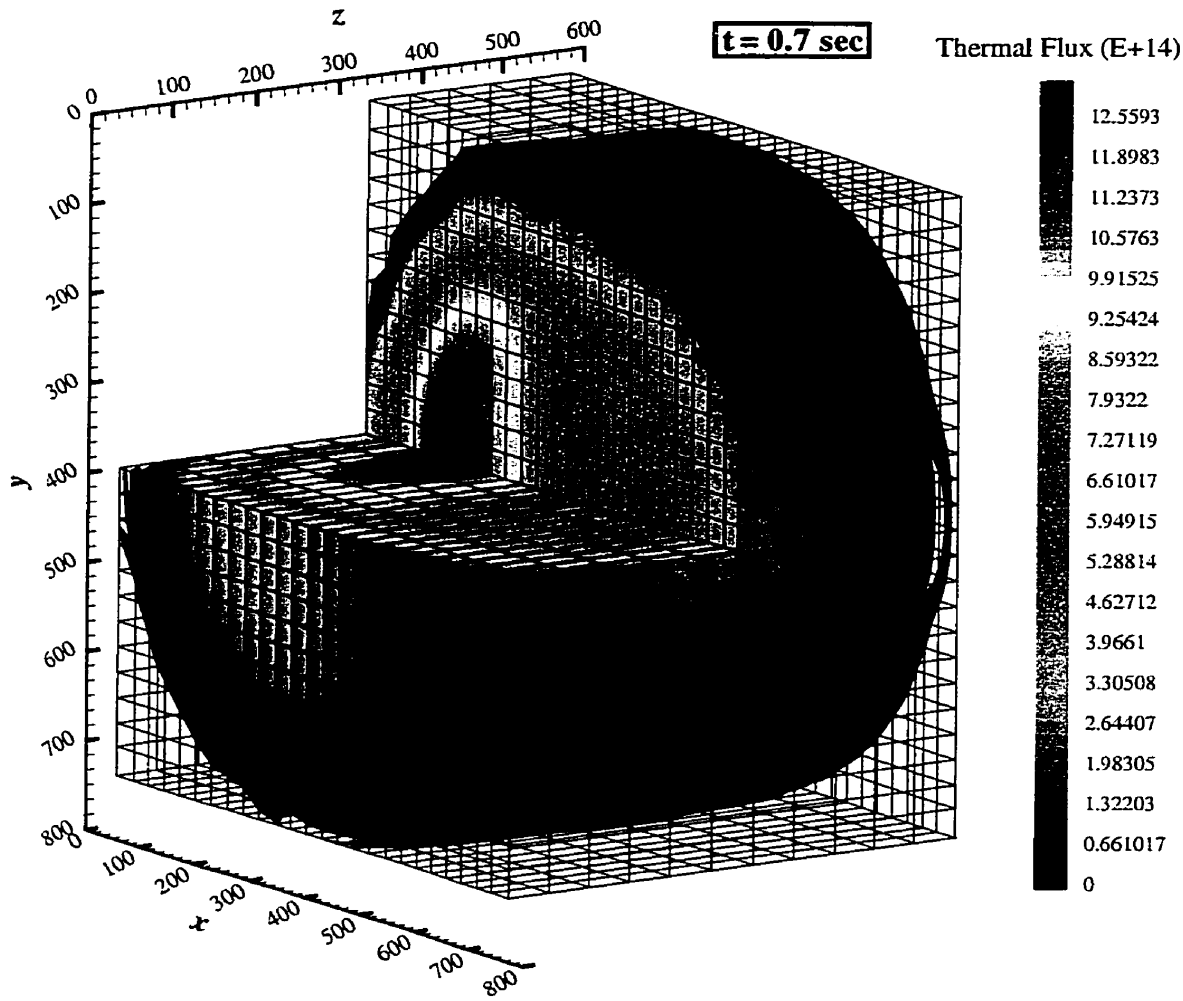

Figure III.3: Thermal neutron flux distribution at $t = 0.7$ s.

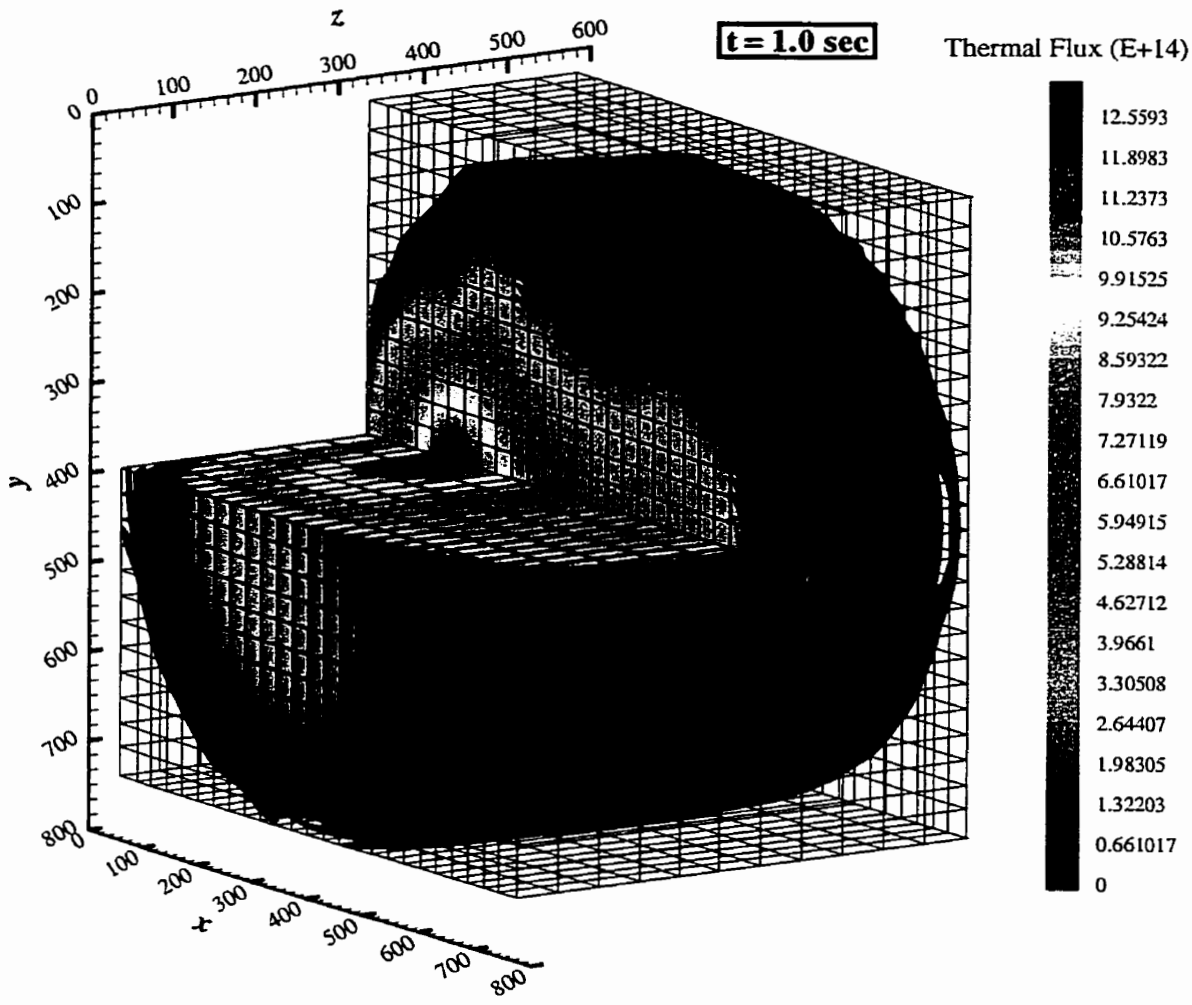

Figure III.4: Thermal neutron flux distribution at $t = 1.0$ s.

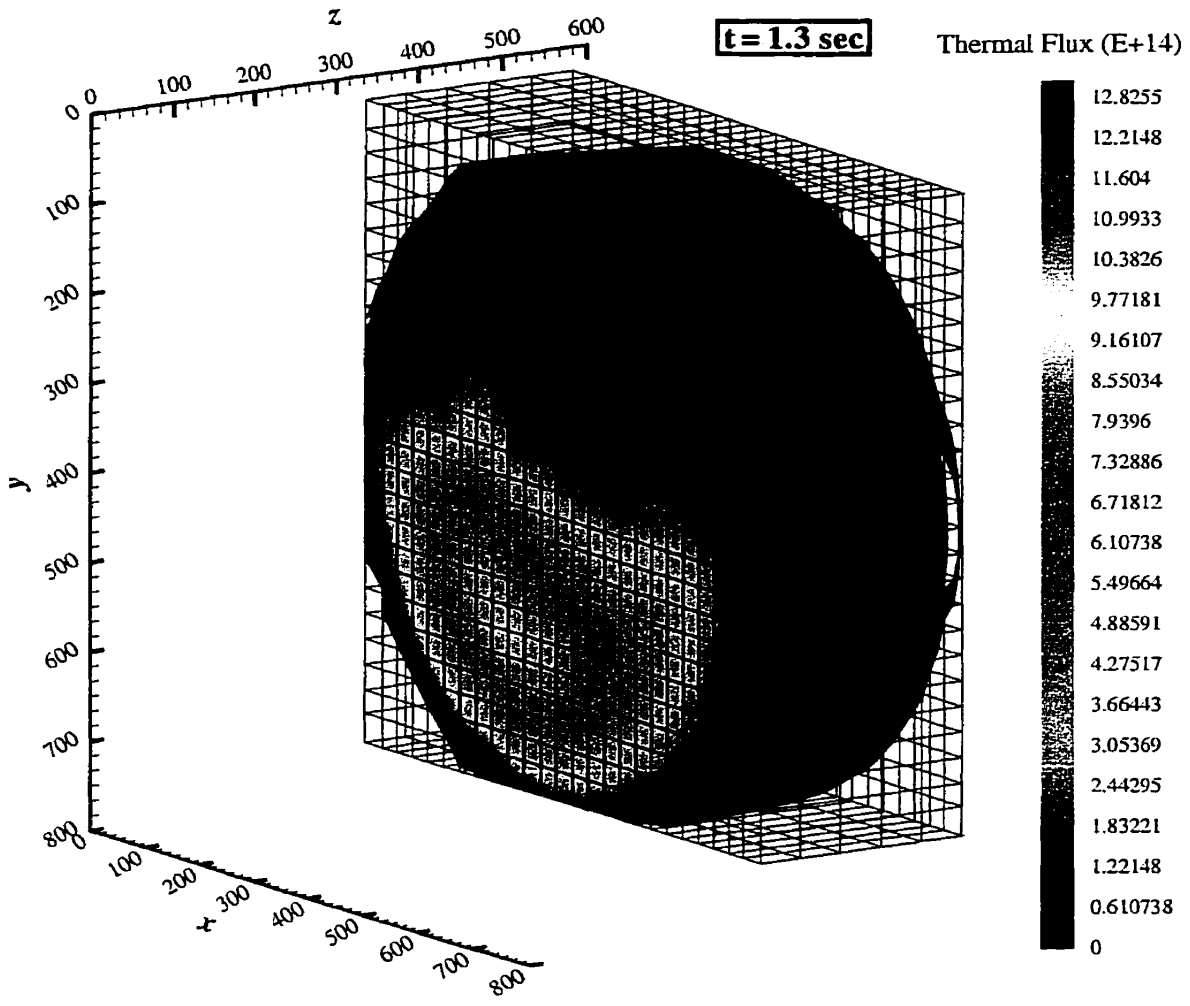

Figure III.5: Thermal neutron flux distribution at $t = 1.3$ s.

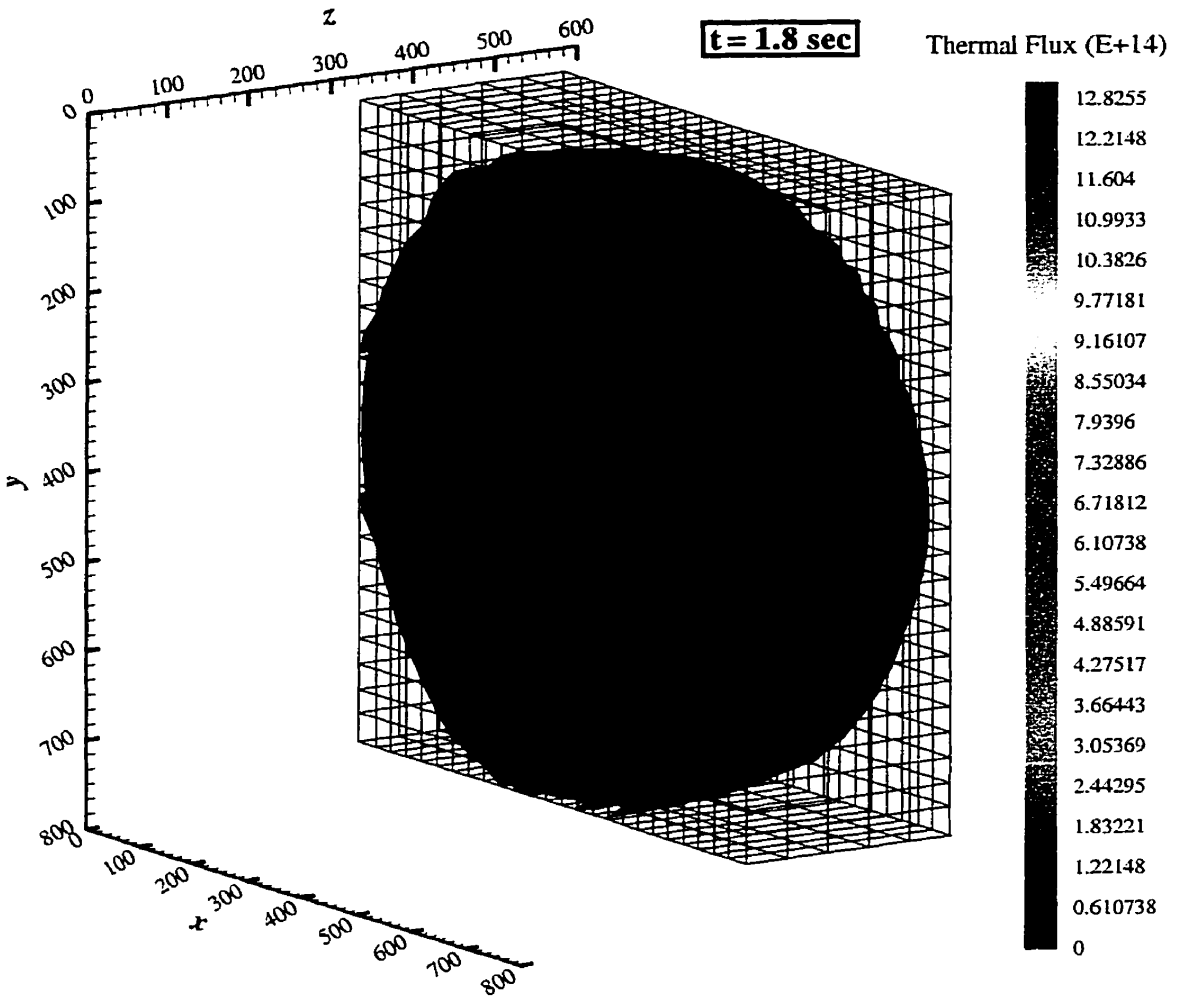

Figure III.6: Thermal neutron flux distribution at $t = 1.8$ s.

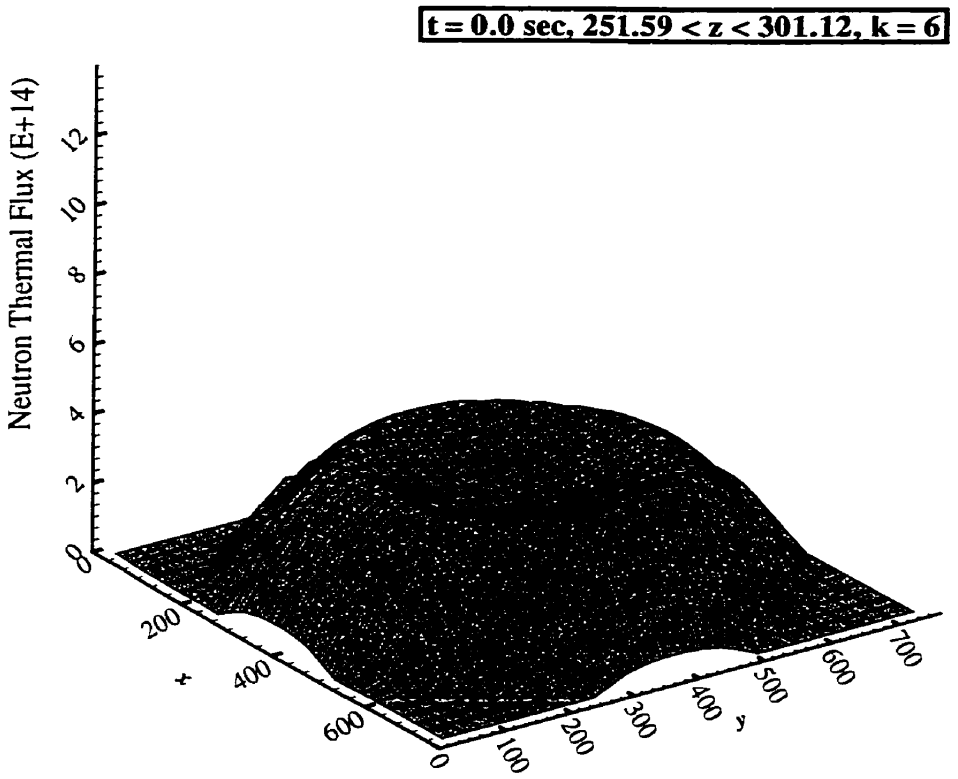

Figure III.7: Thermal neutron flux distribution at $t = 0.0$ s for selected z-plane

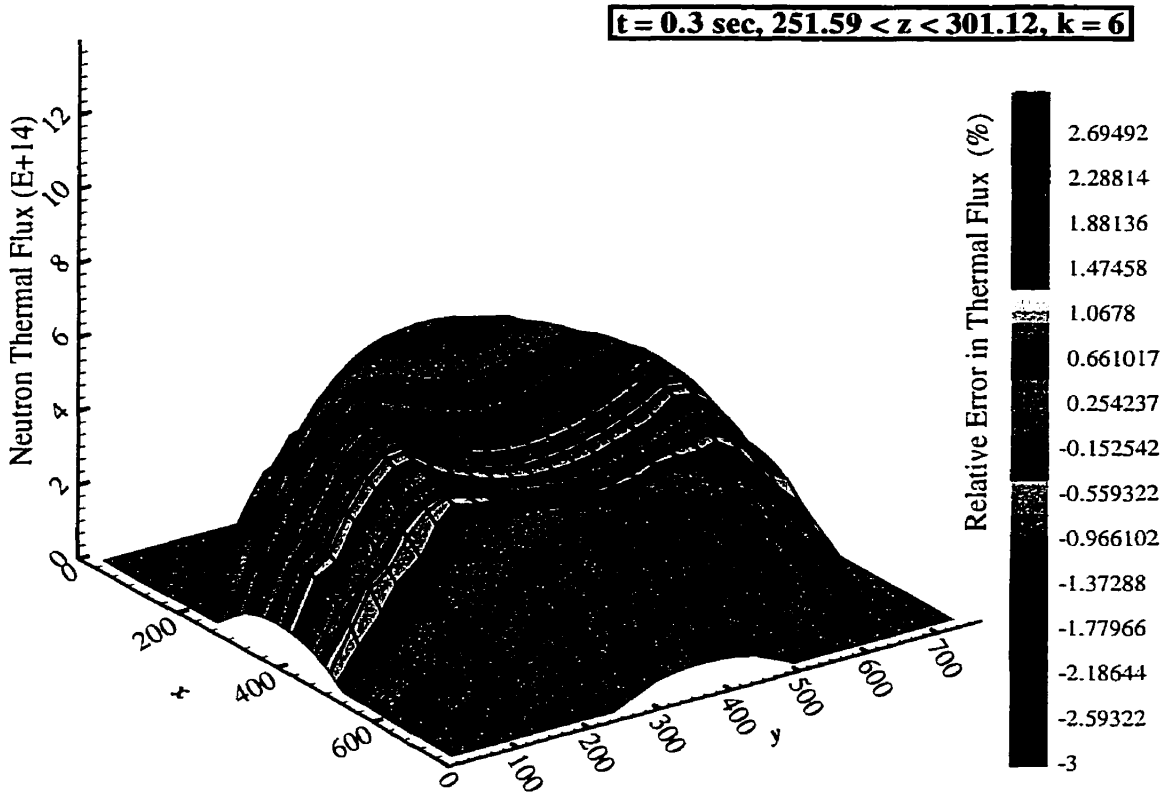

Figure III.8: Error in thermal neutron flux distribution at $t = 0.3$ s for selected z-plane

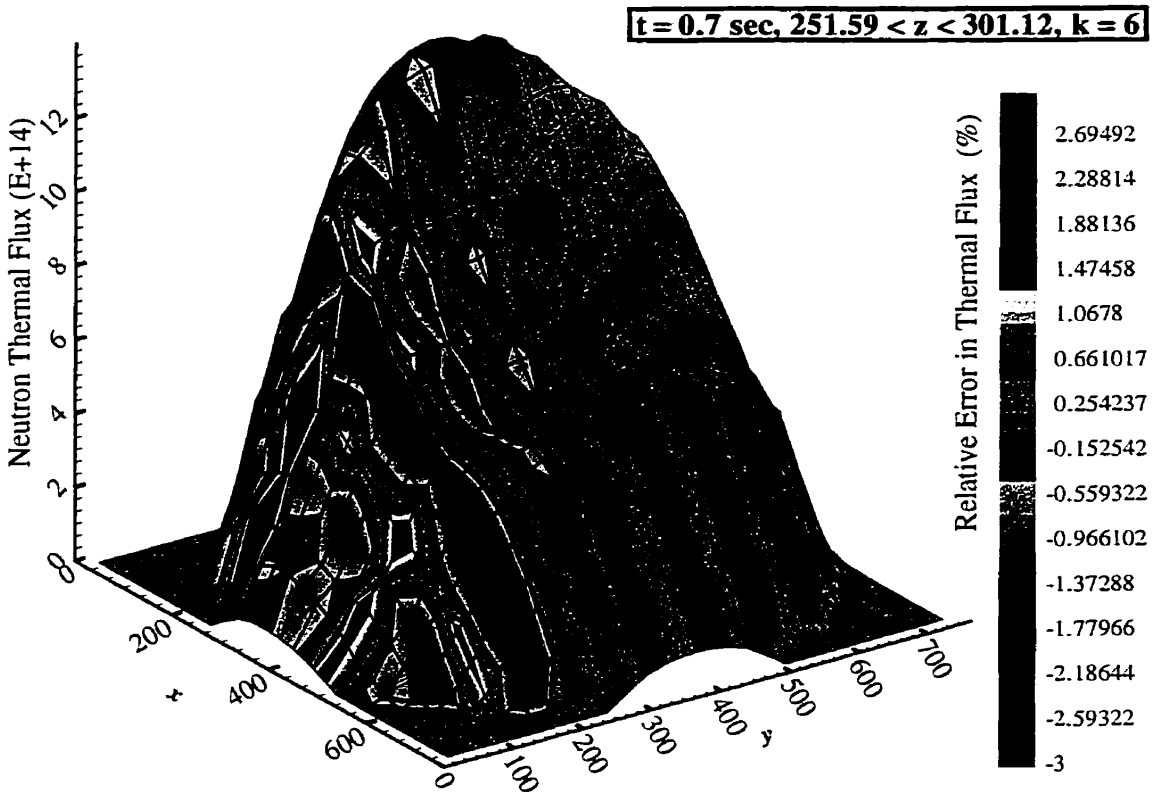

Figure III.9: Error in thermal neutron flux distribution at $t = 0.7$ s for selected z-plane

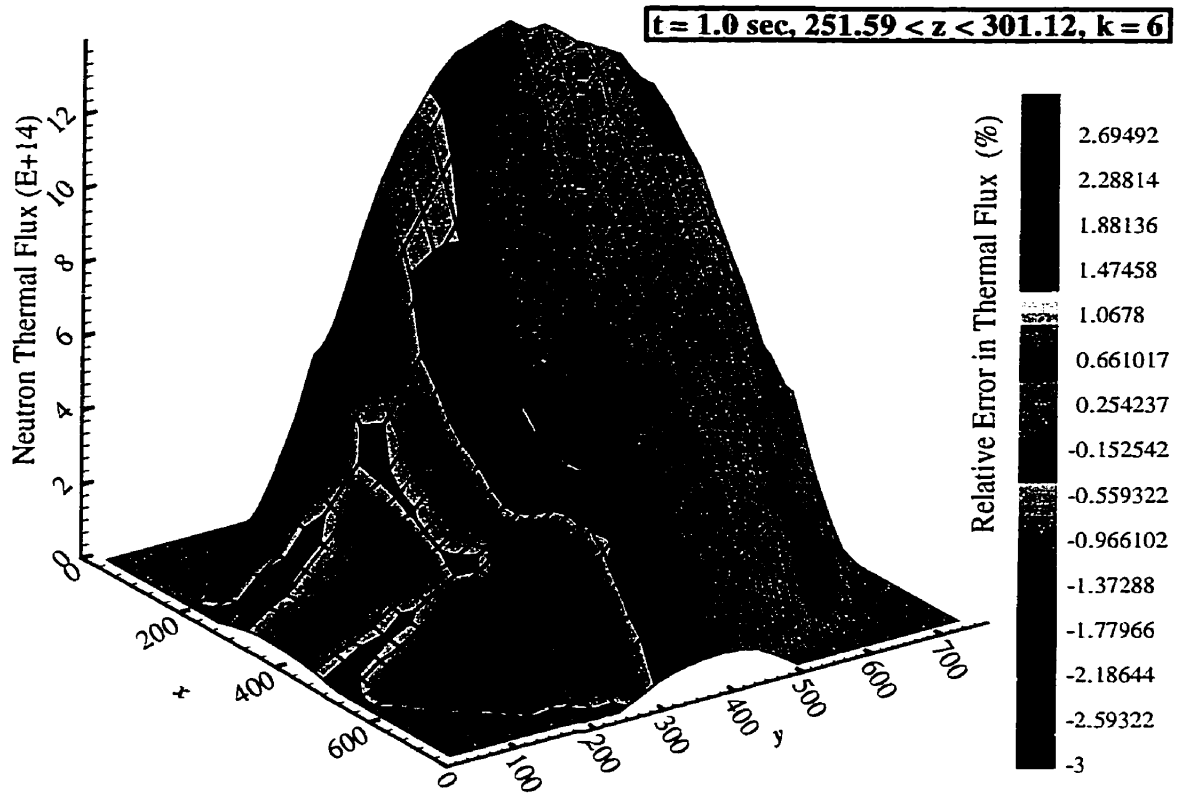

Figure III.10: Error in thermal neutron flux distribution at $t = 1.0$ s for selected z-plane

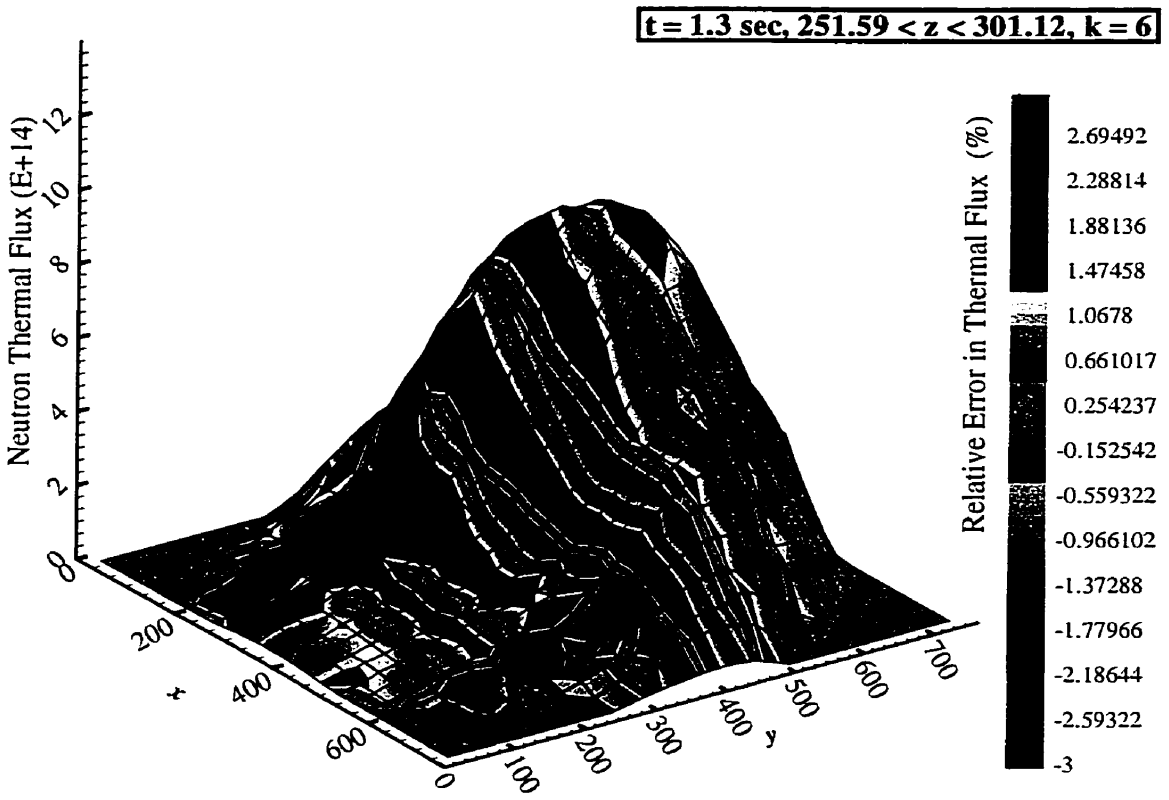

Figure III.11: Error in thermal neutron flux distribution at $t = 1.3$ s for select z-plane

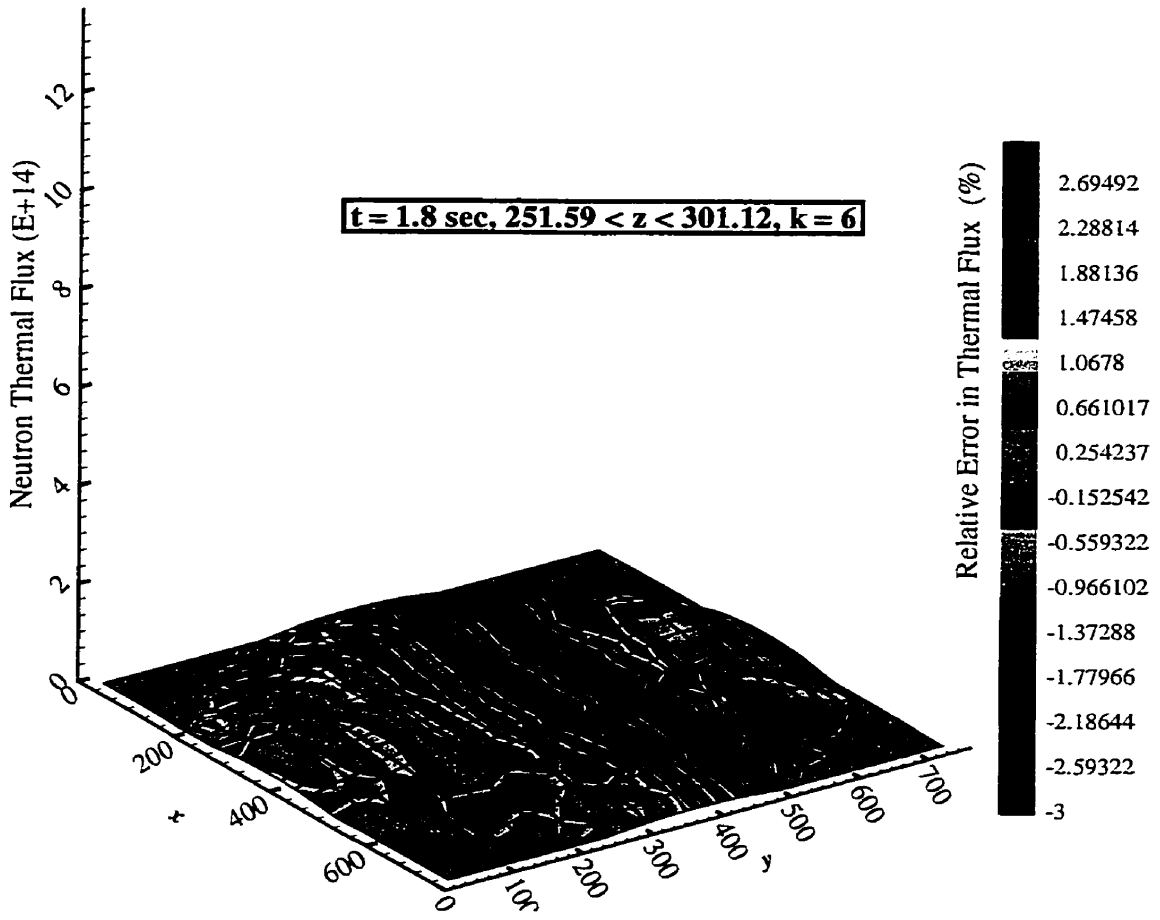

Figure III.12: Error in thermal neutron flux distribution at $t = 1.8$ s for select z-plane

APPENDIX IV: INPUT FILES FOR 3-D CANDU BENCHMARK

In this appendix, some of input files for 3-D CANDU benchmark are presented. The input files are designed based on procedure control language CLE 2000 (Roy and Hébert, 2000). This approach provides a template to establish the sequence of calculations by linking independent modules, each one performing an elementary task. All presented files are commented to clearly show how the calculations are performed.

```
!*************************************************************
! Argonne National Laboratory 3D CANDU Benchmark (1985)      *
!                                                            *
!*************************************************************
! file: zinput.c2m                                           *
!                                                            *
! Siamak Kaveh, 2000                                         *
!*************************************************************
 PROCEDURE   GeoB      macBINI      deviceB
             devprocB  statcalB     DIRECTB
             DYNIQSB   DYNNQSB                              ;

 MODULE      FREE: INIMAC: LINKDS: DECLARE: DELETE: END:
             NDFASCII:                                      ;

!// File declarations
 LINKED_LIST GEO2 INDEX MACRO DEVICE MACRO2 PROCEDE
             POWERFLUX ADJFLUX MACRO4 MACRO3
             TRKNDF TRANS POWERDISCON MACDISCON TRANS_D
             TRKDISCON MACDISCON_1                          ;

!// Local variables
 REAL        TMAX DELTAT DELTATS DELTATF                    ;
! //
 INTEGER     IDIRECT IIQS ITJIQS MPK MCF INWSTATIC          ;
!//
 STRING      FILEHDF FILERMS FILEPKP                        ;

!//==================
!// Solution Method
!// IDIRECT= 1 ==> method direct (with or without multigrid)
!// IIQS   = 1 ==> Conventional Improved Quasi-Static
!// ITJIQS = 1 ==> Extended Improved Quasi-Static Method
!//                (Time-Hierarchical Nodal Kinetics)
!//==================

 EVALUATE  IDIRECT   := 1                                   ;
 EVALUATE  IIQS      := 0                                   ;
 EVALUATE  ITJIQS    := 0                                   ;

!// Call GeoB to initialize fine mesh geometry
 GEO2 INDEX  := GeoB                                        ;

!// Call macBINI to initialize physical properties
 MACRO := macBINI                                           ;
```

```
!// Call deviceB to initialize
!// device geometrical informations
 DEVICE INDEX := deviceB     INDEX GEO2                          ;

!// Call devproc to initialize
!// device operational informations
 PROCEDE := devprocB     DEVICE                                  ;

!// Preparing the INDEXED macrolib
 MACRO2 := INIMAC: MACRO INDEX                                   ;

!// Set initial position for static calculations
 PROCEDE := FREE: PROCEDE                                        ;
 DEVICE  := FREE: DEVICE                                         ;
 DEVICE PROCEDE := LINKDS: DEVICE PROCEDE GEO2 ::
                           EDIT 4 DEVC
                           TYPE CONTROLLED
                           ROD ADJUSTER
                           POS ALL 0.0 END                       ;

!// Call statcalB to Perform initial static calculations
    REAL  intr        := 1.00E-08                                ;
    REAL  CorePower   := 1.00E+20                                ;
 INTEGER  USELIBRARY  := 0                                       ;
 INTEGER  MAKELIBRARY := 0                                       ;
 EVALUATE FILEHDF     := "DATABASE.HDF"                          ;
 ADJFLUX POWERFLUX TRKNDF TRKDISCON MACRO4 MACRO3
 POWERDISCON MACDISCON
 := statcalB
 MACRO2 DEVICE GEO2 PROCEDE ::
                             <<intr>> <<USELIBRARY>>
                             <<MAKELIBRARY>> <<FILEHDF>>
                             <<CorePower>>                       ;

!// Breaking dependencies
 PROCEDE     := FREE: PROCEDE                                    ;
 DEVICE      := FREE: DEVICE                                     ;
 MACRO       := FREE: MACRO                                      ;
 INDEX       := FREE: INDEX                                      ;
 GEO2        := FREE: GEO2                                       ;
 MACRO2      := FREE: MACRO2                                     ;
 MACDISCON_1 := MACDISCON                                        ;
 MACDISCON   := FREE: MACDISCON                                  ;
```

```
!// dynamic calculations
 TRANS      := DECLARE: :: L_TRANS                                    ;
 TRANS_D    := DECLARE: :: L_TRANS                                    ;

!// Method Direct, IDirect = 1
 IF IDIRECT 1 = THEN
    EVALUATE TMAX     :=  2.5                                        ;
    EVALUATE DELTAT   :=  0.01                                       ;
    EVALUATE FILERMS  := "RMS_DIRECT.DAT"                            ;
    EVALUATE FILEPKP  := "PKPAR_DIRECT.DAT"                          ;

!// Call DIRECTB
    TRANS POWERFLUX TRKNDF MACRO4 PROCEDE DEVICE GEO2 MACRO3
    ADJFLUX MACRO2 INDEX TRKDISCON
    := DIRECTB
    TRANS POWERFLUX TRKNDF MACRO4 PROCEDE DEVICE GEO2 MACRO3
    ADJFLUX MACRO2 INDEX TRKDISCON
                 :: <<TMAX>> <<DELTAT>>
                    <<FILEHDF>> <<FILERMS>> <<FILEPKP>>    ;
 ENDIF                                                               ;

!// Method IQS, DELTATS= DELTAT_SHAPE, IIQS = 1
 IF IIQS  1 = THEN
    EVALUATE  TMAX      := 2.5                                       ;
    EVALUATE  DELTATS   := 2.5                                       ;
    EVALUATE  MPK       := 2500                                      ;
    EVALUATE  FILEHDF   := "DATABASE.HDF"                            ;
    EVALUATE  FILERMS   := "RMS_IQS.DAT"                             ;
    EVALUATE  FILEPKP   := "PKPAR_IQS.DAT"                           ;

!// Call DYNIQSB
    TRANS POWERFLUX TRKNDF MACRO4 PROCEDE DEVICE
    GEO2 MACRO3 ADJFLUX MACRO2 INDEX
    := DYNIQSB
    TRANS POWERFLUX TRKNDF MACRO4 PROCEDE DEVICE
    GEO2 MACRO3 ADJFLUX MACRO2 INDEX
                 :: <<TMAX>> <<DELTATS>> <<MPK>>
                    <<FILEHDF>> <<FILERMS>> <<FILEPKP>>    ;
 ENDIF                                                               ;

!// Extended Quasi-Static Approach (Time Hierarchy)
!// ITJIQS = 1
 IF ITJIQS 1 = THEN
    EVALUATE  TMAX      := 2.5                                       ;
    EVALUATE  DELTATF   := 0.05                                      ;
```

```
    EVALUATE  MPK       := 10                                   ;
    EVALUATE  MCF       := 5                                    ;
    EVALUATE  FILEHDF   := "DATABASE.HDF"                       ;
    EVALUATE  FILERMS   := "RMS_NQS.DAT"                        ;
    EVALUATE  FILEPKP   := "PKPAR_NQS.DAT"                      ;

!// Call DYNNQSB
    TRANS_D TRANS POWERFLUX POWERDISCON TRKNDF
    TRKDISCON MACRO4 PROCEDE DEVICE GEO2 MACRO3
    MACDISCON ADJFLUX MACRO2 MACDISCON_1 INDEX
    := DYNNQSB
    TRANS_D TRANS POWERFLUX  POWERDISCON TRKNDF
    TRKDISCON MACRO4 PROCEDE DEVICE GEO2 MACRO3
    MACDISCON ADJFLUX MACRO2 MACDISCON_1 INDEX
                             :: <<TMAX>>
                                <<DELTATF>> <<MPK>>
                                <<MCF>> <<FILEHDF>>
                                <<FILERMS>>
                                <<FILEPKP>>                     ;
 ENDIF                                                          ;
!//

 END:                                                           ;
```

```
!************************************************************
! Argonne National Laboratory 3D CANDU Benchmark (1985)     *
!                                                           *
!************************************************************
! file: GeoB.c2m                                            *
!                                                           *
! Siamak Kaveh, 2000                                        *
!************************************************************

 PARAMETER   GEO2 INDEX ::

             ::: LINKED_LIST GEO2 INDEX  ;
                                         ;
 LINKED_LIST GEOM                        ;
 MODULE      END: GEOD: USPLIT:          ;
!
 GEOM := GEOD: :: CAR3D 18 18 10
                 EDIT  0

                 X- ZERO        X+ ZERO
                 Y- ZERO        Y+ ZERO
                 Z- ZERO        Z+ ZERO

 MIX

 PLAN    1

  0  0  0  0  1  1  4  4  4  4  4  4  3  3  0  0  0  0
  0  0  0  0  1  1  4  4  4  4  4  4  3  3  0  0  0  0
  0  0  1  1  1  1 10 10 10  9  9  9  3  3  3  3  0  0
  0  0  1  1  1  1 10 10 10  9  9  9  3  3  3  3  0  0
  1  1  1  1  5  5 10 10 10  9  9  9  8  8  3  3  3  3
  1  1  1  1  5  5 10 10 10  9  9  9  8  8  3  3  3  3
  1  1  5  5  5  5 11 11 11 12 12 12  8  8  8  8  3  3
  1  1  5  5  5  5 11 11 11 12 12 12  8  8  8  8  3  3
  1  1  5  5  5  5 11 11 11 12 12 12  8  8  8  8  3  3
  1  1  5  5  5  5 11 11 11 12 12 12  8  8  8  8  3  3
  1  1  5  5  5  5 11 11 11 12 12 12  8  8  8  8  3  3
  1  1  5  5  5  5 11 11 11 12 12 12  8  8  8  8  3  3
  1  1  1  1  5  5  6  6  6  7  7  7  8  8  3  3  3  3
  1  1  1  1  5  5  6  6  6  7  7  7  8  8  3  3  3  3
  0  0  1  1  1  1  6  6  6  7  7  7  3  3  3  3  0  0
  0  0  1  1  1  1  6  6  6  7  7  7  3  3  3  3  0  0
  0  0  0  0  1  1  2  2  2  2  2  2  3  3  0  0  0  0
  0  0  0  0  1  1  2  2  2  2  2  2  3  3  0  0  0  0
```

```
PLAN     6

 0  0  0  0 13 13 16 16 16 16 16 16 15 15  0  0  0  0
 0  0  0  0 13 13 16 16 16 16 16 16 15 15  0  0  0  0
 0  0 13 13 13 13 22 22 22 21 21 21 15 15 15 15  0  0
 0  0 13 13 13 13 22 22 22 21 21 21 15 15 15 15  0  0
13 13 13 13 17 17 22 22 22 21 21 21 20 20 15 15 15 15
13 13 13 13 17 17 22 22 22 21 21 21 20 20 15 15 15 15
13 13 17 17 17 17 23 23 23 24 24 24 20 20 20 20 15 15
13 13 17 17 17 17 23 23 23 24 24 24 20 20 20 20 15 15
13 13 17 17 17 17 23 23 23 24 24 24 20 20 20 20 15 15
13 13 17 17 17 17 23 23 23 24 24 24 20 20 20 20 15 15
13 13 17 17 17 17 23 23 23 24 24 24 20 20 20 20 15 15
13 13 17 17 17 17 23 23 23 24 24 24 20 20 20 20 15 15
13 13 13 13 17 17 18 18 18 19 19 19 20 20 15 15 15 15
13 13 13 13 17 17 18 18 18 19 19 19 20 20 15 15 15 15
 0  0 13 13 13 13 18 18 18 19 19 19 15 15 15 15  0  0
 0  0 13 13 13 13 18 18 18 19 19 19 15 15 15 15  0  0
 0  0  0  0 13 13 14 14 14 14 14 14 15 15  0  0  0  0
 0  0  0  0 13 13 14 14 14 14 14 14 15 15  0  0  0  0


PLAN 2  SAME 1
PLAN 3  SAME 1
PLAN 4  SAME 1
PLAN 5  SAME 1
PLAN 7  SAME 6
PLAN 8  SAME 6
PLAN 9  SAME 6
PLAN 10 SAME 6

MESHX    0.0  60.0  90.0 120.0 150.0 180.0 210.0 270.0 330.0
       390.0 450.0 510.0 570.0 600.0 630.0 660.0 690.0 720.0
       780.0

MESHY    0.0  60.0  90.0 120.0 150.0 180.0 210.0 270.0 330.0
       390.0 450.0 510.0 570.0 600.0 630.0 660.0 690.0 720.0
       780.0

MESHZ    0.0  60.0 120.0 180.0 240.0 300.0 360.0 420.0 480.0
       540.0 600.0

!// Splitting Option
```

```
! SPLITX 2 2 2 2 2 2 2 2 2 2 2 2 2 2 2 2 2 2
! SPLITY 2 2 2 2 2 2 2 2 2 2 2 2 2 2 2 2 2 2
! SPLITZ 2 2 2 2 2 2 2 2 2 2

      ;

 GEO2 INDEX := USPLIT: GEOM ::  MAXR 100000 ;

 END: ;
```

```
!************************************************************
! Argonne National Laboratory 3D CANDU Benchmark (1985)     *
!                                                           *
!************************************************************
! file: MacBINI.c2m                                         *
!                                                           *
! Siamak Kaveh, 2000                                        *
!************************************************************
 PARAMETER   MACRO ::
             ::: LINKED_LIST MACRO  ;
                                    ;
!
 MODULE      MACD: END:             ;
!
 MACRO :=  MACD: ::
           EDIT 1  NGRO 2 NMIX 25  READ
!////////
 MIX      1
      DIFFX  1.3100E+00 0.8695E+00
      TOTAL  1.0180E-02 2.1170E-04
     NUSIGF  0.0000E+00 0.0000E+00
        CHI  1.0000E+00 0.0000E+00
  H-FACTORS  0.0000E+00 0.0000E+00
       SCAT  1 1 0.0 2 2 0.0 1.0180E-02
 MIX      2
      DIFFX  1.3100E+00 0.8695E+00
      TOTAL  1.0180E-02 2.1170E-04
     NUSIGF  0.0000E+00 0.0000E+00
        CHI  1.0000E+00 0.0000E+00
  H-FACTORS  0.0000E+00 0.0000E+00
       SCAT  1 1 0.0 2 2 0.0 1.0180E-02
 MIX      3
      DIFFX  1.3100E+00 0.8695E+00
      TOTAL  1.0180E-02 2.1170E-04
     NUSIGF  0.0000E+00 0.0000E+00
        CHI  1.0000E+00 0.0000E+00
  H-FACTORS  0.0000E+00 0.0000E+00
       SCAT  1 1 0.0 2 2 0.0 1.0180E-02
 MIX      4
      DIFFX  1.3100E+00 0.8695E+00
      TOTAL  1.0180E-02 2.1170E-04
     NUSIGF  0.0000E+00 0.0000E+00
        CHI  1.0000E+00 0.0000E+00
  H-FACTORS  0.0000E+00 0.0000E+00
       SCAT  1 1 0.0 2 2 0.0 1.0180E-02
```

```
*!/////////
 MIX      5
      DIFFX  1.2640E+00 0.9328E+00
      TOTAL  8.1540E-03 4.0140E-03
     NUSIGF  0.0000E+00 4.7230E-03
        CHI  1.0000E+00 0.0000E+00
  H-FACTORS  0.0000E+00 4.7230E-03
       SCAT  1 1 0.0 2 2 0.0 7.3680E-03

 MIX      6
      DIFFX  1.2640E+00 0.9328E+00
      TOTAL  8.1540E-03 4.0140E-03
     NUSIGF  0.0000E+00 4.7230E-03
        CHI  1.0000E+00 0.0000E+00
  H-FACTORS  0.0000E+00 4.7230E-03
       SCAT  1 1 0.0 2 2 0.0 7.3680E-03
 MIX      7
      DIFFX  1.2640E+00 0.9328E+00
      TOTAL  8.1540E-03 4.0140E-03
     NUSIGF  0.0000E+00 4.7230E-03
        CHI  1.0000E+00 0.0000E+00
  H-FACTORS  0.0000E+00 4.7230E-03
       SCAT  1 1 0.0 2 2 0.0 7.3680E-03
 MIX      8
      DIFFX  1.2640E+00 0.9328E+00
      TOTAL  8.1540E-03 4.0140E-03
     NUSIGF  0.0000E+00 4.7230E-03
        CHI  1.0000E+00 0.0000E+00
  H-FACTORS  0.0000E+00 4.7230E-03
       SCAT  1 1 0.0 2 2 0.0 7.3680E-03
 MIX      9
      DIFFX  1.2640E+00 0.9328E+00
      TOTAL  8.1540E-03 4.0140E-03
     NUSIGF  0.0000E+00 4.7230E-03
        CHI  1.0000E+00 0.0000E+00
  H-FACTORS  0.0000E+00 4.7230E-03
       SCAT  1 1 0.0 2 2 0.0 7.3680E-03
 MIX     10
      DIFFX  1.2640E+00 0.9328E+00
      TOTAL  8.1540E-03 4.0140E-03
     NUSIGF  0.0000E+00 4.7230E-03
        CHI  1.0000E+00 0.0000E+00
  H-FACTORS  0.0000E+00 4.7230E-03
       SCAT  1 1 0.0 2 2 0.0 7.3680E-03
!/////////
```

```
 MIX     11
      DIFFX  1.2640E+00 0.9328E+00
      TOTAL  8.1540E-03 4.1000E-03
     NUSIGF  0.0000E+00 4.5620E-03
        CHI  1.0000E+00 0.0000E+00
  H-FACTORS  0.0000E+00 4.5620E-03
       SCAT  1 1 0.0 2 2 0.0 7.3680E-03
  MIX     12
      DIFFX  1.2640E+00 0.9328E+00
      TOTAL  8.1540E-03 4.1000E-03
     NUSIGF  0.0000E+00 4.5620E-03
        CHI  1.0000E+00 0.0000E+00
  H-FACTORS  0.0000E+00 4.5620E-03
       SCAT  1 1 0.0 2 2 0.0 7.3680E-03
!/////////
 MIX     13
      DIFFX  1.3100E+00 0.8695E+00
      TOTAL  1.0180E-02 2.1170E-04
     NUSIGF  0.0000E+00 0.0000E+00
        CHI  1.0000E+00 0.0000E+00
  H-FACTORS  0.0000E+00 0.0000E+00
       SCAT  1 1 0.0 2 2 0.0 1.0180E-02
 MIX     14
      DIFFX  1.3100E+00 0.8695E+00
      TOTAL  1.0180E-02 2.1170E-04
     NUSIGF  0.0000E+00 0.0000E+00
        CHI  1.0000E+00 0.0000E+00
  H-FACTORS  0.0000E+00 0.0000E+00
       SCAT  1 1 0.0 2 2 0.0 1.0180E-02
 MIX     15
      DIFFX  1.3100E+00 0.8695E+00
      TOTAL  1.0180E-02 2.1170E-04
     NUSIGF  0.0000E+00 0.0000E+00
        CHI  1.0000E+00 0.0000E+00
  H-FACTORS  0.0000E+00 0.0000E+00
       SCAT  1 1 0.0 2 2 0.0 1.0180E-02
 MIX     16
      DIFFX  1.3100E+00 0.8695E+00
      TOTAL  1.0180E-02 2.1170E-04
     NUSIGF  0.0000E+00 0.0000E+00
        CHI  1.0000E+00 0.0000E+00
  H-FACTORS  0.0000E+00 0.0000E+00
       SCAT  1 1 0.0 2 2 0.0 1.0180E-02
!/////////
 MIX     17
```

```
      DIFFX  1.2640E+00 0.9328E+00
      TOTAL  8.1540E-03 4.0140E-03
     NUSIGF  0.0000E+00 4.7230E-03
        CHI  1.0000E+00 0.0000E+00
  H-FACTORS  0.0000E+00 4.7230E-03
       SCAT  1 1 0.0 2 2 0.0 7.3680E-03
  MIX    18
      DIFFX  1.2640E+00 0.9328E+00
      TOTAL  8.1540E-03 4.0140E-03
     NUSIGF  0.0000E+00 4.7230E-03
        CHI  1.0000E+00 0.0000E+00
  H-FACTORS  0.0000E+00 4.7230E-03
       SCAT  1 1 0.0 2 2 0.0 7.3680E-03
 MIX     19
      DIFFX  1.2640E+00 0.9328E+00
      TOTAL  8.1540E-03 4.0140E-03
     NUSIGF  0.0000E+00 4.7230E-03
        CHI  1.0000E+00 0.0000E+00
  H-FACTORS  0.0000E+00 4.7230E-03
       SCAT  1 1 0.0 2 2 0.0 7.3680E-03
 MIX     20
      DIFFX  1.2640E+00 0.9328E+00
      TOTAL  8.1540E-03 4.0140E-03
     NUSIGF  0.0000E+00 4.7230E-03
        CHI  1.0000E+00 0.0000E+00
  H-FACTORS  0.0000E+00 4.7230E-03
       SCAT  1 1 0.0 2 2 0.0 7.3680E-03
 MIX     21
      DIFFX  1.2640E+00 0.9328E+00
      TOTAL  8.1540E-03 4.0140E-03
     NUSIGF  0.0000E+00 4.7230E-03
        CHI  1.0000E+00 0.0000E+00
  H-FACTORS  0.0000E+00 4.7230E-03
       SCAT  1 1 0.0 2 2 0.0 7.3680E-03
 MIX     22
      DIFFX  1.2640E+00 0.9328E+00
      TOTAL  8.1540E-03 4.0140E-03
     NUSIGF  0.0000E+00 4.7230E-03
        CHI  1.0000E+00 0.0000E+00
  H-FACTORS  0.0000E+00 4.7230E-03
       SCAT  1 1 0.0 2 2 0.0 7.3680E-03
!/////////
 MIX     23
      DIFFX  1.2640E+00 0.9328E+00
      TOTAL  8.1540E-03 4.1000E-03
```

```
      NUSIGF  0.0000E+00 4.5620E-03
         CHI  1.0000E+00 0.0000E+00
   H-FACTORS  0.0000E+00 4.5620E-03
        SCAT  1 1 0.0 2 2 0.0 7.3680E-03
 MIX     24
       DIFFX  1.2640E+00 0.9328E+00
       TOTAL  8.1540E-03 4.1000E-03
      NUSIGF  0.0000E+00 4.5620E-03
         CHI  1.0000E+00 0.0000E+00
   H-FACTORS  0.0000E+00 4.5620E-03
        SCAT  1 1 0.0 2 2 0.0 7.3680E-03
!////////// Device
 MIX     25
       TOTAL  0.0000E+00 6.1500E-04      ;
!
END: ;
```

```
!*************************************************************
! Argonne National Laboratory 3D CANDU Benchmark (1985)     *
!                                                           *
!*************************************************************
! file: Device8.c2m                                         *
!                                                           *
! Siamak Kaveh, 2000                                        *
!*************************************************************
 PARAMETER   DEVICE INDEX GEO2 ::
             ::: LINKED_LIST GEO2 DEVICE INDEX ;
                                               ;

 MODULE      INIDEV:  END:                     ;
!
 DEVICE INDEX := INIDEV: INDEX GEO2 ::
                 NDEV  3  NODEL  NDESC  3
!
 DEVICE CONTROLLED ADJUSTER ADJ_R01
        390.00 570.00 -2780.00 780.00 0.00 300.00
     Y  520.00 0.00 0.00
 ADJR01 390.00 570.00 -2780.00 780.00 0.00 300.00
 25   0
 ENDDEV
!
 DEVICE CONTROLLED ADJUSTER ADJ_R02
         210.00 390.00 -2780.00 780.00 300.00 600.00
      Y  520.00 0.00 0.00
 ADJR02  210.00 390.00 -2780.00 780.00 300.00 600.00
 25   0
 ENDDEV
 DEVICE CONTROLLED ADJUSTER ADJ_R03
         390.00 570.00 -2780.00 780.00 300.00 600.00
      Y  520.00 0.00 0.00
 ADJR03  390.00 570.00 -2780.00 780.00 300.00 600.00
 25   0
 ENDDEV                                              ;
!
 END: ;
```

```
!************************************************************
! Argonne National Laboratory 3D CANDU Benchmark (1985)     *
!                                                           *
!************************************************************
! file: DevprocB.c2m                                        *
!                                                           *
! Siamak Kaveh, 2000                                        *
!************************************************************

 PARAMETER   PROCEDE DEVICE ::
             :::  LINKED_LIST PROCEDE DEVICE      ;
                                                  ;
 MODULE      END: INPROC: READ:  ;
!
 PROCEDE := INPROC: DEVICE ::  EDIT 5  TYPE CONTROLLED  END

            ROD ADJUSTER NAME ADJ_R01 NB 1 NBANC 1 TIME 1.500 END
            ROD ADJUSTER NAME ADJ_R02 NB 1 NBANC 1 TIME 1.500 END
            ROD ADJUSTER NAME ADJ_R03 NB 1 NBANC 1 TIME 1.500 END ;
END: ;
```

```
!************************************************************
! Argonne National Laboratory 3D CANDU Benchmark (1985)     *
!                                                           *
!************************************************************
! file: Statcal8.c2m                                        *
!                                                           *
! Siamak Kaveh, 2000                                        *
!************************************************************
 PARAMETER    ADJFLUX POWERFLUX TRKNDF TRKDISCON MACRO4
              MACRO3 POWERDISCON MACDISCON MACRO2
              DEVICE GEO2 PROCEDE
              ::
 :::
 LINKED_LIST ADJFLUX POWERFLUX TRKNDF MACRO4 MACRO3
              MACRO2 DEVICE GEO2 PROCEDE MACDISCON
              TRKDISCON POWERDISCON
              ;
 ;
 LINKED_LIST MACDISCOND
              ;

!
 REAL         intr CorePower
              ;
!
 INTEGER      STANDARD ADJOINT USELIBRARY MAKELIBRARY
              ;
!
 STRING       FILEHDF
              ;
!
 MODULE       NEWMAC: FREE: END: GREP:
              XEN: NMACX: DELETE:
              DECLARE: SETNDF: MAKTRKDF: MAKMACDF:
              DRAWCOR: CMPFLX: MAKLIB:
              ;
!
 PROCEDURE    GETFLUX
              ;
!
 :: >>intr<<          >>USELIBRARY<<
    >>MAKELIBRARY<<   >>FILEHDF<<
    >>CorePower<<                          ;

!//1) Declaring linked lists...
 POWERFLUX     := DECLARE: :: L_POWER     ;
 TRKNDF        := DECLARE: :: L_TRKNDF    ;
 ADJFLUX       := DECLARE: :: L_ADJOINT   ;
 POWERDISCON   := DECLARE: :: L_POWER     ;
 TRKDISCON     := DECLARE: :: L_TRKNDF    ;
 MACDISCON     := DECLARE: :: L_MACROLIB  ;

!//2) Evaluating adj or forward ...
 EVALUATE  STANDARD := 1                  ;
 EVALUATE  ADJOINT  := 2                  ;

!//3) Making macrolib based on device position...
 MACRO3 := NEWMAC: DEVICE MACRO2 GEO2 ::
           TYPE CONTROLLED XFAC  1.0      ;
 MACRO4 := MACRO3                         ;
 MACRO3 := FREE: MACRO3                   ;
 MACRO4 := FREE: MACRO4                   ;

!//4) Defining coarse mesh...
 TRKNDF := SETNDF: TRKNDF MACRO3 GEO2 ::
 NEDTX 5 LMESHX 0.0 180.00 330.00 450.00 600.00 780.00
 NEDTY 5 LMESHY 0.0 180.00 330.00 450.00 600.00 780.00
```

```
 NEDTZ 4 LMESHZ 0.0 180.00 300.00 420.00 600.00       ;

!//5) Defining coarse mesh...
 TRKDISCON := MAKTRKDF: TRKDISCON TRKNDF ::
 NEDTX 5 LMESHX 0.0 180.00 330.00 450.00 600.00 780.00
 NEDTY 5 LMESHY 0.0 180.00 330.00 450.00 600.00 780.00
 NEDTZ 4 LMESHZ 0.0 180.00 300.00 420.00 600.00       ;

!//6) Calculating standard flux...
POWERFLUX := GETFLUX POWERFLUX MACRO4 TRKNDF
          :: <<STANDARD>> NODISCON 5.E-6 5.E-6 0 <<CorePower>> ;
 MACRO4 := FREE: MACRO4 ;

!//7) Calculating adjoint flux...
ADJFLUX := GETFLUX ADJFLUX MACRO4 TRKNDF
           :: <<ADJOINT>> NODISCON 5.E-6 5.E-6 0 1.00     ;
 MACRO4 := FREE: MACRO4 ;

!//8) Calculating coarse macrolib discontinuity factors from scratch....
     MACDISCON  := MAKMACDF: MACDISCON TRKDISCON TRKNDF
                   POWERFLUX ADJFLUX MACRO4 PROCEDE ::
                   1 PRINTER_FLAG 1 PUT_AL
                                                                    ;
 MACDISCOND := MACDISCON                                            ;
 MACDISCOND := FREE: MACDISCOND                                     ;

!//9) Making HDF library...
IF MAKELIBRARY 1 = THEN
     := MAKLIB: POWERFLUX TRKNDF
        TRKDISCON MACDISCOND PROCEDE ::
        TECPLOT_ON FINEL.DAT COARSEL.DAT
        HDF_ON <<FILEHDF>>                                          ;
ENDIF                                                               ;

!//---->
 POWERDISCON  := GETFLUX POWERDISCON MACDISCON TRKDISCON
              :: <<STANDARD>> DISCON 1.E-6 1.E-6 0
                 <<CorePower>>                                      ;
 END:                                                               ;
```

```
!************************************************************
! Argonne National Laboratory 3D CANDU Benchmark (1985)     *
!                                                           *
!************************************************************
! file: Getflux.c2m                                         *
!                                                           *
! Jean Koclsa, Siamak Kaveh, 2000                           *
!************************************************************

PARAMETER POWER MACLIB TRK      ::
                               :::
LINKED_LIST POWER MACLIB TRK     ;
                                 ;

!
INTEGER TYPE     PF PF1           ;
REAL    EPSK     EPSPHI CorePower ;
STRING  IDISCON                   ;

!
MODULE UTL:     FREE:       DELETE:      END:   GREP:    DECLARE:
       CPLING: FLXNRMNDF: STATICNDF:  OUTER: INITER: INIPOWER: ;

!
LINKED_LIST FLUX MATRIX OUTER ITER RHS ;
SEQ_ASCII RHSDIS MATRIXDIS FLUXDIS     ;


!1) Reading input options...
:: >>TYPE<< >>IDISCON<< >>EPSK<< >>EPSPHI<< >>PF<< >>CorePower<< ;

!
ECHO ' TYPE      IS ' TYPE          ;
ECHO ' IDISCON   IS ' IDISCON       ;
ECHO ' EPSK      IS ' EPSK          ;
ECHO ' EPSPHI    IS ' EPSPHI        ;
ECHO ' PF        IS ' PF            ;
ECHO ' CorePower IS ' CorePower     ;


!2) Declaring linked lists...
MATRIX   RHS   OUTER := DECLARE: ::
L_MATRIX L_RHS L_OUTER             ;
FLUX   ITER := DECLARE: ::
L_FLUXNDF L_ITER                   ;
```

```
!(*********************************************)
!(* ///// CALCULATE COUPLING COEFFICIENTS ///// *)
!(*********************************************)
MATRIX := CPLING: MATRIX MACLIB TRK ::
PRINT_FLAG <<PF>> TYPE <<TYPE>> DF <<IDISCON>> ;
MATRIX := FREE: MATRIX ;

!(*******************************************)
!(* ///// INITIALIZE BOTH FLUX AND KEFF ///// *)
!(*******************************************)
FLUX := FLXNRMNDF: FLUX TRK  POWER :: FLUX KEFF 1.0 TYPE <<TYPE>> ;
FLUX := FREE: FLUX ;

!(*****************************************)
!(* ///// INITIALIZE INNER ITERATIONS ///// *)
!(*****************************************)
ITER := INITER: ITER TRK ::
ITERMETHOD CCSI 1.2
GROUPMETHOD SIMULTANEOUS
ORDERING REDBLACK
SPECTRAL METHOD2
EPSPHI <<EPSPHI>> ;

!(*****************************************)
!(* ///// INITIALIZE OUTER ITERATIONS ///// *)
!(*****************************************)
OUTER FLUX := OUTER: OUTER FLUX ITER ::
WIELAND
EPSK <<EPSK>>
MAXOUTER 25 ;
FLUX := FREE: FLUX ;
ITER := FREE: ITER ;
OUTER := FREE: OUTER ;

!(*********************************)
!(* ///// CALCULATE SOLUTION///// *)
!(*********************************)
OUTER := FREE: OUTER ;
ITER := FREE: ITER ;

!
FLUX MATRIX ITER OUTER := STATICNDF:
FLUX MATRIX ITER OUTER TRK MACLIB ::
PRINT_FLAG <<PF>> ;
```

```
!
ITER   := FREE:   ITER ;
OUTER  := FREE:   OUTER ;
MATRIX := FREE:   MATRIX ;
MATRIX := DELETE: MATRIX ;
ITER   := DELETE: ITER ;
OUTER  := DELETE: OUTER ;

!*
IF IDISCON 'NODISCON' = THEN
   POWER := INIPOWER: POWER FLUX MACLIB TRK ::
                      POWER <<CorePower>> COLLAPSE ;
ENDIF ;

!*
IF IDISCON 'DISCON' = THEN
   POWER := INIPOWER: POWER FLUX MACLIB TRK ::
                      POWER <<CorePower>> ECHO FLUX ;
ENDIF ;

!*
FLUX := FREE: FLUX ;
POWER  := FREE: POWER ;
FLUX := DELETE: FLUX ;

!
END: ;
```

```
!************************************************************
! Argonne National Laboratory 3D CANDU Benchmark (1985)     *
!                                                           *
!************************************************************
! file: DirectB.c2m                                         *
!                                                           *
! Siamak Kaveh, 2000                                        *
!************************************************************
 PARAMETER     TRANS POWER TRKNDF MACRO4 PROCEDE DEVICE GEO2
               MACRO3 ADJFLUX MACRO2 INDEX TRKDISCON
               ::
 :::
 LINKED_LIST   TRANS POWER TRKNDF MACRO4 PROCEDE DEVICE GEO2
               MACRO3 ADJFLUX MACRO2  INDEX TRKDISCON
               ;
 ;
!*
 LINKED_LIST   MACRO
               ;

!*
 MODULE        INITRANS: PREC0: DIRECTINT: PKPAR: TETAUDF:
               END: FREE: DELETE: GREP: DECLARE: XEN:
               NEWMAC: LINKDS: MOVDEV:  INIMAC: NDFASCII:
               DETECT: DIRECTMDF: THETA: DYNCOLLAPSE:
               CMPFLX: NEWMACHDF: DETECTNDF: KEYVAR: SOLVERDVF:
               ;
!
 INTEGER       I MAXITER
               ;
!
 REAL          TMAX DELTAT TIME RSigma2A RSigma2B
               pth pth0 dSigma IR
               ;
!
 STRING        FILEHDF FILERMS FILEPKP
               ;
!
 PROCEDURE     macB
               ;

! First reading input parameters...
 :: >>TMAX<< >>DELTAT<< >>FILEHDF<<
    >>FILERMS<< >>FILEPKP<<            ;
```

```
!
 POWER   := FREE: POWER                ;

! Evaluating local variables...
 EVALUATE I         := 0               ;
 EVALUATE TIME      := 0.              ;
 EVALUATE RSigma2A  := 4.0140E-03      ;
 EVALUATE RSigma2B  := 4.1000E-03      ;
 EVALUATE IR        := I        I_TO_R ;

! Initiating the transition procedure...
 TRANS TRKNDF := INITRANS: TRANS TRKNDF :: NDG 6
                 BET 0.000417 LAMBDA 0.01244
                 BET 0.001457 LAMBDA 0.03063
                 BET 0.001339 LAMBDA 0.1139
                 BET 0.003339 LAMBDA 0.3079
                 BET 0.000897 LAMBDA 1.198
                 BET 0.00032  LAMBDA 3.212
                 CHID 1.0 1.0 1.0 1.0 1.0 1.0
                 0.0 0.0 0.0 0.0 0.0 0.0
               <<TMAX>>
               <<DELTAT>>
                 ITERMETHOD SOR 1.4
                 GROUPMETHOD SIMULTANEOUS
                 ORDERING REDBLACK
                 EPSPHI 1.E-7
                                       ;

! Initiating delayed neutron precursors...
 POWER := PRECO:  POWER MACRO4
                  TRANS TRKNDF ::      ;

! Searching for nominal power
 GREP: POWER :: GETVAL POWER 1 >>pth<<       ;
 GREP: POWER :: GETVAL POWER 1 >>pth0<<      ;
 EVALUATE pth      := pth pth0 /             ;

!
 EVALUATE MAXITER := TMAX DELTAT /
                     R_TO_I            ;
!=============================================================!*
!            Starting transient ...                           !*
!=============================================================!*
 REPEAT
!
```

```
    EVALUATE I  := I 1 +                                    ;
    EVALUATE IR := I  I_TO_R                                ;
    EVALUATE TIME :=  IR DELTAT *                           ;

! IF  T <= 0.4  ELSE T > 0.4  ENDIF
    IF TIME 0.4 <= THEN
       EVALUATE dSigma   := DELTAT -1.00E-04 *              ;
       EVALUATE RSigma2A := RSigma2A dSigma  +              ;
       EVALUATE RSigma2B := RSigma2B dSigma  +              ;
    ELSE
       EVALUATE dSigma   := DELTAT -8.88889E-06 *           ;
       EVALUATE RSigma2A := RSigma2A dSigma     +           ;
       EVALUATE RSigma2B := RSigma2B dSigma     +           ;
    ENDIF                                                   ;

! IF T > 0.6 THEN move device
    IF TIME 0.6 >  THEN
       DEVICE   := FREE: DEVICE                             ;
       DEVICE   := MOVDEV: DEVICE PROCEDE GEO2 ::
                   EDIT 10 TYPE CONTROLLED
                   TIME <<DELTAT>>
                   ROD ADJUSTER                             ;
    ENDIF                                                   ;
!
    MACRO := macB      :: <<RSigma2A>> <<RSigma2B>>         ;

! Preparing the INDEXED macrolib
    MACRO2 := FREE: MACRO2 ;
    MACRO2 := DELETE: MACRO2 ;
    MACRO2 := INIMAC: MACRO INDEX                           ;

!
    MACRO2   := FREE:   MACRO2                              ;
    MACRO3   := FREE:   MACRO3                              ;
    MACRO3   := DELETE: MACRO3                              ;
    MACRO3   := NEWMAC: DEVICE MACRO2 GEO2 ::
                EDIT 1 TYPE CONTROLLED XFAC  1.0            ;
    MACRO4   := FREE:   MACRO4                              ;
    MACRO4   := DELETE: MACRO4                              ;
    MACRO4   := MACRO3                                      ;
    MACRO3   := FREE: MACRO3                                ;
!
    PRINT 'RESULTS AT TIME:  ' TIME                         ;
    PRINT '(Fine implicte DIRECTINT) --->'                  ;
    MACRO := FREE:   MACRO   ;
```

```
    MACRO := DELETE: MACRO    ;


! flux calculations...
    POWER     := FREE: POWER                          ;
    MACRO4    := FREE: MACRO4                         ;
    TRANS     := FREE: TRANS                          ;

    POWER  TRANS  := SOLVERDVF: POWER     TRANS
                                ADJFLUX   MACRO4
                                TRKNDF    TRKDISCON
                                ::
                                PRINTER_FLAG 1
                                DELTA_T <<DELTAT>>
                                NO_MULTIGRID
                                1000
                                1.E-6
                                TIME_PROFILE
                                DFLUX_NOM.DAT
                                TIMING_NOM.DAT
                                1
! // for multigrid
!                                MULTIGRID
!                                1000
!                                500
!                                1.E-6
!                                1.E-6
!                                TIME_PROFILE
!                                DFLUX_MUL.DAT
!                                TIMING_MUL.DAT
!                                1
                                                        ;

   GREP: POWER :: GETVAL POWER 1 >>pth<<                ;
   EVALUATE pth := pth pth0 /                           ;
   ECHO 'fine(implicit)------->' pth                    ;
!
 UNTIL I MAXITER >                                      ;
 END:                                                   ;
```

```
!************************************************************
! Argonne National Laboratory 3D CANDU Benchmark (1985)     *
!                                                           *
!************************************************************
! file: DYNIQSB.c2m                                         *
!                                                           *
! Siamak Kaveh, 2000                                        *
!************************************************************
 PARAMETER     TRANS POWER TRKNDF MACRO4 PROCEDE DEVICE GEO2
               MACRO3 ADJFLUX MACRO2 INDEX
               ::
 :::
 LINKED_LIST   TRANS POWER TRKNDF MACRO4 PROCEDE DEVICE GEO2
               MACRO3 ADJFLUX MACRO2 INDEX
               ;
 ;
 SEQ_ASCII     SMACR.f90
               ;
!
 LINKED_LIST   MACRO POWER_R NDINI NDTRA
               ;

!
 MODULE        INITRANS: PREC0: DIRECTINT: PKPAR: TETAUDF:
               END: FREE: DELETE: GREP: DECLARE: XEN:
               NEWMAC: LINKDS: MOVDEV:  INIMAC: NDFINI:
               DETECT: DIRECTMDF: THETA: DYNCOLLAPSE:
               CMPFLX: NEWMACHDF: DETECTNDF: KEYVAR:
               NDFTRAPK: NDFSHAPE: NDFASCII:
               ;
!
 INTEGER       I MAXITER MPK IPOINT
               ;
!
 REAL          TMAX DELTAT TIME RSigma2A RSigma2B
               pth pth0 dSigma IR RMAXITER MPK_R
               DELTAT_PK
               ;
!
 STRING        FILEHDF FILERMS FILEPKP
               ;
!
 PROCEDURE     macB
               ;
```

```
! First reading input parameters...
 :: >>TMAX<<      >>DELTAT<<
    >>MPK<<       >>FILEHDF<<
    >>FILERMS<<   >>FILEPKP<<          ;

!
 NDINI    := DECLARE: :: L_NDFINI      ;
 NDTRA    := DECLARE: :: L_NDFTRA      ;
 POWER_R  := POWER                     ;
 POWER    := FREE: POWER               ;

! Evaluating local variables...
 EVALUATE I         := 0               ;
 EVALUATE TIME      := 0.              ;
 EVALUATE RSigma2A  := 4.0140E-03      ;
 EVALUATE RSigma2B  := 4.1000E-03      ;
 EVALUATE IR        := I         I_TO_R ;
 EVALUATE MPK_R     := MPK       I_TO_R ;
 EVALUATE DELTAT_PK :=
                   DELTAT MPK_R  /     ;

! Initiating the transient procedure...
 TRANS TRKNDF := INITRANS: TRANS TRKNDF :: NDG 6
                 BET 0.000417 LAMBDA 0.01244
                 BET 0.001457 LAMBDA 0.03063
                 BET 0.001339 LAMBDA 0.1139
                 BET 0.003339 LAMBDA 0.3079
                 BET 0.000897 LAMBDA 1.198
                 BET 0.00032  LAMBDA 3.212
                 CHID 1.0 1.0 1.0 1.0 1.0 1.0
                 0.0 0.0 0.0 0.0 0.0 0.0
               <<TMAX>>
               <<DELTAT>>
                 ITERMETHOD SOR 1.4
                 GROUPMETHOD SIMULTANEOUS
                 ORDERING REDBLACK
                 EPSPHI 1.E-7
                                       ;

! Initiating delayed neutron precursors...
 POWER := PRECO:  POWER MACRO4
                  TRANS TRKNDF ::      ;

! Searching for nominal power
 GREP: POWER :: GETVAL POWER 1 >>pth<<      ;
```

```
 GREP: POWER :: GETVAL POWER 1 >>pth0<<     ;
 EVALUATE pth     := pth pth0 /             ;

! Preparing transition...
 NDINI NDTRA := NDFINI: NDINI NDTRA
                TRANS TRKNDF POWER
                ADJFLUX MACRO4 ::
                ANALYSIS_ERROR_ON
                DISCON_OFF
                OUTPUT_OFF
                PRINTER_FLAG 2
                T_MIN    0.0
                T_MAX  <<TMAX>>
                DELTAT_PK      <<DELTAT_PK>>
                DELTAT_FINE    <<DELTAT>>
                DELTAT_COARSE <<DELTAT>>
                                          ;
 NDINI  := FREE:  NDINI                   ;
 NDTRA  := FREE:  NDTRA                   ;
 TRANS  := FREE:  TRANS                   ;

!
 EVALUATE RMAXITER := TMAX DELTAT_PK / ;
 EVALUATE MAXITER  := RMAXITER R_TO_I  ;
!
!=================================================!*
!            Starting transient ...               !*
!=================================================!*
 REPEAT
!
    EVALUATE I      := I 1 +                       ;
    EVALUATE IPOINT := I I MPK / MPK * -           ;
    EVALUATE IR     := I I_TO_R                    ;
    EVALUATE TIME   := IR DELTAT_PK *              ;

! IF  T <= 0.4  ELSE T > 0.4  ENDIF
    IF TIME 0.4 <= THEN
       EVALUATE dSigma   := DELTAT_PK -1.00E-04 *  ;
       EVALUATE RSigma2A := RSigma2A dSigma  +     ;
       EVALUATE RSigma2B := RSigma2B dSigma  +     ;
    ELSE
       EVALUATE dSigma   := DELTAT_PK -8.88889E-06 * ;
       EVALUATE RSigma2A := RSigma2A dSigma     +  ;
       EVALUATE RSigma2B := RSigma2B dSigma     +  ;
    ENDIF                                          ;
```

```
! IF T > 0.6 THEN move device
    IF TIME 0.6 >  THEN
       DEVICE   := FREE: DEVICE                          ;
       DEVICE   := MOVDEV: DEVICE PROCEDE GEO2 ::
                   EDIT 10 TYPE CONTROLLED
                   TIME <<DELTAT_PK>>
                   ROD ADJUSTER                          ;
    ENDIF                                                ;
!
    MACRO := macB     :: <<RSigma2A>> <<RSigma2B>>       ;

! Preparing the INDEXED macrolib
    MACRO2 := FREE: MACRO2                               ;
    MACRO2 := DELETE: MACRO2                             ;
    MACRO2 := INIMAC: MACRO INDEX                        ;
!
    MACRO2   := FREE:   MACRO2                           ;
    MACRO3   := FREE:   MACRO3                           ;
    MACRO3   := DELETE: MACRO3                           ;
    MACRO3   := NEWMAC: DEVICE MACRO2 GEO2 ::
                EDIT 1 TYPE CONTROLLED XFAC  1.0         ;
    MACRO4   := FREE:   MACRO4                           ;
    MACRO4   := DELETE: MACRO4                           ;
    MACRO4   := MACRO3                                   ;
    MACRO3   := FREE: MACRO3                             ;
!
    ECHO  'RESULTS AT TIME:  ' TIME                      ;
    ECHO  '(Fine implicte DIRECTINT) --->'               ;
    MACRO := FREE:   MACRO   ;
    MACRO := DELETE: MACRO   ;

! flux calculations...
!// point kinetics
 IF IPOINT 0 <> THEN
    NDTRA  := FREE:  NDTRA                               ;
    TRANS  := FREE:  TRANS                               ;
    POWER  := FREE:  POWER                               ;
    NDTRA  POWER
          := NDFTRAPK:
             NDTRA POWER TRANS
             TRKNDF ADJFLUX MACRO4 ::
             DISCON_OFF
             DELTA_T <<DELTAT_PK>>
             UPDATE_POWER_ON
```

```
            TIME <<TIME>>
            PRINTER_FLAG 3
            OUTPUT_ON
            POINT.DAT
            METHOD_GRK4A                                    ;
!    pth   := GREP: NDTRA ::
!                              GETVAL POWER_PK 1                    ;
!    EVALUATE pth := pth pth0 /                              ;
 ENDIF ;
!// shape calculations
 IF IPOINT 0 = THEN
!
    NDTRA  := FREE:  NDTRA                                  ;
    TRANS  := FREE:  TRANS                                  ;
    POWER  := FREE:  POWER                                  ;
    NDTRA  POWER
          := NDFTRAPK:
            NDTRA POWER TRANS
            TRKNDF ADJFLUX MACRO4 ::
            DISCON_OFF
            DELTA_T <<DELTAT_PK>>
            UPDATE_POWER_ON
            TIME <<TIME>>
            PRINTER_FLAG 3
            OUTPUT_ON
            POINT.DAT
            METHOD_GRK4A                                    ;
!
    TRANS := FREE: TRANS                                    ;
    POWER := FREE: POWER                                    ;
    NDTRA := FREE: NDTRA                                    ;
    NDTRA TRANS POWER := NDFSHAPE:
            NDTRA TRANS
            TRKNDF POWER ADJFLUX
            MACRO4 ::
            DISCON_OFF
            UPDATE_POWER_ON
            NORMALIZE_SHAPE_ON
            CHECK_NEW_PRECURSOR_ON
            DELTA_T <<DELTAT>>
            PRINTER_FLAG 3
            OUTPUT_OFF
            METHOD_IMPLICIT                                 ;
 ENDIF                                                      ;
```

```
 GREP: POWER :: GETVAL POWER 1 >>pth<<                ;
 EVALUATE pth := pth pth0 /                           ;
 ECHO  'IQS(implicit)------->' pth                    ;
!
 UNTIL I MAXITER >                                    ;
 END:                                                 ;
```

```
!************************************************************
! Argonne National Laboratory 3D CANDU Benchmark (1985)     *
!                                                           *
!************************************************************
! file: macB.c2m                                            *
!                                                           *
! Siamak Kaveh, 2000                                        *
!************************************************************

 PARAMETER     TRANS_D TRANS POWER POWER_D TRKNDF TRKDISCON
               MACRO4 PROCEDE DEVICE GEO2 MACRO3 MACDISCON ADJFLUX
               MACRO2 MACDISCON_1 INDEX
               ::
 :::
 LINKED_LIST   TRANS_D TRANS POWER POWER_D TRKNDF TRKDISCON
               MACRO4 PROCEDE DEVICE GEO2 MACRO3 MACDISCON ADJFLUX
               MACRO2 MACDISCON_1 INDEX
               ;
 ;
!
 LINKED_LIST   NDINI NDTRA NDINI_D NDTRA_D
               RATIOS RECFLUX POWER_R MACRO MACRO_REF
               ;
!
 MODULE        INITRANS: PREC0: DIRECTINT: PKPAR: TETAUDF:
               END: FREE: DELETE: GREP: DECLARE: XEN:
               NEWMAC: LINKDS: MOVDEV:  INIMAC: NDFINI:
               DETECT: DIRECTMDF: THETA: DYNCOLLAPSE:
               CMPFLX: NEWMACHDF: DETECTNDF: KEYVAR:
               NDFTRAPK: NDFSHAPE: FLUXRATIO: MAKMACDF:
               DEHOM: NEWPOWER: NDFASCII: NDFCORDF:
               ;
!
 INTEGER       I ITOF MAXITER MPK IPOINT
               MCF NFINE
               ;
!
 REAL          TMAX DELTAT TIME RSigma2A RSigma2B
               pth pth0 dSigma IR RMAXITER MPK_R
               DELTAT_PK MCF_R DELTAT_C0 pth_d pth0_d
               ;
!
 CHARACTER     FILEHDF FILERMS FILEPKP
               ;
!
```

```
 PROCEDURE     macB
               ;

! First reading input parameters...
 :: >>TMAX<<    >>DELTAT<<  >>MPK<<
    >>MCF<<     >>FILEHDF<< >>FILERMS<<
    >>FILEPKP<<                          ;

!
 RATIOS     := DECLARE: :: L_FLUXRATIO  ;
 RECFLUX    := DECLARE: :: L_DEHOM      ;
 NDINI      := DECLARE: :: L_NDFINI     ;
 NDTRA      := DECLARE: :: L_NDFTRA     ;
 NDINI_D    := DECLARE: :: L_NDFINI     ;
 NDTRA_D    := DECLARE: :: L_NDFTRA     ;
 POWER_R    := POWER                    ;
 POWER      := FREE: POWER              ;
 MACRO_REF  := MACDISCON                ;
 MACRO_REF  := FREE: MACRO_REF          ;
 MACDISCON  := FREE: MACDISCON          ;

! Evaluating local variables...
 EVALUATE I         := 0                ;
 EVALUATE NFINE     := MPK MCF *        ;
 EVALUATE TIME      := 0.               ;
 EVALUATE RSigma2A  := 4.0140E-03       ;
 EVALUATE RSigma2B  := 4.1000E-03       ;
!
 EVALUATE IR        := I        I_TO_R  ;
 EVALUATE MCF_R     := MCF      I_TO_R  ;
 EVALUATE MPK_R     := MPK      I_TO_R  ;
 EVALUATE DELTAT_CO :=
                       DELTAT MCF_R  /  ;
 EVALUATE DELTAT_PK :=
                       DELTAT_CO MPK_R /  ;

! Initiating the transient procedure...
 TRANS TRKNDF := INITRANS: TRANS TRKNDF :: NDG 6
                 BET 0.000417 LAMBDA 0.01244
                 BET 0.001457 LAMBDA 0.03063
                 BET 0.001339 LAMBDA 0.1139
                 BET 0.003339 LAMBDA 0.3079
                 BET 0.000897 LAMBDA 1.198
                 BET 0.00032  LAMBDA 3.212
                 CHID 1.0 1.0 1.0 1.0 1.0 1.0
```

```
                0.0 0.0 0.0 0.0 0.0 0.0
              <<TMAX>>
              <<DELTAT>>
                ITERMETHOD SOR 1.4
                GROUPMETHOD SIMULTANEOUS
                ORDERING REDBLACK
                EPSPHI 1.E-7
                                        ;
!
 TRANS_D TRKDISCON := INITRANS: TRANS_D TRKDISCON ::
                NDG 6
                BET 0.000417 LAMBDA 0.01244
                BET 0.001457 LAMBDA 0.03063
                BET 0.001339 LAMBDA 0.1139
                BET 0.003339 LAMBDA 0.3079
                BET 0.000897 LAMBDA 1.198
                BET 0.00032  LAMBDA 3.212
                CHID 1.0 1.0 1.0 1.0 1.0 1.0
                0.0 0.0 0.0 0.0 0.0 0.0
              <<TMAX>>
              <<DELTAT_CO>>
                ITERMETHOD SOR 1.4
                GROUPMETHOD SIMULTANEOUS
                ORDERING REDBLACK
                EPSPHI 1.E-7
                                        ;
! Initiating delayed neutron precursors...
 POWER := PREC0:  POWER MACRO4
                  TRANS TRKNDF ::       ;
! coarse level...
 POWER_D := PREC0: POWER_D MACDISCON_1
            TRANS_D TRKDISCON ::        ;

! Searching for nominal power
 GREP: POWER :: GETVAL POWER 1 >>pth<<      ;
 GREP: POWER :: GETVAL POWER 1 >>pth0<<     ;
 EVALUATE pth     := pth pth0 /         ;

! second coarse level...
 GREP: POWER :: GETVAL POWER 1 >>pth_d<<      ;
 GREP: POWER :: GETVAL POWER 1 >>pth0_d<<     ;
 EVALUATE pth_d   := pth_d pth0_d /    ;

! Preparing transient...
 NDINI NDTRA := NDFINI: NDINI NDTRA
```

```
                TRANS TRKNDF POWER
                ADJFLUX MACRO4 ::
                ANALYSIS_ERROR_ON
                DISCON_OFF
                OUTPUT_OFF
                PRINTER_FLAG 2
                T_MIN     0.0
                T_MAX  <<TMAX>>
                DELTAT_PK      <<DELTAT_PK>>
                DELTAT_FINE    <<DELTAT>>
                DELTAT_COARSE <<DELTAT_CO>> (*not used*)
                                          ;
 NDINI  := FREE:  NDINI                   ;
 NDTRA  := FREE:  NDTRA                   ;
!
 NDINI_D NDTRA_D := NDFINI: NDINI_D NDTRA_D
                TRANS_D TRKDISCON POWER_D
                ADJFLUX MACDISCON ::
                ANALYSIS_ERROR_ON
                DISCON_ON
                OUTPUT_OFF
                PRINTER_FLAG 2
                T_MIN         0.0
                T_MAX       <<TMAX>>
                DELTAT_PK  <<DELTAT_PK>>
                DELTAT_FINE    <<DELTAT>>
                DELTAT_COARSE <<DELTAT_CO>>
                                          ;
!
 NDINI_D  := FREE:  NDINI_D               ;
 NDTRA_D  := FREE:  NDTRA_D               ;

! Calculating initial fluxratio
 POWER       := FREE: POWER               ;
 RATIOS      := FREE: RATIOS              ;
 RATIOS      := FLUXRATIO: RATIOS
                POWER TRKNDF ::           ;
 RATIOS      := FREE: RATIOS              ;
!
 EVALUATE RMAXITER := TMAX DELTAT_PK / ;
 EVALUATE MAXITER  := RMAXITER R_TO_I  ;
!================================================!*
!            Starting transient ...              !*
!================================================!*
 REPEAT
```

```
!
    EVALUATE I      := I 1 +                          ;
    EVALUATE IR     := I   I_TO_R                     ;
    EVALUATE TIME :=  IR DELTAT_PK *                  ;

! IF  T <= 0.4  ELSE T > 0.4  ENDIF
    IF TIME 0.4 <= THEN
       EVALUATE dSigma   := DELTAT_PK -1.00E-04 *     ;
       EVALUATE RSigma2A := RSigma2A dSigma  +        ;
       EVALUATE RSigma2B := RSigma2B dSigma  +        ;
    ELSE
       EVALUATE dSigma   := DELTAT_PK -8.88889E-06 * ;
       EVALUATE RSigma2A := RSigma2A dSigma     +     ;
       EVALUATE RSigma2B := RSigma2B dSigma     +     ;
    ENDIF                                             ;

! IF T > 0.6 THEN move device
    IF TIME 0.6 >  THEN
       DEVICE   := FREE: DEVICE                       ;
       DEVICE   := MOVDEV: DEVICE PROCEDE GEO2 ::
                   EDIT 10 TYPE CONTROLLED
                   TIME <<DELTAT_PK>>
                   ROD ADJUSTER                       ;
    ENDIF                                             ;
!
    MACRO := macB     :: <<RSigma2A>> <<RSigma2B>>    ;
! Preparing the INDEXED macrolib
    MACRO2 := FREE: MACRO2                            ;
    MACRO2 := DELETE: MACRO2                          ;
    MACRO2 := INIMAC: MACRO INDEX                     ;
!
    MACRO2   := FREE:   MACRO2                        ;
    MACRO3   := FREE:   MACRO3                        ;
    MACRO3   := DELETE: MACRO3                        ;
    MACRO3   := NEWMAC: DEVICE MACRO2 GEO2 ::
                EDIT 1 TYPE CONTROLLED XFAC  1.0      ;
    MACRO4   := FREE:   MACRO4                        ;
    MACRO4   := DELETE: MACRO4                        ;
    MACRO4   := MACRO3                                ;
    MACRO3   := FREE: MACRO3                          ;
! coarse level  //OPTION: Updating Cross-Sections
    MACDISCON := FREE: MACDISCON                      ;
    MACDISCON := MAKMACDF: MACDISCON TRKDISCON
                 TRKNDF POWER ADJFLUX
                 MACRO4 PROCEDE ::
```

```
                1
                PRINTER_FLAG 0
                PUT_XS                                  ;
    MACDISCON := FREE: MACDISCON                        ;
!
    MACRO := FREE:   MACRO                              ;
    MACRO := DELETE: MACRO                              ;
!
    PRINT 'RESULTS AT TIME:  ' TIME                     ;
    EVALUATE ITOF   := I I NFINE / NFINE * -            ;

! // Fine Calculation... ITOF = 0
 IF ITOF 0 = THEN
    TRANS := FREE: TRANS                                ;
    POWER := FREE: POWER                                ;
    NDTRA := FREE: NDTRA                                ;
!// Calculating new shape...and new L_POWER
!// Updating point kinetics parameters coarse
    NDTRA_D  := FREE:  NDTRA_D                          ;
    TRANS_D  := FREE:  TRANS_D                          ;
    POWER_D  := FREE:  POWER_D                          ;
    NDTRA_D  POWER_D
             := NDFTRAPK:
                NDTRA_D POWER_D TRANS_D
                TRKDISCON ADJFLUX MACDISCON ::
                DISCON_ON
                DELTA_T <<DELTAT_PK>>
                UPDATE_POWER_ON
                TIME <<TIME>>
                PRINTER_FLAG 3
                OUTPUT_OFF
                METHOD_GRK4A                            ;
!// Updating point kinetics parameters fine
    NDTRA  := FREE:  NDTRA                              ;
    TRANS  := FREE:  TRANS                              ;
    POWER  := FREE:  POWER                              ;
    NDTRA  POWER
           := NDFTRAPK:
              NDTRA POWER TRANS
              TRKNDF ADJFLUX MACRO4 ::
              DISCON_OFF
              DELTA_T <<DELTAT_PK>>
              UPDATE_POWER_ON
              TIME <<TIME>>
              PRINTER_FLAG 3
```

```
                OUTPUT_ON
                POINT.DAT
                METHOD_GRK4A                                    ;
!//Calculating fine shape
    NDTRA TRANS POWER := NDFSHAPE:
                NDTRA TRANS
                TRKNDF POWER ADJFLUX
                MACRO4 ::
                DISCON_OFF
                UPDATE_POWER_ON
                NORMALIZE_SHAPE_ON
                CHECK_NEW_PRECURSOR_ON
                DELTA_T <<DELTAT>>
                PRINTER_FLAG 3
                OUTPUT_OFF
                METHOD_IMPLICIT                                 ;
!//Updating Discontinuity factors
    MACDISCON := FREE: MACDISCON                                ;
    MACDISCON := MAKMACDF: MACDISCON TRKDISCON
                   TRKNDF POWER ADJFLUX
                   MACRO4 PROCEDE ::
                   1
                   PRINTER_FLAG 1
                   PUT_AL                                       ;
    MACDISCON := FREE: MACDISCON                                ;
!//Updating  Flux Ratios
    POWER       := FREE: POWER                                  ;
    RATIOS      := FREE: RATIOS                                 ;
    RATIOS      := FLUXRATIO: RATIOS POWER TRKNDF ::            ;

 ENDIF                                                          ;
!// NO Fine Calculation... ITOF <> 0
 IF ITOF 0 <> THEN
    EVALUATE IPOINT  := I I MPK / MPK * -                       ;
    PRINT 'IPOINT ====>' IPOINT                                 ;
!// Coarse calculation...IPOINT = 0
 IF IPOINT 0 = THEN
!// Updating point kinetics parameters fine
    NDTRA  := FREE:  NDTRA                                      ;
    TRANS  := FREE:  TRANS                                      ;
    POWER  := FREE:  POWER                                      ;
    NDTRA  POWER
           := NDFTRAPK:
              NDTRA POWER TRANS
              TRKNDF ADJFLUX MACRO4 ::
```

```
                DISCON_OFF
                DELTA_T <<DELTAT_PK>>
                UPDATE_POWER_ON
                TIME <<TIME>>
                PRINTER_FLAG 3
                OUTPUT_ON
                POINT.DAT
                METHOD_GRK4A                                    ;
!// Updating point kinetics parameters coarse
    NDTRA_D  := FREE:  NDTRA_D                                  ;
    TRANS_D  := FREE:  TRANS_D                                  ;
    POWER_D  := FREE:  POWER_D                                  ;
    NDTRA_D  POWER_D
             := NDFTRAPK:
                NDTRA_D POWER_D TRANS_D
                TRKDISCON ADJFLUX MACDISCON ::
                DISCON_ON
                DELTA_T <<DELTAT_PK>>
                UPDATE_POWER_ON
                TIME <<TIME>>
                PRINTER_FLAG 3
                OUTPUT_OFF
                METHOD_GRK4A                                    ;
!Solving coarse shape...
    TRANS_D := FREE: TRANS_D                                    ;
    POWER_D := FREE: POWER_D                                    ;
    NDTRA_D := FREE: NDTRA_D                                    ;
    NDTRA_D TRANS_D POWER_D := NDFSHAPE:
                NDTRA_D TRANS_D
                TRKDISCON POWER_D ADJFLUX
                MACDISCON ::
                DISCON_ON
                UPDATE_POWER_ON
                NORMALIZE_SHAPE_ON
                CHECK_NEW_PRECURSOR_ON
                DELTA_T <<DELTAT_CO>>
                PRINTER_FLAG 3
                OUTPUT_OFF
                METHOD_IMPLICIT                                 ;
   GREP: POWER :: GETVAL POWER 1 >>pth_d<<                      ;
   PRINT ' Pth_d===>' pth_d                                     ;
   EVALUATE pth_d := pth_d pth0_d /                             ;
!// Reconstruction of flux
    RECFLUX := FREE:  RECFLUX                                   ;
    RECFLUX := DEHOM: RECFLUX
```

```
                    RATIOS POWER_D TRKNDF ::        ;
!// Updating L_POWER
    POWER   := FREE: POWER                          ;
    POWER   := NEWPOWER: POWER
                    RECFLUX MACRO4 TRKNDF ::        ;
  ENDIF                                             ;
!!// Solving Point kinetics...
  IF IPOINT 0 <> THEN
    NDTRA  := FREE:  NDTRA                          ;
    TRANS  := FREE:  TRANS                          ;
    POWER  := FREE:  POWER                          ;
    NDTRA  POWER
          := NDFTRAPK:
             NDTRA POWER TRANS
             TRKNDF ADJFLUX MACRO4 ::
             DISCON_OFF
             DELTA_T <<DELTAT_PK>>
             UPDATE_POWER_ON
             TIME <<TIME>>
             PRINTER_FLAG 3
             OUTPUT_ON
             POINT.DAT
             METHOD_GRK4A                           ;
!
    NDTRA_D  := FREE:  NDTRA_D                      ;
    TRANS_D  := FREE:  TRANS_D                      ;
    POWER_D  := FREE:  POWER_D                      ;
    NDTRA_D  POWER_D
             := NDFTRAPK:
             NDTRA_D POWER_D TRANS_D
             TRKDISCON ADJFLUX MACDISCON ::
             DISCON_ON
             DELTA_T <<DELTAT_PK>>
             UPDATE_POWER_ON
             TIME <<TIME>>
             PRINTER_FLAG 3
             OUTPUT_OFF
             METHOD_GRK4A                           ;
   GREP: POWER :: GETVAL POWER 1 >>pth_d<<          ;
   PRINT ' Pth_d===>' pth_d                         ;
   EVALUATE pth_d := pth_d pth0_d /                 ;
!// Reconstructing flux
      RECFLUX := FREE:  RECFLUX                     ;
      RECFLUX := DEHOM: RECFLUX
                 RATIOS POWER_D TRKNDF ::           ;
```

```
!// Updating L_POWER
      POWER    := FREE:     POWER                    ;
      POWER    := NEWPOWER: POWER
                  RECFLUX MACRO4 TRKNDF ::          ;
   ENDIF                                            ;
!//endif ITOF
 ENDIF                                              ;

!
 GREP: POWER :: GETVAL POWER 1 >>pth<<              ;
 EVALUATE pth := pth pth0 /                         ;
!
 UNTIL I MAXITER >                                  ;
 END:                                               ;
```

```
!************************************************************
! Argonne National Laboratory 3D CANDU Benchmark (1985)     *
!                                                           *
!************************************************************
! file: DevprocB.c2m                                        *
!                                                           *
! Siamak Kaveh, 2000                                        *
!************************************************************
 PARAMETER   MACRO ::
 :::
 LINKED_LIST MACRO  ;
 ;
!//
!//
 MODULE      MACD: END:          ;
!//
 REAL        RSigma2A   RSigma2B ;
!//
 :: >>RSigma2A<< >>RSigma2B<<    ;
!//
 MACRO :=  MACD: ::
           EDIT 0  NGRO 2 NMIX 25  READ
!//////////
  MIX      1
      DIFFX  1.3100E+00 0.8695E+00
      TOTAL  1.0180E-02 2.1170E-04
     NUSIGF  0.0000E+00 0.0000E+00
        CHI  1.0000E+00 0.0000E+00
  H-FACTORS  0.0000E+00 0.0000E+00
       SCAT  1 1 0.0 2 2 0.0 1.0180E-02
MIX       2
      DIFFX  1.3100E+00 0.8695E+00
      TOTAL  1.0180E-02 2.1170E-04
     NUSIGF  0.0000E+00 0.0000E+00
        CHI  1.0000E+00 0.0000E+00
  H-FACTORS  0.0000E+00 0.0000E+00
       SCAT  1 1 0.0 2 2 0.0 1.0180E-02
MIX       3
      DIFFX  1.3100E+00 0.8695E+00
      TOTAL  1.0180E-02 2.1170E-04
     NUSIGF  0.0000E+00 0.0000E+00
        CHI  1.0000E+00 0.0000E+00
  H-FACTORS  0.0000E+00 0.0000E+00
       SCAT  1 1 0.0 2 2 0.0 1.0180E-02
MIX       4
```

```
      DIFFX  1.3100E+00 0.8695E+00
      TOTAL  1.0180E-02 2.1170E-04
     NUSIGF  0.0000E+00 0.0000E+00
        CHI  1.0000E+00 0.0000E+00
  H-FACTORS  0.0000E+00 0.0000E+00
       SCAT  1 1 0.0 2 2 0.0 1.0180E-02
!////////////
 MIX      5
      DIFFX  1.2640E+00 0.9328E+00
      TOTAL  8.1540E-03 <<RSigma2A>>
     NUSIGF  0.0000E+00 4.7230E-03
        CHI  1.0000E+00 0.0000E+00
  H-FACTORS  0.0000E+00 4.7230E-03
       SCAT  1 1 0.0 2 2 0.0 7.3680E-03

 MIX      6
      DIFFX  1.2640E+00 0.9328E+00
      TOTAL  8.1540E-03 <<RSigma2A>>
     NUSIGF  0.0000E+00 4.7230E-03
        CHI  1.0000E+00 0.0000E+00
  H-FACTORS  0.0000E+00 4.7230E-03
       SCAT  1 1 0.0 2 2 0.0 7.3680E-03
 MIX      7
      DIFFX  1.2640E+00 0.9328E+00
      TOTAL  8.1540E-03 4.0140E-03
     NUSIGF  0.0000E+00 4.7230E-03
        CHI  1.0000E+00 0.0000E+00
  H-FACTORS  0.0000E+00 4.7230E-03
       SCAT  1 1 0.0 2 2 0.0 7.3680E-03
 MIX      8
      DIFFX  1.2640E+00 0.9328E+00
      TOTAL  8.1540E-03 4.0140E-03
     NUSIGF  0.0000E+00 4.7230E-03
        CHI  1.0000E+00 0.0000E+00
  H-FACTORS  0.0000E+00 4.7230E-03
       SCAT  1 1 0.0 2 2 0.0 7.3680E-03
 MIX      9
      DIFFX  1.2640E+00 0.9328E+00
      TOTAL  8.1540E-03 4.0140E-03
     NUSIGF  0.0000E+00 4.7230E-03
        CHI  1.0000E+00 0.0000E+00
  H-FACTORS  0.0000E+00 4.7230E-03
       SCAT  1 1 0.0 2 2 0.0 7.3680E-03
 MIX     10
      DIFFX  1.2640E+00 0.9328E+00
```

```
      TOTAL  8.1540E-03 <<RSigma2A>>
     NUSIGF  0.0000E+00 4.7230E-03
        CHI  1.0000E+00 0.0000E+00
  H-FACTORS  0.0000E+00 4.7230E-03
       SCAT  1 1 0.0 2 2 0.0 7.3680E-03
!///////////
 MIX     11
      DIFFX  1.2640E+00 0.9328E+00
      TOTAL  8.1540E-03 <<RSigma2B>>
     NUSIGF  0.0000E+00 4.5620E-03
        CHI  1.0000E+00 0.0000E+00
  H-FACTORS  0.0000E+00 4.5620E-03
       SCAT  1 1 0.0 2 2 0.0 7.3680E-03
  MIX     12
      DIFFX  1.2640E+00 0.9328E+00
      TOTAL  8.1540E-03 4.1000E-03
     NUSIGF  0.0000E+00 4.5620E-03
        CHI  1.0000E+00 0.0000E+00
  H-FACTORS  0.0000E+00 4.5620E-03
       SCAT  1 1 0.0 2 2 0.0 7.3680E-03
!///////////
 MIX     13
      DIFFX  1.3100E+00 0.8695E+00
      TOTAL  1.0180E-02 2.1170E-04
     NUSIGF  0.0000E+00 0.0000E+00
        CHI  1.0000E+00 0.0000E+00
  H-FACTORS  0.0000E+00 0.0000E+00
       SCAT  1 1 0.0 2 2 0.0 1.0180E-02
 MIX     14
      DIFFX  1.3100E+00 0.8695E+00
      TOTAL  1.0180E-02 2.1170E-04
     NUSIGF  0.0000E+00 0.0000E+00
        CHI  1.0000E+00 0.0000E+00
  H-FACTORS  0.0000E+00 0.0000E+00
       SCAT  1 1 0.0 2 2 0.0 1.0180E-02
 MIX     15
      DIFFX  1.3100E+00 0.8695E+00
      TOTAL  1.0180E-02 2.1170E-04
     NUSIGF  0.0000E+00 0.0000E+00
        CHI  1.0000E+00 0.0000E+00
  H-FACTORS  0.0000E+00 0.0000E+00
       SCAT  1 1 0.0 2 2 0.0 1.0180E-02
 MIX     16
      DIFFX  1.3100E+00 0.8695E+00
      TOTAL  1.0180E-02 2.1170E-04
```

```
    NUSIGF  0.0000E+00 0.0000E+00
       CHI  1.0000E+00 0.0000E+00
 H-FACTORS  0.0000E+00 0.0000E+00
      SCAT  1 1 0.0 2 2 0.0 1.0180E-02
!///////////
 MIX     17
     DIFFX  1.2640E+00 0.9328E+00
     TOTAL  8.1540E-03 <<RSigma2A>>
    NUSIGF  0.0000E+00 4.7230E-03
       CHI  1.0000E+00 0.0000E+00
 H-FACTORS  0.0000E+00 4.7230E-03
      SCAT  1 1 0.0 2 2 0.0 7.3680E-03
 MIX     18
     DIFFX  1.2640E+00 0.9328E+00
     TOTAL  8.1540E-03 <<RSigma2A>>
    NUSIGF  0.0000E+00 4.7230E-03
       CHI  1.0000E+00 0.0000E+00
 H-FACTORS  0.0000E+00 4.7230E-03
      SCAT  1 1 0.0 2 2 0.0 7.3680E-03
 MIX     19
     DIFFX  1.2640E+00 0.9328E+00
     TOTAL  8.1540E-03 4.0140E-03
    NUSIGF  0.0000E+00 4.7230E-03
       CHI  1.0000E+00 0.0000E+00
 H-FACTORS  0.0000E+00 4.7230E-03
      SCAT  1 1 0.0 2 2 0.0 7.3680E-03
 MIX     20
     DIFFX  1.2640E+00 0.9328E+00
     TOTAL  8.1540E-03 4.0140E-03
    NUSIGF  0.0000E+00 4.7230E-03
       CHI  1.0000E+00 0.0000E+00
 H-FACTORS  0.0000E+00 4.7230E-03
      SCAT  1 1 0.0 2 2 0.0 7.3680E-03
 MIX     21
     DIFFX  1.2640E+00 0.9328E+00
     TOTAL  8.1540E-03 4.0140E-03
    NUSIGF  0.0000E+00 4.7230E-03
       CHI  1.0000E+00 0.0000E+00
 H-FACTORS  0.0000E+00 4.7230E-03
      SCAT  1 1 0.0 2 2 0.0 7.3680E-03
 MIX     22
     DIFFX  1.2640E+00 0.9328E+00
     TOTAL  8.1540E-03 <<RSigma2A>>
    NUSIGF  0.0000E+00 4.7230E-03
       CHI  1.0000E+00 0.0000E+00
```

```
  H-FACTORS  0.0000E+00 4.7230E-03
       SCAT  1 1 0.0 2 2 0.0 7.3680E-03
!///////////
 MIX     23
      DIFFX  1.2640E+00 0.9328E+00
      TOTAL  8.1540E-03 <<RSigma2B>>
     NUSIGF  0.0000E+00 4.5620E-03
        CHI  1.0000E+00 0.0000E+00
  H-FACTORS  0.0000E+00 4.5620E-03
       SCAT  1 1 0.0 2 2 0.0 7.3680E-03
 MIX     24
      DIFFX  1.2640E+00 0.9328E+00
      TOTAL  8.1540E-03 4.1000E-03
     NUSIGF  0.0000E+00 4.5620E-03
        CHI  1.0000E+00 0.0000E+00
  H-FACTORS  0.0000E+00 4.5620E-03
       SCAT  1 1 0.0 2 2 0.0 7.3680E-03
!///////////// Device
 MIX     25
      TOTAL  0.0000E+00 6.1500E-04      ;
!//
END: ;
```